5-14-2021

Clay Mineralogy And Geochemistry Of Pleistocene Sediments From Paleolake Olduvai, Tanzania

Nabil Murshed
Georgia State University

CLAY MINERALOGY AND GEOCHEMISTRY OF PLEISTOCENE SEDIMENTS FROM PALEOLAKE OLDUVAI, TANZANIA

by

NABIL MURSHED

Under the Direction of W. Crawford Elliott, Ph.D.

ABSTRACT

Sediment cores were studied from the oldest yet known, newly revealed, deepest area of the Olduvai paleolake in northern Tanzania as part of the *Olduvai Gorge Coring Project* (OGCP). Illite was the predominant mineral identified in the X-ray Diffraction (XRD) analyses of 112 samples from Core 2A (between fifth and FLK faults) at 156 - 215.3 meters below the surface (mbs). The illite was aluminous based on the (060) d-spacing values of 1.511Å, confirming the dioctahedral phase. This aluminous illite is in contrast to the well-known magnesium-rich illite in younger deposits, and the magnesian illite was deposited in a less saline Olduvai paleolake >2 Ma ago.f That lake water composition contrasted with the hypersaline, hyper alkaline lake waters known from the geochemical and mineralogical analyses of the younger units of Olduvai Beds I and II. The octahedral composition of illite (Mg/(Al+Fe) varied from 0.09 to 0.24. A lower MgO anomaly was observed in the claystone geochemistry restricted to the studied interval.

INDEX WORDS: Authigenic Clays, Paleoclimate, Human evolution, Diagenesis, Paleolimnology, East African Rift

CLAY MINERALOGY AND GEOCHEMISTRY OF PLEISTOCENE SEDIMENTS FROM PALEOLAKE OLDUVAI, TANZANIA

by

NABIL MURSHED

A Thesis Submitted in Partial Fulfillment of the Requirements for the Degree of

Master of Science

in the College of Arts and Sciences

Georgia State University

2021

CLAY MINERALOGY AND GEOCHEMISTRY OF PLEISTOCENE SEDIMENTS FROM PALEOLAKE OLDUVAI, TANZANIA

by

NABIL MURSHED

Committee Chair: W. Crawford Elliott

Committee: Daniel M. Deocampo

Daniel Gebregiorgis

Lindsay J. McHenry

Electronic Version Approved: May 2021

Office of Graduate Studies

College of Arts and Sciences

Georgia State University

May 2021

DEDICATION

I dedicate this thesis to my mother, Monira Nazneen, who provided constant support throughout my life, passed along her passion for life and desire to pursue knowledge. My mother has and always will be my biggest inspiration. I am proud and lucky to have her in my life.

It is further dedicated to all my family members, mentors, and peers at the Geoscience department. The mentors' guidance and peers' support at Georgia State University, without which this work wouldn't be possible, was very much appreciated.

ACKNOWLEDGEMENTS

I would like to express my deepest gratitude to my advisor Dr. Crawford Elliott, who has taken the challenges of advising me and providing me the utmost support regarding both educational and professional quests. His comments and direction did not let me go off track. I would also like to thank committee members Dr. Daniel Gebregiorgis, Dr. Daniel Deocampo, and Dr. Lindsay McHenry whose help pushed me forward.

I would like to thank Prof. Stanley A. Mertzman Jr. of Franklin & Marshall College for XRF analysis.

The National Science Foundation award (Award Number 1349599) to Dr. Daniel M. Deocampo provided both access to samples and the needed contextual information to study them.

I am incredibly thankful to Georgia State University's Department of Geosciences for giving me this opportunity to prove my potential. Heartiest thanks to all the faculty members of the Department of Geosciences, who was and will be inspirations for myself and for researchers everywhere.

TABLE OF CONTENTS

LIST OF TABLES

LIST OF FIGURES

LIST OF ABBREVIATIONS

LacCore	National Lacustrine Core Laboratory
LOI	Loss of Ignition
m	Meters
µm	Microns
mA	Milliamps
Ma	Million years
mbs	meters below surface
mg	Milligram
XRD	X-ray Diffraction
XRF	X-ray Fluorescence
wt.%	Weight Percent
>	Greater than
<	Less than
Å	Angstrom

1 INTRODUCTION

Reconstruction of the terrestrial Quaternary paleoenvironment is essential to understand the role of climate in the evolution of hominins and other vertebrates. Paleolakes can provide essential archives of past climate change, hominin evolution, and ecosystem change, using a wide array of climate proxies. These proxies often include biotic (fossil) indicators, geochemical indicators, and mineralogical indicators for an individual locality. Plant microfossils, diatoms, pollen, and ostracodes can be proxies of paleoenvironmental conditions. Biotic indicators such as ostracodes and diatoms are repressed in lacustrine settings. Thus, recent studies underscore the potential of phyllosilicate minerals (pedogenic and authigenic) as possible lacustrine salinity proxies (Deocampo et al., 2009). However, authigenic phyllosilicate minerals can be difficult to implement as climate proxies, partly due to challenges in obtaining purified authigenic phases, poorly defined geochemical reactions, a lack of understanding of the prevailing geochemical conditions, and prevailing geochemical conditions and relationships between limnology and climate. This is especially true for the Olduvai Basin, a closed basin in a saline-alkaline setting (Hay, 1976).

Paleolake basins along the East African Rift are important archives of paleontological fossil assemblages of early hominid species. In northern Tanzania, Olduvai Gorge, on the shoulder of the rift valley, has provided a wealth of information on terrestrial ecosystem evolution (Ashley & Hay, 2002). Previous studies on the East African Rift have focused on finding evidence of environmental fluctuations, hominin extinction, speciation, and behavioral events associated with changes in the African climate over the past 5 million years. Some of the critical behavioral breakthroughs are clustered between 2.9 and 1.6 Ma (deMenocal, 2011; Deocampo & Tactikos, 2010). Several scientific drilling projects were conducted to obtain continuous sediment cores to

generate high-resolution lake core records to help unravel the link between environmental change and human evolution. East African Rift valley lakes are generally shallow and alkaline, and the lacustrine deposits usually lack biotic proxies such as diatoms, ostracods, phytoliths, and pollen. At the same time, the high alkalinity, Mg, and silica contents are consistent with the presence of authigenic clays. Authigenic clays are preferable to pre-existing (detrital) clays for paleoclimatic reconstruction. Detrital paleoclays can provide information about their areas of provenance, if the clay mineral assemblages have not been affected by post-depositional changes (Singer, 1984). Paleoclimatic interpretation is feasible if the paleoclay is authigenic, assuming that it stored a record of the depositional conditions, with no post-burial diagenesis in clay composition or mineralogy. In continental sediments, the distinction between detrital and authigenic clays is often troublesome. Intermediate weathering products and a lack of information on local conditions unrelated to climate can make it difficult to interpret whether a clay is authigenic. The distinction should be based on clay morphology, structure, composition, distribution, and textural properties (Singer, 1984). Polytypes have also been used to show provenance of illite in argillaceous rocks (Pevear, 1999). Another indicator for the paleoclimatic conditions can be the isotopic composition of the paleoclays. The isotopic composition of clay minerals can reflect the isotopic composition of meteoric water involved in forming or transforming these clay minerals (Singer, 1980). At Olduvai, authigenic clay minerals provide sole proxy data to help determine the paleohydrology and paleoenvironment of the basin (Deocampo, 2015).

While there is no modern lake in the Olduvai Basin, paleolacustrine sediments are exposed in a 2 Ma sedimentary record (Ashley & Hay, 2002). Olduvai records a paleolake expansion at 1.79 Ma that lasted about 10,000 years (Deocampo, 2004). The Olduvai Basin was a saline, alkaline lake basin with low detrital input that allowed the accumulation of authigenic silicates. It

is well known for its record of hominin fossils, stone tools, high-resolution paleoenvironmental reconstructions associated with many archaeological sites (Ashley et al., 2010; Hay, 1976). Central Basin clays recorded limnological fluctuations in their compositions and relative abundances of authigenic clay mineral phases (Hay & Kyser, 2001; Hover & Ashley, 2003). The sedimentary deposits include volcanic and volcaniclastic deposits, with basalt flows, pyroclastic air falls, ground surges, and ignimbrites from the eruptive Ngorongoro volcanic complex. The paleo landscape had a central lake basin filled with detrital sediment, carbonate rocks, and tephra (Hay, 1976). The detrital deposition was provided both by rivers sourced in the Ngorongoro complex and by Precambrian rocks of the Serengeti to the north and west.

1.1 Geologic Background

Olduvai Gorge is located at the Eastern Rift Valley's western margin in Northern Tanzania, where the Gorge cuts a valley within the Serengeti Plains. The elevation of the Serengeti Plain is 1219 to 1402 meters. Olduvai is divided into two branches; a southern, smaller branch, or Side Gorge, and a northern, larger branch, or Main Gorge.

The Pleistocene sediment beds cut by the Gorge overlie the rhyolitic Naabi Ignimbrite (2.038+/-0.005 Ma). The Naabi Ignimbrite overlies Precambrian metamorphic basement where it is exposed in the far western Olduvai basin. Deposits of tuff and volcaniclastics were overlain by (and interfingered with) the Pleistocene sediment beds, and were sourced from the Eastern Rift Valley’s volcanoes, including Ngorongoro.

Basin stratigraphic analysis of Olduvai Gorge was initiated by Hay (1976). This work primarily covers the eastern part of the Main Gorge, with Bed I basaltic lava flows considered a basement layer. This basement was overlain by sedimentary beds that were subdivided into five units. The units were first termed Bed I, Bed II, Bed III, Bed IV, and Bed V (Hay, 1971) but

updated to include seven units (Beds I-IV, Masek, Ndutu, and Naisisusiu Beds) (Hay, 1976). Numerous horizontal or nearly horizontal faults cut these beds. These faults numbered from east to west: First, Second, Third, Fourth, and Fifth faults, with the FLK fault between the Fourth and Fifth (Figure 1-1). The offset from these faults ranged from 6 to 36.6 meters. The Fifth fault was similar to the other faults. The Fifth Fault showed the maximum displacement, causing a significant down drop that provided accommodation space for sediment accumulation. Olduvai Gorge dropped down about 121.9 meters into the Ol'Balbal fault graben, along the First Fault (Hay, 1971).

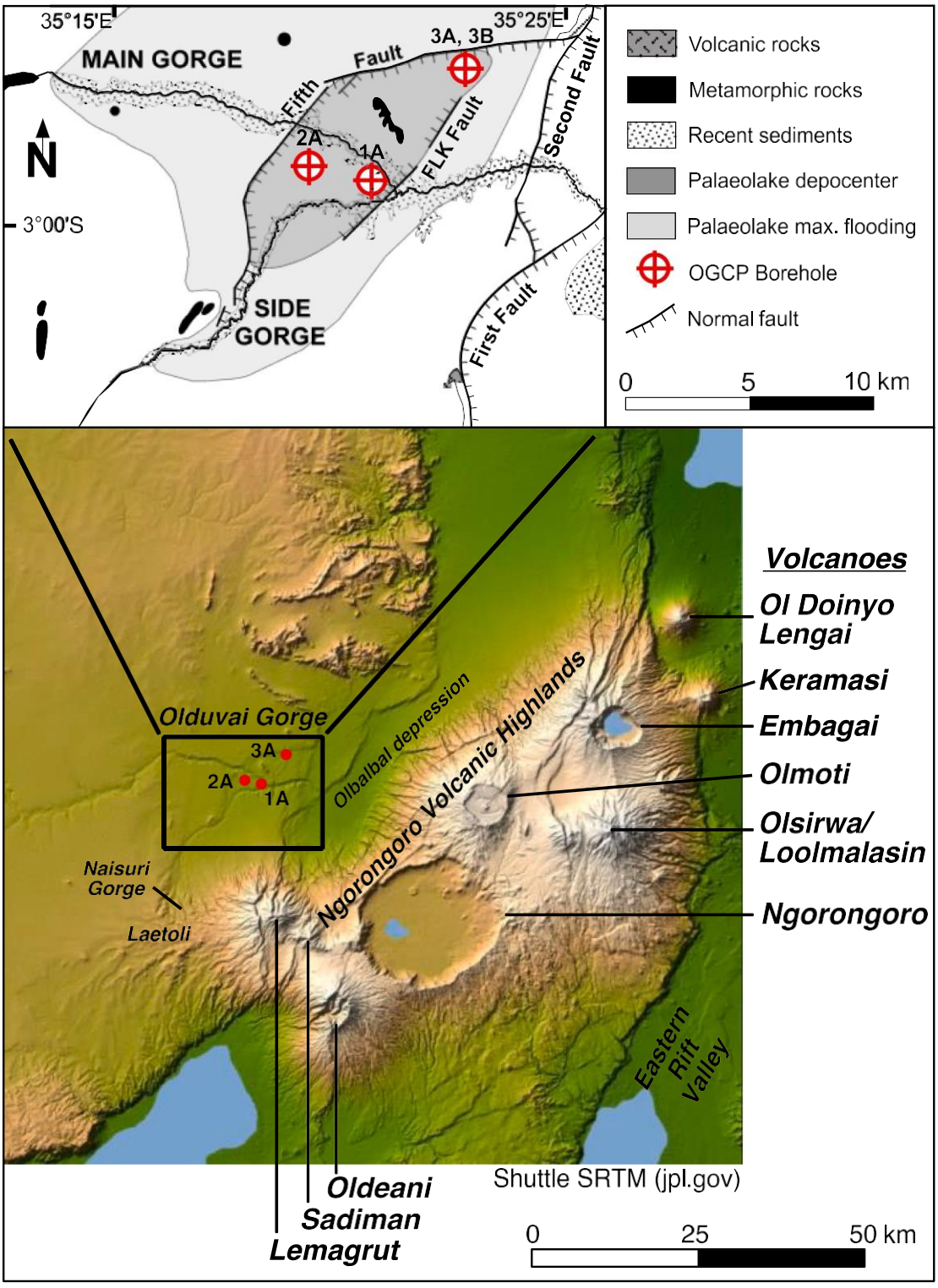

Figure 1-1 Regional map showing major geological and topographic features in the area surrounding Olduvai Gorge, location of three OGCP borehole sites (red circle). A diagrammatic reconstruction of paleolake Olduvai outline during the Early Pleistocene modified from Hay

(1976) illustrating the Main and Side Gorges mentioned in the text. The borehole site shown between Fifth and FLK Faults (faults by hachured lines) based on Deino et al., (2020)

The subdivision into Beds I-IV was adopted by Hay (1976) in subsequent studies. All of the deposits between Naabi Ignimbrite and Bed II were then considered as Bed I, including the Bed I basaltic lavas at the base of the section in the eastern gorge. The Bed II member included the previously described Aeolian Tuff Member. Bed III is mostly claystone and sandstone, which are overlain by Bed IV's claystone and sandstone where the two Beds can be distinguished. The two are not distinguishable to the west, where Bed III loses its characteristic red color. The uppermost part of Bed IV consists mostly of aeolian tuffs and is termed the Norkilili member. The erosion-resistant Norkilili member forms a cliff along the rim to the west side of Gorge. The current study focused on Bed I, which is indicated in Figure 2-1 and Figure 2-2.

1.2 Climatic setting

Large areas of East Africa experience bimodal rains from March to May (the long rains) and October to December (the short rains), owing to the northward and southward migration of the African rain belt (also widely referred to as the ITCZ) (Nicholson, 2000). Note that eastern Africa's long and short rains occur between the northeast and southwest monsoon (e.g., Indian monsoon) domains, and the peak monsoon months (July - September, and December - February) typically correspond to East Africa's two dry seasons. The northeast monsoon, having mostly continental origins, brings relatively dry air passing over Somali, running parallel to the Indian Ocean coast and the Ethiopian highlands (McGregor & Nieuwolt, 1998; Nicholson, 2017). The climatology of East Africa, however, is complex due to large scale atmospheric circulations (e.g., Walker circulation), regional circulations (e.g., Localized convergence, moisture transport), coastal influences (e.g., Frictional uplift), and complex interrelationships between these factors

(Nicholson, 2017; Yang et al., 2015). Interannual rainfall variability in Northern Tanzania is particularly sensitive to sea surface temperature (SST) changes in the tropical oceans (Shemsanga et al., 2010) and the El Niño Southern Oscillation (ENSO) or the Indian Ocean SST dipole (IOD) phenomenon, with the warming of the tropical oceans (e.g., such as during El Niño and positive IOD phases) leading to an increase in rainfall over much of East Africa, including at Olduvai Gorge (Conway et al., 2007). Typically, however, Olduvai Gorge receives a relatively meager total rainfall of about ~60-180 cm per annum (Shemsanga et al., 2010).

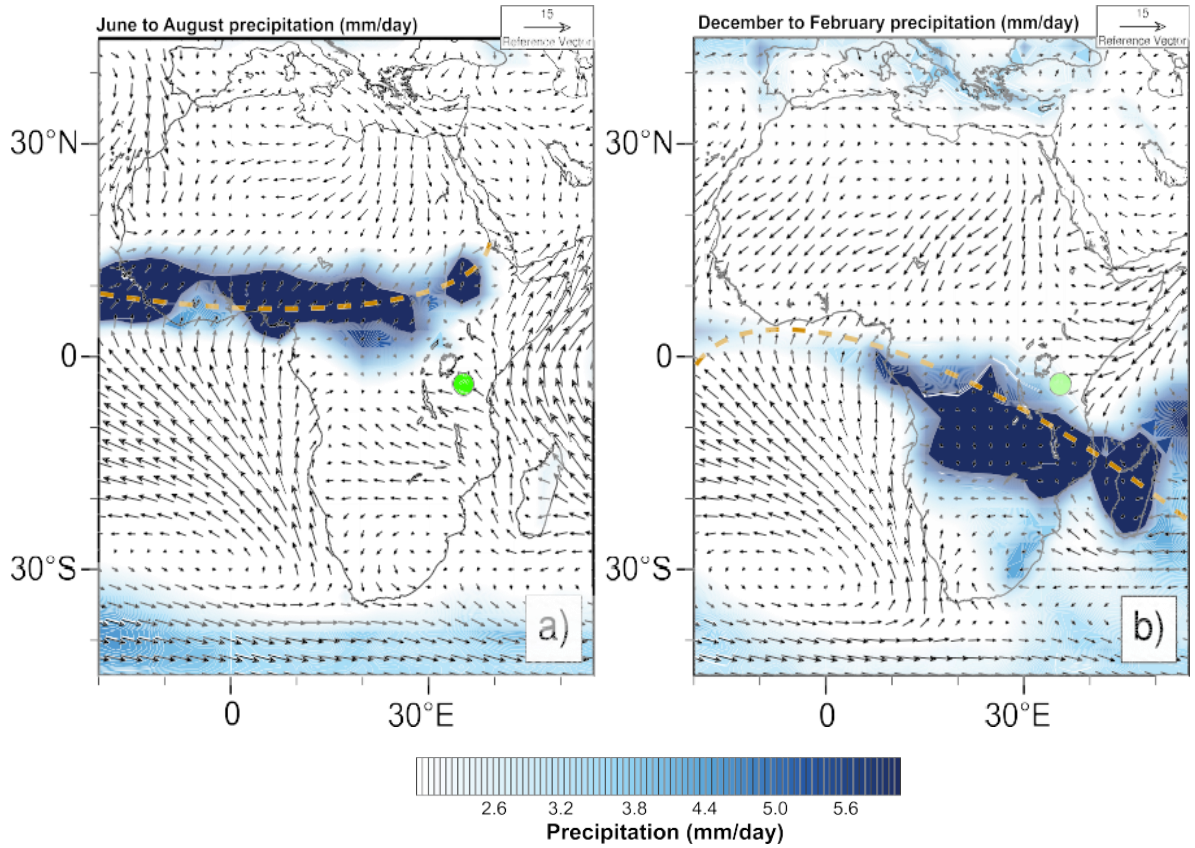

Figure 1-2 East African seasonal mean precipitation (mm/day) for the period of 1975-2015 and surface wind vectors (a) June-August, (b) December-February. Olduvai Gorge shown with a green circle and tropical rain belt shown with broken lines for respective months b based on (Gebregiorgis et al., 2020).

1.3 Clay Minerals in East African Lakes

The deposited clastic sediment material in marine, lacustrine, and fluvial environments can alter because of climate variation, depositional environment, and sedimentary structure. Clay minerals form in part by weathering (meteoric alteration) of rocks and pedogenesis (formation of soils). These processes transform rocks into loose material, including clay minerals. Lacustrine and fluvial *in-situ* water interacts with clay minerals during alteration and form *in-situ* mineral facies. These mineral facies preserve a record of Earth surface processes (e.g., soil formation, sedimentation) and shallow processes in the upper crust (e.g., hydrothermal processes, sedimentary diagenesis) (Meunier, 2005). These clays are essential components for many sediments. Clay minerals mostly preserve near-surface environmental information, albeit some clay minerals form at higher temperatures near igneous minerals after crystallization (Manuella et al., 2012). The alteration of clastic deposit related to burial diagenesis is an essential indicator of depositional processes (Deocampo, 2015).

Clay mineralogy in marine and terrestrial sediments differ from each other in several key aspects. In terrestrial basins, the sediment sources are close, so the basin reflects the mineralogy of proximal sediment sources. In contrast, marine sedimentary pore water is dominated by seawater. The geochemistry of terrestrial and groundwater is more diverse, as is the water chemistry of evaporite systems. Identifying clays, whether detrital or authigenic, within lake sediments can shed light on paleoenvironmental indicators (Jones & Deocampo, 2003).

Aqueous surface water geochemistry depends on the host rock's geology, surrounding climate, and hydrology of surface water. Clays forming *in situ* mineral facies are linked directly with the lake's hydrology, especially for closed lake basins due to the higher ion concentration.

The alteration of minerals is also much more significant in closed basins than in other lacustrine settings.

At Olduvai, sand-sized euhedral calcite crystals were widespread in the saline-alkaline lake deposits of Beds I and Bed II (Hay and Kyser, 2001). Fine-grained dolomite and chert nodules of unusual shapes are indicators for saline, alkaline lake water. Zeolites and potassium feldspar are also found in the Olduvai lake beds, and are also commonly associated with saline, alkaline water. The lake beds are chemically similar to saline lakes of the same origin in an arid and semiarid climate (Hay, 1976).

1.4 Purpose of the Study

This research aims to improve our understanding of the paleoclimatological environmental response to global climate change in Quaternary environments and to help quantify time-series records that address the preservation bias in the fresher-water paleolake records through the analysis of authigenic clay minerals. The study's central aim is to study a Paleolake Olduvai core to help understand the paleoenvironmental and paleoclimatic history of the basin. New geochemical and mineralogical data are presented from a paleolake interval that underlies the previously known Olduvai Beds in the Northern Tanzania, within East African Rift. Primary research questions include:

- Does the aluminum enrichment reflect the freshwater flushing of the watershed or the open lake basin associated with the early state of the lake basin?
- What are the most dominant climatic shifts and how are prevailing paleoclimatic conditions linked to overall trends in hominin evolution?

We hypothesize that:

The mineralogy and geochemistry of the OGDP-OLD14-2A core likely to reflects a hydrologically open lake that was subject to regional desiccation over 2 Ma years ago. The variable whole-rock geochemistry likely reflects the evaporation concentration of long-term aridification in the region. Greater aridity is predicted based on previous studies of outcrops of the younger interval (~1.8 Ma) of Olduvai Gorge. This would be consistent with closed-basin conditions and associated octahedral magnesium enrichment in clays, which would indicate high salinity within hydrologically steady-state conditions (Deocampo & Tactikos, 2010). Whole-rock geochemical results are supposed to show peak magnesium trends.

2 MATERIALS AND METHODS

2.1 2A core (New locality)

The borehole (2A) located at (S 02° 57′ 13.9″ E 035° 15′ 33.2″) was drilled where the Olduvai Basin was expected to be deepest, between the fifth and FLK faults (Figure 1-1). Extracting the core of 245 m doubled the previously known stratigraphy, which was ~100 m of cumulative thickness based on outcrops. The new 245 mbs core (~2.24 Ma) extended the earlier record for ~210 kyr of oldest exposed Olduvai strata, and this can provide multiple age calibration points (Deino et al., 2020). There was a major unconformity between the Bed I basalt and CFCT (Coarse Feldspar Crystal Tuff) contact (Stanistreet et al., 2020b) in Core 2A, resulting in the absence of Lower Bed I sediments in this core (such sediments are preserved in Core 3A).

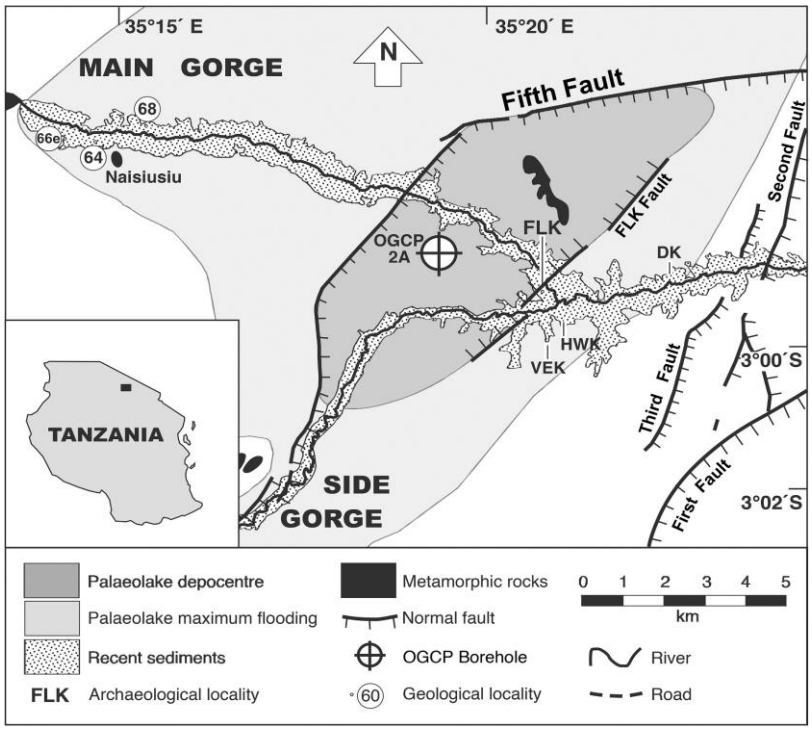

Figure 2-1 Location of OGCP borehole 2A (study location) and important localities mentioned in the description and newly revealed basin depocenter and the deepest area of Paleolake Olduvai per Stanistreet et al. (2020c)

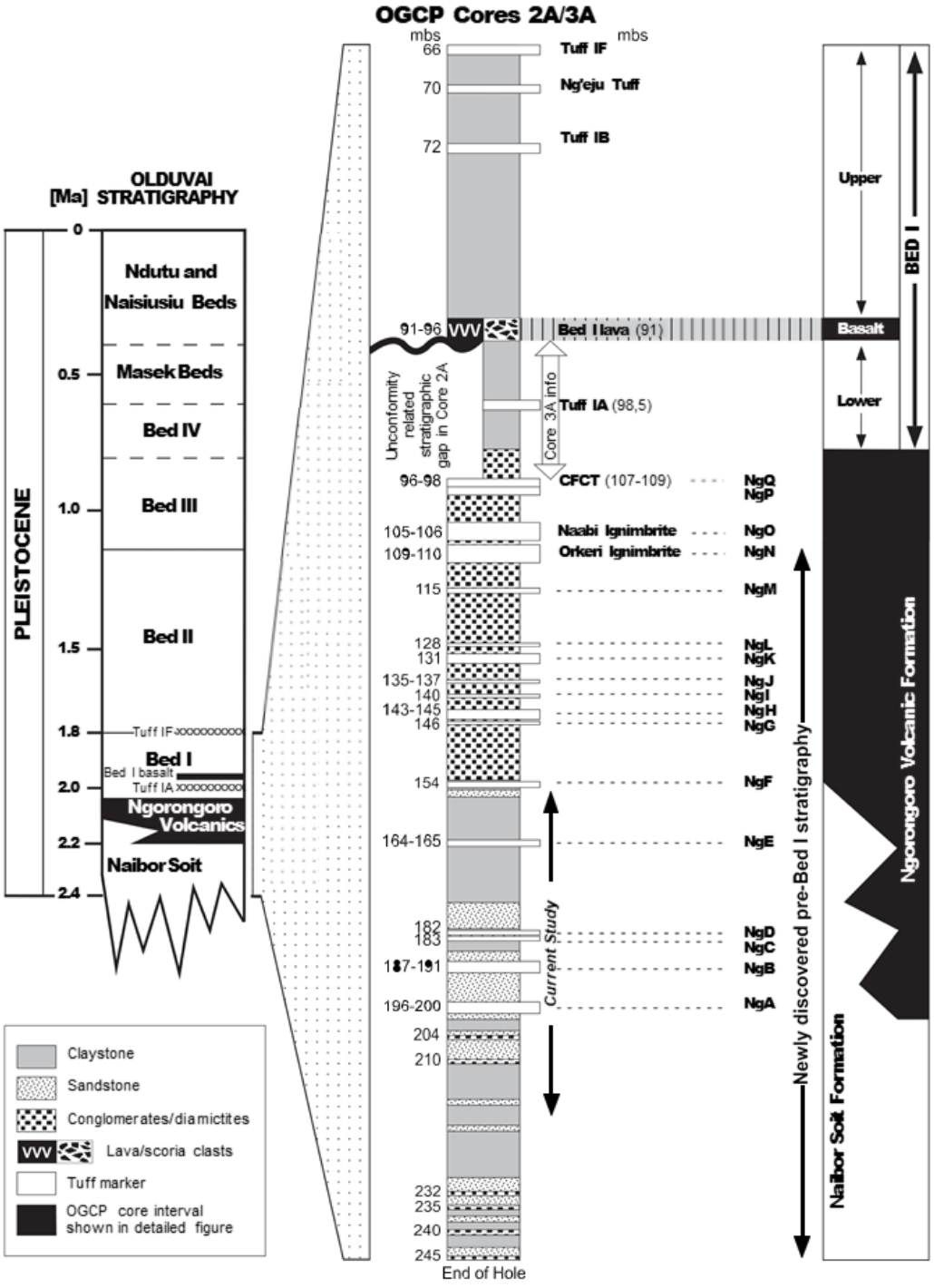

Figure 2-2 Olduvai Stratigraphy (Generalized), left column, based on Hay (1976). Middle stratigraphic column providing Core 2A stratigraphy with a combination of Core 3A per Stanistreet et al., (2020a). Numbers to the left of the stratigraphic column indicating mbs positions of marker beds. CFCT to Bed I lava interval was missing in Core 2A due to an unconformity. Right column indicating sub-Bed I strata (Naibor Soit and Ngorongoro Volcanic formations) (Stanistreet et al., 2020c). Black vertical arrows delineate the newly discovered Bed I stratigraphy and the target interval of the current study.

2.2 Sample collection

Representative samples of sediment were collected from cores drilled at Olduvai Gorge within Arusha Region, Tanzania. The cores were drilled in 2014 as part of the Olduvai Gorge Coring Project (OGCP). Four holes were drilled (1A, 2A, 3A, and 3B) at three different locations. One of the holes, designated as OGDP-OLD-2A, was drilled on 17 August 2014 for 254 meters. The hole's elevation was 1393 m from the surface 0 (m). For this study, the core 2A sample used is from 156.9 meters below the surface (mbs) to 215.3 meters below the surface (mbs). Each core sample was approximately 1.5 cm long, and sample spacing was a few cm. The water depth was 0 (m). Every few cm, samples were collected for detailed clay mineralogical study and geochemical investigation to determine the nature of the deposit.

2.2.1 Core Description

At the center of palaeolake Olduvai Basin, four boreholes 1A, 2A, 3A, and 3B were drilled at three sites by the Olduvai Gorge Coring Project (OGCP). The upper part of the cores (termed as Beds I, II, III, IV) all contained at least some lacustrine facies, and are correlated to outcrop equivalents at Olduvai Gorge (Stanistreet et al., 2020). The lacustrine sediments below the Bed I basalts and above the main Ngorongoro sourced fan body are attributed to Lower Bed I, and were recovered only from Core 3A. Core 2A penetrated beneath the level known from natural outcrops, exposing another 135 m of sediment below. This newly recovered material includes a fan-delta sourced from Ngorongoro Volcano below Olduvai Bed I (termed the Ngorongoro Volcanic Formation: Stanistreet et al., 2020), and includes previously-known marker tuffs CFCT (Coarse Feldspar Crystal Tuff) and the Naabi Ignimbrite near the top. There is an interval of fluvio-lacustrine non-volcaniclastic sediments underlying the fan sequence, referred to as the Naibor Soit Formation, named after the Naibor Soit Inselberg that lies between Cores 2A and 3A. The

Ngorongoro Formation contains primary Tuff Markers NgA to NgQ, volcaniclastic fan-delta deposits that interfinger with and overlie claystones and interbedded sandstones of the fluvio-lacustrine Naibor Soit Formation. An older Ngorongoro-derived fan delta underlies these lactusrine sediments, and below it (approaching the base of the core) lies the deepest fluvio-lacustrine sediments yet recovered (Stanistreet et al., 2020c).

LacCore (National institute Core Facility) described these cores initially including the current study. Per LacCore, most of the core sections were composed of sandy claystone with carbonate nodules with a few limestone nodules. About 175.5 (m) meters below the surface, there was a section of green clay underlying with an unnamed volcanic grayish-green fine-grained formation or pumice section. For this study, the core was sampled from 156.9 meters below the surface (mbs) to 215.3 meters below the surface (mbs). A layer of coarse black claystone and sandy claystone occurred below the volcanic formation.

2.3 Sample preparation for geochemical and mineralogical analysis

Each 2 gram subsample collected from the core was placed in a small beaker containing deionized (DI) water. The soaked bulk samples were crushed gently with a ceramic mortar and pestle by hand. The crushed sample was ultrasound sonicated for 1 minute with Branson Model, 450 Digital sonicator. This agitation reduced some particle sizes. The sonication also dispersed the clay coatings from mineral grains. No dispersing agents were added. The samples were centrifuged for 90 minutes at 18,000 rpm with a Sorvall RC 5B Plus Centrifuge to extract the clay fraction. The clay fraction remained supernatant, while the coarser fraction sunk to the bottom of the centrifuge tube. The clay fraction was scraped off the top of the residue at the bottom of the centrifuge tube, and was used for further mineral and chemical analyses.

2.4 X-ray diffractometry

X-ray diffractometry (XRD) was used to identify the minerals in the clay fractions. A Panalytical X-Pert Pro diffractometer was used in this study. CuKα radiation was generated at 45 kilovolts (kV) and 40 milliamps (mA). The incident Cu X-radiation was filtered using a Ni-filter to remove CuKβ radiation and to generate monochromatic CuKα radiation (λ = 1.5418 Å). The wavelength of this monochromatic X-radiation was used in Bragg's Law to calculate the d-spacing values of each observed diffraction peak. Bragg's Law is summarized below.

$$n\lambda = 2d(\sin\theta) \qquad \textit{Equation 2-1}$$

In equation 2.1, λ= wavelength of Ni-filtered CuKα radiation (Å); d is the d-spacing value between planes of atoms (Å); θ is the angle between the incident beam of monochromatic CuKα X-rays and the surface of the mounting material. The parameter n is the order of diffraction, n = 1 for all the diffraction peaks. The conditions used in the XRD analyses are summarized in Table 2-1. Operationally, the d-spacing values of the observed diffraction peaks were determined using the XRD software within the X'Pert Pro Diffractometer using Bragg's Law. The types of mounts used in this study are described in the following 2.4.1 section.

2.4.1 Sample Preparation for X-Ray Diffractometry

Clay fractions were analyzed as oriented mounts. An oriented mount was produced by dropping of wet clay fraction material that scrapped the supernatant onto a petrographic slide (23 mm by 46 mm) and dried in air. One hundred and twelve oriented samples were prepared in this way for this study. In this oriented mount, the a-b planes of phyllosilicate minerals were mostly parallel to the petrographic slide. Their c-axes were more perpendicular to the slides. Consequently, the planes parallel to the c-axis were preferentially diffracted (00l), greatly

simplifying the identification of phyllosilicate minerals using X-ray diffraction. These mounts were analyzed by X-ray diffractometry after drying first in the air. Oriented mounts were solvated in ethylene glycol at room temperature for 24 hours. An air-dried oriented mount was heated at 550° C for one hour to distinguish the presence of kaolinite or chlorite.

Oriented mounts were solvated in ethylene glycol vapor for 24 hours. After analysis of the glycol-solvated oriented mount, this mount was left to evaporate in air. The material was then scraped off from the slides and mounted onto a zero-background slide for the 060 reflection analysis. This type of mount produced a random orientation of individual grains or clay particles. The 060 scans of these randomly oriented samples allowed for the identification of the presence of trioctahedral or dioctahedral sheets in the phyllosilicate minerals present in clay fractions (Moore & Reynolds, 1997).

Table 2-1 XRD Scan particularization (Instrument in use is PANalytical X'Pert Pro XRD)

		Oriented Scans	060 Scans
Instrument Settings	X-ray tube	Empyrean Cu LFF HR (9430 033 7310x)	
	Voltage	45 kV	45 kV
	Current	40 mA	40 mA
	Scan Time	68 mins	68 mins
	Scan Axis	3.0˚-60.0˚	59.0˚-63.0˚
	Step Size	0.0262˚	0.0131
	Sample Stage	PW3071/xx Bracket	Reflection-Transmission Spinner PW 3064/60
	Sample changer	n/a	Changer PW 3065/12
Incident Beam	Soller Slit	0.04 rad.	0.04 rad.
	Programmable Divergence Slit (PDS)	1/32˚	1/8˚
	Fixed Incident Beam Mask	10 mm	10 mm

	Anti-scatter slit	Fixed 1/16˚	Fixed 1/4˚
	Beam attenuator	None	None
Diffracted Beam Optics	Beta Filter	Ni	Ni
	Programmable Anti-Scatter Slit (PASS)	Fixed 1/32˚	Fixed 1/8
	PIXcel1D detector: Active length (2˚ Theta)	2.009˚	3.347˚
	Number of active channels	153	255
	Soller Slit	0.04 rad.	0.04 rad.

2.4.2 Mineral Identification

The minerals observed in the diffraction scans were identified using diffraction data from Moore and Reynolds (1997). Other texts were consulted as (Brindley & Brown, 1980). The d-spacings used to identify the minerals present in these sub-samples were tallied below (Table 2-2 and Table 2-3).

Table 2-2 Diagnostic diffraction d-spacing values (d_{hkl}) for observed minerals

d (001)	**d (002)**	**d (003)**	**d hkl**	**Minerals**
10.0 9.91 9.81	5.0 4.9	3.33 3.32		Illite
			6.3- 6.6 3.23- 3.26 3.24*	K- feldspar
			6.3- 6.6 3.15- 3.21 3.19	Plagioclase Feldspar
			7.16 4.36 3.59 2.34	Kaolinite
			4.30 – 4.33 4.30 3.40	Quartz

			3.34	
			7.61 4.28 3.07 2.87	Gypsum
			2.89 2.67	Dolomite

* The most intense peaks are underlined

Table 2-3 Diagnostic diffraction d-spacing values (d_{hkl}) for zeolite minerals per mineralogy database and based on (Moore & Reynolds, 1997).

Zeolite	Heulandite		Clinoptilolite	Phillipsite		Analcime	Chabazite
	<u>8.96</u>	3.18	8	8.11	3.27	9.14	9.35
	7.94	3.13	95	7.18	<u>3.21</u>	5.6	5.02
	5.26	3.07	4.65	7.16	3.14	4.85	4.32
	<u>5.1</u>	2.99	3.98	6.42	3.13	<u>3.43</u>	3.87
	4.65	<u>2.97</u>	3.91	5.38	2.93	2.93	3.59
	3.98	2.81	3.17	5.07	2.76	2.69	2.92
	3.9		3.12	4.94		2.51	2.89
	3.84		3	4.13		2.23	
	3.43		2.97	4.12			
	3.41		2.79	4.06			

2.5 X-ray Fluorescence

X-ray fluorescence spectroscopy (XRF) is one of the most intensive and powerful techniques for characterizing the chemical composition of minerals, size fractions, and whole-rock samples. The intensity of fluorescent radiation given by each element was recorded. The weight percentage of major elements were derived from the measured intensities of those elements from each sample against element-specific calibration curves (Boyd & Mertzman, 1987). Loss on

ignition (LOI) along with major element oxides data is shown in Table 3-3. The wt.% of major elements is converted to oxides using the appropriate gravimetric conversions. Fe was reported as wt.% Fe_2O_3. All the XRF analyses were done by Prof. Stanley A. Mertzman Jr. of Franklin & Marshall College.

2.5.1 Sample preparation for XRF

Twenty (20) core samples, whose clay fractions exhibited 060 reflection d-spacing values corresponding to illite per XRD, were crushed by hand with a mortar and pestle with a starting material of 4 grams. 40 ml of DI water was added and agitated using ultrasound sonication for 1 minute. This agitation reduces the presence of clumps of clay coatings. The wet sample was spun at 19,000 rpm for 1.5 hours to recover the clay fraction entirely with Sorvall RC-5B Centrifuge. The top clear natant was discarded. The wet material was dried and crushed again by hand with mortar and pestle. This crushed material was passed through a 400 mesh sieve to produce the < 37 µm size fraction. One gram of these subsamples of the clay fraction were shipped to Franklin & Marshall College for further XRF analysis. LOI was first determined on this material. The remaining material was fused with Lithium Tetraborate in a platinum crucible, heated and quenched major element determination.

3 RESULTS

3.1 Lithological description of the core

The core lithology for this study was described from a depth of 156.0 mbs (meters below the surface) to 215.3 mbs based on drilling logs. Core recovery was incomplete from 156 to 157.8 mbs, where sandy sediments were washed away with logging fluid.

The top layer of the studied interval was a 302.8 cm thick sandy claystone. This sandy claystone was olive-colored sandy (waxy) claystone with carbonate nodules (which were < 3 m diameter). The claystone continues with waxy features and limestone nodules for a thickness of 298.1 cm. Another 284.8 cm thick of similar olive-colored waxy claystone material without limestone nodules were present with linear core collection from 168.0 mbs to 177.0 mbs. The waxy claystone material started to get greenish/ blackish at 174.0 mbs. Dark color clay mixed with volcaniclastic materials (ash, tuff) continued from 180.0 mbs to 182.9 mbs. A fine-grained deposit of grayish-volcanic rocks was sampled for 291.6 cm at a depth of 189.0 mbs. These deposits appeared to be ignimbrite. These deposits were present from 186.0 mbs to 192.0 mbs; the top interval (186.0 mbs to 189.0 mbs) is fine-grained and dark green colored and pumice and feldspar bearing, while the lower interval (189.0 mbs to 192.0 mbs), is coarse-grained.

Feldspar-rich coarse ash was found from 192.0 mbs to 195.0 mbs. From 201.0 mbs to 204.0 mbs, only the top part was black-coarse ash, and the base of the section was brown claystone. From 204.0 mbs to 206.8 mbs, the sediments consist of sand with some gravel. Quartz rich sand was found at from 207.0 mbs to 208.2 mbs. The tube collapsed with little recovery from 210.0 mbs to 211.1 mbs within the formation of quartzite pebble rich siliciclastic sandstone. Sandy claystone was found from 213.0 to 215.3 mbs. At a depth of 201.0 mbs, the recovered core was coarse black

ash and brown claystone. At 210.0 mbs, where the whole core was retrieved, and it contained pebble rich siliciclastic sandstone (McHenry et al., 2020; Stanistreet et al., 2020c).

3.2 Mineralogy

The mineral assemblages were determined from the oriented clay fraction mounts from selected samples from the core. The minerals found in clay fractions included the following phases: illite, feldspar (both plagioclase feldspar and K-feldspar), quartz, kaolinite, and carbonate (dolomite), and various zeolites (Table 3-1). The peaks used to identify each mineral are listed in Table 2-2 and Table 2-3. The X-ray diffraction patterns provided a qualitative estimate based on the intensity of each mineral's characteristic d-spacings (Appendix B). Illite was found in these sediments from 156 mbs to 160.4 mbs, mostly without other minerals except in a few sections (Figure 3-1). In one section, kaolinite, alkali feldspar, and quartz were found with illite. In another section, plagioclase feldspar and dolomite (a carbonate mineral) were found along with illite. Plagioclase feldspar, alkali feldspar, kaolinite, quartz, gypsum, and dolomite were also identified in the XRD patterns of clay fraction (Table 3-1, Figure 3-1, Figure 3-3). Smectite (or and expandable phyllosilicate) was noted at 172.3 mbs (Figure 3-2, Table 3-1).

Kaolinite, K-feldspar, and quartz were found at about 160.4 mbs, in addition to illite. Illite was found as the predominant mineral from 156.0 mbs to 215.3 mbs. Dolomite was observed at around 161.9 mbs along with illite. Gypsum and plagioclase feldspar were found at 162.0 mbs and plagioclase feldspar and quartz were found within 164.9 mbs to 169.0 mbs. Zeolite minerals were found between 183.0 mbs to 189.0 mbs within the volcanoclastic fan (Stanistreet et al., 2020c). All through the section, the zeolite presence was minor, whereas carbonates were more often present. Dolomite is the predominant carbonate mineral (Figure 3-3).

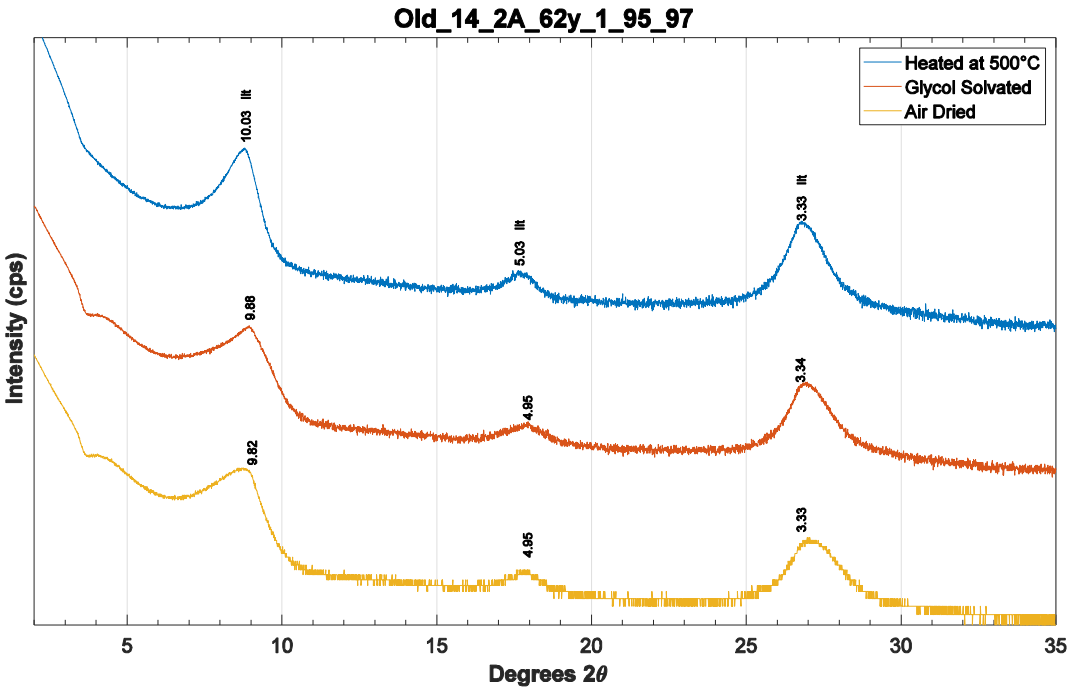

Figure 3-1 X-ray diffraction traces and d-spacings values of the sample's oriented mount located at a depth of 159.0 mbs. Three traces were shown (heated, glycol-solvated, and air-dried). Illite (Ilt) was identified in the sample.

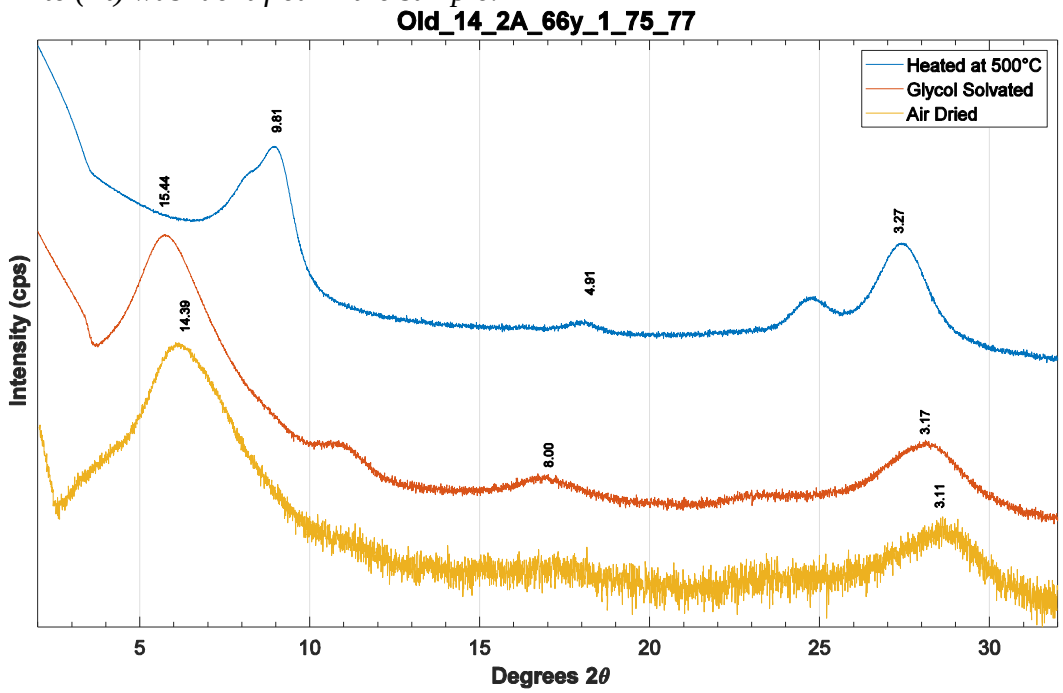

Figure 3-2 X-ray diffraction traces and d-spacings values of the sample's oriented mount located at a depth of 172.3 mbs. Three traces were shown (heated, glycol-solvated, and air-dried). Smectite (Sme) was identified in the sample.

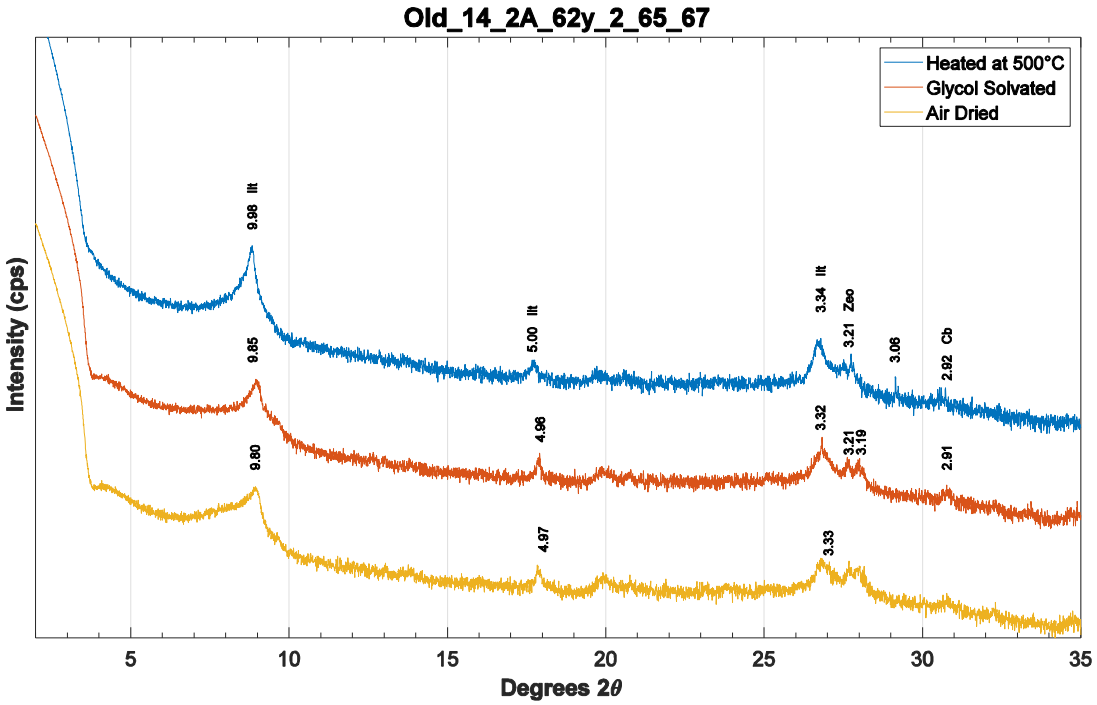

Figure 3-3 X-ray diffraction traces and d-spacings values of the sample's oriented mount located at a depth of 160.4 mbs. Three traces were shown (heated, glycol-solvated, and air-dried). Illite (Ilt), zeolite (Zeo), and carbonate (Cb) were identified in the sample.

We initially identified ankerite (a carbonate mineral) based on its d-spacing of 2.9 (Appendix E.1), but the overall pattern is better explained by chabazite, which has a dominant peak at 2.92 (Table 2-3). (McHenry et al., 2020) identified chabazite in the bulk XRD patterns of many samples from the same core interval (confirmed on multiple peaks in addition to the 2.92 angstrom peak) and did not identify ankerite. In general, XRD mineral identifications on the bulk samples have zeolite n almost every sample, usually chabazite and/or erionite. However, zeolite peaks are infrequently identified in the clay fractions in this study. Except for the presence of illite, there is little overlap in the minerals identified in both studies (McHenry et al., 2020). This could be because the oriented clay mounts are less suitable for identifying hkl phases like zeolites (compared to clay mineral phases), or because minerals other than clays are more abundant in the coarser size fractions and rarer in the clay separates. The results of the current study therefore

reflect the mineralogical composition of the fine size fraction but not the mineral assemblages of the whole rock.

The chronostratigraphic data shown in (Table 3-1) obtained directly from individual core samples using $^{40}Ar/^{39}Ar$ for volcanic units from combined core and outcrop experiments (Deino et al., 2020).

Table 3-1 Identified minerals from clay fraction (Abbreviations are; Afs: alkali feldspar, Cb: carbonate mineral (Ank: Ankerite, Dol: Dolomite, Str: Strontianite), Ilt: illite, Kln: kaolinite, Pl: plagioclase feldspar, Qz: quartz, Sme: smectite, Zeo: zeolite (Anl: Analcime, Cpt: Clinoptilolite, Hul: Heulandite, Php: Phillipsite)) (Whitney & Evans, 2009). Age calculated using the K-feldspar phenocryst materials. MSE: modified standard error (standard error expanded by root MSWE if MSWD >1. Here MSWE: Mean Squared Weighted Deviation).

Depth	Section ID									Age	Error
Top-Bottom mbs	Name	Ilt	Kln	Afs	Pl	Qz	Zeo	Cb		(Ma)	±1s MSE
156.0 - 156.9	61y-1-84-86	1								2.0937	0.0030
156.9 - 157.8	61y-2-10-12	1									
	61y-2-30-32	1									
	61y-2-40-42	1									
	61y-2-50-52	1									
	61y-2-60-62	1			1						
159.0 - 160.4	62y-1-20-22	1									
	62y-1-35-37	1									
	62y-1-50-52	1									
	62y-1-65-67	1									
	62y-1-80-82	1	1	1	1	1		Ank			
	62y-1-95-97	1									
	62y-1-110-112	1									
	62y-1-140-142	1									
160.4 - 161.9	62y-2-5-7	1									
	62y-2-35-37	1									
	62y-2-50-52	1			1						
	62y-2-65-67	1					Php	Ank			
	62y-2-80-82	1			1			Ank			
	62y-2-95-97	1									
	62y-2-125-127	1									
	62y-2-140-142	1					Php	Ank			

161.9 - 162.0	62y-3-7-9	1			1			Dol			
162.0 - 163.5	63y-1-5-7	1									
	63y-1-31-33	1									
	63y-1-80-82	1									
	63y-1-123-125	1									
163.5 - 164.9	63y-2-5-7	1			1					2.1371	0.0016
	63y-2-35-37	1									
	63y-2-121-123	1		1	1		Anl				
165.0 166.4	64y-1-20-22	1									
	64y-1-50-52	1		1			Php				
	64y-1-65-67	1									
	64y-1-83-85	1		1			Php				
	64y-1-112-114	1									
	64y-1-128-130	1						Ank			
166.4 - 167.8	64y-2-18-20	1		1			Php			2.1227	0.0044
	64y-2-75-77	1		1			Php				
	64y-2-88-90	1			1			Ank			
	64y-2-105-107	1			1			Ank			
	64y-2-119-121	1			1	1		Ank			
167.8 - 168.0	64y-3-15-17	1									
168.0 - 169.4	65y-1-20-22	1									
	65y-1-50-52	1									
	65y-1-65-67	1									
	65y-1-80-82	1									
	65y-1-110-112	1									
	65y-1-125-127	1									
	65y-1-138-140	0									
169.4 - 170.9	65y-2-5-7	0									
	65y-2-33-35	1		1			Php				
	65y-2-52-54	0									
	65y-2-80-82	1									
	65y-2-110-112	1									
	65y-2-122-124	0									
	65y-2-148-150	1									
171.0 - 172.3	66y-1-15-17	1									
	66y-1-31-33	1		1							
	66y-1-45-47			1	1				Sme		
	66y-1-60-62								Sme		

	66y-1-75-77								Sme		
	66y-1-90-92	1									
	66y-1-105-107	0									
	66y-1-120-122	1			1						
172.3 - 173.6	66y-2-5-7	1		1			Php				
	66y-2-20-22	1									
	66y-2-35-37	0									
	66y-2-50-52	1									
	66y-2-66-68	1			1						
	66y-2-91-93	0			1						
	66y-2-102-104	1									
	66y-2-125-127	1			1						
174.0 - 175.5	67y-1-5-7	1	1	1			1				
	67y-1-50-52	0									
	67y-1-95-97	0									
	67y-1-110-112	0									
	67y-1-125-127	1		1							
	67y-1-140-142	0			1						
175.5 - 176.9	67y-2-10-12	1									
	67y-2-40-42	0									
	67y-2-70-72	0									
	67y-2-98-100	1									
	67y-2-142-144	1									
177.0 - 178.5	68y-1-12-14	1		1				1	Gp	2.1632	0.0022
181.5 - 182.9	69y-2-142-143				1						
183.0 - 184.4	70y-1-15-17	1		1		1	1	Ank			
	70y-1-25-27			1		1		Ank			
	70y-1-40-42				1	1					
	70y-1-70-72					1	1				
	70y-1-85-87			1	1	1					
	70y-1-115-117	1			1	1					
	70y-1-130-132	1		1		1	Php Hul				
184.4 - 185.8	70y-2-5-7	1									
	70y-2-20-22	1									
	70y-2-35-37	1			1			Ank Str			
	70y-2-50-52	1									

	70y-2-65-67	1	1	1			Php Hul				
	70y-2-80-82	1			1			Str			
	70y-2-10-12	1	1		1						
	70y-2-125-127	1			1	1		Str Ank			
	70y-2-135-137	1		1		1		Ank	Gp		
201.0 - 202.5	76y-1-67-69	1									
202.5 - 203.9	76y-2-6-9	1		1		1				2.1671	0.0019
213.0 - 214.2	80y-1-5-7	1									
	80y-1-71-73	1									
	80y-1-113-115	1									
214.2 - 215.3	80y-2-11-13	1		1	1	1	Php Anl	Ank			
	80y-2-26-28	1			1	1		Ank			
	80y-2-42-44	1									
	80y-2-90-92	1		1	1						
	80y-2-103-105	1					Anl				
	80y-2-113-115	1			1	1		Ank Dol			

3.2.1 060 Peaks

The d-spacing values of the (060) reflection permitted the identification of the octahedral charge. Measurement was done using randomly oriented mounts. For 060 reflection scans, 20 samples were analyzed to represent the complete interval of the study.

Table 3-2 Values of d (060) for the samples

Sample ID*	d (060)	Sample ID*	d (060)
61y-1-84-86	1.512	65y-2-52-54	1.512
61y-2-40-42	1.509	66y-1-75-77	1.514
62y-1-140-142	1.512	66y-1-90-92	1.512
62y-2-65-67	1.509	66y-2-50-52	1.511
63y-1-5-7	1.511	66y-2-102-104	1.511
63y-1-123-125	1.518	67y-2-10-12	1.509
64y-1-20-22	1.512	67y-2-142-144	1.510
64y-1-65-67	1.511	70y-2-20-22	1.513

64y-3-15-17	1.512	76y-1-67-69	1.513
65y-1-50-52	1.513	80y-1-71-73	1.510

The maximum value for 060 is 1.518 Å, and the minimum value is 1.509 Å, whereas the average is 1.5117 Å at61.21º2θ (Table 3-2, Figure 3-4). The 060 peak position indicates that the clay is dioctahedral. The 060 values are dominated by 1.511Å, the coefficient of variation is low, and the standard deviation is very low (0.002), which strengthens the interpretation that the samples were dioctahedral. The peak is near 1.511Å, which corresponds to glauconite clays. The peak around 10.0 Å indicated a mica group mineral or illite (Figure 3-1). The positions of the peaks were unaffected by ethylene glycol saturation treatment or even heating at 550°C or higher (Figure 3-1). With the increase of temperature, the peaks were observed to be sharper (less wide). The intense 001 peak was asymmetrical at low angles, indicating that some degree of interstratification is present for a few samples. Chlorite-smectite identified was very rare (Figure 3-2). The 001 illite d-spacing (10 Å) followed by (4.9 Å) was indicative of illite for most samples and inconsistent with glauconite, which would not have the (4.9 Å) peak. The 001 peaks in most of the samples indicated low-charge illite, and since the peaks were (10 Å), these minerals were identified as illite. Glycol solvation and heat treatment seemed to have no change in the d-spacings for most of the patterns.

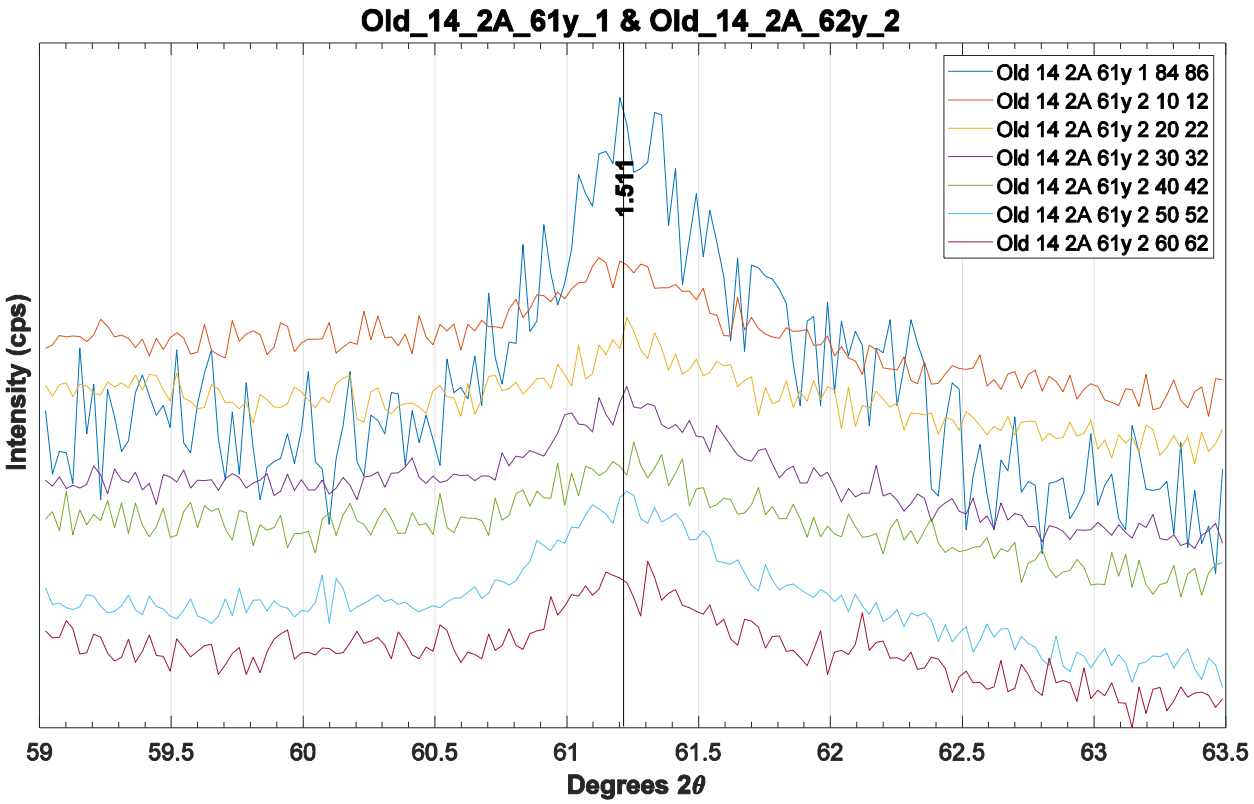

Figure 3-4 X-ray diffraction traces for 060 reflections for randomly oriented powders. The 060 reflections were identified as dioctahedral occupancy in the octahedral sheet.

3.3 Geochemistry

The major element compositions of the clay fraction showed high concentrations of SiO_2, TiO_2, Al_2O_3, and Fe_2O_3 (Table 3-3). Where one mineral was predominant, namely illite, the formulae for the minerals were calculated from the major elements. The chemical composition of the clay fraction is shown (Table 3-4) with corresponding chemical formulas shown (Table 3-5). Moreover, these formula calculations were presented in Appendix D.

The clay fractions contained silicon (57.26- 65.20 wt.% SiO_2), aluminum (13.27- 16.23 wt.% Al_2O_3), magnesium (1.3- 4.3 wt.% MgO), iron (5.19- 14.66 wt.% Fe_2O_3), and titanium (0.81- 2.21 wt.% TiO_2). Silicon was most likely housed in the tetrahedral sheets of the illite clays (Table 3-4). The clay fractions also contained calcium (0.25- 6.27 wt.% CaO), sodium (1.89- 5.01 wt.%Na_2O),

and potassium (3.16- 5.96 wt.%K_2O). The highest absolute variability was seen in Fe_2O_3, SiO_2, and CaO.

The total presence of chlorine, phosphorus, and manganese was less than five weight percentage. The maximum weight % of chlorine in any one sample was 0.24 wt.%. The maximum wt. % of phosphorus was 0.75 wt.%. The highest abundance of manganese was 0.23 wt.%. Loss on ignition (LOI) was high (6.9 wt. % to 20.8 wt. %). The high LOI signified both the hydrous nature of the phyllosilicates and the presence of carbonate cement.

Table 3-3 Geochemical composition of clay fraction of Olduvai Gorge. All individual analysis was shown here.

Section ID*	SiO_2	TiO_2	Al_2O_3	Fe_2O_3	MgO	CaO	Na_2O	K_2O	LOI	Total
61y-1-84-86*	64.80	0.88	14.22	7.29	1.97	1.37	3.82	4.84	6.91	99.46
61y-2-40-42	61.62	1.34	15.03	8.00	2.38	1.87	3.78	4.84	8.47	99.39
62y-1-140-142	61.88	1.39	15.40	7.78	2.25	1.67	4.01	4.57	9.71	99.53
62y-2-65-67	59.68	1.52	15.71	8.80	2.31	2.18	4.07	4.58	9.98	99.68
63y-1-5-7	57.77	1.80	15.16	11.97	2.99	0.81	3.17	5.23	11.30	99.58
63y-1-123-125	59.57	1.70	15.69	10.52	2.64	0.60	3.69	4.91	10.61	99.73
64y-1-20-22	58.49	2.21	13.27	14.66	2.79	0.35	1.89	5.56	11.54	99.55
64y-1-65-67	59.86	1.48	15.50	10.92	2.89	1.48	2.24	4.92	11.91	99.62
64y-2-18-20	59.72	1.46	15.57	10.96	2.56	0.71	3.10	4.93	20.77	99.55
64y-3-15-17	60.10	1.46	15.85	9.67	2.53	1.78	3.45	4.65	12.61	99.95
65y-1-50-52	61.08	1.18	14.77	7.27	1.95	4.81	3.78	4.27	11.62	99.44
65y-2-52-54	58.24	1.43	14.22	10.41	3.16	4.05	2.90	4.68	18.59	99.54
66y-1-75-77	60.89	1.35	13.54	7.90	1.74	6.27	4.29	3.16	12.52	99.51
66y-2-50-52	65.20	0.94	15.05	6.51	1.58	1.54	4.55	4.00	8.08	99.61
66y-2-102-104	64.13	1.06	15.60	6.75	1.74	1.22	4.69	4.23	10.25	99.67
67y-1-140-142	63.79	0.81	15.70	5.19	1.31	3.17	4.90	4.38	13.77	99.55
67y-2-10-12	62.01	1.20	15.05	9.00	2.17	1.52	3.86	4.59	12.13	99.77
67y-2-142-144	62.88	1.30	14.86	9.24	2.24	0.25	3.64	5.07	16.53	99.76

76y-1-67-69	61.98	0.99	16.23	6.30	2.12	1.86	5.01	4.94	8.07	99.78
80y-1-71-73	57.26	1.45	15.04	12.52	4.32	0.70	1.99	5.96	12.34	99.71

* Complete section ID designated as OGDP-OLD14-2A-61Y-1-84-86, but for brevity, sample numbers referred to in this thesis will be recorded by the shortened form.

The highest coefficient of variability (standard deviation divided by the mean), are found in CaO (0.814) and P_2O_5 (0.683). The coefficient of variability of other analysis were consecutively Cl (0.552), MnO (0.410), MgO (0.279), Fe_2O_3 (0.263), TiO_2 (0.247), Na_2O (0.245), K_2O (0.123), Al_2O_3 (0.051), and SiO_2 (0.038). The correlation between K_2O and MgO, and Fe_2O_3 and TiO_2 are presented in Figure 3-5.

A

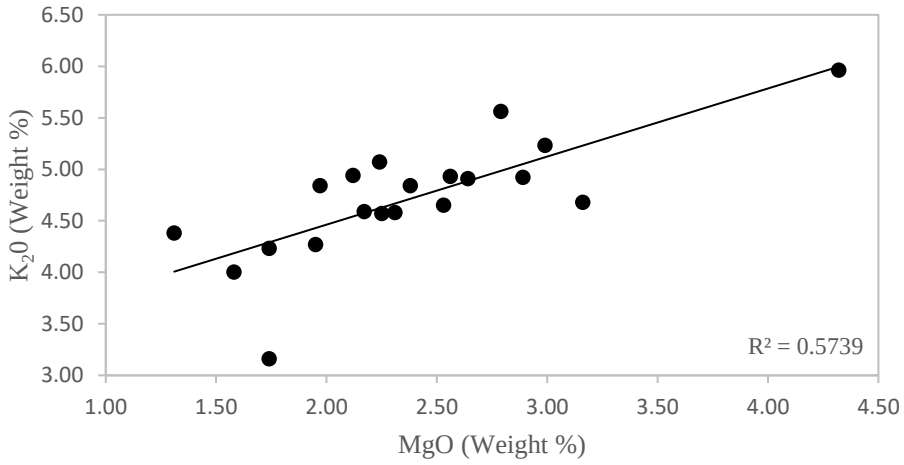

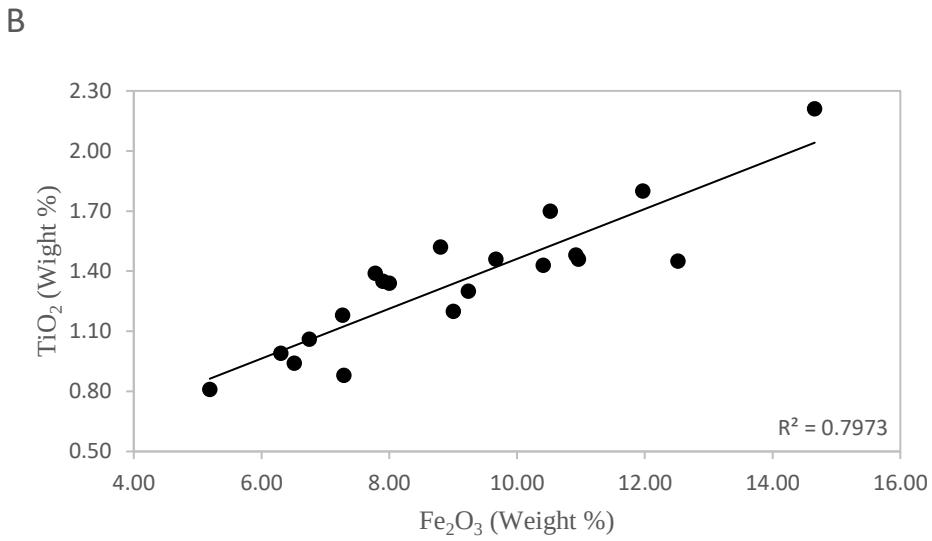

Figure 3-5 Correlations of major element data. Reported p-values are one-tailed

3.4 Structural Formula calculation

The formulae derived from the major element analyses for illite showed a high octahedral charge (Table 3-5, Appendix D). The formula was deficient in some tetrahedral charges (i.e., not equal to four atoms). There was also a deficiency in octahedral charge (i.e., not equal to a sum of two octahedral atoms, Table 3-4). Nonetheless, the octahedral charge's amount permitted the identification of the 2:1 clay as illite. The alkali metals showed high amounts of K and Na. Chemical variation mostly falls among Al, Fe, and Mg. Ti is in the octahedral layer, whereas Si is in the tetrahedral layer. The octahedral charge was calculated based on 2:1 clay, which was dioctahedral. Furthermore, the interlayer charge is fulfilled with the Ca, Na, and K distributed between the dioctahedral sheets.

The formula would determine the total number of octahedral cations and assign layer charge to tetrahedral or octahedral sheets. The formula 2:1-layer silicate structure was calculated with 22 negative charged cations to formulate the octahedral cation composition. Charges for the

tetrahedral sheet were done first, then to the octahedral sheet, followed by the interlayer cation position.

Table 3-4 Formulas for the clay minerals calculated from the volcanic basement of Olduvai George. Calculation of structural formulas of layer silicates based on a formula unit of 11 oxygen (H2O not considered).

Name	Depth Top(mbs)	Mineral Formula (2:1 Clays)
61y-1-84-86	156.0	$(Ca_{0.09}Na_{0.46}K_{0.39})\ (Ti_{0.04}Al_{1.05}Fe^{3+}_{0.34}Mg_{0.18})\ (Si_{4.06}O_{10})\ (OH)_2$
61y-2-40-42	156.9	$(Ca_{0.12}Na_{0.46}K_{0.39})\ (Ti_{0.06}Al_{1.12}Fe^{3+}_{0.38}Mg_{0.22})\ (Si_{3.91}O_{10})\ (OH)_2$
62y-1-140-142	159.0	$(Ca_{0.11}Na_{0.49}K_{0.36})\ (Ti_{0.06}Al_{1.14}Fe^{3+}_{0.37}Mg_{0.21})\ (Si_{3.91}O_{10})\ (OH)_2$
62y-2-65-67	160.4	$(Ca_{0.14}Na_{0.50}K_{0.37})\ (Ti_{0.07}Al_{1.18}Fe^{3+}_{0.42}Mg_{0.22})\ (Si_{3.81}O_{10})\ (OH)_2$
63y-1-5-7	162.0	$(Ca_{0.05}Na_{0.39}K_{0.43})\ (Ti_{0.08}Al_{1.15}Fe^{3+}_{0.58}Mg_{0.28})\ (Si_{3.73}O_{10})\ (OH)_2$
63y-1-123-125	163.5	$(Ca_{0.04}Na_{0.45}K_{0.39})\ (Ti_{0.08}Al_{1.17}Fe^{3+}_{0.50}Mg_{0.25})\ (Si_{3.79}O_{10})\ (OH)_2$
64y-1-20-22	165.0	$(Ca_{0.02}Na_{0.23}K_{0.45})\ (Ti_{0.10}Al_{1.01}Fe^{3+}_{0.71}Mg_{0.26})\ (Si_{3.78}O_{10})\ (OH)_2$
64y-1-65-67	166.1	$(Ca_{0.10}Na_{0.27}K_{0.39})\ (Ti_{0.07}Al_{1.16}Fe^{3+}_{0.52}Mg_{0.27})\ (Si_{3.80}O_{10})\ (OH)_2$
64y-2-18-20	166.4	$(Ca_{0.04}Na_{0.38}K_{0.40})\ (Ti_{0.07}Al_{1.17}Fe^{3+}_{0.52}Mg_{0.24})\ (Si_{3.81}O_{10})\ (OH)_2$
64y-3-15-17	167.8	$(Ca_{0.12}Na_{0.42}K_{0.37})\ (Ti_{0.07}Al_{1.18}Fe^{3+}_{0.46}Mg_{0.23})\ (Si_{3.81}O_{10})\ (OH)_2$
65y-1-50-52	168.0	$(Ca_{0.32}Na_{0.46}K_{0.34})\ (Ti_{0.05}Al_{1.10}Fe^{3+}_{0.34}Mg_{0.18})\ (Si_{3.89}O_{10})\ (OH)_2$
65y-2-52-54	169.4	$(Ca_{0.28}Na_{0.36}K_{0.38})\ (Ti_{0.06}Al_{1.08}Fe^{3+}_{0.50}Mg_{0.30})\ (Si_{3.76}O_{10})\ (OH)_2$
66y-1-75-77	171.0	$(Ca_{0.42}Na_{0.53}K_{0.25})\ (Ti_{0.06}Al_{1.02}Fe^{3+}_{0.38}Mg_{0.16})\ (Si_{3.89}O_{10})\ (OH)_2$
66y-2-50-52	172.3	$(Ca_{0.10}Na_{0.54}K_{0.31})\ (Ti_{0.04}Al_{1.10}Fe^{3+}_{0.30}Mg_{0.14})\ (Si_{4.05}O_{10})\ (OH)_2$
66y-2-102-104	173.0	$(Ca_{0.08}Na_{0.56}K_{0.33})\ (Ti_{0.05}Al_{1.14}Fe^{3+}_{0.31}Mg_{0.16})\ (Si_{4.00}O_{10})\ (OH)_2$
67y-1-140-142	174.0	$(Ca_{0.21}Na_{0.59}K_{0.35})\ (Ti_{0.03}Al_{1.16}Fe^{3+}_{0.24}Mg_{0.12})\ (Si_{4.00}O_{10})\ (OH)_2$
67y-2-10-12	175.5	$(Ca_{0.10}Na_{0.47}K_{0.37})\ (Ti_{0.05}Al_{1.12}Fe^{3+}_{0.42}Mg_{0.20})\ (Si_{3.91}O_{10})\ (OH)_2$
67y-2-142-144	176.9	$(Ca_{0.01}Na_{0.44}K_{0.40})\ (Ti_{0.06}Al_{1.10}Fe^{3+}_{0.43}Mg_{0.21})\ (Si_{3.95}O_{10})\ (OH)_2$
76y-1-67-69	201.0	$(Ca_{0.12}Na_{0.61}K_{0.39})\ (Ti_{0.04}Al_{1.20}Fe^{3+}_{0.29}Mg_{0.19})\ (Si_{3.90}O_{10})\ (OH)_2$
80y-1-71-73	213.0	$(Ca_{0.04}Na_{0.24}K_{0.49})\ (Ti_{0.07}Al_{1.14}Fe^{3+}_{0.60}Mg_{0.41})\ (Si_{3.69}O_{10})\ (OH)_2$

Table 3-5 Results of the chemical analysis and average structural formulae for each of 20 samples.

Name	Si	Al	Fe^{3+}	Mg	Ti	Σoct	Na	K	Ca
61y-1-84-86	4.06	1.05	0.34	0.18	0.04	1.61	0.46	0.39	0.09
61y-2-40-42	3.91	1.12	0.38	0.22	0.06	1.78	0.46	0.39	0.12
62y-1-140-142	3.91	1.14	0.37	0.21	0.06	1.78	0.49	0.36	0.11
62y-2-65-67	3.81	1.18	0.42	0.22	0.07	1.89	0.50	0.37	0.14
63y-1-5-7	3.73	1.15	0.58	0.28	0.08	2.09	0.39	0.43	0.05
63y-1-123-125	3.79	1.17	0.50	0.25	0.08	2.00	0.45	0.39	0.04
64y-1-20-22	3.78	1.01	0.71	0.26	0.10	2.08	0.23	0.45	0.02
64y-1-65-67	3.80	1.16	0.52	0.27	0.07	2.02	0.27	0.39	0.10
64y-2-18-20	3.81	1.17	0.52	0.24	0.07	2.00	0.38	0.40	0.04
64y-3-15-17	3.81	1.18	0.46	0.23	0.07	1.94	0.42	0.37	0.12
65y-1-50-52	3.89	1.10	0.34	0.18	0.05	1.67	0.46	0.34	0.32
65y-2-52-54	3.76	1.08	0.50	0.30	0.06	1.94	0.36	0.38	0.28
66y-1-75-77	3.89	1.02	0.38	0.16	0.06	1.62	0.53	0.25	0.42
66y-2-50-52	4.05	1.10	0.30	0.14	0.04	1.58	0.54	0.31	0.10
66y-2-102-104	4.00	1.14	0.31	0.16	0.05	1.66	0.56	0.33	0.08
67y-1-140-142	4.00	1.16	0.24	0.12	0.03	1.55	0.59	0.35	0.21
67y-2-10-12	3.91	1.12	0.42	0.20	0.05	1.79	0.47	0.37	0.10
67y-2-142-144	3.95	1.10	0.43	0.21	0.06	1.80	0.44	0.40	0.01
76y-1-67-69	3.90	1.20	0.29	0.19	0.04	1.72	0.61	0.39	0.12
80y-1-71-73	3.69	1.14	0.60	0.41	0.07	2.22	0.24	0.49	0.04

4 DISCUSSION

4.1 Down core variations of whole-rock and clay geochemistry

The chemical composition of lower Bed II and upper Bed I were reported and described in (Deocampo et al., 2009; Deocampo & Tactikos, 2010). The current study is on the Naibor Soit Formation, which underlies a thick section of Ngorongoro-derived volcaniclastic material beneath the Naabi Ignimbrite much older than Bed I (Stanistreet et al., 2020c). The claystone composition of the volcanoclastic sediments was generally siliceous. A few vital observations are the major element analysis showed that Al_2O_3 (13.27 - 16.23 wt. %) was much more abundant than MgO (1.3 - 4.3 wt.%). These results suggested the samples in the current study were freshwater lake sediments, as the higher amount (wt. %) magnesium tends to occur with greater aridity. The samples from the interval under study are consistent with formation in a less arid environment and tropical climate.

The alkaline lake basin of Olduvai Beds I and II contained Mg-rich clays, wherein the Mg substituted for Al in octahedral sheet. Clay geochemistry varied across the field area, showing a wide range of paleosalinity from a freshwater to the highly saline water environment (Deocampo, 2005). Saline and alkaline lakes have higher Mg enrichment Mg/(Al+Fe) ranging from 0.7 to 2.3 (Deocampo, 2005; Deocampo & Tactikos, 2010).

The clays in the current study show less Mg enrichment, indicated by Mg and (Al + Fe) ratio. This ratio had a maximum of 0.24 and a minimum of 0.09, with an average of 0.14 (Figure 4-1). The Mg, Al, and Fe atom ratio was conducted based on (Table 3-5) assuming charge balance with 11 oxygen atoms.

The current clay chemistry findings were inconsistent with clays forming in a saline, alkaline paleolake Olduvai, like that previously described for Beds I and II. The lower Mg/ (Al+Fe)

of illite clays are interpreted as being detrital in origin. Saline, alkaline environment was previously interpreted as the secondary diagenetic reaction where Mg leached in a freshwater paleoenvironment for Beds I and II. So in this instance, the diagenetic process did not occur, or the deposition site was influenced by the influx of non-saline waters.

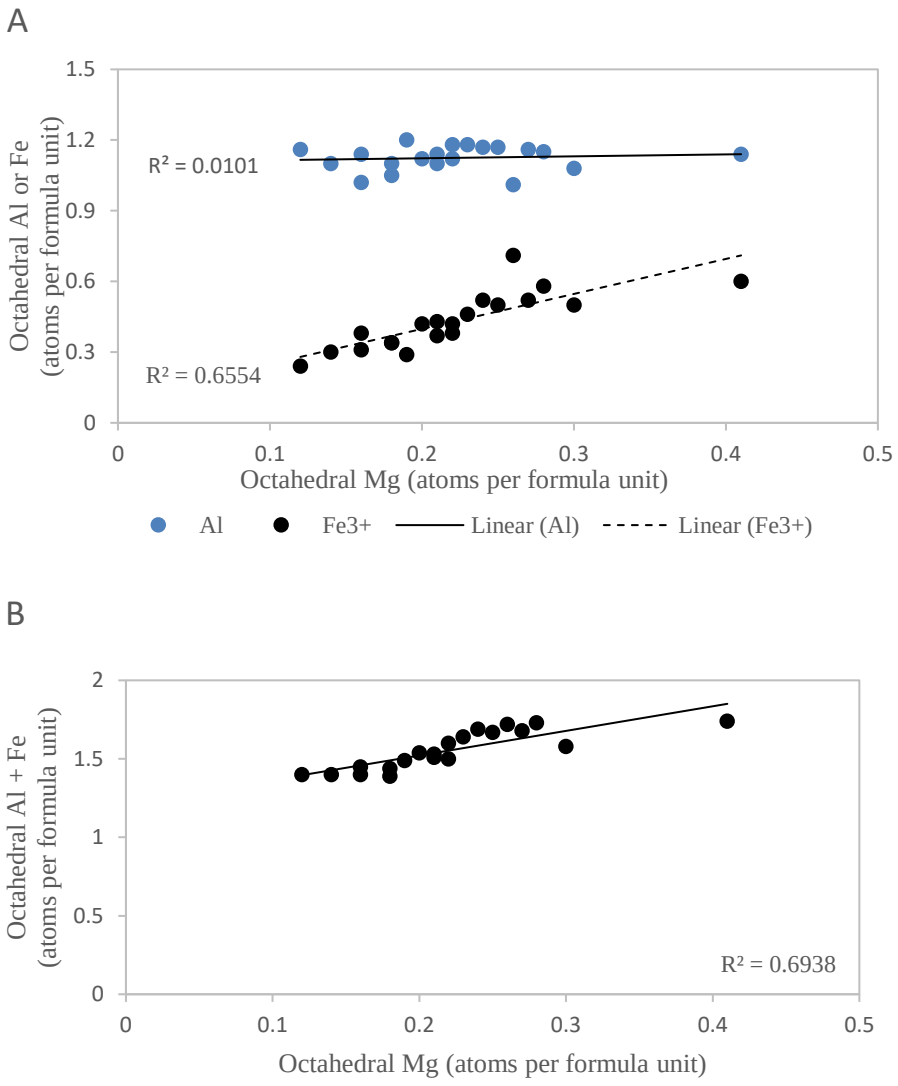

Figure 4-1 Octahedral occupancies of ultrafine clay minerals for core 2A are reported as the number of atoms per formula unit.

The ternary plot (Figure 4-2) of the octahedral composition indicated that clays from the 2A core have more aluminum than magnesium. Compared to lake-margin clays, the illite clays

have similar or more aluminum and less magnesium with the previous findings (Deocampo & Tactikos, 2010; Hover & Ashley, 2003). The higher aluminum is consistent with a terrestrial origin for this illite.

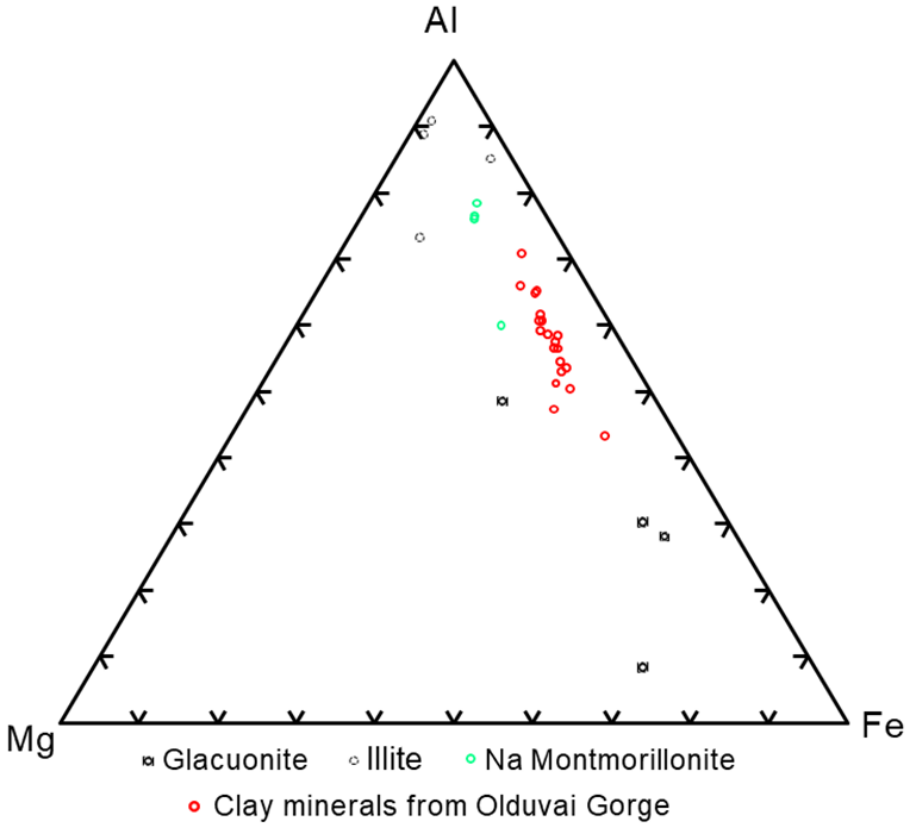

Figure 4-2 Reported compositions for glauconite, illite, and Na montmorillonite samples collected from (Newman, 1987). Red circles are clay minerals analysis for the core samples (2A).

Higher concentrations of magnesium was found in the younger Olduvai Bed I and II lacustrine sediments (Deocampo et al., 2017). These units were deposited in waters with elevated salinity in the lake basin (Table 3-3, Figure 4-1). The increased salinity likely resulted from hydrologic closure and higher evaporation. Higher magnesium content has been associated with more saline basins, such as Olduvai (Hay & Kyser, 2001; Jones & Deocampo, 2003). The higher

aluminum in the samples from the current study contrast with the higher magnesium observed in the younger Olduvai Bed I and II paleolake sediments, and suggests a less saline environment. The 2:1-layer silicate structure formula was calculated to show the octahedral, tetrahedral, and layer charge within the octahedral sheet (Appendix D). Fourteen of the 20 samples analyzed have less than two dioctahedral atoms in this formula (Table 3-4). The lower octahedral atoms in this formula (give amounts) suggested the clay fraction might have contained a mixture of minerals with small amounts of quartz and feldspar. These calculated formulae did not provide definitive results as to the provenance of the illite clays.

Deocampo (2004) analyzed (by electron microprobe) and calculated structural formulas for ultrafine clays (< 0.1μm) from East African basins with a wide chemical variability. The structural formula for < 0.1μm clays for the Olduvai paleo-alluvial fan from detrital sources is $(Ca_{0.01}Na_{0.3}K_{0.4})$ $(Ti_{0.05}Al_{0.3}Fe^{3+}_{1.3}Mg_{0.4})$ $(Si_{3.5}Al_{0.5}O_{10})$ $(OH)_2$, the structural formula for < 0.1μm clay for Olduvai paleo-wetlands from intermediate clays is $(Ca_{0.05}Na_{0.2}K_{0.3})$ $(Ti_{0.04}Al_{0.9}Fe^{3+}_{0.5}Mg_{0.9})$ $(Si_{3.9}Al_{0.1}O_{10})$ $(OH)_2$ (Deocampo, 2004), and the structural formula of < 0.1μm clay from lowermost Bed II in the eastern lake margin of Olduvai Gorge is $(Ca_{0.16}Na_{0.99}K_{0.22})$ $(Al_{0.43}Fe^{3+}_{0.49}Mg_{0.84})$ $(Si_{3.83}Al_{0.17}O_{10})$ $(OH)_2$ (Deocampo & Tactikos, 2010). The average structural formula of ultrafine clays (< 0.1μm) from the southern Kenya rift (Olorgesailie formation) is $(Ca_{0.01}Na_{0.32}K_{0.26})$ $(Ti_{0.04}Al_{0.86}Fe^{3+}_{0.68}Mg_{0.42})$ $(Si_{3.76}Al_{0.24}O_{10})$ $(OH)_2$ (Deocampo et al., 2010). For the current study, the average calculated structural formula for the Al-rich clay fraction is $(Ca_{0.09}Na_{0.46}K_{0.39})$ $(Ti_{0.04}Al_{1.05}Fe^{3+}_{0.34}Mg_{0.18})$ $(Si_{4.06}O_{10})$ $(OH)_2$ for core 2A, though it should be noted that the size fraction analyzed was much coarser than in previous studies. The source of Ca can be the plagioclase feldspars, traced back to weathered volcanic rock. The source of Ca can be the plagioclase feldspars, traced back to weathered volcanic rock.

4.2 Down core variations in mineralogy

The predominant minerals found in the section from XRD analysis of clay fraction were illite and plagioclase feldspar. Illite was present in the entire section with minimal smectite (Fig 3-3). Minerals identified from the XRD diffraction patterns were consistent with terrigenous sediment. Illite, dolomite, plagioclase feldspar, alkali feldspar, and quartz were observed in sandy claystone, with some carbonate nodules. Illite, plagioclase feldspar, alkali feldspar, and quartz were found in the sediment samples of waxy claystone, limestone nodule, and dark green claystone. The volcanic deposits appeared at 177.0 mbs. Pumice, mafic minerals, or zeolites that appeared in the core sediments probably correspond to several unidentified peaks in the XRD patterns.

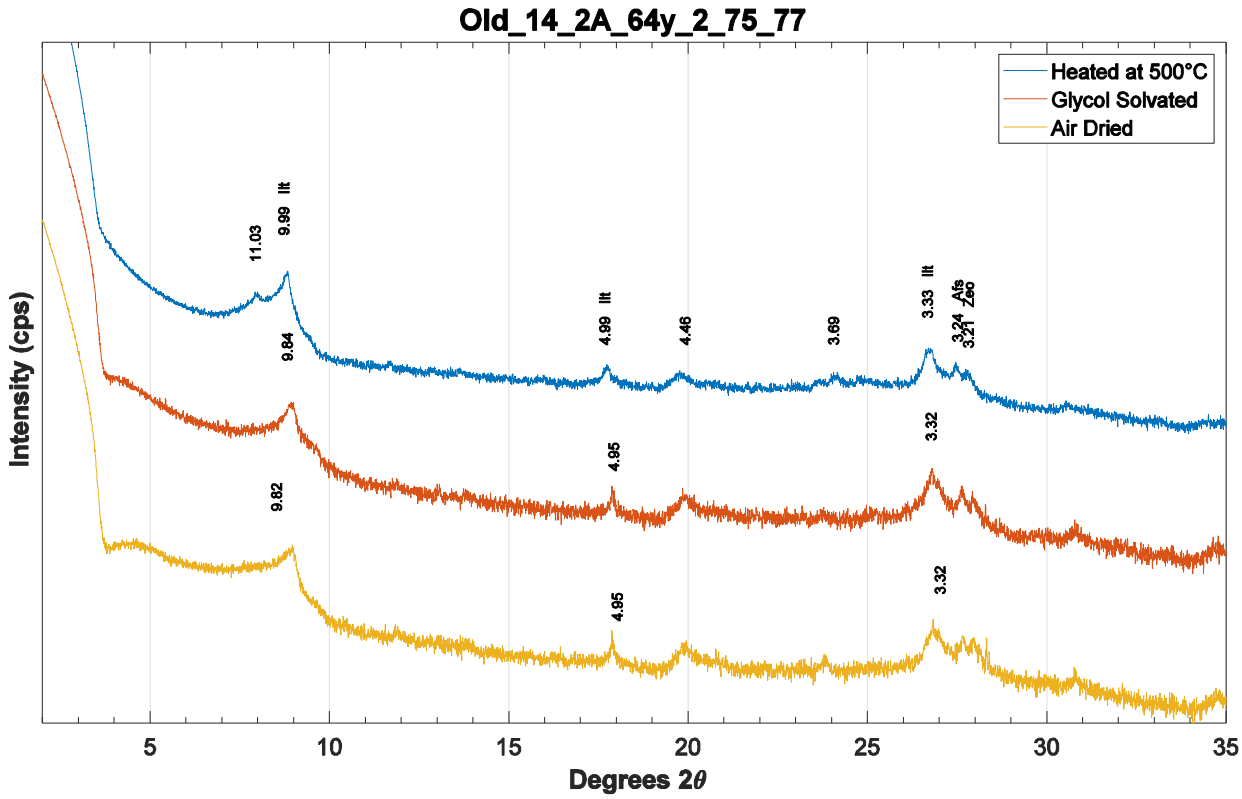

Figure 4-3 X-ray diffraction traces and d-spacings values of the sample's oriented mount located at a depth of 166.4 mbs. Three traces were shown (heated, glycol-solvated, and air-

dried). Illite (Ilt), zeolite (Zeo), and alkali feldspar (Afs) were identified in the sample. Unidentified peaks were 11.03, 3.69 Å consistent for several samples.

The clay mineralogy was interpreted to be detrital clays that were deposited in a freshwater lake basin. The primary reason was that these clays contained Al-rich illite, which forms from the weathering of crustal rocks. However, there was no illite based on d (060) reflection data; instead, these 060 reflections showed the presence of glauconite. Moreover, the octahedral composition was dioctahedral, and some new d-spacing values (11.10 Å, 5.54 Å, and 3.68 Å) appeared only when samples were heated at 500-degree Celsius and not in the air-dried or glycol-solvated samples. The inherent reason for these d-spacings was unknown and could not be determined (Figure 4-3) (Brindley & Brown, 1980; Moore & Reynolds, 1997).

Analysis of 20 powdered clay fractions showed that the d (060) value is 1.511Å on average (Figure 3-4), which is consistent with glauconite. Note that the value of d (060) for illite is 1.490Å (Moore & Reynolds, 1997). Analysis for average octahedral d-spacing in younger clays was 1.509Å (Deocampo et al., 2009), slightly lower than the current study. The standard deviation of 060 peaks is less than one, which strengthens the interpretation that glauconite is present.

4.3 The occurrence of glauconite and illite and Glauconite controversy

Glauconite is an iron-rich hydrous phyllosilicate with a dioctahedral 2:1 layer structure. It typically forms at the sediment-water interface in recent and paleo sediments. Most glauconite is dark green and common in marine clay. Sand to pebble-sized green particles are usually termed glauconite (or glaucony pellets). The term glauconite is used interchangeably to designate morphologically specific minerals of the glaucony facies and glauconitic smectite and glauconitic mica that are end members of the glauconitic mineral family. Glauconitization requires micaceous parent clay minerals (2:1 clay), which were degraded. Usually, carbonate minerals, argillaceous

(kaolinite) faecal pallets, and various rock fragments gradually transform into green grains (Odin & Matter, 1981).

The glauconitization process occurred as authigenic growth of automorphous crystallites within the pore space of the substrate. Gradually the substrate was replaced, and new altered grains formed. Smectites that are formed are subsequently modified with potassium to form glauconite (mica) that is non-expandable. The evolution of smectite (like glaucony) to mica (like glauconite) is analogous to the conversion of smectite to illite.

Moreover, glauconite is very diverse mineralogically based on the degree of evolution. The balance between the micro-environment and availability of iron and potassium controls the glauconitizaiton process (Odin & Matter, 1981). Glauconite minerals form between the oxidizing and reducing pore water conditions in sediments that resided for a long time, as sediment accumulation takes considerable time in continental shelves. The reason for the presence of glauconite composition in Olduvai lake is still unknown. The presence of glauconite usually indicates a low sedimentation rate in marine environments (Harris & Whiting, 2000).

The terms “illite” and “glauconite” can be problematic because of nomenclature issues and term “illite” is avoided altogether over the past disagreement. (Gaudette et al., 1966) showed that illites were not essentially mixed-layer structures. The U.S. system of soil taxonomy for soils indicated clayey size particle that has clay with illite (hydrous mica) by weight and commonly >4% K_2O. Based on major element analysis, K_2O was >4% for 19 samples out of 20 samples. Based on the formula's low layer charge (~ +0.66), it can be satisfied that the minerals were either illite or glauconite. Due to these difficulties, the CMS Nomenclature Committee in 1984 recommended a few requirements to define illite. The mineral must have a non-expandable micaceous layer and a dioctahedral sheet. Furthermore, the maximum interlayer charge is about

+0.8, and the minimum charge is near +0.6 without expansibility uncertainty. The representative formula where the octahedral charge is equal to interlayer deficiency is $K_{0.75}(Al_{1.75}R^{2+}_{0.25})(Si_{3.50}Al_{0.50}O_{10})(OH)_2$ (Fanning et al., 1989).

The interlayer charge was about +0.66 based on the calculation (Appendix D). The 060 identified dioctahedral composition, and the K_2O was >4%, which easily can be interpreted as the illite. The calculated formula was $(Ca_{0.09}Na_{0.46}K_{0.39})$ $(Ti_{0.04}Al_{1.05}Fe^{3+}_{0.34}Mg_{0.18})$ $(Si_{4.06}O_{10})$ $(OH)_2)$.

Again, XRD can be used to identify glauconite and illite definitively with the 002 reflection. Glauconite has weak to near non-existence 002 reflection. Glauconite has a higher 001/ 003 ratio than illite, and most importantly, the 002 reflection for illite is quite visible (Moore & Reynolds, 1997). All the profiles showed a 002 reflection at (4.9 Å), which undeniably indicates illite.

4.4 Pleistocene Paleoclimate

A high Al_2O_3/ MgO ratio was an indicator of fresher waters (i.e., freshening events) in the last six freshening events documented for Paleolake Olduvai between 1.78 Ma and 1.92 Ma (Deocampo et al., 2017). Al-rich clays found in the central basin suggested freshwater. The presence of Mg-rich clays are interpreted to represent phases of elevated salinity (Hover & Ashley, 2003). However, Mg enrichment could also be related to source rock type as magnesium values are typically highest when basaltic magmatism is the primary source and lower with a rhyolitic source (Stanistreet et al., 2020a).

The observed mineralogy and clay chemistry indicates that the environment at Olduvai was generally fresher in the older Naibor Soit formation. In the younger Olduvai Bed I and II paleolake, interlayered illite-smectite clays are common but in this instance (Naibor Soit Formation) mineral assemblages indicate that illite is dominant with very little to no illite-smectite interlayering. The

dominance of illite indicates a fresher environment and by extension stronger the prevalence of an East African monsoon regime. The high Al_2O_3/ MgO ratio and the presence of illite rather than smectite reflects fresher water conditions, potentially due to a hydrologically open lake system. Al-rich clays found in the central basin suggest freshwater, and they were likely derived from the weathering of rhyolitic source rock or freshwater flushing in an open basin during the 2.09 – 2.16 Ma interval of paleolake Olduvai.

The freshwater markers (phytoliths results, diatoms, sponge spicules, and chrysophyte cysts) in claystone facies derive from Palaeolake Olduvai. Phytoliths may be displaced and transported within the plant into the lake from catchment areas from adjacent areas by agents (water, wind, mudflows). The transportation of phytoliths can happen before or after the plant decayed. The preservation depends on post-depositional conditions, and for the former have well preservation, and the latter have poorer preservation. Phytoliths were not in high abundance in any sample. A savannah-type environment was identified based on phytoliths' morphology and the D/P index, with an influential presence of C_3 Pooideae grasses over C_4 Chloridoideae grasses and associated bushy/tree vegetation. The C_3 Pooideae grasses is dominant throughout most of the time interval and would equate to more humid intervals (Rodríguez-Cintas et al., 2020). The meroplanktic (e.g., *Nitzschia*, *Encyonema*, and *Ulnaria*) diatoms could be reliable identification of deeper water of lacustrine or riverine environments due to well preservation potential. These diatoms were either growing in the lake during less saline periods or were transported from the adjacent area. And *Hantzschia* and *Luticola* are found in moist soils, mosses, riverbanks, and other aerophytic environments that eroded to the lake sediment (Wehr et al., 2015). Other siliceous microremains (e.g., sponge spicules and chrysophyte cysts) can indicate aqueous paleoenvironment. The presence of microremains indicates a fresher environment. The spicules

recovered from samples and usually evidenced by closer proximity of freshwater sponge. Chrysophytes are algae that live in freshwater that linked to the resting phase in the algal life cycle. Palaeovegetation and environmental setting for core 2A deciphered by phytoliths, diatoms, and sponge spicules signifying stable environments with moderate pH and suggesting the phytoliths were eroded from close to paleolake and during lower salinity periods from ~2.09 Ma to 2.12 Ma covering ~30 kyr suggest that the presence of freshwater system (Rodríguez-Cintas et al., 2020).

An alternative explanation for the record of a fresher water paleolake is that the lake basin itself had a more open hydrology than younger phases of the lake, rather than being solely controlled by climate. If the lake was more open, with water draining out a spillway perhaps toward the Serengeti or one of the axial rift basins, or into groundwater recharge, then evaporative concentration would not have occurred to enhance salinity (Deocampo & Jones, 2014). Such a hydrologic condition may have been promoted by regional tectonic adjustments during uplift of the rift shoulder, and enhanced in combination with generally wetter paleoclimate to raise lake levels and generate greater hydraulic head (Rosen, 1994).

4.5 A note on human evolution and theories

The discoveries of Olduvai Hominids (OH) 5 and 7 by Louis and Mary Leakey in 1959 at the FLK site at Olduvai Gorge were the first recognized ancient hominin fossils from East Africa. The cranium found at the FLK site is still referred informally by its genus name *Zinjanthropus*. These discoveries established East Africa as a significant depository of evidence for human origin and evolution (Blumenschine et al., 2012). The evolution of two distinct bipedal lineages predating Olduvai originated from a single ancestral bipedal line between 3.0 and 2.5 Ma. The earliest members of the australopithecine lineage occurred near 2.7 Ma (in fossil records). A second lineage, the earliest members of our genus Homo, first occurred near 1.9 Ma (in fossil records

found in East African sediments) (deMenocal, 1995). The fossil *Homo habilis* was similar to the australopithecines in morphology, with a slightly larger brain size, classified as *Homo*. The appearance of *Homo erectus sensu lato,* that has more changes in brain size, life history, and body shape-size. *H. erectus* was very similar to modern humans anatomically except cranium (Maslin et al., 2014). The presence of a freshwater lake in the Olduvai basin from 2.09-2.16 Ma could have provided a more hospitable environment for hominins than the later saline-alkaline lake that dominated the landscape of Beds I-II.

Early hominin evolution in East Africa was affected strongly by climate change that can be traced back to terrestrial records. The use of paleoenvironmental proxies can point to hominin evolution and paleoecology (deMenocal, 2004; Deocampo, 2004). In summary, the literature provided three competing hypotheses (savanna hypothesis, turnover pulse hypothesis, variability selection hypothesis) to explain the role of the human evolution environment. For example, the savanna hypothesis suggests that hominins moved out to form their forest habitat to open grassland on the savannas. Savannas replaced woodland forest in East Africa over a long period of time as the land turns more arid. Accelerated aridification helped expand the savannas that increased speciation progression (deMenocal, 2004, 2011; Trauth et al., 2005; Vrba et al., 1995). The turnover pulse hypothesis, on the other hand, argues against the proposed link between hominin evolution with aridification in East Africa. This theory further suggests that faunal turnover occurred due to speciation and adaptation results over hundreds of thousands of years and unrelated to climate-change events. The increased diversity would lead to much higher turnover rates, followed by increased speciation, and ended with extinction. This mechanism allowed hominin adaptation and further evolution within the ecosystem (Carto et al., 2009; Potts et al., 1999; Vrba et al., 1995; Wynn, 2004). The variability selection hypothesis suggests that regional

climate variability with the variability of floodplain habitats control species diversity across the savanna in East Africa during the Plio-Pleistocene transition. Evolution of flora and fauna in floodplain habitats changed due to episodic flooding and aridity. These events created opportunities for new species to develop and fill the void and more opportunity for early hominins to exploit the resulting genus *Homo* (deMenocal, 2004; Potts, 1996; Wynn, 2004).

Key events in hominin evolution occurred when deep lakes would form in the East African Rift landscape. The appearance of the genus *Homo* during the Pleistocene between 1.8 and 2.5 Ma is suggested by the fossil records (1.8 to 1.9 million-year-old EARS deposits). The notion that major global climate change forced significant evolutionary changes in hominins remains relevant, although the idea of exactly when and how remains debatable. The prevalence of a relatively stronger monsoon during the Pleistocene as our results and the indication of the impacts on human evolution similarly remains unclear (Maslin et al., 2014). Determining the most dominant climatic shifts and paleoclimatic conditions that are linked to overall hominin evolution trends is difficult due to the project's short time interval (2.09 – 2.16 Ma), the lack of outcrop of this age in the Olduvai area, and the need to distinguish between tectonic and climatic forcing of local environmental changes.

5 CONCLUSIONS

The following conclusions were derived in this study.

The paleoenvironmental history of Olduvai Gorge reveals a freshening interval from 2.09 – 2.16 Ma where illite was present in its paleolacustrine sediments. Mineralogical evidence indicates the predominant presence of illite throughout the 156.9 mbs to 215.3 mbs interval of lake sediment from core 2A. Plagioclase feldspar is the second most dominant mineral, followed by alkali feldspar, and quartz. Carbonate minerals, kaolinite, and zeolites were rare in clay fraction.

Analysis of the elemental compositions of the core samples indicates that the claystones were siliceous and derived from detrital sources. The volcanoclastic sediments are aluminum-rich with a lower amount of magnesium. This Al-rich clay had the following formula $(Ca_{0.09}Na_{0.46}K_{0.39})$ $(Ti_{0.04}Al_{1.05}Fe^{3+}_{0.34}Mg_{0.18})$ $(Si_{4.06}O_{10})$ $(OH)_2$). The 060 peak positions of selected monomineralic clay fractions showed that the samples were dioctahedral.

The geochemistry of the core sediments suggests a low-salinity environment. The associated fine size fraction shows Al-rich clay geochemistry instead of Mg enrichment, and the Mg was lower compared to the overlying units. Al-rich clay chemistry is interpreted as detrital sources with the end-member as dioctahedral illite was likely derived from detrital sources.

REFERENCES

Ashley, G. M., Dominguez-Rodrigo, M., Bunn, H. T., Mabulla, A. Z. P., & Baquedano, E. (2010). Sedimentary Geology and Human Origins: A Fresh Look at Olduvai Gorge, Tanzania. *Journal of Sedimentary Research, 80*(8), 703-709.

Ashley, G. M., & Hay, R. L. (2002). Sedimentation Patterns in a Plio-Pleistocene Volcaniclastic Rift-Platform Basin, Olduvai Gorge, Tanzania. In *Sedimentation in Continental Rifts* (pp. 107-122).

Blumenschine, R. J., Stanistreet, I. G., & Masao, F. T. (2012). Olduvai Gorge and the Olduvai landscape paleoanthropology project. *J Hum Evol, 63*(2), 247-250. https://www.ncbi.nlm.nih.gov/pubmed/22727946

Boyd, F., & Mertzman, S. (1987). Composition and structure of the Kaapvaal lithosphere, southern Africa. In *Magmatic processes: physicochemical principles* (Vol. 1, pp. 13-24): The Geochemical Society.

Brindley, G. W., & Brown, G. (1980). Crystal Structures of Clay Minerals and their X-Ray Identification. *Mineralogical Society of Great Britain and Ireland*.

Carto, S. L., Weaver, A. J., Hetherington, R., Lam, Y., & Wiebe, E. C. (2009). Out of Africa and into an ice age: on the role of global climate change in the late Pleistocene migration of early modern humans out of Africa. *J Hum Evol, 56*(2), 139-151. https://www.ncbi.nlm.nih.gov/pubmed/19019409

Conway, D., Hanson, C. E., Doherty, R., & Persechino, A. (2007). GCM simulations of the Indian Ocean dipole influence on East African rainfall: Present and future. *Geophysical Research Letters, 34*(3).

Deino, A. L., Heil, C., King, J., McHenry, L. J., Stanistreet, I. G., Stollhofen, H., et al. (2020). Chronostratigraphy and age modeling of Pleistocene drill cores from the Olduvai Basin, Tanzania (Olduvai Gorge Coring Project). *Palaeogeography, Palaeoclimatology, Palaeoecology*.

deMenocal, P. B. (1995). Plo-Pleistocene African Climate. *Science, 270*, 53-59.

deMenocal, P. B. (2004). African climate change and faunal evolution during the Pliocene–Pleistocene. *Earth and Planetary Science Letters, 220*(1-2), 3-24.

deMenocal, P. B. (2011). Climate and Human Evolution. *Science, 331*, 540-542.

Deocampo, D. M. (2004). Authigenic clays in East Africa: Regional trends and paleolimnology at the Plio-Pleistocene boundary, Olduvai Gorge, Tanzania. *Journal of Paleolimnology, 31*, 1-9.

Deocampo, D. M. (2005). Evaporative evolution of surface waters and the role of aqueous CO2 in magnesium silicate precipitation: Lake Eyasi and Ngorongoro Crater, northern Tanzania. *South African Journal of Geology, 108*(4), 493-504.

Deocampo, D. M. (2015). Authigenic clay minerals in lacustrine mudstones. In *Paying Attention to Mudrocks: Priceless!* (pp. 49-64).

Deocampo, D. M., Behrensmeyer, A. K., & Potts, R. (2010). Ultrafine clay minerals of the Pleistocene Olorgesailie Formation, southern Kenya Rift: diagenesis and paleoenvironments of early hominins. *Clays and Clay Minerals, 58*(3), 294-310.

Deocampo, D. M., Berry, P. A., Beverly, E. J., Ashley, G. M., & Jarrett, R. E. (2017). Whole-rock geochemistry tracks precessional control of Pleistocene lake salinity at Olduvai Gorge, Tanzania: A record of authigenic clays. *Geology*.

Deocampo, D. M., Cuadros, J., Wing-dudek, T., Olives, J., & Amouric, M. (2009). Saline lake diagenesis as revealed by coupled mineralogy and geochemistry of multiple ultrafine clay phases: Pliocene Olduvai Gorge, Tanzania. *American Journal of Science, 309*(9), 834-868.

Deocampo, D. M., & Jones, B. F. (2014). *Geochemistry of Saline Lakes. Treatise on Geochemistry 2nd Edition* (J. I. Drever Ed. Vol. 7: Surface and Groundwater, Weathering, and Soils).

Deocampo, D. M., & Tactikos, J. C. (2010). Geochemical gradients and artifact mass densities on the lowermost Bed II eastern lake margin (~ 1.8 Ma), Olduvai Gorge, Tanzania. *Quaternary Research, 74*(3), 411-423.

Fanning, D. S., Keramidas, V. Z., & El-Desoky, M. A. J. M. i. s. e. (1989). Micas. *1*, 551-634.

Gaudette, H. E., Eades, J. L., & Grim, R. E. (1966). The Nature of Illite. *Clays and Clay Minerals, 13*, 33-48.

Gebregiorgis, D., Deocampo, D. M., Longstaffe, F. J., Simpson, A., Ashley, G. M., Beverly, E. J., et al. (2020). Oxygen Isotopes in Authigenic Clay Minerals: Toward Building a Reliable Salinity Proxy. *Geophysical Research Letters, 47*(3).

Harris, L. C., & Whiting, B. M. (2000). Sequence-stratigraphic significance of Miocene to Pliocene glauconite-rich layers, on- and offshore of the US Mid-Atlantic margin. *Sedimentary Geology, 134* 129–147.

Hay, R. L. (1971). Geologic Background Of Beds I And II Stratigraphic Summary. In M. D. Leakey (Ed.), *Olduvai Gorge* (Vol. 3, pp. 9-18). Cambridge University Press.

Hay, R. L. (1976). *Geology of the Olduvai Gorge*. Berkeley, California: University of California Press.

Hay, R. L., & Kyser, T. K. (2001). Chemical sedimentology and paleoenvironmental history of Lake Olduvai, a Pliocene lake in northern Tanzania. *GSA Bulletin, 113*(12), 1505–1521.

Hover, V. C., & Ashley, G. M. (2003). Geochemical signatures of paleodepositional and diagenetic environments: a STEM/ AEM study of authigenic clay minerals form an arid rift basin, Olduvai Gorge, Tanzania. *Clays and Clay Minerals, 51*(3), 231-251.

Jones, B. F., & Deocampo, D. M. (2003). Geochemistry of saline lakes. *TrGeo, 5*, 605.

Manuella, F. C., Carbone, S., & Barreca, G. (2012). Origin of Saponite-Rich Clays in a Fossil Serpentinite-Hosted Hydrothermal System in the Crustal Basement of the Hyblean Plateau (Sicily, Italy). *Clays and Clay Minerals, 60*(1), 18-31.

Maslin, M. A., Brierley, C. M., Milner, A. M., Shultz, S., Trauth, M. H., & Wilson, K. E. (2014). East African climate pulses and early human evolution. *Quaternary Science Reviews, 101*, 1-17.

McGregor, G. R., & Nieuwolt, S. (1998). *Tropical Climatology : An Introduction to the Climates of the Low Latitudes* (Vol. Second). New York: Wiley.

McHenry, L. J., Stanistreet, I. G., Stollhofen, H., Njau, J. K., Toth, N., & Schick, K. (2020). Tuff fingerprinting and correlations between OGCP cores and outcrops for Pre-Bed I and Beds I/II at Olduvai Gorge, Tanzania. *Palaeogeography, Palaeoclimatology, Palaeoecology, 548*.

Meunier, A. (2005). *Clays*. Germany: Springer.

Moore, D. M., & Reynolds, R. C. (1997). *X-ray Diffraction and the Identification and Analysis of Clay Minerals* (Second ed.): Oxford University Press (OUP).

Newman, A. C. D. (1987). Chemistry of Clays and Clays Minerals, Mineralogical Society Monograph, No. 6.

Nicholson, S. E. (2000). The nature of rainfall variability over Africa on time scales of decades to millenia. *Global and Planetary Change, 26*, 137-158.

Nicholson, S. E. (2017). Climate and climatic variability of rainfall over eastern Africa. *Reviews of Geophysics, 55*(3), 590-635.

Odin, G. S., & Matter, A. (1981). De glauconiarum origine. *Sedimentology, 28*, 611–641.

Potts, R. (1996). Evolution and Climate Variability. *Science, 273*(5277), 922-923.

Potts, R., Behrensmeyer, A. K., & Ditchfield, P. (1999). Paleolandscape variation and Early Pleistocene hominid activities: Members 1 and 7, Olorgesailie Formation, Kenya. *Journal of Human Evolution, 37*, 747–788.

Rodríguez-Cintas, A., Albert, R. M., Bamford, M. K., Stanistreet, I. G., Stollhofen, H., Stone, J. R., et al. (2020). Palaeovegetation changes recorded in Palaeolake Olduvai OGCP Core 2A (2.09–2.12 Ma) Naibor Soit Formation Olduvai Gorge, Tanzania. *Palaeogeography, Palaeoclimatology, Palaeoecology, 557*.

Rosen, M. R. (1994). The importance of groundwater in playas: A review of playa classifications and the sedimentology and hydrology of playas. In *Paleoclimate and Basin Evolution of Playa Systems* (pp. 1-18).

Shemsanga, C., Omambia, A. N., & Gu, Y. (2010). The Cost of Climate Change in Tanzania: Impacts and Adaptations. *Journal of American Science, 6*, 182-196.

Singer, A. (1980). The paleoclimatic interpretation of clay minerals in soils and weathering profiles. *Earth-Science Reviews, 15*, 303-326.

Singer, A. (1984). The paleoclimatic interpretation of clay minerals in sediments - a review. *Earth-Science Reviews, 21*, 251-293.

Stanistreet, I. G., Boyle, J. F., Stollhofen, H., Deocampo, D. M., Deino, A., McHenry, L. J., et al. (2020a). Palaeosalinity and palaeoclimatic geochemical proxies (elements Ti, Mg, Al) vary with Milankovitch cyclicity (1.3 to 2.0 Ma), OGCP cores, Palaeolake Olduvai, Tanzania. *Palaeogeography, Palaeoclimatology, Palaeoecology, 546*.

Stanistreet, I. G., Doyle, C., Hughes, T., Rushworth, E. D., Stollhofen, H., Toth, N., et al. (2020b). Changing depocentre environments of Palaeolake Olduvai and carbonates as marker horizons for hiatuses and lake-level extremes. *Palaeogeography, Palaeoclimatology, Palaeoecology, 560*.

Stanistreet, I. G., Stollhofen, H., Deino, A. L., McHenry, L. J., Toth, N. P., Schick, K. D., & Njau, J. K. (2020c). New Olduvai Basin stratigraphy and stratigraphic concepts revealed by OGCP cores into the Palaeolake Olduvai depocentre, Tanzania. *Palaeogeography, Palaeoclimatology, Palaeoecology, 554*.

Trauth, M. H., Maslin, M. A., Deino, A. L., & Streccker, M. R. (2005). Late Cenozoic Moisture History of East Africa. *Science, 309*(5743), 2051-2053.

Vrba, E. S., Denton, G. H., Partridge, T. C., & Burckle, L. H. (1995). *Paleoclimate and Evolution: with Emphasis on Human Origins*: Yale University. Bookcrafters Inc. Chelsea, MI.

Wehr, J. D., Sheath, R. G., & Kociolek, J. P. (2015). *Freshwater algae of North America: ecology and classification*: Elsevier.

Whitney, D. L., & Evans, B. W. (2009). Abbreviations for names of rock-forming minerals. *American Mineralogist, 95*(1), 185-187.

Wynn, J. G. (2004). Influence of Plio-Pleistocene aridification on human evolution: evidence from paleosols of the Turkana Basin, Kenya. *Am J Phys Anthropol, 123*(2), 106-118. https://www.ncbi.nlm.nih.gov/pubmed/14730645

Yang, W., Seager, R., Cane, M. A., & Lyon, B. (2015). The Annual Cycle of East African Precipitation. *Journal of Climate, 28*(6), 2385-2404.

APPENDICES

Appendix A: Core description of the study area

The data was arranged with the section length and scaled top depth and bottom depth. Complete section ID designated as OGDP-OLD14-2A-61Y-1-84-86; however, the OGDP-OLD14-2A was excluded since it is identical for all samples in this study. The expedition was OGDP, location name was Olduvai Gorge, location id was OLD, time of expedition was at 2014, site of the hole was 2A, core identifier was 61, the tool was designated as Y, and number of the section was 61 and following.

Section ID	**Section Length** *cm*	**Depth Top, scaled** *mbs*	**Depth Bottom, scaled** *mbs*	**Core Comments**
61Y-1	0.916	156.0	156.9	Incomplete core recovery in the 3-meter run. Much sandy sediment, some likely washed away. No core catcher. 183.2 cm=total length of recovered core in liner.
61Y-2	0.916	156.9	157.8	Incomplete core recovery in the 3-meter run. Much sandy sediment, some likely washed away. No core catcher. 183.2 cm=total length of recovered core in liner.
62Y-1	1.516	159.0	160.4	302.8 cm=total core recovery in plastic liner. 30 cm at the top is very sandy claystone. Rest: Olive sandy, waxy claystone with carbonate nodules <3m.
62Y-2	1.517	160.4	161.9	302.8 cm=total core recovery in plastic liner. 30 cm at the top is very sandy claystone. Rest: Olive sandy, waxy claystone with carbonate nodules <3m.
62Y-3	0.12	161.9	162.0	302.8 cm=total core recovery in plastic liner. 30 cm at the top is very sandy claystone. Rest: Olive sandy, waxy claystone with carbonate nodules <3m.
63Y-1	1.496	162.0	163.5	298.1 cm = total core recovery in plastic liner. Olive waxy claystone with limestone nodules.
63Y-2	1.492	163.5	164.9	298.1 cm = total core recovery in plastic liner. Olive waxy claystone with limestone nodules.
63Y-3	0.063	164.9	165.0	298.1 cm = total core recovery in plastic liner. Olive waxy claystone with limestone nodules.

				Comments: *ORIGINALLY LABELED 63Y-2*
64Y-1	1.416	165.0	166.4	Total length in tube=284.8 cm. Sandy waxy claystone, with small limestone nodules in section 2.
64Y-2	1.432	166.4	167.8	Total length in tube=284.8 cm. Sandy waxy claystone, with small limestone nodules in section 2.
64Y-3	0.205	167.8	168.0	Total length in tube=284.8 cm. Sandy waxy claystone, with small limestone nodules in section 2.
65Y-1	1.531	168.0	169.4	Total core recovery in liner = 306 cm. Olive waxy claystone.
65Y-2	1.548	169.4	170.9	Total core recovery in liner = 306 cm. Olive waxy claystone.
65Y-3	0.113	170.9	171.0	Total core recovery in liner = 306 cm. Olive waxy claystone.
66Y-1	1.282	171.0	172.3	Total core recovery in liner= 256.6 cm. Olive waxy claystone.
66Y-2	1.289	172.3	173.6	Total core recovery in liner= 256.6 cm. Olive waxy claystone.
66Y-3	0.094	173.6	173.7	Total core recovery in liner= 256.6 cm. Olive waxy claystone.
67Y-1	1.551	174.0	175.5	305.1= total core recovery in liner. Section 1: Olive waxy claystone. Section 2: Olive waxy claystone; lower 30 cm dark green/blackish claystone.
67Y-2	1.518	175.5	176.9	305.1= total core recovery in liner. Section 1: Olive waxy claystone. Section 2: Olive waxy claystone; lower 30 cm dark green/blackish claystone.
67Y-3	0.075	176.9	177.0	305.1= total core recovery in liner. Section 1: Olive waxy claystone. Section 2: Olive waxy claystone; lower 30 cm dark green/blackish claystone.
68Y-1	1.466	177.0	178.5	296.7= total core recovery in liner. Topmost 5 cm: dark green clay. Rest of core: black (lava) or other dark volcanic deposit.
68Y-2	1.479	178.5	179.9	296.7= total core recovery in liner. Topmost 5 cm: dark green clay. Rest of core: black (lava) or other dark volcanic deposit.
68Y-3	0.035	179.9	180.0	296.7= total core recovery in liner. Topmost 5 cm: dark green clay. Rest of core: black (lava) or other dark volcanic deposit.
69Y-1	1.461	180.0	181.5	291.6 cm = total core recovery in liner. No core catcher. Dark grayish-green volcanic -(?lava or) ?ignimbrite, fine-grained.
69Y-2	1.46	181.5	182.9	291.6 cm = total core recovery in liner. No core catcher. Dark grayish-green volcanic -(?lava or) ?ignimbrite, fine-grained.

70Y-1	1.379	183.0	184.4	276.3 cm total length in liner. Mafic ?ash; dark green to black with pumice <1 cm.
70Y-2	1.386	184.4	185.8	276.3 cm total length in liner. Mafic ?ash; dark green to black with pumice <1 cm.
70Y-3	0.19	185.8	186.0	276.3 cm total length in liner. Mafic ?ash; dark green to black with pumice <1 cm.
71Y-1	1.387	186.0	187.4	276.8 cm total in liner. [Naabi Ignimbrite]: Feldspar and pumice-bearing fine-grained dark green ignimbrite.
71Y-2	1.391	187.4	188.8	276.8 cm total in liner. [Naabi Ignimbrite]: Feldspar and pumice-bearing fine-grained dark green ignimbrite.
71Y-3	0.198	188.8	189.0	276.8 cm total in liner. [Naabi Ignimbrite]: Feldspar and pumice-bearing fine-grained dark green ignimbrite.
72Y-1	1.455	189.0	190.4	291.1 total in liner. Coarser-grained ignimbrite.
72Y-2	1.459	190.4	191.8	291.1 total in liner. Coarser-grained ignimbrite.
72Y-3	0.158	191.8	192.0	291.1 total in liner. Coarser-grained ignimbrite.
73Y-1	1.435	192.0	193.4	287.6 cm total in liner. Feldspar-rich coarse ash.
73Y-2	1.44	193.4	194.9	287.6 cm total in liner. Feldspar-rich coarse ash.
73Y-3	0.127	194.9	195.0	287.6 cm total in liner. Feldspar-rich coarse ash.
74Y-1	0.099	195.0	195.1	284.7 total length in liner. Top portion detached=Section 1.
74Y-2	1.416	195.1	196.5	284.7 total length in liner. Top portion detached=Section 1.
74Y-3	1.43	196.5	197.9	284.7 total length in liner. Top portion detached=Section 1.
74Y-4	0.052	197.9	198.0	284.7 total length in liner. Top portion detached=Section 1.
75Y-1	1.45	198.0	199.5	
75Y-2	1.448	199.5	200.9	
75Y-3	0.094	200.9	201.0	
76Y-1	1.531	201.0	202.5	Total cm = 305.5; Section 1 and top of section 2: black coarse ash; base of section 2=brown claystone Have run out of drilling pipe; have put in an order with Mal at Layne to send more, 100m, to arrive by Sunday, hopefully in the morning. In meantime, will log site up to casing, then start angled bore.
76Y-2	1.526	202.5	203.9	Total cm = 305.5; Section 1 and top of section 2: black coarse ash; base of section 2=brown claystone Have run out of drilling pipe; have put in an order with Mal at Layne to send more, 100m, to arrive by Sunday, hopefully in the morning. In meantime, will log site up to casing, then start angled bore.

76Y-3	0.068	203.9	204.0	Total cm = 305.5; Section 1 and top of section 2: black coarse ash; base of section 2=brown claystone Have run out of drilling pipe; have put in an order with Mal at Layne to send more, 100m, to arrive by Sunday, hopefully in the morning. In meantime, will log site up to casing, then start angled bore.
77Y-1	1.383	204.0	205.4	Sand with some gravels. Total length in liner=276.5 cm. No orientation. Water used for 2A starting with Core 77 had been brought in a truck previously used for fuel, and has slight diesel smell. Not in lacustrine facies in core 77, fluvial. Has been brought to drill site in Layne truck tank from the water truck tank, and put into poly container at drill site.
77Y-2	1.384	205.4	206.8	Sand with some gravels. Total length in liner=276.5 cm. No orientation. Water used for 2A starting with Core 77 had been brought in a truck previously used for fuel, and has slight diesel smell. Not in lacustrine facies in core 77, fluvial. Has been brought to drill site in Layne truck tank from the water truck tank, and put into poly container at drill site.
77Y-3	0.057	206.8	206.8	Sand with some gravels. Total length in liner=276.5 cm. No orientation. Water used for 2A starting with Core 77 had been brought in a truck previously used for fuel, and has slight diesel smell. Not in lacustrine facies in core 77, fluvial. Has been brought to drill site in Layne truck tank from the water truck tank, and put into poly container at drill site.
78Y-1	1.242	207.0	208.2	No core catcher. Quartz-rich sands at base of section 2. Total length in liner = 248.4 cm. Top of section 1= clayey sandstone. Top of section 2=base of section 1= clayey sandstone. **Comments:** *Base: clayey sandstone.*
78Y-2	1.242	208.2	209.5	No core catcher. Quartz-rich sands at base of section 2. Total length in liner = 248.4 cm. Top of section 1= clayey sandstone. Top of section 2=base of section 1= clayey sandstone. **Comments:** *Top: clayey sandstone; base: quartz-rich sands.*
79Y-1	0.935	210.0	210.9	Tube collapsed; little recovery. Whole core retrieved: Quartzite pebble-rich siliciclastic sandstone.
79Y-2	0.082	210.9	211.0	Tube collapsed; little recovery. Whole core retrieved: Quartzite pebble-rich siliciclastic sandstone.

79Y-3	0.068	211.0	211.1	Tube collapsed; little recovery. Whole core retrieved: Quartzite pebble-rich siliciclastic sandstone.
80Y-1	1.163	213.0	214.2	232 cm total length in liner. All sections=sandy claystone. Core catcher=sandy claystone.
80Y-2	1.163	214.2	215.3	232 cm total length in liner. All sections=sandy claystone. Core catcher=sandy claystone.

Appendix B: d-spacing of the samples

All the peak values were identified with 2 Theta value and d-spacing's which were the suggestive for specific minerals but in some instances not adequate as the scan axis was set from 3.0˚- 60.0˚ and scan time was set for short duration.

Section ID	d-spacing						
2A-61y-1							
61y-1-84-86-Air	9.92	4.98	3.27				
61y-1-84-86-Glycolated	9.94	4.95	3.31				
61y-1-84-86-Heated@500°C	9.99	5.01	3.33				
2A-61y-2							
61y-2-10-12-Air	25.71	9.92	5.55	4.91	3.31		
61y-2-30-32-Air	21.77		9.87		4.93		3.32
61y-2-30-32-Glycolated	26.85		9.88		4.99		3.33
61y-2-30-32-Heated@500°C		11.11	10.02	5.54	5.01	3.69	3.33
61y-2-40-42-Air	19.77	9.85	4.97	3.32			
61y-2-50-52-Air		9.91	4.98	3.33			
61y-2-50-52-Glycolated	27.99	9.87	4.95	3.32			
61y-2-60-62-Air	20.81	9.78	4.93		3.33		
61y-2-60-62-Glycolated	22.85	9.82	4.99	3.74	3.33		
61y-2-60-62-Heated@500°C	11.07	9.97	5.01	3.68	3.32	3.19	
2A-62y-1							
62y-1-20-22-air	10.59	4.93	3.28				
62y-1-35-37-Air	9.89	4.95	3.33				
62y-1-35-37-Glycolated	9.87	4.97	3.33				
62y-1-50-52-Air	9.97	5.01	3.33				
62y-1-65-67-Air	9.89	4.96	3.33				
62y-1-65-67-Glycolated	9.86	4.95	3.33				
62y-1-80-82-Air	9.83		4.98		3.33		
62y-1-80-82-Glycolated	10.04		5.02		3.36		

62y-1-80-82-K-Saturated	10.06		5.00		3.33			
62y-1-80-82-K-Saturated-Heated@300°C	10.04		4.99		3.24			
62y-1-80-82-K-Saturated-Heated@500°C	11.04	9.96 3.59	7.12 3.55	6.48 3.34	5.53 3.24	4.99 3.20	4.32 2.92	3.70
62y-1-95-97-Air	9.82	4.95	3.33					
62y-1-95-97-Glycolated	9.89	4.95	3.34					
62y-1-95-97-Heated@500°C	10.04	5.03	3.33					
62y-1-110-112-Air	9.83	4.97	3.33	3.19				
62y-1-110-112-Glycolated	10.10	5.01	3.36					
62y-1-140-142-air	9.85	4.94	3.33					
62y-1-140-142-Glycolated	9.85	4.94	3.32					
62y-1-140-142-Heated@500°C	10.01	5.00	3.33					
2A-62y-2								
62y-2-5-7-Air	9.91	4.96	3.30					
62y-2-5-7-Glycolated	9.88	4.99	3.31					
62y-2-35-37-Air	9.93	4.98	3.32					
62y-2-35-37-Glycolated	9.81	4.90	3.32					
62y-2-50-52-Air	9.84	4.98	3.33					
62y-2-50-52-Glycolated	9.79	4.96	3.33	3.19				
62y-2-65-67-Air	9.80	4.97	3.33	3.22	3.19	2.91		
62y-2-65-67-Glycolated	9.85	4.96	3.32	3.23	3.19	2.91		
62y-2-65-67-Heated@500°C	9.98	5.00	3.34	3.21	3.06	2.92		
62y-2-80-82-air	9.86			4.97	3.33	3.20		
62y-2-80-82-Glycolated	9.87	8.34	6.41	4.97	3.33	3.20	3.18	
62y-2-95-97-Air	9.79	4.95	3.33					
62y-2-95-97-Glycolated	9.82	4.94	3.32					
62y-2-95-97-Heated@500°C	9.98	5.02	3.34					
62y-2-125-127-air	9.86	4.96	3.33					

62y-2-125-127-Glycolated	9.86	4.96	3.32				
62y-2-140-142-Air	9.89	4.97	4.48	3.33	3.21		
62y-2-140-142-Glycolated	9.89	4.97	4.46	3.33	3.21		
2A-62y-3							
62y-3-7-9-Air	9.89	4.96	4.27	3.33	3.22	3.20	2.90
62y-3-7-9-Glycolated	9.75	4.95	4.28	3.32	3.23	3.19	2.90
2A-63y-1							
63y-1-5-7-air		9.83	4.94	3.32			
63y-1-5-7-Glycolated		9.85	4.97	3.33			
63y-1-5-7-K-Saturated		10.07	5.02	3.35			
63y-1-5-7-K-Saturated-Heated@300°C		9.99	5.01	3.34			
63y-1-5-7-K-Saturated-Heated@500°C		9.96	5.00	3.33			
63y-1-31-33-Air	9.97	4.96	3.27				
63y-1-31-33-Glycolated	9.73	4.97	3.32				
63y-1-31-33-Heated@500°C	9.74	4.95	3.31				
63y-1-80-82-Air	9.94	4.97	3.32				
63y-1-80-82-Glycolated	9.97	5.03	3.30				
63y-1-80-82-Heated@500°C	9.99	5.01	3.33				
63y-1-123-125-Air	9.82	4.96	3.33				
63y-1-123-125-Glycolated	9.86	4.96	3.33				
63y-1-123-125-Heated@500°C	10.01	5.01	3.33				

2A-63y-2							
63y-2-5-7-Air	10.55	4.96	3.28	3.23	3.20		
63y-2-5-7-Glycolated	9.89	4.93	3.33	3.22	3.20		
63y-2-35-37-Air	10.14	4.90	3.30				
63y-2-35-37-Glycolated	9.67	5.04	3.34				
63y-2-121-123-Air		9.15	4.95	4.47	3.74		
63y-2-121-123-Glycolated		9.15	4.95	4.48	3.73		
63y-2-121-123-Heated@500°C	11.46	9.91	6.87	6.48	5.53		
			4.99	4.31	3.56	3.25	3.20
2A-64y-1							

64y-1-20-22-Air		9.87	4.95		3.30			
64y-1-20-22-Glycolated		9.82	5.02		3.33			
64y-1-20-22-Heated@500°C	11.12	10.01	4.97	3.68	3.33			
64y-1-50-52-Air		9.84	4.93		3.32	3.23	3.19	
64y-1-50-52-Glycolated		9.85	4.96		3.33	3.23	3.19	
64y-1-50-52-Heated@500°C	11.12	10.01	5.00	3.70	3.33	3.25	3.21	
64y-1-65-67-Air		10.03	4.92	3.32				
64y-1-65-67-Glycolated	25.58	9.84	4.95	3.31				
64y-1-83-85-Air		9.96	4.95		3.32			
64y-1-83-85-Glycolated		9.81	4.93		3.32			
64y-1-83-85-Heated@500°C	11.03	9.99	4.99	3.69	3.33	3.25	3.21	
64y-1-112-114-Air		9.91	4.95	3.34				
64y-1-112-114-Glycolated	25.44	9.84	4.94	3.32				
64y-1-128-130-Air	9.84	4.96	4.48	3.32	3.23			
64y-1-128-130-Glycolated	9.82	4.95	4.46	3.32	3.22			
2A-64y-2								
64y-2-18-20-Air		9.84	4.95	4.46	3.74	3.32	3.23	
64y-2-18-20-Glycolated		9.81	4.94	4.46		3.32	3.22	
64y-2-18-20-Heated@500°C	11.13	9.98	4.99	4.49	3.69	3.35	3.25	3.19
64y-2-75-77-air		9.82	4.96	4.47	3.73	3.32	3.22	3.19
64y-2-75-77-Glycolated		9.84	4.96	4.46		3.33	3.23	3.20
64y-2-75-77-Heated@500°C	11.09	10.00	5.00	4.50	3.70	3.33	3.25	3.21
64y-2-88-90-Air	9.83	4.97	4.46	3.33	3.22	3.19		
64y-2-88-90-Glycolated	9.82	4.96	4.46	3.32	3.22	3.18		
64y-2-105-107-Air	9.80		4.96	4.47	4.28	3.33	3.23	
64y-2-105-107-Glycolated	9.83	9.19	4.96	4.46	4.27	3.32	3.23	
64y-2-119-121-Air	9.81	4.96	4.46	4.27	3.56	3.32	3.21	
64y-2-119-121-Glycolated	9.76	4.95	4.47	4.27	3.55	3.32	3.19	
2A-64y-3								
64y-3-15-17-Air		9.79	4.96		3.32			
64y-3-15-17-Glycolated		9.90	4.95		3.32			
64y-3-15-17-Heated@500°C	11.08	10.00	5.00	3.68	3.33			

2A-65y-1			
65y-1-20-22-air	9.81	4.97	3.33
65y-1-20-22-Glycolated	9.87	4.96	3.33
65y-1-20-22-Heated@500°C	10.05	5.01	3.32
65y-1-50-52-Air	9.89	4.95	3.32

65y-1-50-52-Glycolated	9.80	4.97	3.32					
65y-1-65-67-Air	9.89	4.95	4.28	3.33				
65y-1-65-67-Glycolated	9.86	4.95	4.27	3.32				
65y-1-80-82-Air		9.85	4.95		3.34			
65y-1-80-82-Glycolated		9.86	4.96		3.33			
65y-1-80-82-Heated@500°C	11.08	10.00	5.00	3.70	3.34			
65y-1-110-112-Air		9.80		4.95	3.33			
65y-1-110-112-Glycolated		9.83		4.97	3.32			
65y-1-110-112-K-Saturated	11.46	10.05		5.00	3.34			
65y-1-110-112-K-Saturated-Heated@300°C		10.03		4.97	3.34			
65y-1-110-112-K-Saturated-Heated@500°C		9.99	8.98	5.01	3.33	3.24	3.21	
65y-1-125-127-Air	9.89	4.98		3.34				
65y-1-125-127-Glycolated	9.82	4.95	3.83	3.33				
65y-1-138-140-Air	9.81	4.94	3.31					
65y-1-138-140-Glycolated	9.88	4.94	3.32	3.19				

2A-65y-2								
65y-2-5-7-Air	11.16	10.46	9.78	7.44	6.56	4.95	3.33	3.22
65y-2-5-7-Glycolated	11.20		9.77	7.43	6.54	4.95	3.33	
65y-2-33-35-Air		9.82		6.39	4.97	3.31	3.22	3.17
65y-2-33-35-Glycolated		9.82	7.82	6.40	4.97	3.31	3.23	3.17
65y-2-33-35-Heated@500°C	11.10	10.00		6.49	5.00	3.32	3.25	2.21
65y-2-52-54-air	9.87	4.98	3.31	3.23				
65y-2-52-54-Glycolated	9.81	4.94	3.33					
65y-2-80-82-air	10.97	9.95	4.94		3.31			
65y-2-80-82-Glycolated		9.85	4.93		3.32			
65y-2-80-82-Heated@500°C	11.17	9.96	5.00	3.69	3.34			
65y-2-110-112-air		9.80	4.97		3.31	3.27		
65y-2-110-112-Glycolated		9.81	4.92		3.32			
65y-2-110-112-Heated@500°C	11.13	10.01	5.01	3.69	3.34			

65y-2-122-124-air	9.84	4.95	3.32								
65y-2-122-124-Glycolated	9.83	4.93	3.33								

65y-2-148-150-air	11.21	9.90		6.54	4.95	4.29	3.29				
65y-2-148-150-Glycolated		9.88		6.53	4.94	4.28	3.32				
65y-2-148-150-Heated@500°C	11.47	9.97	7.08	6.63	4.99	4.33	3.76	3.57	3.33	3.25	3.21
2A-66y-1											
66y-1-15-17-Air		10.29	4.95	3.26							
66y-1-15-17-Glycolated		10.37	4.99	3.30							
66y-1-31-33-Air				9.89		4.96				3.27	
66y-1-31-33-Glycolated			11.26	9.83	6.56	4.96	4.31			3.29	
66y-1-31-33-Heated@500°C		12.39	11.45	9.97	6.62	4.98	4.34	3.76		3.31	
							3.24	2.87			

66y-1-45-47-Air		14.95			3.40			
66y-1-45-47-Glycolated		17.96	10.03					
66y-1-45-47-Heated@500°C			9.96	4.98	3.33	3.24	3.21	3.19
66y-1-60-62-Air		15.64	5.54	3.40	3.18	3.01		
66y-1-75-77-Air				14.39				3.11
66y-1-75-77-Glycolated		15.44		8.00	5.30			3.17
66y-1-75-77-Heated@500°C			10.86	9.81		4.91		3.27
66y-1-90-92-Air			9.86	5.02		3.32		
66y-1-90-92-Glycolated			10.04	4.95		3.32		
66y-1-90-92-Heated@500°C		11.08	10.00	5.02	3.69	3.32		
66y-1-105-107-Air		9.89	4.95	3.29				
66y-1-105-107-Glycolated		9.88	5.03	3.33				
66y-1-120-122-Air		9.83			3.31	3.22	3.19	
66y-1-120-122-Glycolated		9.83	6.41	4.96	3.33	3.22	3.18	
2A-66y-2								
66y-2-5-7-Air		10.10			4.92	3.32		
66y-2-5-7-Glycolated	11.30	9.79		6.54	4.95	3.33	3.23	3.18
66y-2-5-7-Heated@500°C	11.47	10.00	7.52	6.62	4.98	3.59	3.56	
						3.34	3.25	3.21
66y-2-20-22-Air		9.93	4.89	3.33				
66y-2-20-22-Glycolated		9.89	4.99	3.34				
66y-2-35-37-Air		21.15	10.11	4.95	3.32			
66y-2-35-37-Glycolated			10.04	4.97	3.33			
66y-2-50-52-Air			9.89	4.90		3.32		
66y-2-50-52-Glycolated			9.83	4.96		3.33		
66y-2-50-52-Heated@500°C		11.09	10.00	4.98	3.69	3.34		

66y-2-66-68-Air		9.84			4.96	3.31		
66y-2-66-68-Glycolated	11.21	9.76	6.54	6.40	4.95	3.33	3.22	3.19
66y-2-91-93-Air	10.16		4.90	3.33				
66y-2-91-93-Glycolated	9.85	6.45	4.96	3.33	3.22	3.19		
66y-2-102-104-Air		9.97		4.94	3.31			
66y-2-102-104-Glycolated		9.93		5.01	3.32			
66y-2-102-104-Heated@500°C	11.16	10.10	4.99	3.68	3.33			
66y-2-125-127-Air	9.93	6.40	4.92	3.31	3.23	3.19		
66y-2-125-127-Glycolated	9.94	6.39	4.95	3.33	3.22	3.19		
2A-67y-1								
67y-1-5-7-Air	9.84			4.95	3.32			
67y-1-5-7-Glycolated	9.79			4.94	3.33			
67y-1-5-7-K-Saturated	9.96			4.98	3.33			
67y-1-5-7-K-Saturated-Heated@300°C	9.95		7.55	6.48	4.98	3.32	3.25	3.21
67y-1-5-7-K-Saturated-Heated@500°C	11.07 9.96	8.37	7.54	6.49	4.98	3.77 3.33	3.59 3.25	3.21
67y-1-50-52-Air		9.80	4.93	3.32				
67y-1-50-52-Glycolated		9.74	4.96	3.32				
67y-1-95-97-Air	9.89	4.92	3.32					
67y-1-95-97-Glycolated	9.86	4.94	3.33					
67y-1-110-112-Air	9.78	4.95	3.34					
67y-1-110-112-Glycolated	9.79	4.96	3.33					
67y-1-110-112-Heated@500°C	9.85	4.94	3.31					
67y-1-125-127-air	11.33	9.82	6.42	4.96	3.77	3.33	3.23	3.19
67y-1-125-127-Glycolated		9.80	6.41	4.95	4.22		3.33	3.22
67y-1-125-127-Heated@500°C	11.09	9.97	6.63	4.99	4.26	3.69	3.33	3.25
67y-1-140-142-Air	11.21	9.85	8.81	4.94	3.33	3.18		
67y-1-140-142-Glycolated		9.81	8.81	4.93	3.32	3.18		
2A-67y-2								
67y-2-10-12-air	9.84	4.96	3.31	3.23	3.28			
67y-2-10-12-Glycolated	9.83	4.99	3.30					
67y-2-40-42-air	10.18	4.93	3.31	3.22	3.27			
67y-2-40-42-Glycolated	9.81	4.97	3.31					
67y-2-70-72-Air	9.86	4.97	3.30					
67y-2-70-72-Glycolated	9.76	5.04	3.32					
67y-2-98-100-air		9.88	4.93		3.30	3.24	3.28	
67y-2-98-100-Glycolated		9.85	4.97		3.32			
67y-2-98-100-Heated@500°C	11.09	10.04	5.02	3.67	3.33			
67y-2-142-144-Air	9.91	4.97	3.32	3.26	3.28			

2A-68y-1									
68y-1-12-14-Air	11.21	9.91		4.96		3.31			
68y-1-12-14-Glycolated	11.23	9.88		4.98		3.31			
68y-1-12-14-Heated@500°C	11.46	9.99	6.62	4.99	3.67	3.33	3.24	2.87	
2A-69y-2									
69y-2-142-143-Glycolated	11.13	6.51	4.46	4.29	3.87	3.28	3.22	3.19	
2A-70y-1									
70y-1-15-17-air	11.23	9.13		4.26		3.19			
70y-1-15-17-Glycolated	11.18	9.12	6.53	5.46	4.93	4.27	2.22	3.19	
70y-1-15-17-Heated@500°C	12.72	11.47	10.29	9.30	7.34	6.62	5.53	4.98	
				4.31	3.55	3.24	3.21	2.91	
70y-1-25-27-air		11.18	9.12	4.29	3.22				
70y-1-25-27-Glycolated		11.19	9.12	4.30	3.22				
70y-1-25-27-Heated@500°C	12.66	11.43	9.28	6.61	4.33	4.15	4.10	3.76	
	3.59	3.55	3.31	3.24	3.21	2.91	2.86	2.81	
70y-1-40-42-air		4.30				3.23			
70y-1-40-42-Glycolated	11.28	9.88	9.14	6.78	6.54	5.47	4.94	4.47	
		4.27	3.54	3.33	3.23	3.19	2.90	2.85	
70y-1-70-72-air	9.17	4.28	3.55	3.21					
70y-1-85-87-air	11.29	9.97		6.56		4.29	3.76	3.22	3.19
70y-1-85-87-Glycolated	11.24	9.87	9.15	8.32	6.55	4.93	4.31	3.80	3.54	3.23	3.19
								2.90	2.85	2.70
70y-1-115-117-air	11.22			6.56		4.30			
70y-1-115-117-Glycolated	11.24	9.82		6.53		4.30	3.30	3.19	
70y-1-130-132-air		11.20	9.96	6.54		4.28	3.77	3.54	
					3.29		3.19	2.85	
70y-1-130-132-Glycolated		11.19	9.84	6.53	4.93	4.30	3.80	3.54	
			3.29	3.22	3.18	2.90	2.85	2.80	
70y-1-130-132-Heated@500°C	12.68	11.45	10.07	9.30	8.94	7.92	6.62	4.97	
		4.80	4.33	3.96	3.82	3.75	3.67	3.55	
			3.31	3.25	3.21	2.92	2.87	2.81	
2A-70y-2									
70y-2-5-7-air	9.87				3.30				
70y-2-5-7-Glycolated	11.18	9.85	6.52	4.26	3.53	3.33	2.86		
70y-2-20-22-air	10.76	4.96	3.32	3.24					
70y-2-35-37-air	11.56	9.33			4.30	3.75			3.22
70y-2-35-37-Glycolated	11.22	9.80	6.54	4.93	4.27	3.73	3.54	3.32	3.22
						3.19	2.90	2.85	
70y-2-50-52-air	11.10	10.10		3.26					
70y-2-65-67-air		11.26						3.20	
70y-2-65-67-Glycolated		11.20	7.80	6.54	4.93	4.30	3.93	3.73	
						3.30	3.22	2.85	

70y-2-65-67-Heated@500°C	12.74	11.47	10.01 3.83	7.94 3.75	6.62 3.56 2.92	4.98 3.32 2.87	4.30 3.25 2.82	3.97 3.21
70y-2-80-82-air	11.23		4.27		3.53		3.18	
70y-2-80-82-Glycolated	11.17	9.11 3.54	6.53 3.29	5.55 3.20	4.93 2.90	4.26 2.85	3.73 2.80	2.67
70y-2-110-112-Air			4.29		3.17			
70y-2-110-112-Glycolated		11.21	8.79 3.29	6.53 3.22	4.94 3.16	4.30 2.90	3.73 2.85	3.54
70y-2-110-112-Heated@500°C	12.69	11.46 3.31	9.91 3.24	6.62 3.21	4.98 3.18	4.34 2.92	3.83 2.87	3.56 2.82
70y-2-125-127-air	11.16	9.22	7.01 3.74	3.55	6.55 3.15	5.41	4.95 2.90	4.28 2.85
70y-2-125-127-Glycolated	11.18	9.13 4.30	8.78 3.73	6.10 3.54 2.90	6.53 3.41 2.85	5.67 3.29 2.80	5.46 3.22 2.66	4.93 3.15
70y-2-135-137-air		11.25					4.29	
70y-2-135-137-Glycolated		11.20	9.15	6.99 3.15	2.90	4.94 2.86	4.30	3.73
70y-2-135-137-Heated@500°C	12.74	11.46	9.91 3.56	6.62 3.31	5.52 3.25	4.97 2.92	4.34 2.87	3.75 2.82
2A-76y-1								
76y-1-67-69-Air			9.83	4.96	3.32	3.22		
76y-1-67-69-Glycolated			9.83	4.96	3.33			
76y-1-67-69-Heated@500°C	11.09		10.00	4.99	3.69	3.34		
2A-76y-2								
76y-2-6-9-Air	11.23	9.88	7.04	4.95	4.28	3.55	3.33	2.90
76y-2-6-9-Glycolated		9.87	7.03	4.95	4.28	3.55	3.33	3.17	2.91
76y-2-6-9-Heated@500°C	11.08	10.01	10.00	6.90	5.53	4.99 3.24	4.32 2.93	3.69 2.88	3.34
2A-80y-1								
80y-1-5-7-Air	9.84	4.95	3.33					
80y-1-5-7-Glycolated	9.82	4.97	3.33					
80y-1-71-73-air		9.94	4.97	4.44			3.33	
80y-1-71-73-Glycolated		9.82	5.54	4.96	4.47		3.34	
80y-1-71-73-Heated@500°C	11.07	10.02	5.01			3.70	3.33	
80y-1-113-115-Air	9.87	4.95	3.33	3.22				
80y-1-113-115-Glycolated	9.80	4.95	3.33					
2A-80y-2								
80y-2-11-13-Air	9.82	8.32 3.33		5.53 3.22	4.97 3.22	4.28 3.17	3.74 2.98	3.41 2.91

80y-2-11-13-Glycolated		9.82	8.32	6.96	5.53		4.97	4.45	3.73
					3.40	3.33	3.21	3.17	
80y-2-11-13-Heated@500°C	11.06	9.97		6.47	5.56	5.01	4.50	4.33	3.69
	3.60	3.54	3.34	3.25	3.22	3.21	3.19	2.93	2.90
80y-2-26-28-air	10.26	9.83	5.53		4.93	3.40	3.33	3.23	3.17
					3.01				
80y-2-26-28-Glycolated	9.84		5.52		4.94	3.40	3.32	3.22	
			3.01		2.91				
80y-2-42-44-Air	9.86	4.95			3.33				
80y-2-42-44-Glycolated	9.82	4.94	3.51		3.33				
80y-2-90-92-Air			9.83		6.40		5.54	4.96	4.01
				3.41	3.34	3.23		2.91	2.68
80y-2-90-92-Glycolated			9.86		6.38		5.53	4.94	
80y-2-90-92-Heated@500°C	11.08		10.00	8.43	6.50	6.03	5.46	4.99	4.04
			3.69	3.60	3.33	3.25	3.19	2.84	
80y-2-103-105-Air			9.85	5.54	4.81	3.41	3.33	3.21	2.91
80y-2-103-105-Glycolated			9.80	5.53	4.94	3.40	3.33	3.17	2.90
							2.67		
80y-2-103-105-Heated@500°C	11.08		10.01	8.47	5.39	4.99	4.50	3.69	3.55
				3.44	3.33	3.28	3.22	2.93	2.85
80y-2-113-115-air	9.88	5.54		4.95		3.41	3.34	3.19	2.91
80y-2-113-115-Glycolated	9.89	6.98		5.54	4.98	4.80	3.41	3.33	3.19
							2.91	2.67	

Appendix C: XRF Analysis

X-ray Fluorescence was conducted at Franklin & Marshall College by Prof. Stanley A Mertzman Jr.. The process entailed determining loss of ignition, XRF and major elements techniques.

Appendix C.1

Loss on Ignition (LOI) – Determining the Total Volatile Content

1. Turn muffle furnace on and set control dial at obvious mark. Do so approximately two hours before you want to start procedure in order to bring temperature of furnace up to desired temperature of 950°C.

2. Turn on electronic balance and calibrate it at beginning of the workday.

3. Remove wire basket from large desiccator near furnace. Using a forceps to move crucible, not your fingers, weigh the clean and dry porcelain crucible directly. Note and record its name from the outside bottom of the crucible. Also record sample powder name which is being weighed into crucible. No weighing paper is required. As usual, record all weighing to four decimal places.

4. Add approximately 1 gram of finely ground rock powder.

5. Record weight of crucible plus sample. Make sure bottom of crucible has some identifying mark; if not, make one by scratching bottom of crucible.

6. Do steps 3 through 5 for each of your sample powders. A maximum of 8 samples can be done at one time.

7. Place in muffle furnace for 90 minutes at 950° C.

8. Remove basket from furnace and place in desiccator as quickly as possible. Let cool to room temperature and weigh. (Keep in mind the demonstration of this procedure).

9. Weight of sample before heating minus the weight after heating is “initial” loss on ignition.

(NOTE: if sample has lost weight, the loss is positive; if it has gained weight, the loss is negative).

10. Determine % loss on ignition by dividing “initial loss” by initial weight of sample and multiply by 100.

11. SAVE the LOI sample powder in a small vial labeled with the sample number. Place vial in a desiccator. This material is the starting point for the major element technique.

Last Revised: June 2018

Appendix C.2

X-ray Laboratory Instrumentation

X-ray Laboratory Instrumentation

The X-ray lab contains two major research instruments. The first is a Malvern PANalytical, Inc. Zetium X-ray fluorescence vacuum spectrometer that was installed and calibrated in mid-January 2019. A major step forward with this generation of XRF spectrometers is the 4kW Rh super sharp X-ray tube that maintains its output x-ray intensity over the life of the tube. The sample deck is capable of holding 68 individual samples when fully loaded. The lab also has a Malvern PANalytical X'Pert PRO X-ray diffractometer equipped with a 15-position sample changer and a ceramic Cu X-ray tube. Standard phase identification and Rietveld analysis are our forte. Both instruments are available for contract work. Please contact Dr. Stan Mertzman for details concerning cost per analysis, turnaround time, etc.

The personnel who handle day-to-day operation of the X-ray instrumentation are Dr. Stan Mertzman, the Earl D. Stage and Mary E. Stage Professor of Geosciences, Emily Wilson, Research Specialist, and Karen Mertzman, senior lab technician.

X-Ray Fluorescence

Sample preparation for major element analysis

To start, a total volatile determination (% LOI) is made by weighing out ~1 gram of sample to 4 decimal places, placing in a muffle furnace at 950C for 1.5 hours, removing and cooling to room temperature in a desiccator, and re-weighing and noting the weight change. A portion of this anhydrous sample powder (0.4000 +/- 0.0001 grams) is mixed with lithium tetraborate (3.6000 +/- 0.0002 grams), placed in a platinum crucible and heated with a meeker burner until molten. This molten material is swirled and mixed several time over 10-12 minutes and transferred to a platinum casting dish and quenched. This procedure produces a glass disk that is used for XRF analysis including SiO_2, TiO2, Al_2O_3, Fe2O3 Total, MnO, MgO, CaO, Na2O, K_2O, and P_2O_5,

Working curves for each element are determined by analyzing geochemical rock standards prepared exactly as described in the paragraph above. (See Abbey (1983) and Govindaraju (1994) for chemical analyses of the rock standards). Between 50 and 60 data points are gathered for each working curve; various element interferences are also taken into account. Results are calculated and presented as percent oxide.

Ferrous iron titration and Loss on Ignition

The amount of ferrous Fe is determined by the titration using a modified Reichen and Fahey (1962) method. XRF determines total iron as Fe_2O_3. Loss on ignition is determined by heating an exact aliquot of the sample at 950°C for 1.5 hours.

Important

Always keep in mind that the original rock or mineral powder must be crushed so the ALL of the sample passes through a clean 80-mesh sieve screen. Do NOT use Tungsten Carbide grinding vessels if at all possible. Always use alumina or ceramic crushing implements if available.

References

Bennett, H. and Oliver, G. 1992, XRF Analysis of Ceramic, Minerals and Allied Materials, John Wiley &Sons, LTD (ISBN 0 471 93457 7 (cloth)) pp. 298.

Boyd, F.R., and Mertzman, S.A., (1987): Composition of structure of the Kaapvaal lithosphere, southern Africa: In Magmatic Processes- Physiochemical Principles, B.O. Mysen, Ed., The Geochemical Society, Special Publication #1, pp. 13-24. (Contains description of XRF methodology).

Jenkins, R., 1999, X-Ray Fluorescence Spectrometry, 2nd ed., John Wiley & Sons, Inc. (ISBN 0-471-29942-1 (cloth)) 207 pp.

Mertzman, S.A., 2000, K-Ar results from the Southern Oregon- Northern California Cascade Range. Oregon Geology, V. 62, no. 4, pp.99-122.

Reichen, L.E., Fayey, J.J. (1962) An improvied metod for the determination of FeO in rocks and minerals including garnet. United States Geological Survey Bulletin 1144-B.

Waterton, P., Pearson, D. G., Mertzman, S. A., Mertzman, K. R., Kiarsgaard, B.: Komatiites, basalts and dunites: Plumbing system of a Proterozoic greenstone belt (submitted to Journal of Petrology February 2019)

Last Revised 04-01-2019.

Appendix C.3

Major Element Technique

Major Element Technique

A. Lithium Tetraborate-whole rock powder preparation- Introduction

3.6000 grams +/- 0.0002 of lithium tetraborate is weighed out into a clean glass bottle followed by 0.4000 grams +/- 0.0001 of the anhydrous rock powder that results from the LOI technique. An initial mixing is done by hand, gently rolling the bottle in your hands to gently mix the two powders. After 20 to 30 seconds of hand mixing the bottle is transferred to a Spex Mixer Mill for 10 minutes. The homogenous powder is transferred into a 25 cc. 95% Pt-5% Au crucible, 3-4 drops of a 2% solution of Lithium Iodide is added to the powder to reduce the viscosity of the mixture as it is heated over a Meeker burner while mounted on a standard ring stand. During the heating, the crucible is covered with a 95% Pt-5% Au lid that will also act a mold into which the molten sample will be poured and cast into a disc shape. The bottom of the Pt lid is flat and highly polished, thus, the side of the disc in contact with the Pt lid is the one exposed to the primary X-ray beam.

The heating period is usually 12-15 minutes in duration with the sample being vigorously stirred while holding the crucible with a pair of Nichrome tongs at both the 5-minute and 10 minute marks. After sufficient heating, so that the sample is fully convecting, the Pt lid is removed from the crucible with a pair of tongs and is heated over a second meeker burner until it is red hot. With a second pair of tongs the crucible is removed rapidly from suspension on the ring stand over the first burner and emptied onto the hot Pt lid. With some practice, virtually all of the crucible's contents are transferred to the lid. Immediately upon completing the pouring event, the still hot crucible is dropped into a warm beaker containing sufficient 4N HCl to cover the crucible. With the other hand, the lid, which has been held quite level, is now set down on a flat surface, in our lab this is a flat slab of polished granite. The sample will cool in 3 to 5 minutes so that the glass disc can be labeled with a magic marker, labeled on the side of the disc that was exposed to the air. The sample can be stored indefinitely in a dessicator. The major element oxides, SiO_2, Al_2O_3, Fe_2O_3T (where T = total iron), MnO, K_2O, Na_2O, TiO_2, P_2O_5, CaO, MgO, are determined using this technique together with Sr, Zr, Cr and V.

Safety Warning: Lithium tetraborate poses a hazard to skin, eyes, and internal organs. For more information See www.fishersci.com/msds Acetone poses health and fire hazards. For more information see www.fishersci.com/msds
Lithium iodide poses a hazard to skin, eyes, and respiratory system. For more information see www.fishersci.com/msds

Instructions:

1) Thoroughly clean and dry several glass sample bottles (24 ml glass bottles made by Wheaton) and lids if clean bottles are not already available. The final cleaning step is always to rinse in acetone and lay bottle on its side and the plastic caps up on a paper towel for the purposes of drying.
2) Weigh out 3.6000 +/- 0.0002 of Li_2B_4O7 onto a piece of weighing paper (previously weighed and tared) and transfer to a clean glass bottle. Label glass bottle with magic marker (not lid) with sample number followed by WR (whole rock) or M (major).
3) Weigh out 0.4000 +/- 0.0001 of anhydrous whole rock powder onto a piece of weighing paper (previously weighed and tared) and transfer to the same bottle as in step 2.
4) Carefully rotate sample bottle in your hands so as to mix the powders without letting them touch the lid.
5) Make sure you have labeled the bottle!!!
6) Mix sample for 10 minutes in the Spex mixer mill.
7) If you stop at this step without going onto Part B, store bottle in a dessicator.

B. **Fuse the sample to make the glass disc per demonstration given by your instructor.** Key factor to always remember- mix your liquid sample three times in the Pt crucible, once at the 5-minute mark again at 10-12 minutes, and the third time just before pouring into the Pt lid. Also, be sure to incline the Pt crucible in the flame before pouring to break the surface tension between liquid and metal so that most or the entire sample will be used in casting the glass disc. You must mix three times to insure sample homogeneity.

C. Do not forget the following items:

a) When fusing the sample, always wear safety goggles.
b) Add 2-3 drops of Lithium Iodide (LiI) solution to powder after it has been transferred to Pt crucible, from small, labeled plastic squeeze bottle.

1) Be extremely careful in cleaning Pt lid! DO NOT SCRATCH!!!
2) With a magic marker, label sample number on concave side of the glass disc, which is the side that cools in contact with air.
3) Place ½ of a small kimwipe in the bottom of a pillbox and put glass disc, label side up, into the container and cover with lid. Do not label the pillbox itself.
4) Store pillbox in a dessicator.
5) Clean the glass bottles and caps you used in distilled water, using a scrub brush. Rinse in distilled water and then rinse with acetone and let dry in air on a paper towel for an hour or so. Lay the bottles on their sides to dry. Recap and put back into the storage trays.

Appendix D: 2-1 Clay

The calculation for 2-1 clay minerals formula from selected 20 samples

	Oxide	Valence	*Cation charge*	Wt %	Form. Wt.	Eq. wt.	Charge/ gm. Equiv	Cat. Ch/ f. unit	No. cat./ f. unit
61y-1-84-86	SiO_2	4	4	64.80	60.084	15.021	4.314	16.247	4.062
	TiO_2	4	4	0.88	79.898	19.975	0.044	0.166	0.041
	Al_2O_3	3	6	14.22	101.959	16.993	0.837	3.152	1.051
	Fe_2O_3	3	6	7.29	159.691	26.615	0.274	1.032	0.344
	FeO	2	2		71.846	35.923	0.000	0.000	0.000
	MgO	2	2	1.97	40.304	20.152	0.098	0.368	0.184
	CaO	2	2	1.37	56.079	28.040	0.049	0.184	0.092
	Na_2O	1	2	3.82	61.979	30.990	0.123	0.464	0.464
	K_2O	1	2	4.84	94.195	47.098	0.103	0.387	0.387

Tetra	Octa	Inter	Net	Total positive charge	5.841	Pos. Ch
4.062	1.620	0.648		Total negative charge	22	22.0
0.062	-0.380		-0.318	postive/ negative	0.27	

	Oxide	Valence	*Cation charge*	Wt %	Form. Wt.	Eq. wt.	Charge/ gm. Equiv	Cat. Ch/ f. unit	No. cat./ f. unit
61y-2-40-42	SiO_2	4	4	61.62	60.084	15.021	4.102	15.658	3.914
	TiO_2	4	4	1.34	79.898	19.975	0.067	0.256	0.064
	Al_2O_3	3	6	15.03	101.959	16.993	0.884	3.376	1.125
	Fe_2O_3	3	6	8.00	159.691	26.615	0.301	1.147	0.382
	FeO	2	2		71.846	35.923	0.000	0.000	0.000
	MgO	2	2	2.38	40.304	20.152	0.118	0.451	0.225
	CaO	2	2	1.87	56.079	28.040	0.067	0.255	0.127
	Na_2O	1	2	3.78	61.979	30.990	0.122	0.466	0.466
	K_2O	1	2	4.84	94.195	47.098	0.103	0.392	0.392

Tetra	Octa	Inter	Net	Total positive charge	5.764	Pos. Ch
3.914	1.797	0.647		Total negative charge	22	22.0
-0.086	-0.203		-0.288	postive/ negative	0.26	

	Oxide	Valence	*Cation charge*	Wt %	Form. Wt.	Eq. wt.	Charge/ gm. Equiv	Cat. Ch/ f. unit	No. cat./ f. unit
62y-1-140-142	SiO_2	4	4	61.88	60.084	15.021	4.120	15.665	3.916
	TiO_2	4	4	1.39	79.898	19.975	0.070	0.265	0.066
	Al_2O_3	3	6	15.40	101.959	16.993	0.906	3.446	1.149
	Fe_2O_3	3	6	7.78	159.691	26.615	0.292	1.112	0.371
	FeO	2	2		71.846	35.923	0.000	0.000	0.000
	MgO	2	2	2.25	40.304	20.152	0.112	0.425	0.212
	CaO	2	2	1.67	56.079	28.040	0.060	0.226	0.113
	Na_2O	1	2	4.01	61.979	30.990	0.129	0.492	0.492
	K_2O	1	2	4.57	94.195	47.098	0.097	0.369	0.369

Tetra	Octa	Inter	Net	Total positive charge	5.785	Pos. Ch
3.916	1.798	0.595		Total negative charge	22	22.0
-0.084	-0.202		-0.286	postive/ negative	0.26	

	Oxide	Valence	*Cation charge*	Wt %	Form. Wt.	Eq. wt.	Charge/ gm. Equiv	Cat. Ch/ f. unit	No. cat./ f. unit
62y-2-65-67	SiO_2	4	4	59.68	60.084	15.021	3.973	15.267	3.817
	TiO_2	4	4	1.52	79.898	19.975	0.076	0.292	0.073
	Al_2O_3	3	6	15.71	101.959	16.993	0.924	3.552	1.184
	Fe_2O_3	3	6	8.80	159.691	26.615	0.331	1.271	0.424
	FeO	2	2		71.846	35.923	0.000	0.000	0.000
	MgO	2	2	2.31	40.304	20.152	0.115	0.440	0.220
	CaO	2	2	2.18	56.079	28.040	0.078	0.299	0.149
	Na_2O	1	2	4.07	61.979	30.990	0.131	0.505	0.505
	K_2O	1	2	4.58	94.195	47.098	0.097	0.374	0.374

Tetra	Octa	Inter	Net	Total positive charge	5.725	Pos. Ch
3.817	1.901	0.672		Total negative charge	22	22.0
-0.183	-0.099		-0.282	postive/ negative	0.26	

	Oxide	Valence	*Cation charge*	Wt %	Form. Wt.	Eq. wt.	Charge/ gm. Equiv	Cat. Ch/ f. unit	No. cat./ f. unit
63y-1-5-7	SiO_2	4	4	57.77	60.084	15.021	3.846	14.926	3.732
	TiO_2	4	4	1.80	79.898	19.975	0.090	0.350	0.087
	Al_2O_3	3	6	15.16	101.959	16.993	0.892	3.462	1.154
	Fe_2O_3	3	6	11.97	159.691	26.615	0.450	1.745	0.582
	FeO	2	2		71.846	35.923	0.000	0.000	0.000
	MgO	2	2	2.99	40.304	20.152	0.148	0.576	0.288
	CaO	2	2	0.81	56.079	28.040	0.029	0.112	0.056
	Na_2O	1	2	3.17	61.979	30.990	0.102	0.397	0.397
	K_2O	1	2	5.23	94.195	47.098	0.111	0.431	0.431

Tetra	Octa	Inter	Net	Total positive charge	5.669	Pos. Ch
3.732	2.111	0.543		Total negative charge	22	22.0
-0.268	0.111		-0.157	postive/ negative	0.26	

	Oxide	Valence	*Cation charge*	Wt %	Form. Wt.	Eq. wt.	Charge/ gm. Equiv	Cat. Ch/ f. unit	No. cat./ f. unit
63y-1-123-125	SiO_2	4	4	59.57	60.084	15.021	3.966	15.186	3.797
	TiO_2	4	4	1.70	79.898	19.975	0.085	0.326	0.081
	Al_2O_3	3	6	15.69	101.959	16.993	0.923	3.536	1.179
	Fe_2O_3	3	6	10.52	159.691	26.615	0.395	1.514	0.505
	FeO	2	2		71.846	35.923	0.000	0.000	0.000
	MgO	2	2	2.64	40.304	20.152	0.131	0.502	0.251
	CaO	2	2	0.60	56.079	28.040	0.021	0.082	0.041
	Na_2O	1	2	3.69	61.979	30.990	0.119	0.456	0.456
	K_2O	1	2	4.91	94.195	47.098	0.104	0.399	0.399

Tetra	Octa	Inter	Net	Total positive charge	5.745	Pos. Ch
3.797	2.015	0.481		Total negative charge	22	22.0
-0.203	0.015		-0.188	postive/ negative	0.26	

	Oxide	Valence	*Cation charge*	Wt %	Form. Wt.	Eq. wt.	Charge/ gm. Equiv	Cat. Ch/ f. unit	No. cat./ f. unit
64y-1-20-22	SiO_2	4	4	58.49	60.084	15.021	3.894	15.119	3.780
	TiO_2	4	4	2.21	79.898	19.975	0.111	0.430	0.107
	Al_2O_3	3	6	13.27	101.959	16.993	0.781	3.032	1.011
	Fe_2O_3	3	6	14.66	159.691	26.615	0.551	2.139	0.713
	FeO	2	2		71.846	35.923	0.000	0.000	0.000
	MgO	2	2	2.79	40.304	20.152	0.138	0.538	0.269
	CaO	2	2	0.35	56.079	28.040	0.012	0.048	0.024
	Na_2O	1	2	1.89	61.979	30.990	0.061	0.237	0.237
	K_2O	1	2	5.56	94.195	47.098	0.118	0.458	0.458

Tetra	Octa	Inter	Net	Total positive charge	5.666	Pos. Ch
3.780	2.100	0.507		Total negative charge	22	22.0
-0.220	0.100		-0.121	postive/ negative	0.26	

	Oxide	Valence	*Cation charge*	Wt %	Form. Wt.	Eq. wt.	Charge/ gm. Equiv	Cat. Ch/ f. unit	No. cat./ f. unit
64y-1-65-67	SiO_2	4	4	59.86	60.084	15.021	3.985	15.235	3.809
	TiO_2	4	4	1.48	79.898	19.975	0.074	0.283	0.071
	Al_2O_3	3	6	15.50	101.959	16.993	0.912	3.487	1.162
	Fe_2O_3	3	6	10.92	159.691	26.615	0.410	1.569	0.523
	FeO	2	2		71.846	35.923	0.000	0.000	0.000
	MgO	2	2	2.89	40.304	20.152	0.143	0.548	0.274
	CaO	2	2	1.48	56.079	28.040	0.053	0.202	0.101
	Na_2O	1	2	2.24	61.979	30.990	0.072	0.276	0.276
	K_2O	1	2	4.92	94.195	47.098	0.104	0.399	0.399

Tetra	Octa	Inter	Net	Total positive charge	5.755	Pos. Ch
3.809	2.030	0.601		Total negative charge	22	22.0
-0.191	0.030		-0.161	postive/ negative	0.26	

	Oxide	Valence	*Cation charge*	Wt %	Form. Wt.	Eq. wt.	Charge/ gm. Equiv	Cat. Ch/ f. unit	No. cat./ f. unit
64y-2-18-20	SiO_2	4	4	59.72	60.084	15.021	3.976	15.254	3.814
	TiO_2	4	4	1.46	79.898	19.975	0.073	0.280	0.070
	Al_2O_3	3	6	15.57	101.959	16.993	0.916	3.515	1.172
	Fe_2O_3	3	6	10.96	159.691	26.615	0.412	1.580	0.527
	FeO	2	2		71.846	35.923	0.000	0.000	0.000
	MgO	2	2	2.56	40.304	20.152	0.127	0.487	0.244
	CaO	2	2	0.71	56.079	28.040	0.025	0.097	0.049
	Na_2O	1	2	3.10	61.979	30.990	0.100	0.384	0.384
	K_2O	1	2	4.93	94.195	47.098	0.105	0.402	0.402

Tetra	Octa	Inter	Net	Total positive charge	5.734	Pos. Ch
3.814	2.012	0.499		Total negative charge	22	22.0
-0.186	0.012		-0.174	postive/ negative	0.26	

	Oxide	Valence	*Cation charge*	Wt %	Form. Wt.	Eq. wt.	Charge/ gm. Equiv	Cat. Ch/ f. unit	No. cat./ f. unit
64y-3-15-17	SiO_2	4	4	60.10	60.084	15.021	4.001	15.257	3.814
	TiO_2	4	4	1.46	79.898	19.975	0.073	0.279	0.070
	Al_2O_3	3	6	15.85	101.959	16.993	0.933	3.557	1.186
	Fe_2O_3	3	6	9.67	159.691	26.615	0.363	1.385	0.462
	FeO	2	2		71.846	35.923	0.000	0.000	0.000
	MgO	2	2	2.53	40.304	20.152	0.126	0.479	0.239
	CaO	2	2	1.78	56.079	28.040	0.063	0.242	0.121
	Na_2O	1	2	3.45	61.979	30.990	0.111	0.425	0.425
	K_2O	1	2	4.65	94.195	47.098	0.099	0.376	0.376

Tetra	Octa	Inter	Net	Total positive charge	5.769	Pos. Ch
3.814	1.956	0.619		Total negative charge	22	22.0
-0.186	-0.044		-0.229	postive/ negative	0.26	

	Oxide	Valence	*Cation charge*	Wt %	Form. Wt.	Eq. wt.	Charge/ gm. Equiv	Cat. Ch/ f. unit	No. cat./ f. unit
65y-1-50-52	SiO_2	4	4	61.08	60.084	15.021	4.066	15.562	3.890
	TiO_2	4	4	1.18	79.898	19.975	0.059	0.226	0.057
	Al_2O_3	3	6	14.77	101.959	16.993	0.869	3.326	1.109
	Fe_2O_3	3	6	7.27	159.691	26.615	0.273	1.045	0.348
	FeO	2	2		71.846	35.923	0.000	0.000	0.000
	MgO	2	2	1.95	40.304	20.152	0.097	0.370	0.185
	CaO	2	2	4.81	56.079	28.040	0.172	0.656	0.328
	Na_2O	1	2	3.78	61.979	30.990	0.122	0.467	0.467
	K_2O	1	2	4.27	94.195	47.098	0.091	0.347	0.347

Tetra	Octa	Inter	Net	Total positive charge	5.749	Pos. Ch
3.890	1.699	1.003		Total negative charge	22	22.0
-0.110	-0.301		-0.411	postive/ negative	0.26	

	Oxide	Valence	*Cation charge*	Wt %	Form. Wt.	Eq. wt.	Charge/ gm. Equiv	Cat. Ch/ f. unit	No. cat./ f. unit
65y-2-52-54	SiO_2	4	4	58.24	60.084	15.021	3.877	15.041	3.760
	TiO_2	4	4	1.43	79.898	19.975	0.072	0.278	0.069
	Al_2O_3	3	6	14.22	101.959	16.993	0.837	3.246	1.082
	Fe_2O_3	3	6	10.41	159.691	26.615	0.391	1.517	0.506
	FeO	2	2		71.846	35.923	0.000	0.000	0.000
	MgO	2	2	3.16	40.304	20.152	0.157	0.608	0.304
	CaO	2	2	4.05	56.079	28.040	0.144	0.560	0.280
	Na_2O	1	2	2.90	61.979	30.990	0.094	0.363	0.363
	K_2O	1	2	4.68	94.195	47.098	0.099	0.385	0.385

Tetra	Octa	Inter	Net	Total positive charge	5.671	Pos. Ch
3.760	1.961	0.946		Total negative charge	22	22.0
-0.240	-0.039		-0.278	postive/ negative	0.26	

	Oxide	Valence	*Cation charge*	Wt %	Form. Wt.	Eq. wt.	Charge/ gm. Equiv	Cat. Ch/ f. unit	No. cat./ f. unit
66y-1-75-77	SiO_2	4	4	60.89	60.084	15.021	4.054	15.563	3.891
	TiO_2	4	4	1.35	79.898	19.975	0.068	0.259	0.065
	Al_2O_3	3	6	13.54	101.959	16.993	0.797	3.059	1.020
	Fe_2O_3	3	6	7.90	159.691	26.615	0.297	1.140	0.380
	FeO	2	2		71.846	35.923	0.000	0.000	0.000
	MgO	2	2	1.74	40.304	20.152	0.086	0.331	0.166
	CaO	2	2	6.27	56.079	28.040	0.224	0.858	0.429
	Na_2O	1	2	4.29	61.979	30.990	0.138	0.531	0.531
	K_2O	1	2	3.16	94.195	47.098	0.067	0.258	0.258

Tetra	Octa	Inter	Net	Total positive charge	5.730	Pos. Ch
3.891	1.630	1.116		Total negative charge	22	22.0
-0.109	-0.370		-0.479	postive/ negative	0.26	

	Oxide	Valence	*Cation charge*	Wt %	Form. Wt.	Eq. wt.	Charge/ gm. Equiv	Cat. Ch/ f. unit	No. cat./ f. unit
66y-2-50-52	SiO_2	4	4	65.20	60.084	15.021	4.341	16.232	4.058
	TiO_2	4	4	0.94	79.898	19.975	0.047	0.176	0.044
	Al_2O_3	3	6	15.05	101.959	16.993	0.886	3.312	1.104
	Fe_2O_3	3	6	6.51	159.691	26.615	0.245	0.915	0.305
	FeO	2	2		71.846	35.923	0.000	0.000	0.000
	MgO	2	2	1.58	40.304	20.152	0.078	0.293	0.147
	CaO	2	2	1.54	56.079	28.040	0.055	0.205	0.103
	Na_2O	1	2	4.55	61.979	30.990	0.147	0.549	0.549
	K_2O	1	2	4.00	94.195	47.098	0.085	0.318	0.318

Tetra	Octa	Inter	Net	Total positive charge	5.883	Pos. Ch
4.058	1.599	0.523		Total negative charge	22	22.0
0.058	-0.401		-0.342	postive/ negative	0.27	

	Oxide	Valence	*Cation charge*	Wt %	Form. Wt.	Eq. wt.	Charge/ gm. Equiv	Cat. Ch/ f. unit	No. cat./ f. unit
66y-2-102-104	SiO_2	4	4	64.13	60.084	15.021	4.269	16.014	4.004
	TiO_2	4	4	1.06	79.898	19.975	0.053	0.199	0.050
	Al_2O_3	3	6	15.60	101.959	16.993	0.918	3.444	1.148
	Fe_2O_3	3	6	6.75	159.691	26.615	0.254	0.951	0.317
	FeO	2	2		71.846	35.923	0.000	0.000	0.000
	MgO	2	2	1.74	40.304	20.152	0.086	0.324	0.162
	CaO	2	2	1.22	56.079	28.040	0.044	0.163	0.082
	Na_2O	1	2	4.69	61.979	30.990	0.151	0.568	0.568
	K_2O	1	2	4.23	94.195	47.098	0.090	0.337	0.337

Tetra	Octa	Inter	Net	Total positive charge	5.865	Pos. Ch
4.004	1.677	0.500		Total negative charge	22	22.0
0.004	-0.323		-0.320	postive/ negative	0.27	

	Oxide	Valence	*Cation charge*	Wt %	Form. Wt.	Eq. wt.	Charge/ gm. Equiv	Cat. Ch/ f. unit	No. cat./ f. unit
67y-1-140-142	SiO_2	4	4	63.79	60.084	15.021	4.247	16.011	4.003
	TiO_2	4	4	0.81	79.898	19.975	0.041	0.153	0.038
	Al_2O_3	3	6	15.70	101.959	16.993	0.924	3.483	1.161
	Fe_2O_3	3	6	5.19	159.691	26.615	0.195	0.735	0.245
	FeO	2	2		71.846	35.923	0.000	0.000	0.000
	MgO	2	2	1.31	40.304	20.152	0.065	0.245	0.123
	CaO	2	2	3.17	56.079	28.040	0.113	0.426	0.213
	Na_2O	1	2	4.90	61.979	30.990	0.158	0.596	0.596
	K_2O	1	2	4.38	94.195	47.098	0.093	0.351	0.351

Tetra	Octa	Inter	Net	Total positive charge	5.835	Pos. Ch
4.003	1.567	0.777		Total negative charge	22	22.0
0.003	-0.433		-0.430	postive/ negative	0.27	

	Oxide	Valence	*Cation charge*	Wt %	Form. Wt.	Eq. wt.	Charge/ gm. Equiv	Cat. Ch/ f. unit	No. cat./ f. unit
67y-2-10-12	SiO_2	4	4	62.01	60.084	15.021	4.128	15.670	3.917
	TiO_2	4	4	1.20	79.898	19.975	0.060	0.228	0.057
	Al_2O_3	3	6	15.05	101.959	16.993	0.886	3.362	1.121
	Fe_2O_3	3	6	9.00	159.691	26.615	0.338	1.284	0.428
	FeO	2	2		71.846	35.923	0.000	0.000	0.000
	MgO	2	2	2.17	40.304	20.152	0.108	0.409	0.204
	CaO	2	2	1.52	56.079	28.040	0.054	0.206	0.103
	Na_2O	1	2	3.86	61.979	30.990	0.125	0.473	0.473
	K_2O	1	2	4.59	94.195	47.098	0.097	0.370	0.370

Tetra	Octa	Inter	Net	Total positive charge	5.796	Pos. Ch
3.917	1.810	0.576		Total negative charge	22	22.0
-0.083	-0.190		-0.273	postive/ negative	0.26	

	Oxide	Valence	*Cation charge*	Wt %	Form. Wt.	Eq. wt.	Charge/ gm. Equiv	Cat. Ch/ f. unit	No. cat./ f. unit
67y-2-142-144	SiO_2	4	4	62.88	60.084	15.021	4.186	15.829	3.957
	TiO_2	4	4	1.30	79.898	19.975	0.065	0.246	0.062
	Al_2O_3	3	6	14.86	101.959	16.993	0.874	3.307	1.102
	Fe_2O_3	3	6	9.24	159.691	26.615	0.347	1.313	0.438
	FeO	2	2		71.846	35.923	0.000	0.000	0.000
	MgO	2	2	2.24	40.304	20.152	0.111	0.420	0.210
	CaO	2	2	0.25	56.079	28.040	0.009	0.034	0.017
	Na_2O	1	2	3.64	61.979	30.990	0.117	0.444	0.444
	K_2O	1	2	5.07	94.195	47.098	0.108	0.407	0.407

Tetra	Octa	Inter	Net	Total positive charge	5.818	Pos. Ch
3.957	1.811	0.441		Total negative charge	22	22.0
-0.043	-0.189		-0.231	postive/ negative	0.26	

	Oxide	Valence	*Cation charge*	Wt %	Form. Wt.	Eq. wt.	Charge/ gm. Equiv	Cat. Ch/ f. unit	No. cat./ f. unit
76y-1-67-69	SiO_2	4	4	61.98	60.084	15.021	4.126	15.636	3.909
	TiO_2	4	4	0.99	79.898	19.975	0.050	0.188	0.047
	Al_2O_3	3	6	16.23	101.959	16.993	0.955	3.619	1.206
	Fe_2O_3	3	6	6.30	159.691	26.615	0.237	0.897	0.299
	FeO	2	2		71.846	35.923	0.000	0.000	0.000
	MgO	2	2	2.12	40.304	20.152	0.105	0.399	0.199
	CaO	2	2	1.86	56.079	28.040	0.066	0.251	0.126
	Na_2O	1	2	5.01	61.979	30.990	0.162	0.613	0.613
	K_2O	1	2	4.94	94.195	47.098	0.105	0.397	0.397

Tetra	Octa	Inter	Net	Total positive charge	5.806	Pos. Ch
3.909	1.752	0.649		Total negative charge	22	22.0
-0.091	-0.248		-0.339	postive/ negative	0.26	

	Oxide	Valence	*Cation charge*	Wt %	Form. Wt.	Eq. wt.	Charge/ gm. Equiv	Cat. Ch/ f. unit	No. cat./ f. unit
80y-1-71-73	SiO_2	4	4	57.26	60.084	15.021	3.812	14.790	3.698
	TiO_2	4	4	1.45	79.898	19.975	0.073	0.282	0.070
	Al_2O_3	3	6	15.04	101.959	16.993	0.885	3.434	1.145
	Fe_2O_3	3	6	12.52	159.691	26.615	0.470	1.825	0.608
	FeO	2	2		71.846	35.923	0.000	0.000	0.000
	MgO	2	2	4.32	40.304	20.152	0.214	0.832	0.416
	CaO	2	2	0.70	56.079	28.040	0.025	0.097	0.048
	Na_2O	1	2	1.99	61.979	30.990	0.064	0.249	0.249
	K_2O	1	2	5.96	94.195	47.098	0.127	0.491	0.491

Tetra	Octa	Inter	Net	Total positive charge	5.670	Pos. Ch
3.698	2.239	0.588		Total negative charge	22	22.0
-0.302	0.239		-0.063	postive/ negative	0.26	

Appendix E: X-ray Diffraction Patterns

Appendix E.1

The patterns were with select d-spacings Labeled (Air Dried, Glycol Solvated, Heated). The used abbreviated symbols are Afs: alkali feldspar, Cb: carbonate mineral (Ank: Ankerite, Dol: Dolomite, Str: Strontianite), Ilt: illite, Kln: kaolinite, Pl: plagioclase feldspar, Qz: quartz, Sme: smectite, Zeo: zeolite (Anl: Analcime, Cpt: Clinoptilolite, Hul: Heulandite, Php: Phillipsite) (Whitney & Evans, 2009).

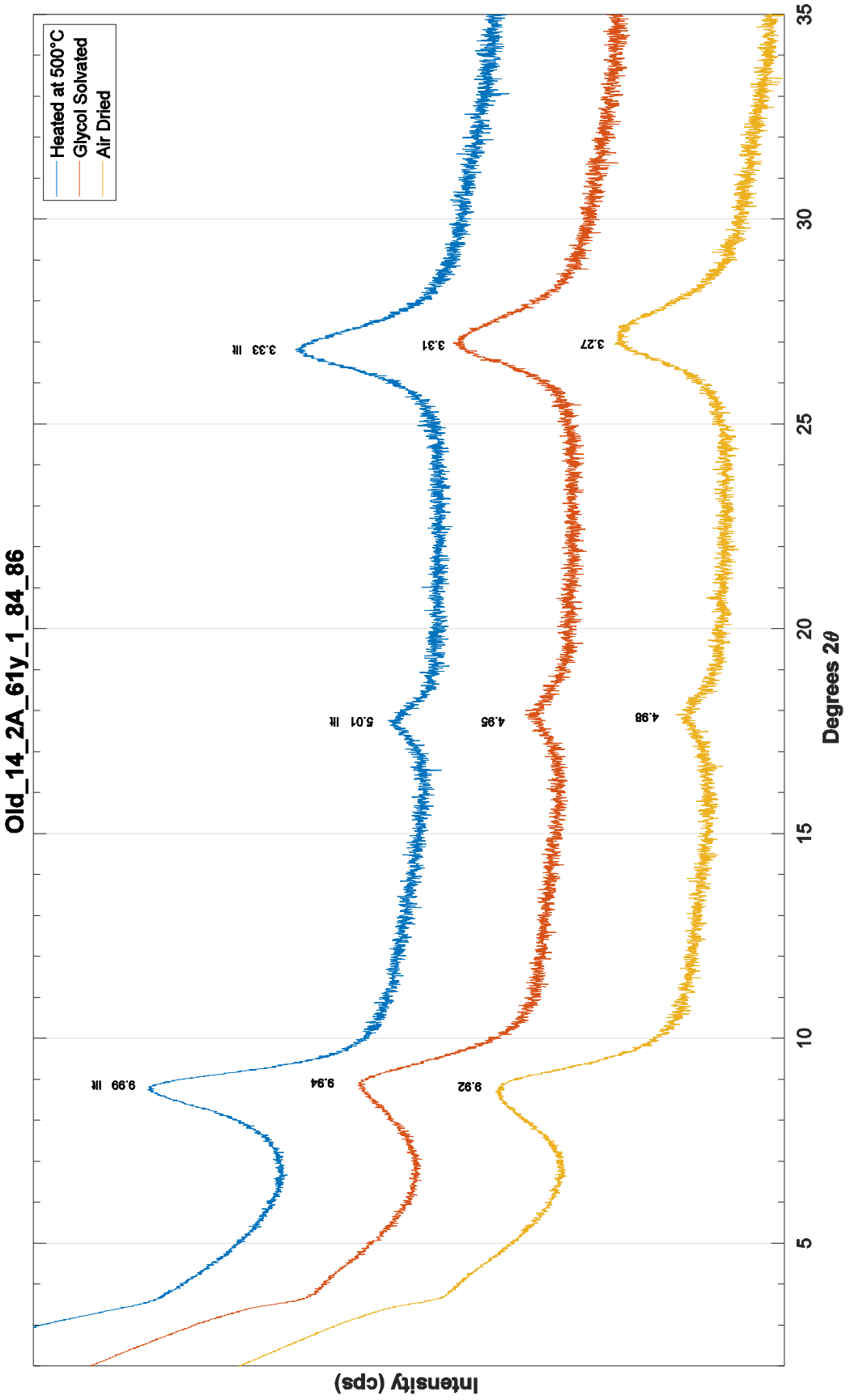
Old_14_2A_61y_1_84_86
Heated at 500°C
Glycol Solvated
Air Dried
9.99 lit
9.94
9.92
5.01 lit
4.85
4.98
3.33 lit
3.31
3.27
Intensity (cps)
Degrees 2θ
5
10
15
20
25
30
35

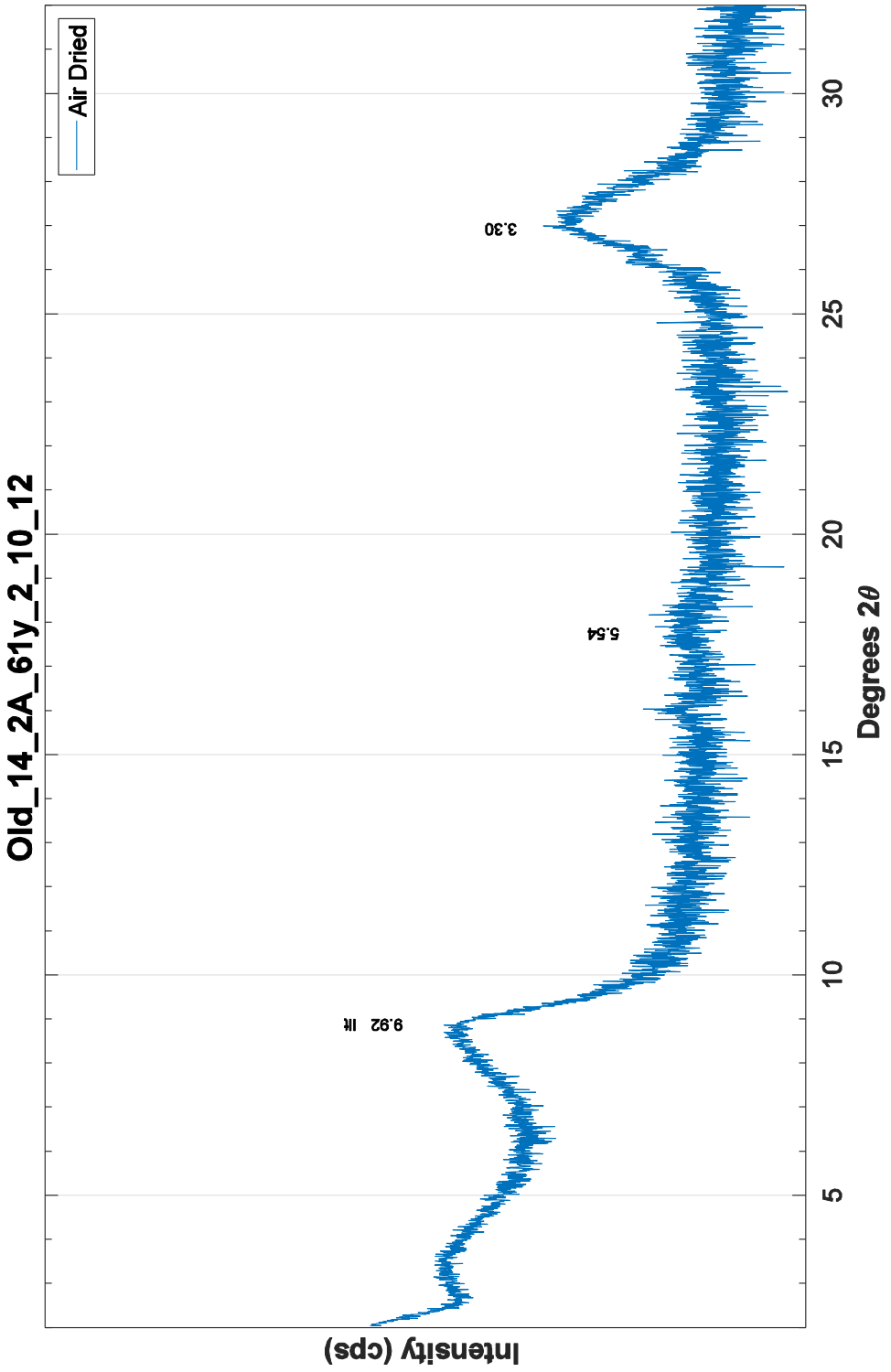
Old_14_2A_61y_2_10_12
Air Dried
Intensity (cps)
Degrees 2θ
5
10
15
20
25
30
9.92 Å
5.54
3.30

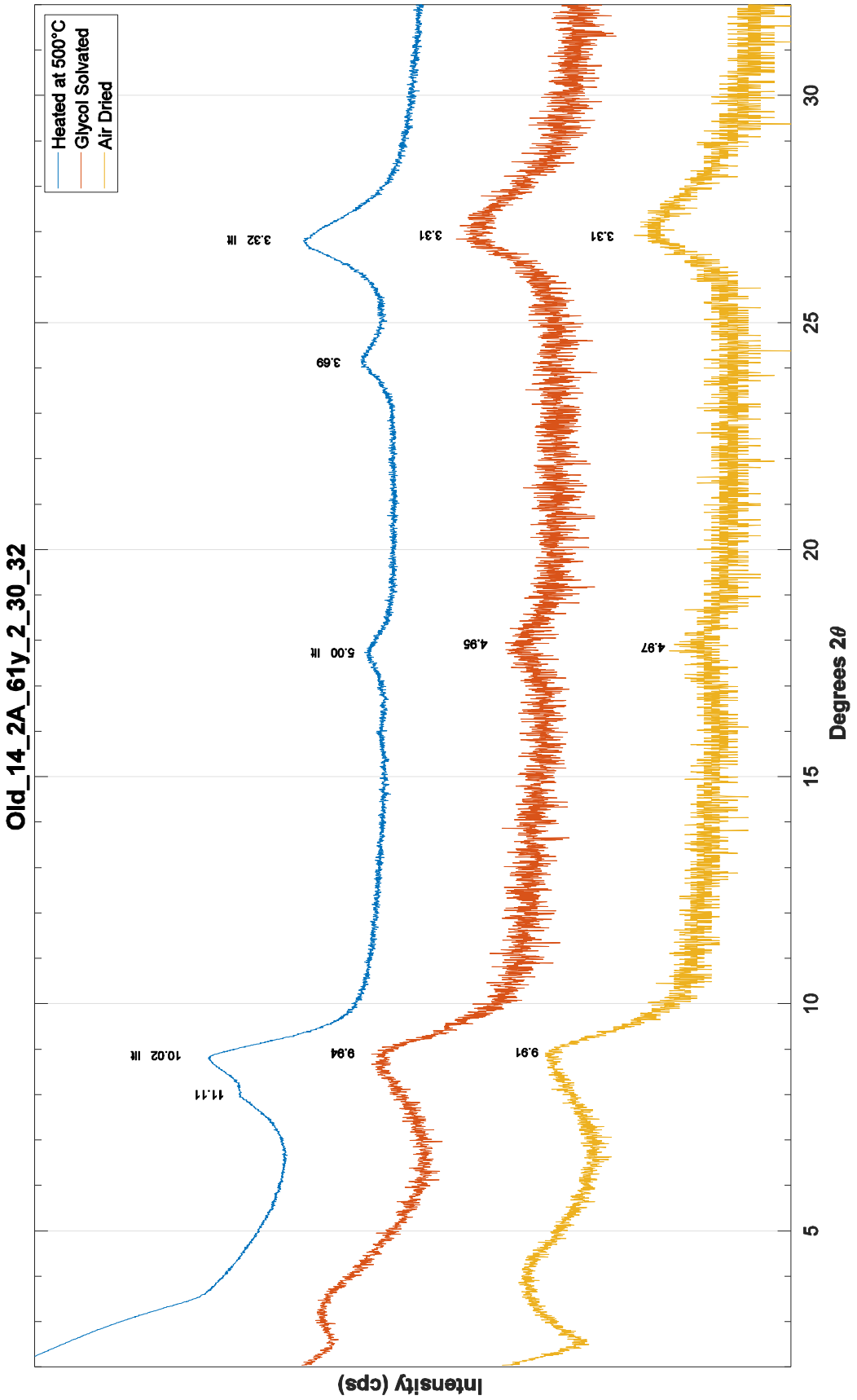
Old_14_2A_61y_2_30_32
Heated at 500°C
Glycol Solvated
Air Dried
Intensity (cps)
Degrees 2θ
5
10
15
20
25
30
10.02 lR
11.11
9.94
9.91
5.00 lR
4.85
4.97
3.69
3.32 lR
3.31
3.31

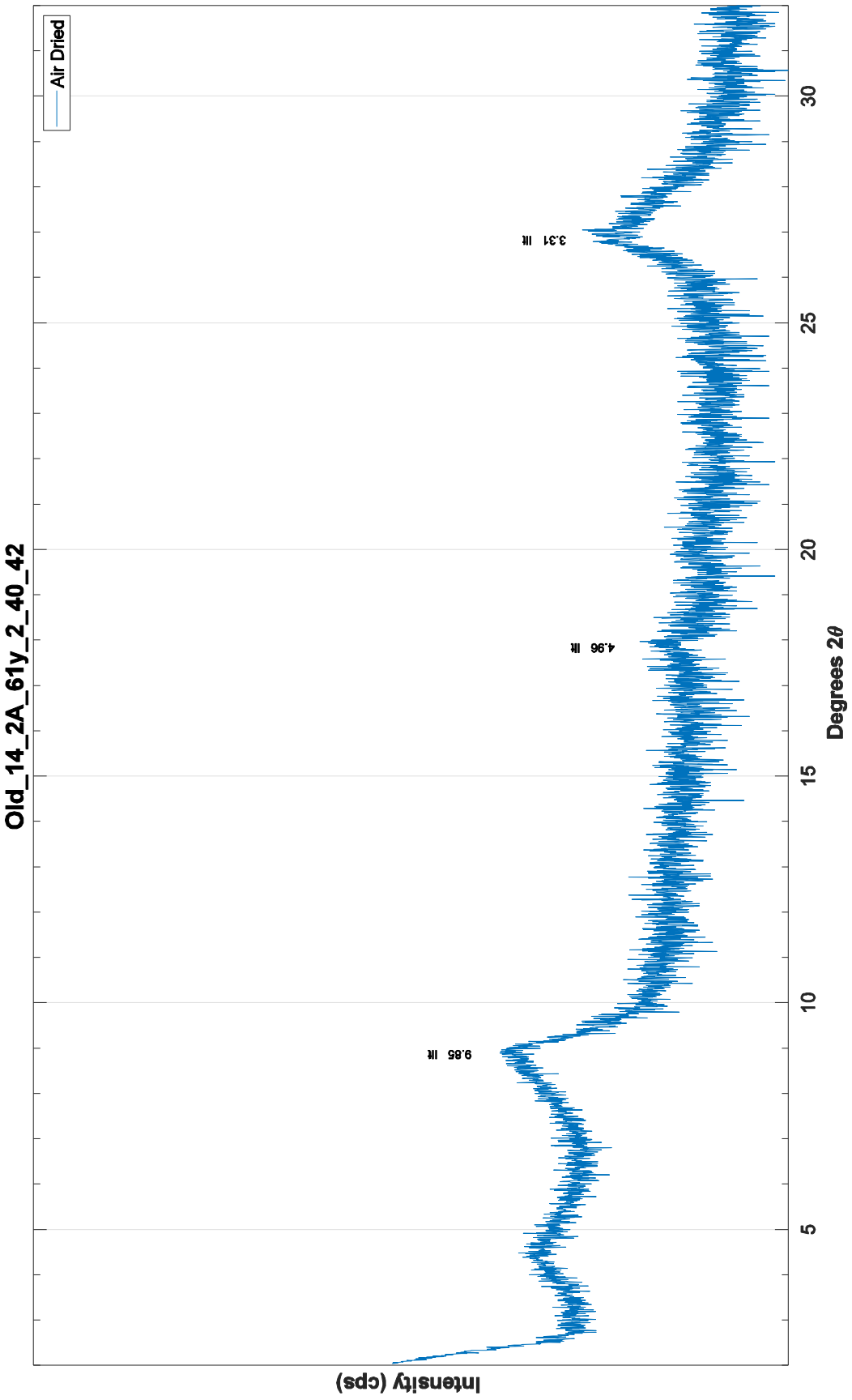
Old_14_2A_61y_2_40_42
Air Dried
Intensity (cps)
Degrees 2θ
5
10
15
20
25
30
9.85 Å
4.96 Å
3.31 Å

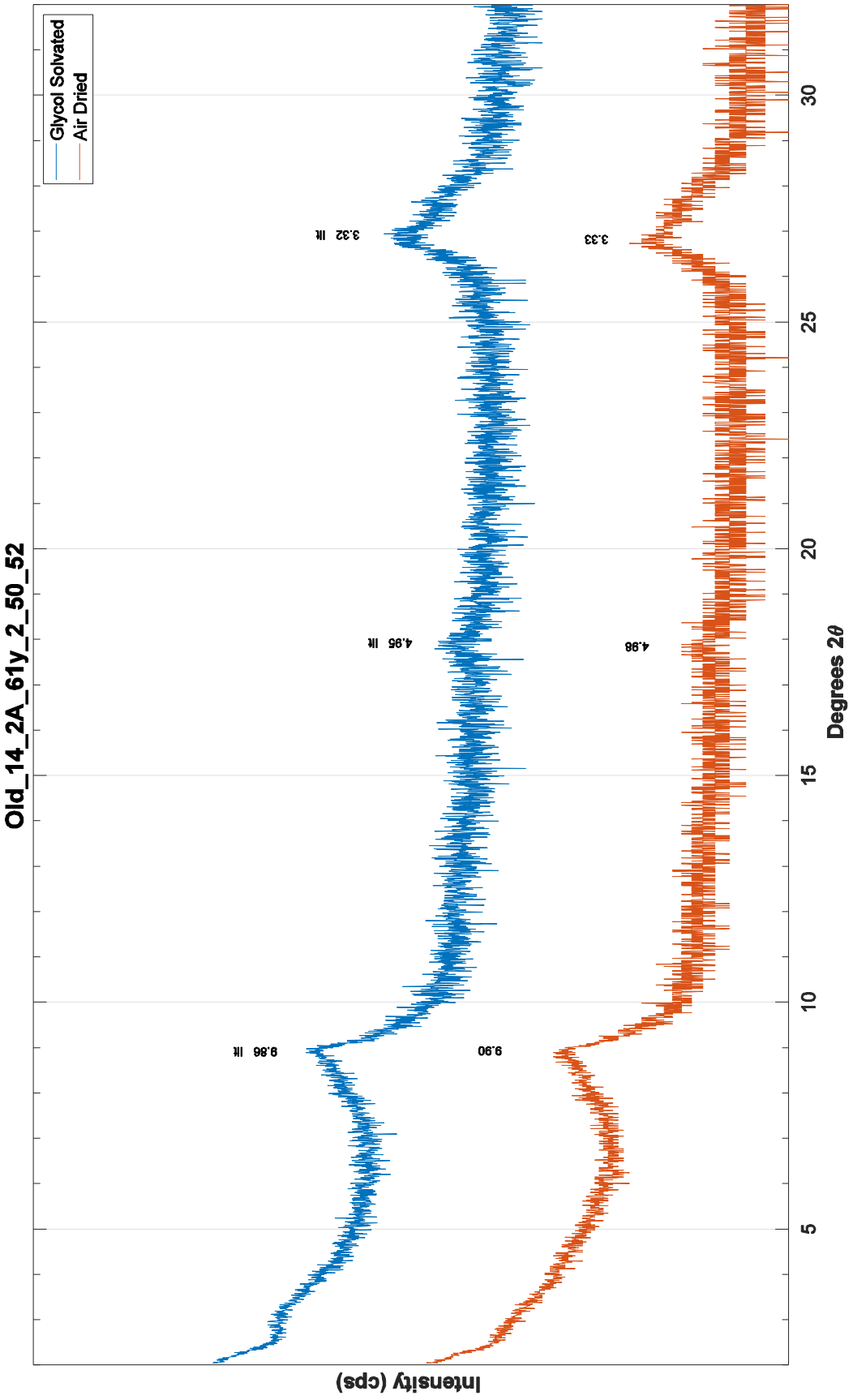
Old_14_2A_61y_2_50_52
Glycol Solvated
Air Dried
9.86 lk
4.95 lk
3.32 lk
9.90
4.98
3.33
Intensity (cps)
Degrees 2θ
5
10
15
20
25
30

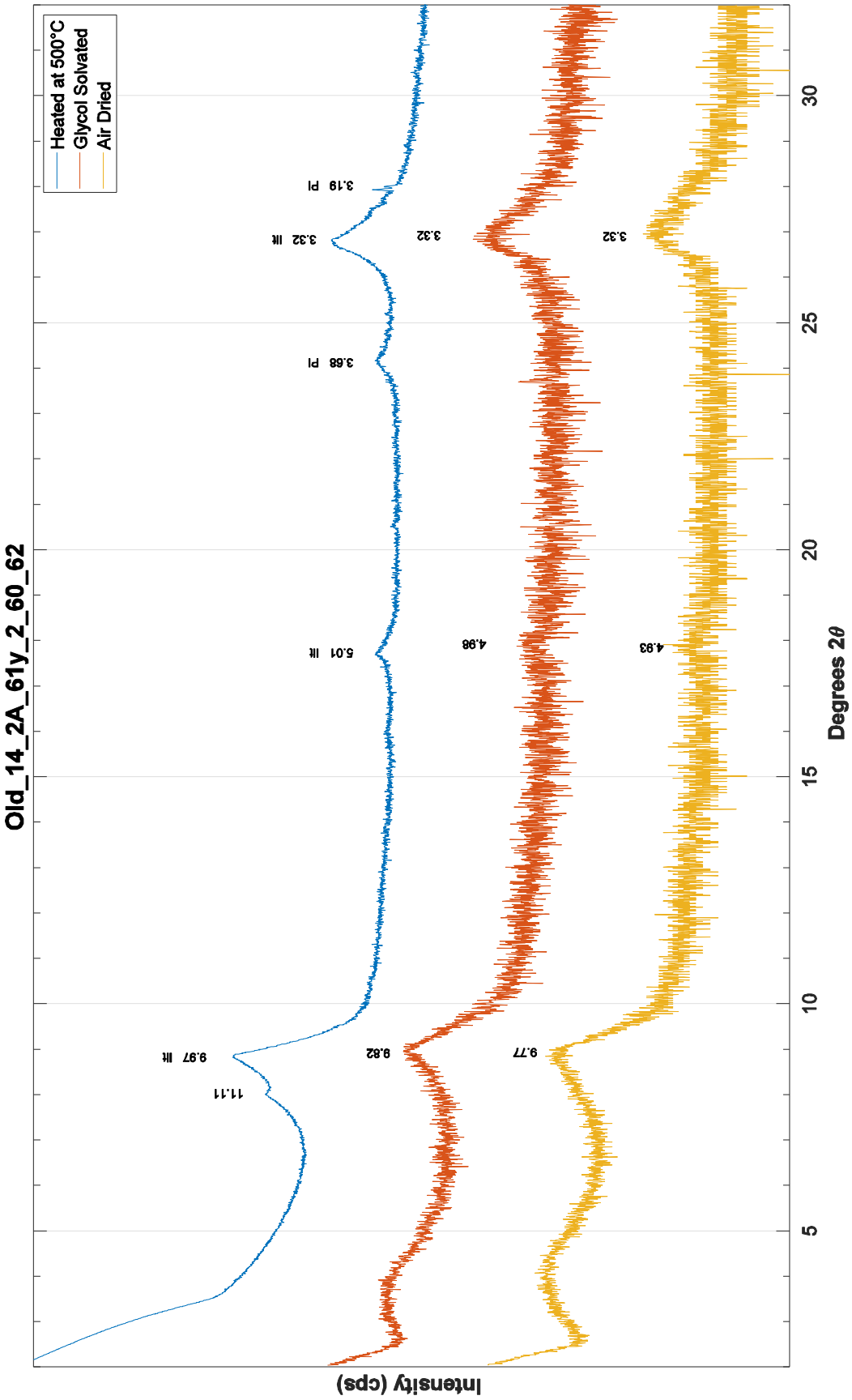
Old_14_2A_61y_2_60_62
Heated at 500°C
Glycol Solvated
Air Dried
Intensity (cps)
Degrees 2θ
5
10
15
20
25
30
11.11
9.97 Ilt
9.82
9.77
5.01 Ilt
4.98
4.93
3.68 Pl
3.32 Ilt
3.32
3.32
3.19 Pl

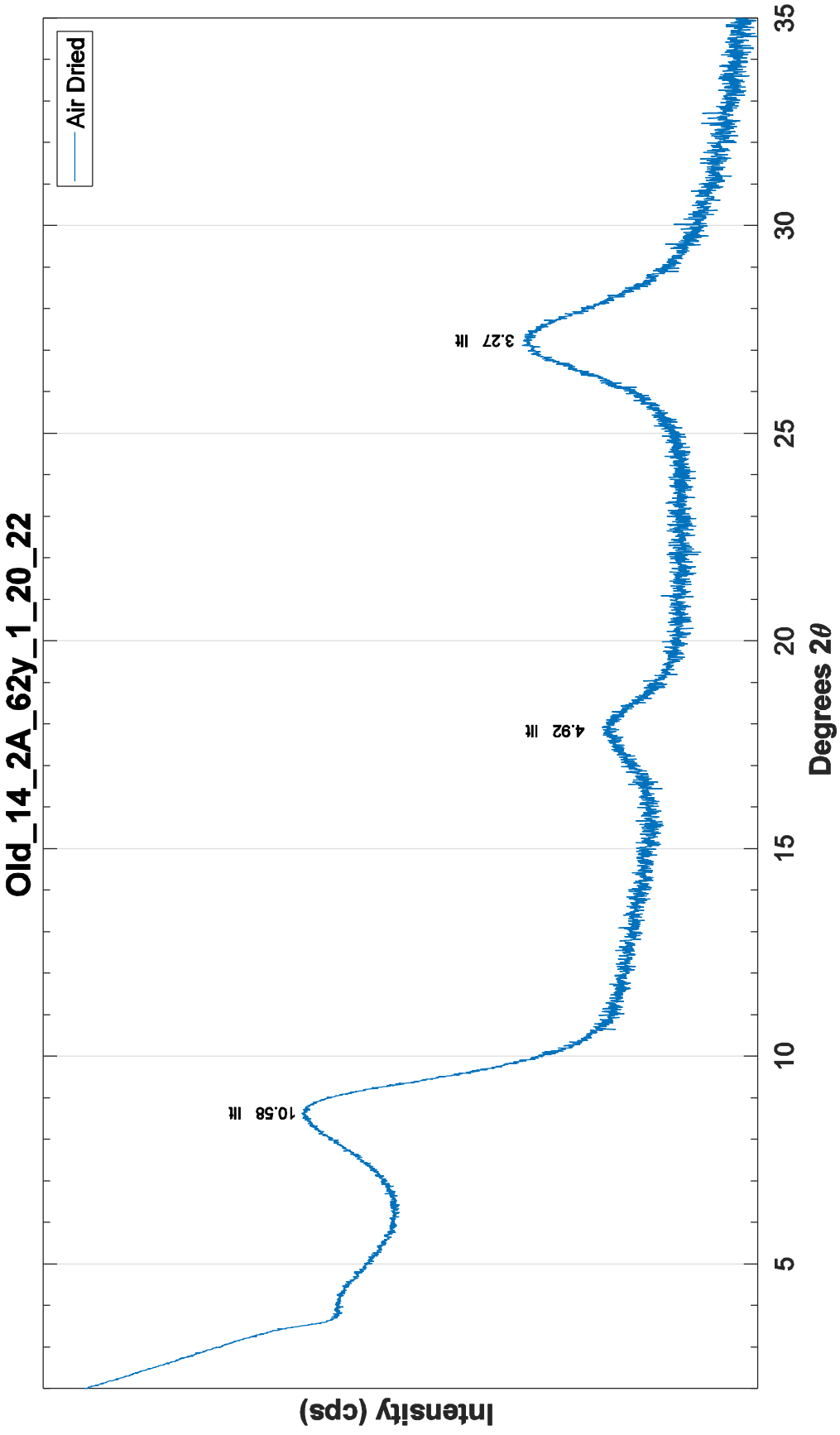
Old_14_2A_62y_1_20_22
Air Dried
10.58 Å
4.92 Å
3.27 Å
Intensity (cps)
Degrees 2θ
5
10
15
20
25
30
35

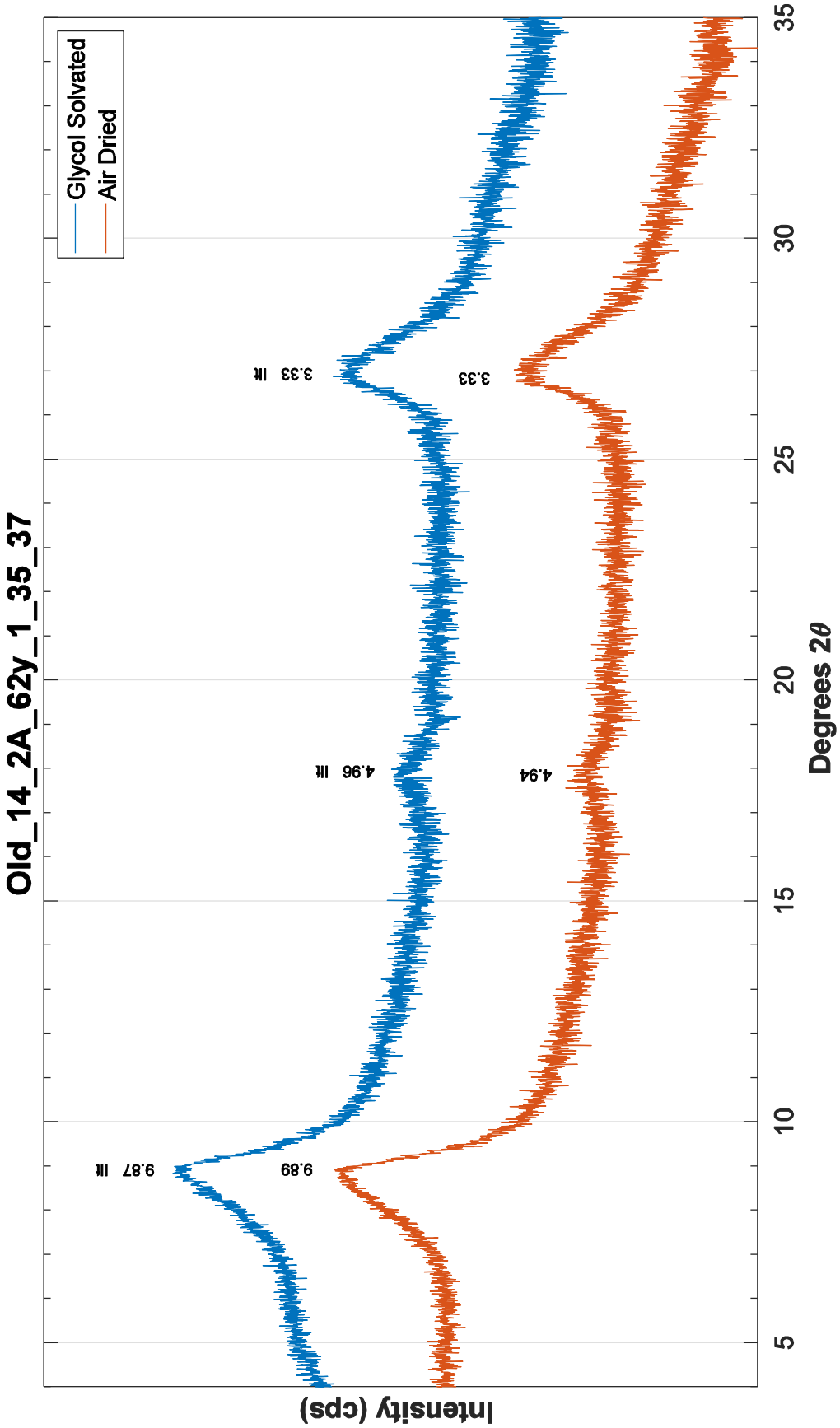
Old_14_2A_62y_1_35_37
Glycol Solvated
Air Dried
9.87 lit
9.89
4.96 lit
4.94
3.33 lit
3.33
Intensity (cps)
Degrees 2θ
5
10
15
20
25
30
35

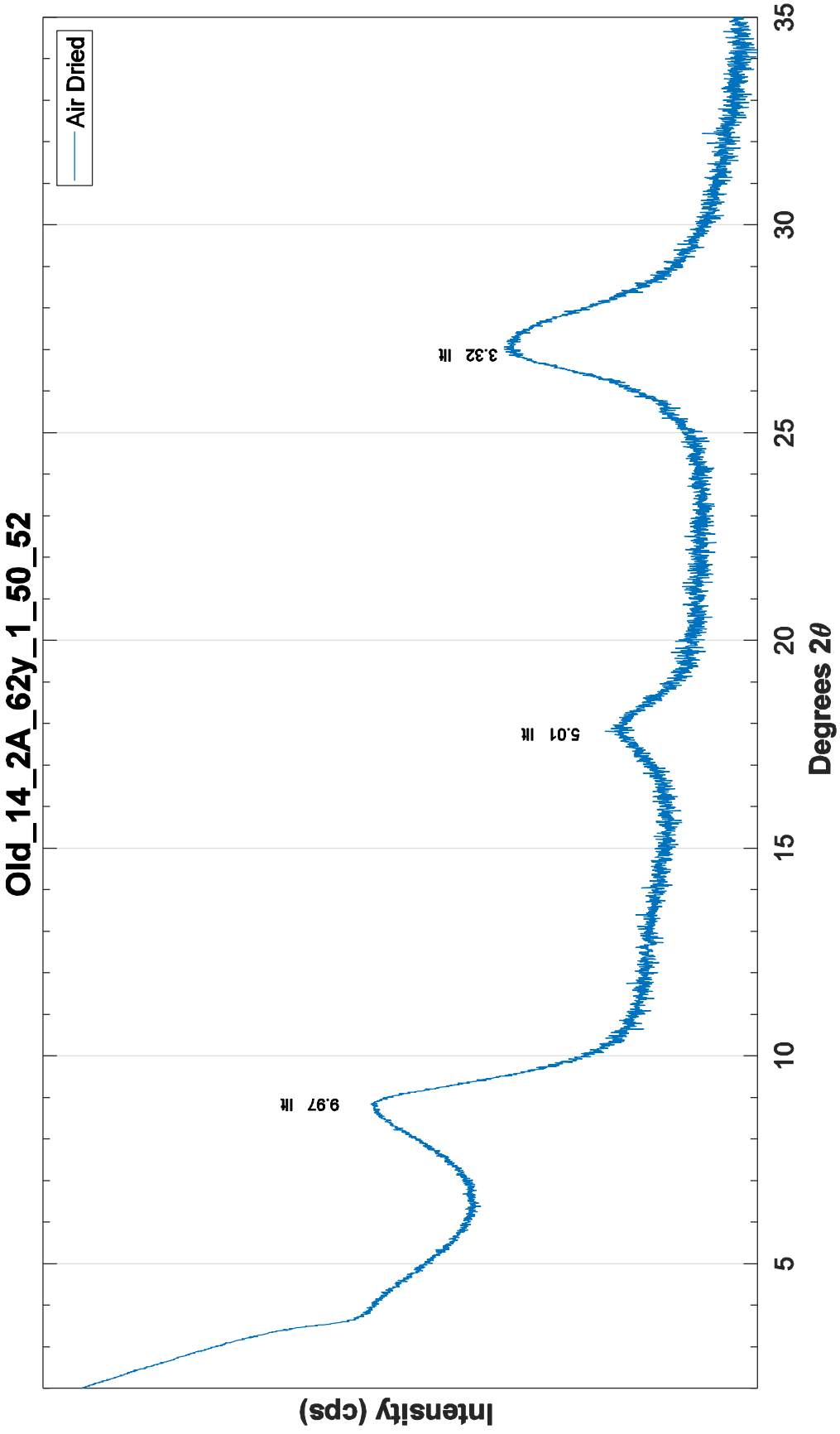
Old_14_2A_62y_1_50_52
Air Dried
9.97 Å
5.01 Å
3.32 Å
Intensity (cps)
Degrees 2θ
5
10
15
20
25
30
35

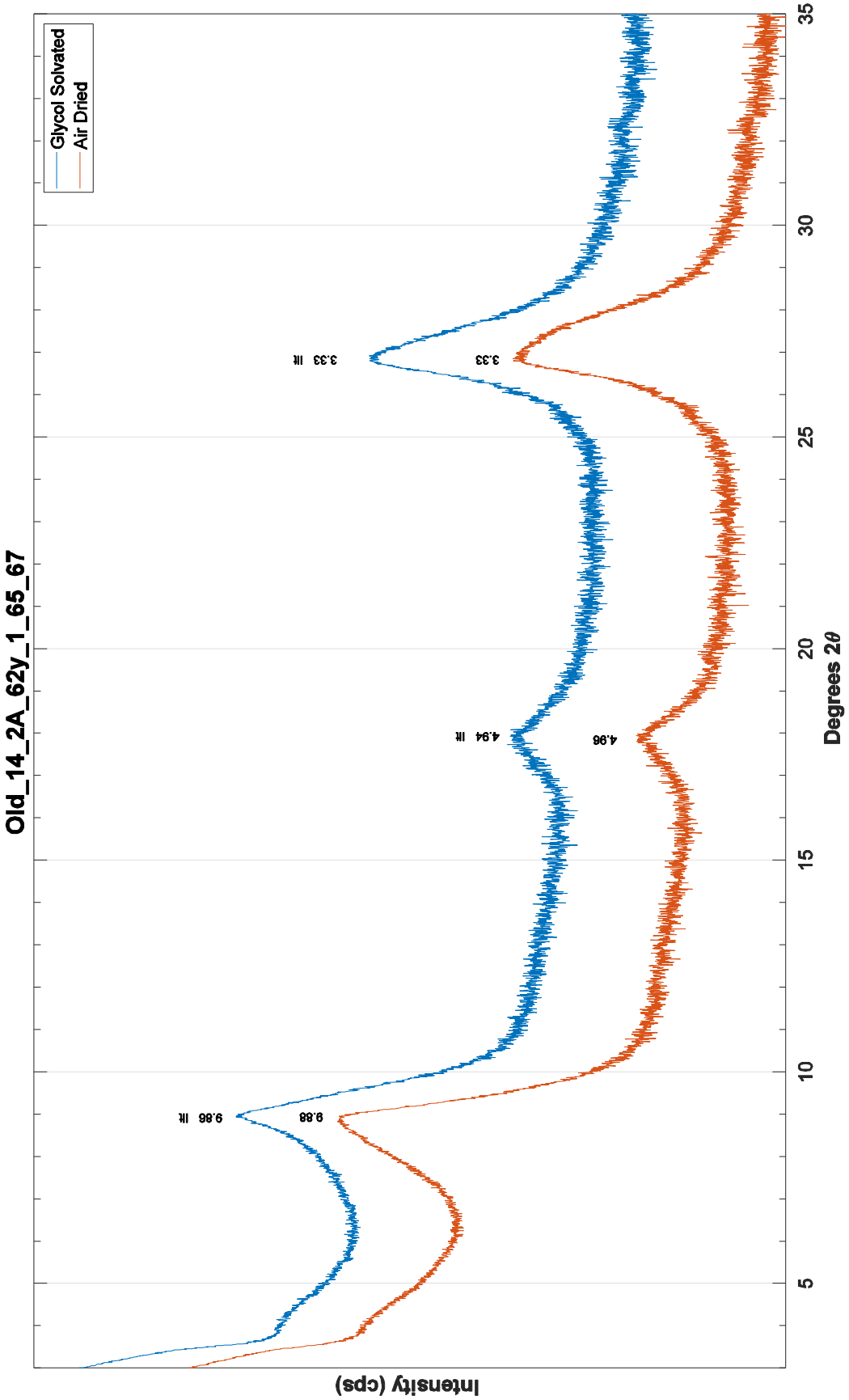
Old_14_2A_62y_1_65_67
Glycol Solvated
Air Dried
9.86 Å
9.88
4.94 Å
4.96
3.33 Å
3.33
Intensity (cps)
Degrees 2θ
5
10
15
20
25
30
35

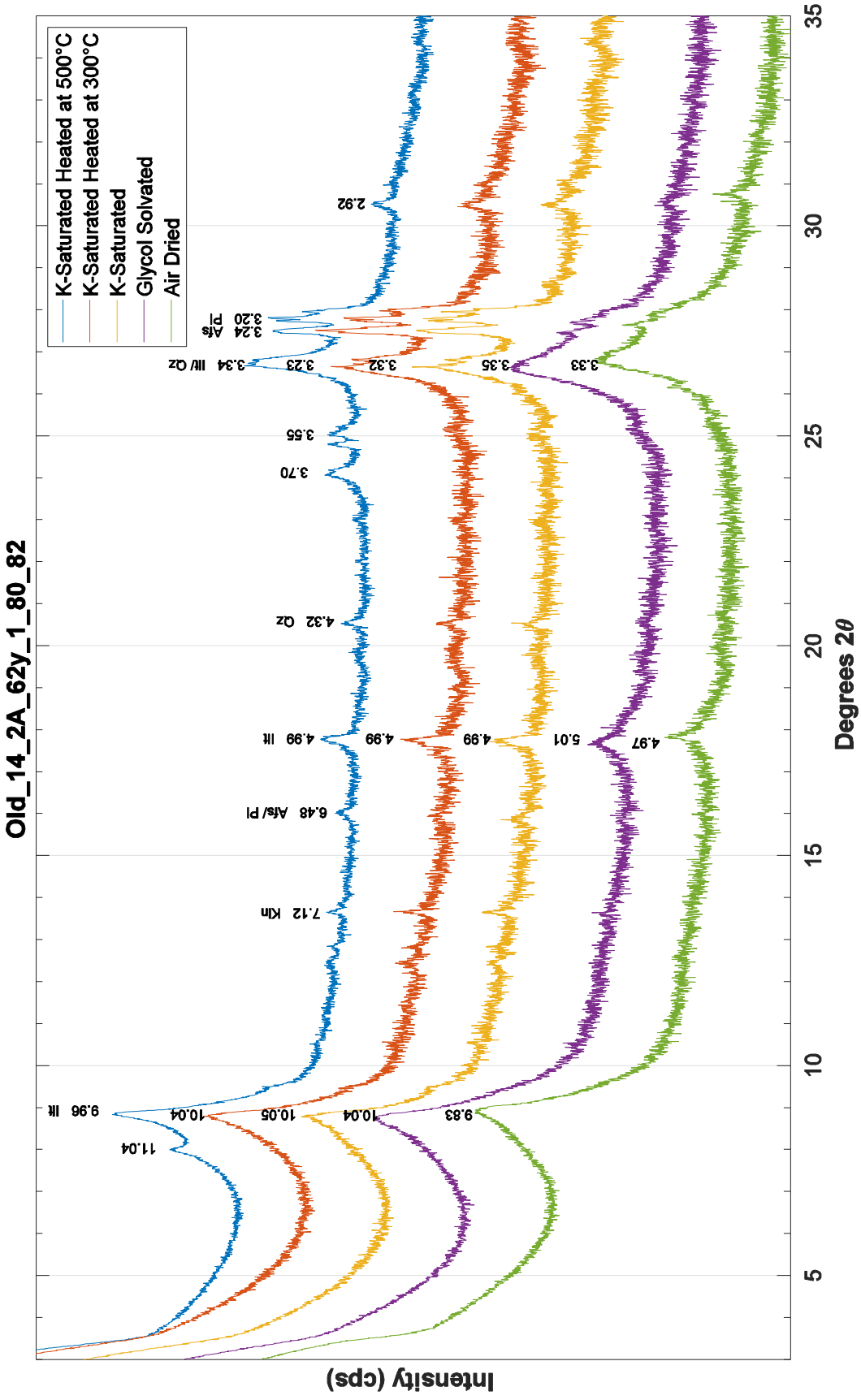
Old_14_2A_62y_1_80_82
Intensity (cps)
Degrees 2θ
K-Saturated Heated at 500°C
K-Saturated Heated at 300°C
K-Saturated
Glycol Solvated
Air Dried
9.96 Ilt
11.04
10.04
10.05
10.04
9.83
7.12 Kln
6.48 Afs/Pl
4.99 Ilt
4.99
4.99
5.01
4.97
4.32 Qz
3.70
3.55
3.34 Ilt/ Qz
3.23
3.32
3.35
3.33
3.24 Afs
3.20 Pl
2.92

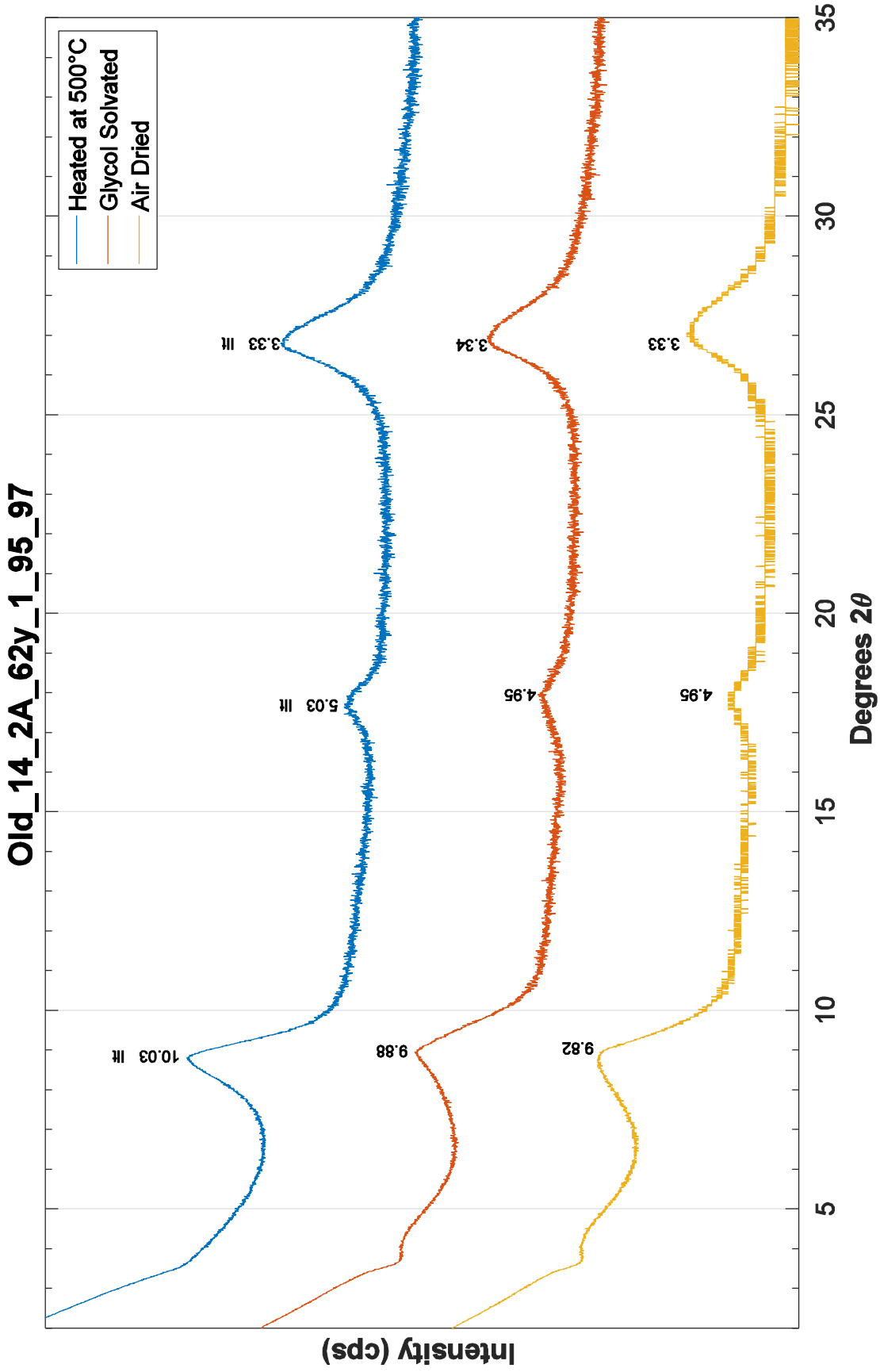
Old_14_2A_62y_1_95_97
Heated at 500°C
Glycol Solvated
Air Dried
10.03 Ill
5.03 Ill
3.33 Ill
9.88
4.95
3.34
9.82
4.95
3.33
Intensity (cps)
Degrees 2θ
5
10
15
20
25
30
35

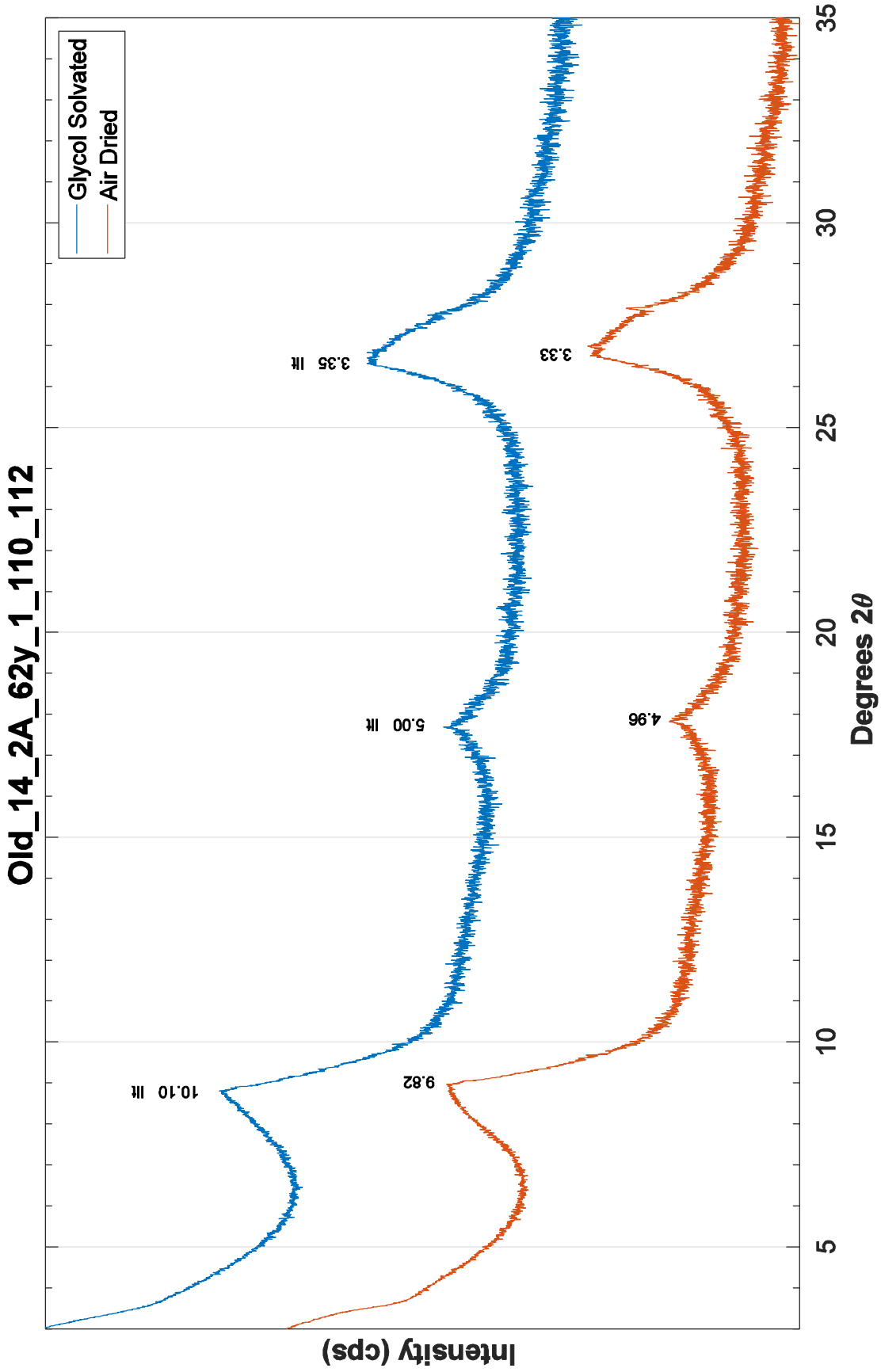
Old_14_2A_62y_1_110_112
Glycol Solvated
Air Dried
10.10 Ilt
9.82
5.00 Ilt
4.96
3.35 Ilt
3.33
Intensity (cps)
Degrees 2θ
5
10
15
20
25
30
35

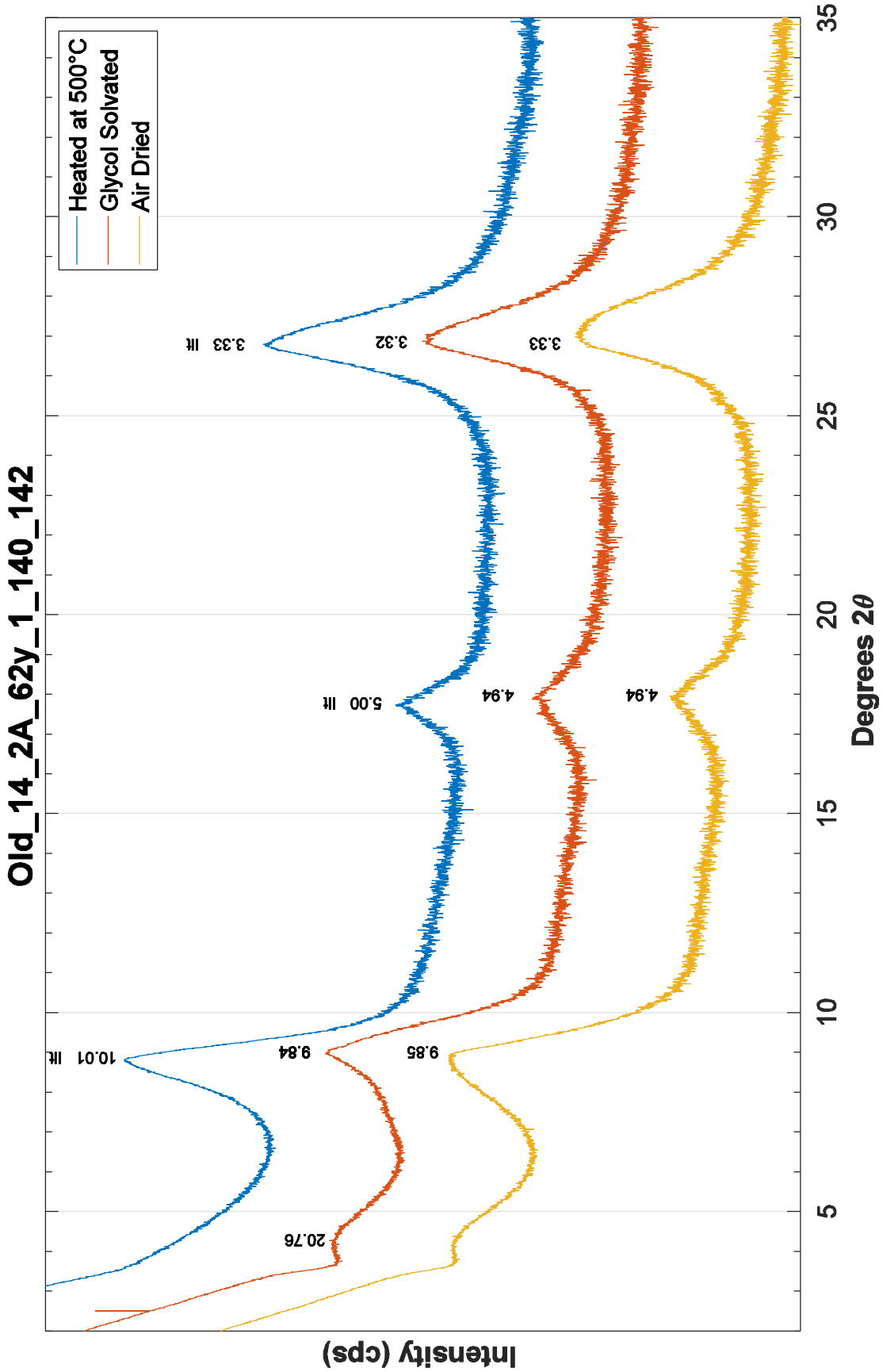
Old_14_2A_62y_1_140_142
Heated at 500°C
Glycol Solvated
Air Dried
Intensity (cps)
Degrees 2θ
5
10
15
20
25
30
35
10.01 lit
9.84
20.76
9.85
5.00 lit
4.94
4.94
3.33 lit
3.32
3.33

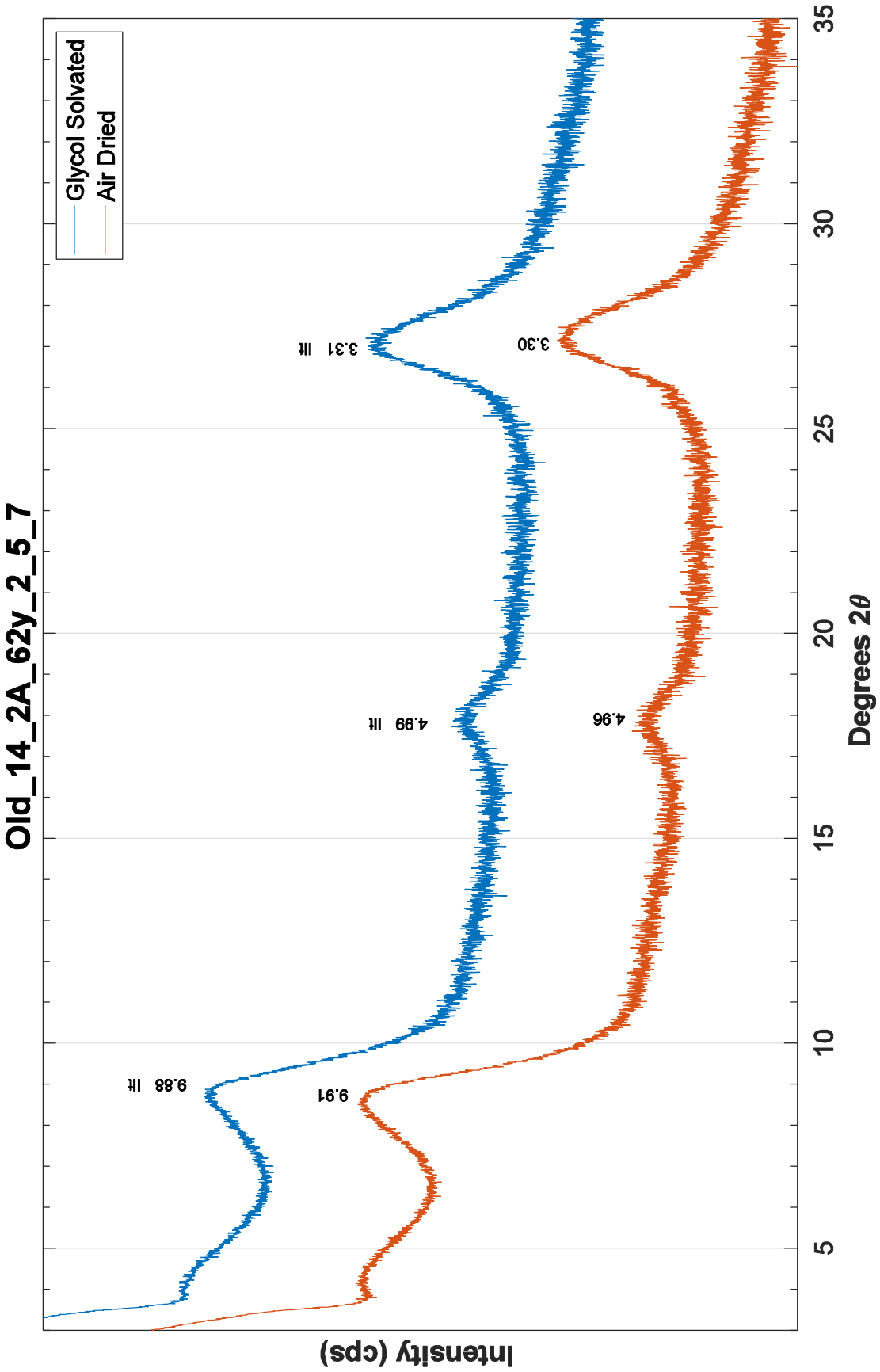
Old_14_2A_62y_2_5_7
Glycol Solvated
Air Dried
9.88 Ilt
9.91
4.99 Ilt
4.96
3.31 Ilt
3.30
Intensity (cps)
Degrees 2θ
5
10
15
20
25
30
35

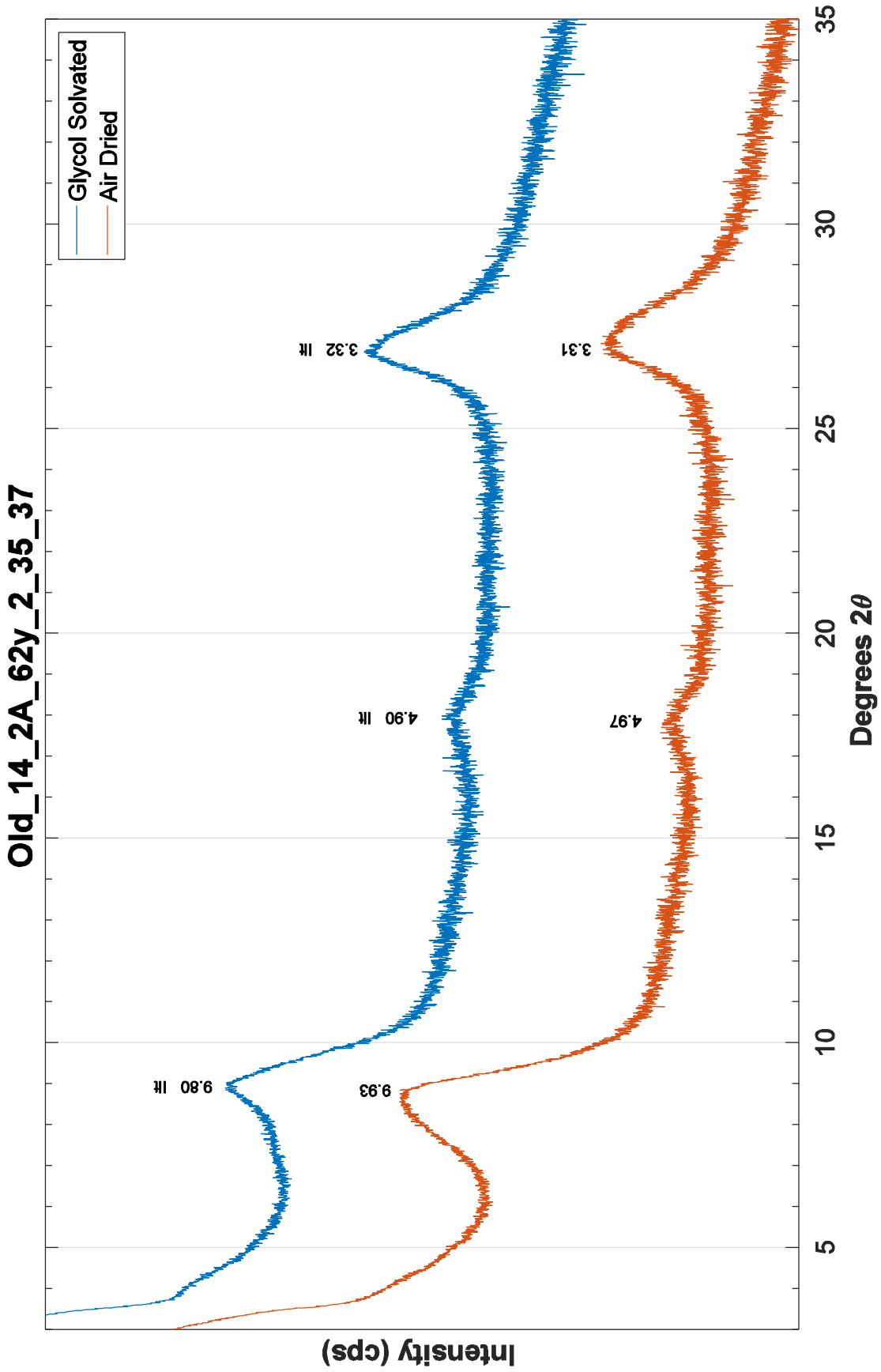
Old_14_2A_62y_2_35_37
Glycol Solvated
Air Dried
9.80 lit
4.90 lit
3.32 lit
9.93
4.97
3.31
Intensity (cps)
Degrees 2θ
5
10
15
20
25
30
35

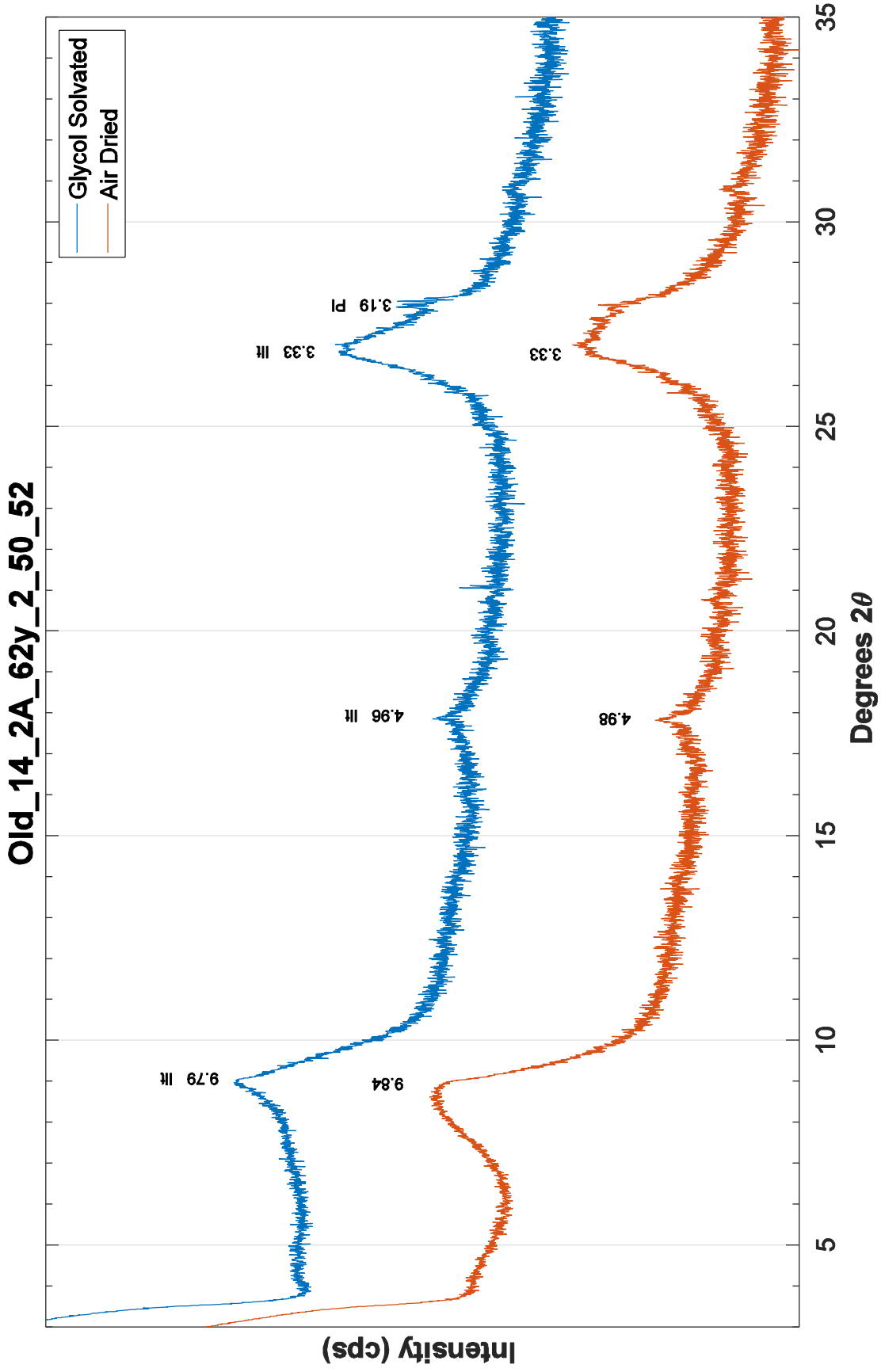
Old_14_2A_62y_2_50_52
Glycol Solvated
Air Dried
Intensity (cps)
Degrees 2θ
5
10
15
20
25
30
35
9.79 Ilt
9.84
4.96 Ilt
4.98
3.33 Ilt
3.33
3.19 Pl

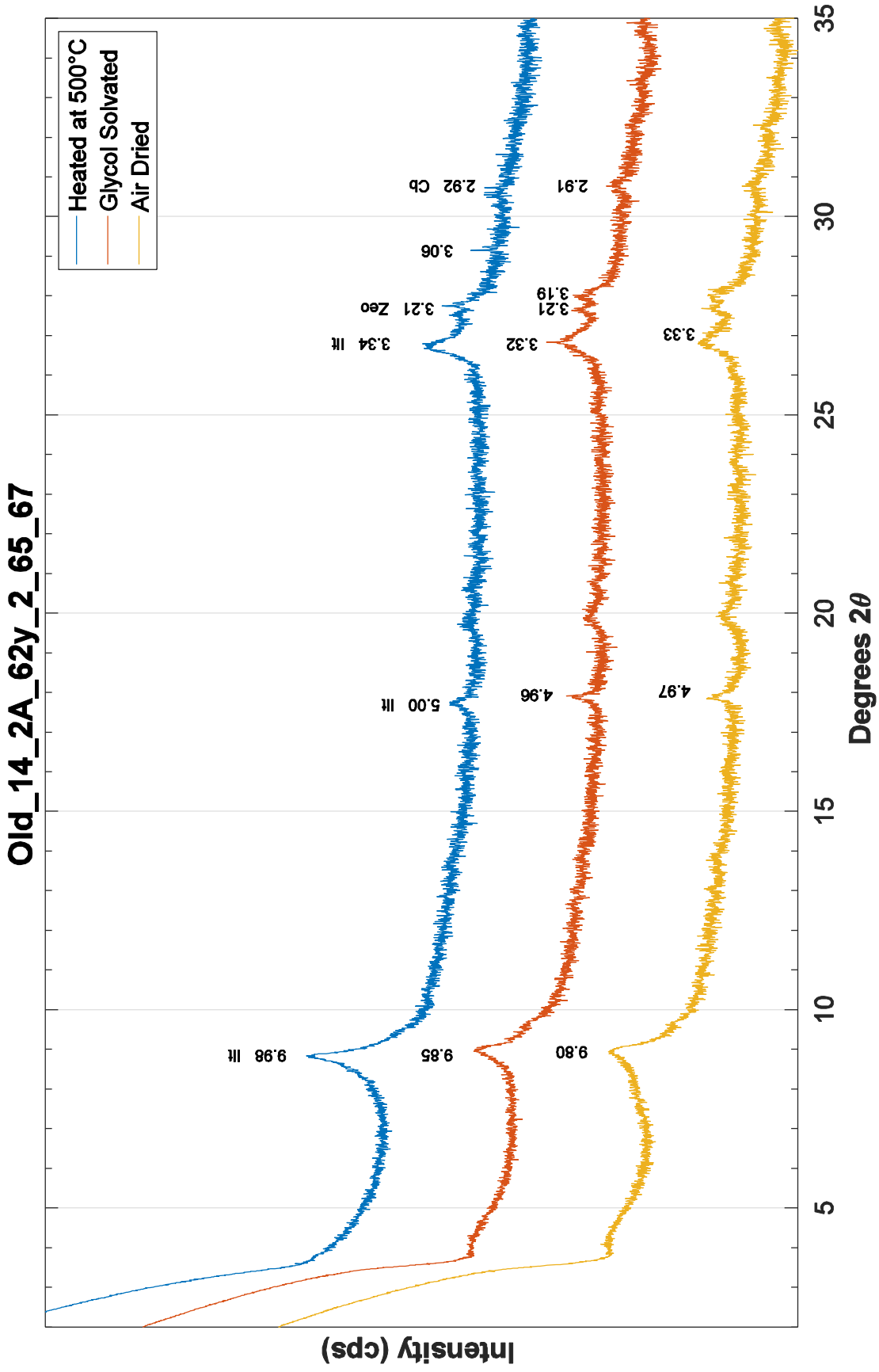
Old_14_2A_62y_2_65_67
Heated at 500°C
Glycol Solvated
Air Dried
Intensity (cps)
Degrees 2θ
5
10
15
20
25
30
35
9.98 Ilt
9.85
9.80
5.00 Ilt
4.96
4.97
3.34 Ilt
3.32
3.33
3.21 Zeo
3.21
3.19
3.06
2.92 Cb
2.91

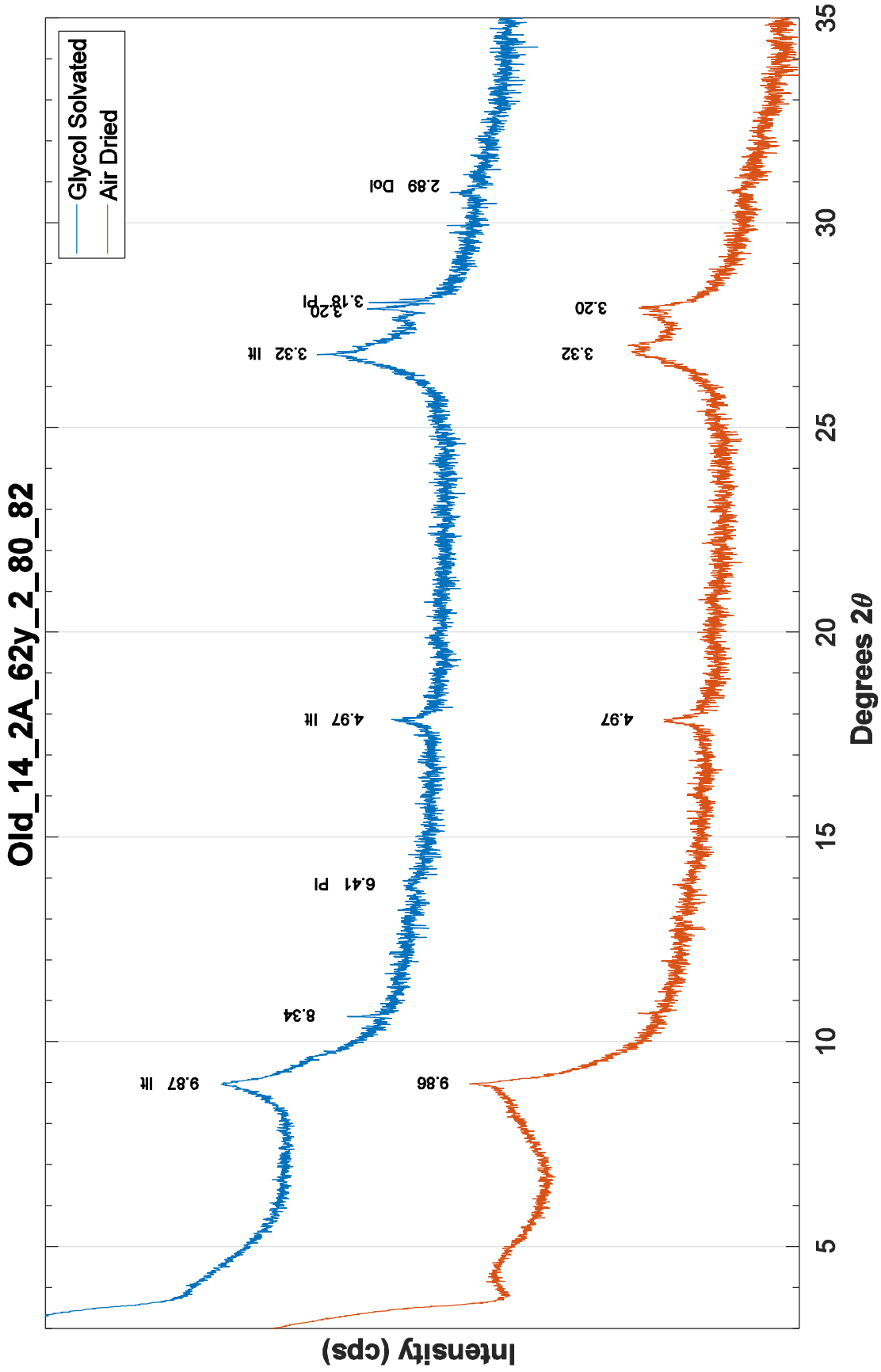
Old_14_2A_62y_2_80_82
Glycol Solvated
Air Dried
Intensity (cps)
Degrees 2θ
5
10
15
20
25
30
35
9.87 Ilt
8.34
6.41 Pl
4.97 Ilt
3.32 Ilt
3.20 Pl
2.89 Dol
9.86
4.97
3.32
3.20

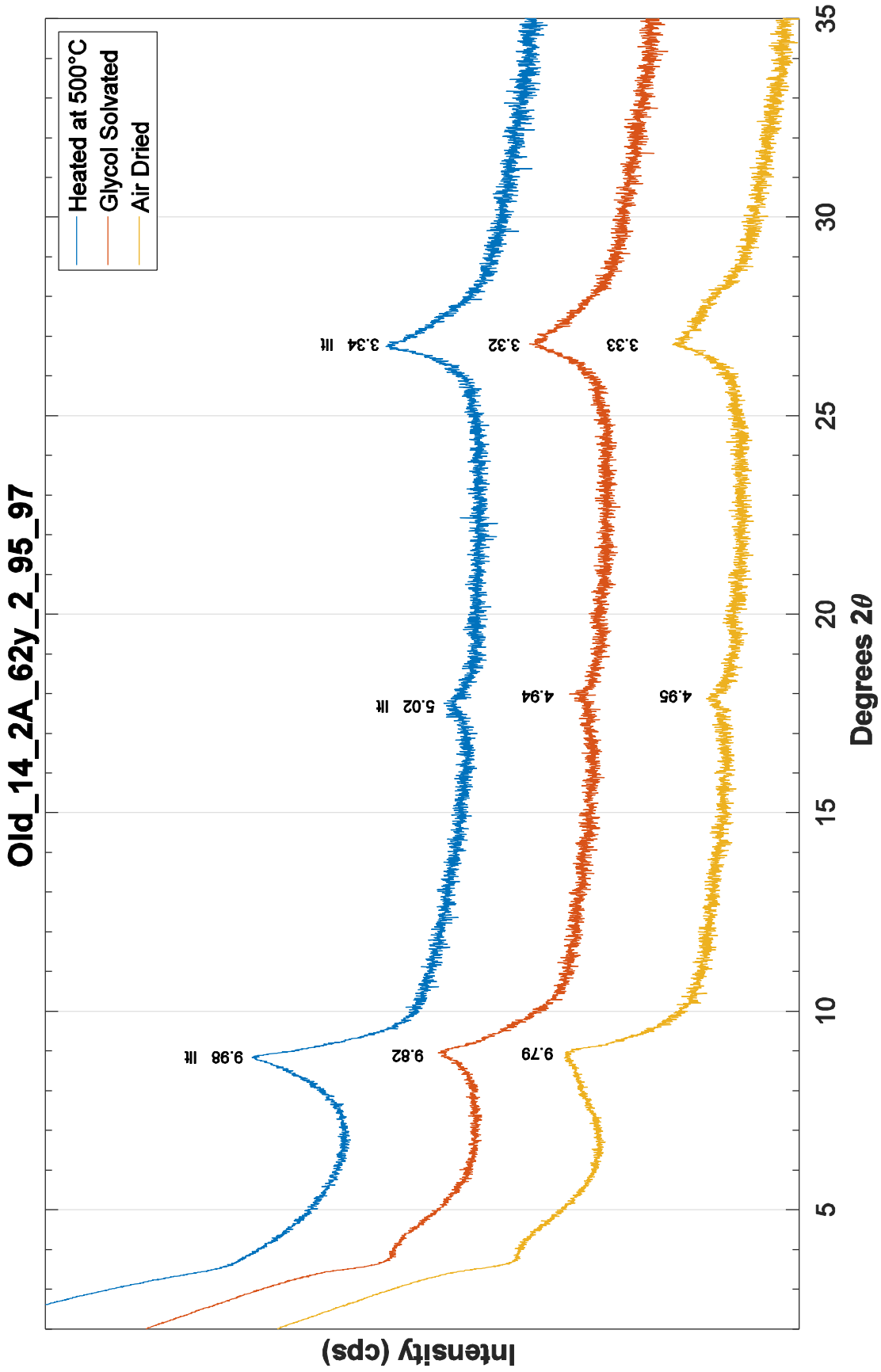
Old_14_2A_62y_2_95_97
Heated at 500°C
Glycol Solvated
Air Dried
Intensity (cps)
Degrees 2θ
5
10
15
20
25
30
35
9.98 lit
9.82
9.79
5.02 lit
4.94
4.95
3.34 lit
3.32
3.33

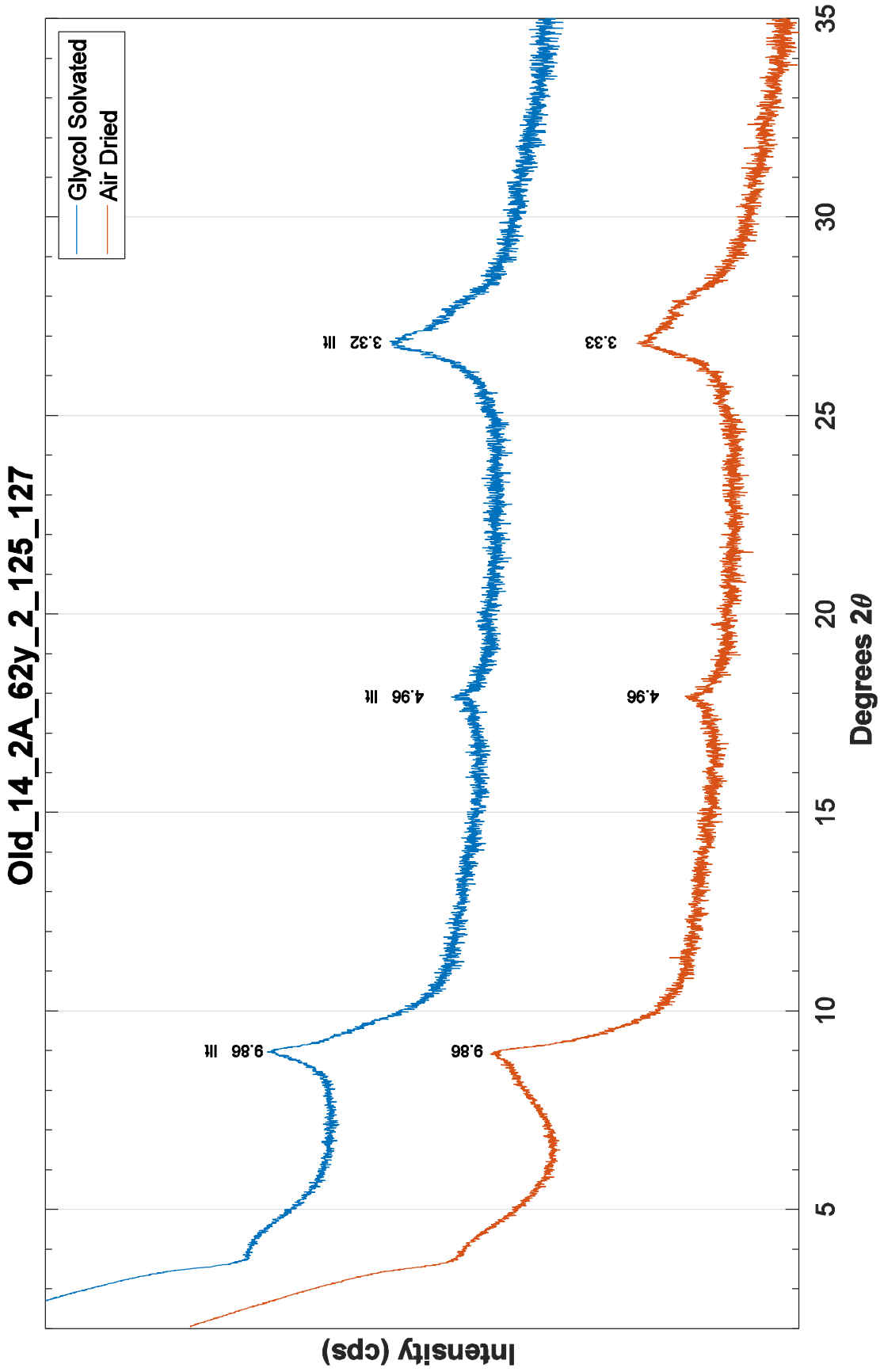
Old_14_2A_62y_2_125_127
Glycol Solvated
Air Dried
9.86 llt
4.96 llt
3.32 llt
9.86
4.96
3.33
Intensity (cps)
Degrees 2θ
5
10
15
20
25
30
35

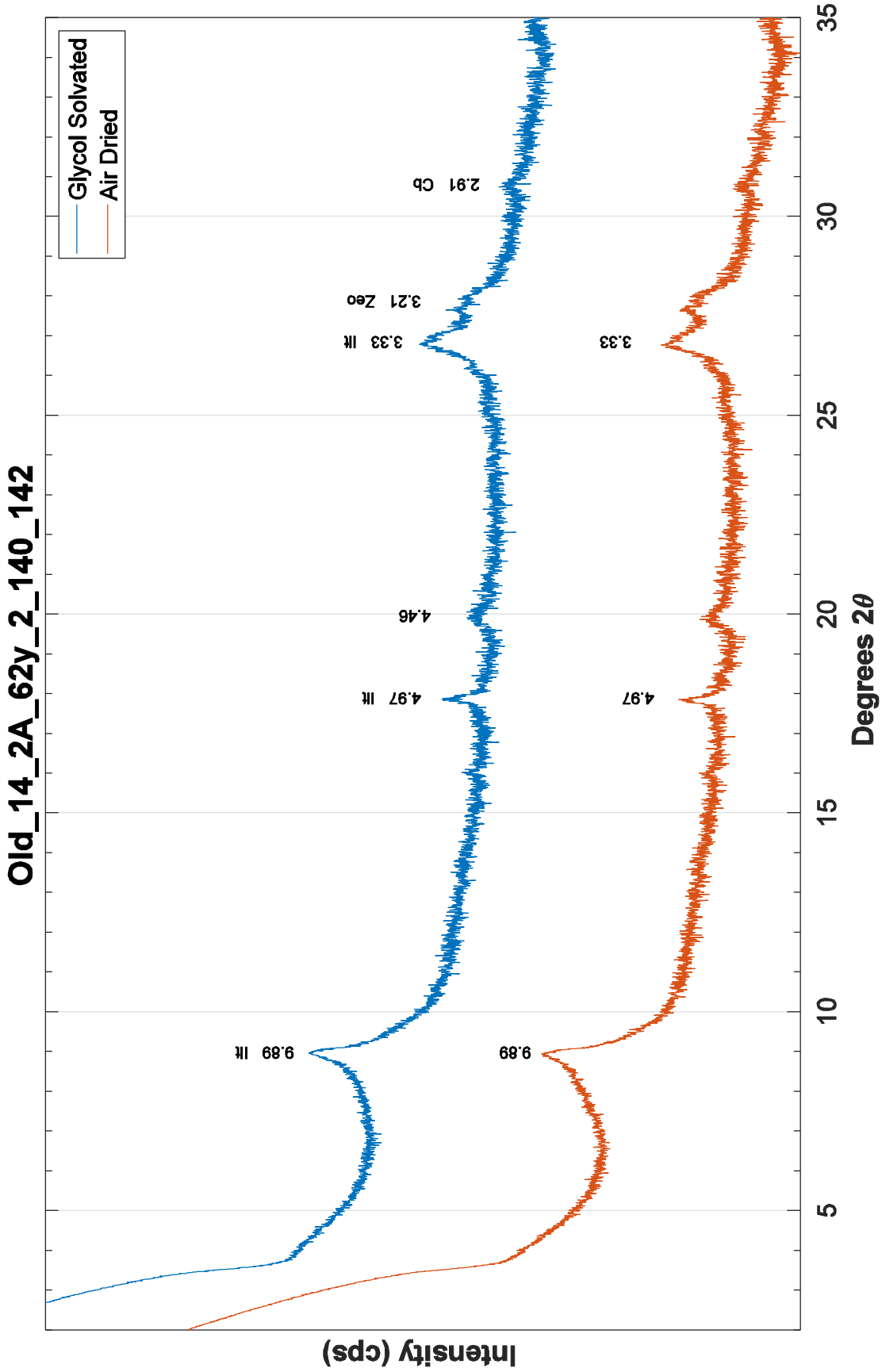
Old_14_2A_62y_2_140_142
Glycol Solvated
Air Dried
Intensity (cps)
Degrees 2θ
5
10
15
20
25
30
35
9.89 Ilt
4.97 Ilt
4.46
3.33 Ilt
3.21 Zeo
2.91 Clb
9.89
4.97
3.33

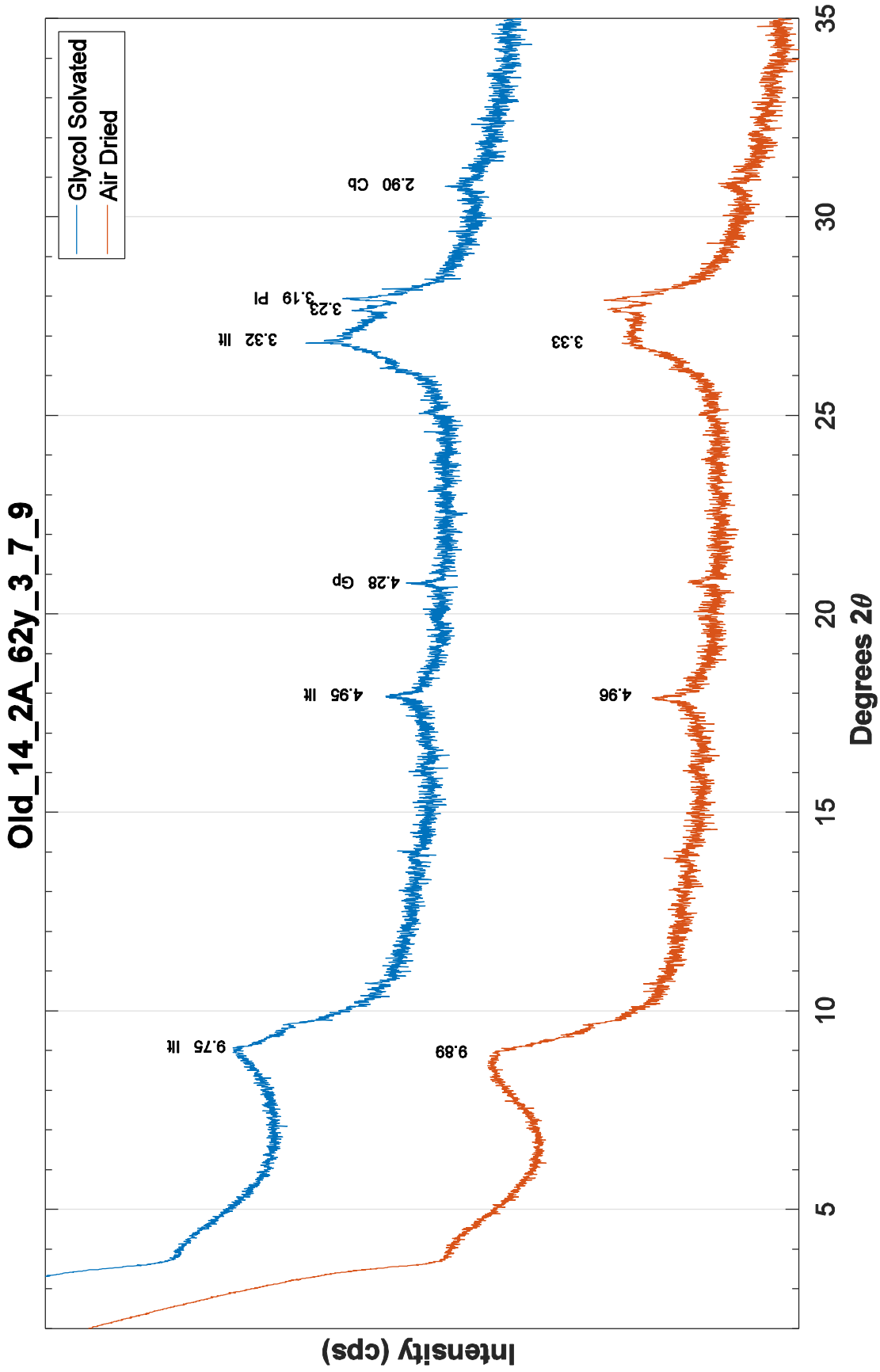
Old_14_2A_62y_3_7_9
Glycol Solvated
Air Dried
Intensity (cps)
Degrees 2θ
5
10
15
20
25
30
35
9.75 Ilt
9.89
4.95 Ilt
4.28 Gp
4.96
3.32 Ilt
3.23
3.19 Pl
3.33
2.90 Cb

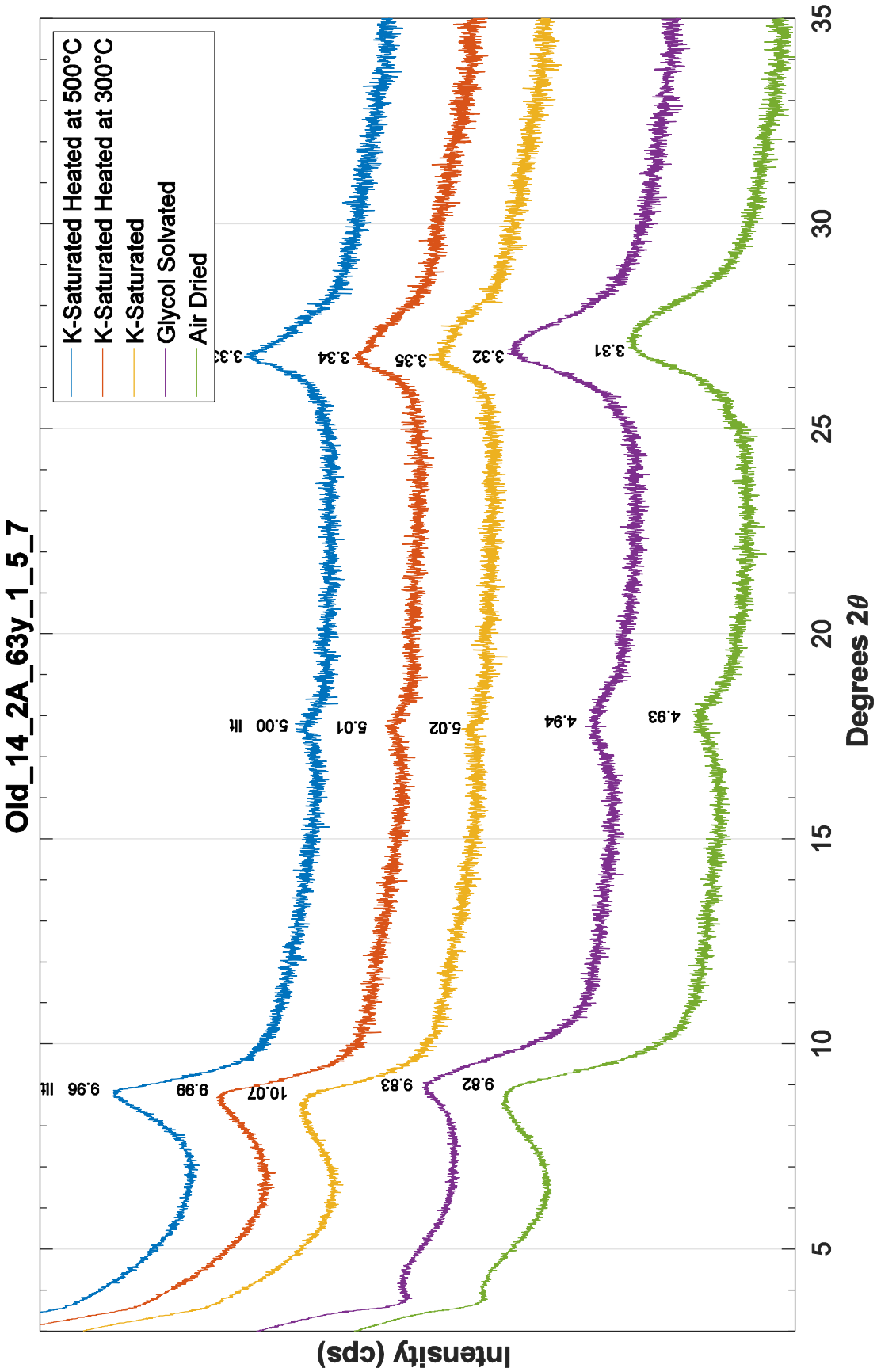
Old_14_2A_63y_1_5_7
K-Saturated Heated at 500°C
K-Saturated Heated at 300°C
K-Saturated
Glycol Solvated
Air Dried
Intensity (cps)
Degrees 2θ
5
10
15
20
25
30
35
9.96
9.99
10.07
9.83
9.82
5.00
5.01
5.02
4.94
4.93
3.34
3.35
3.32
3.31

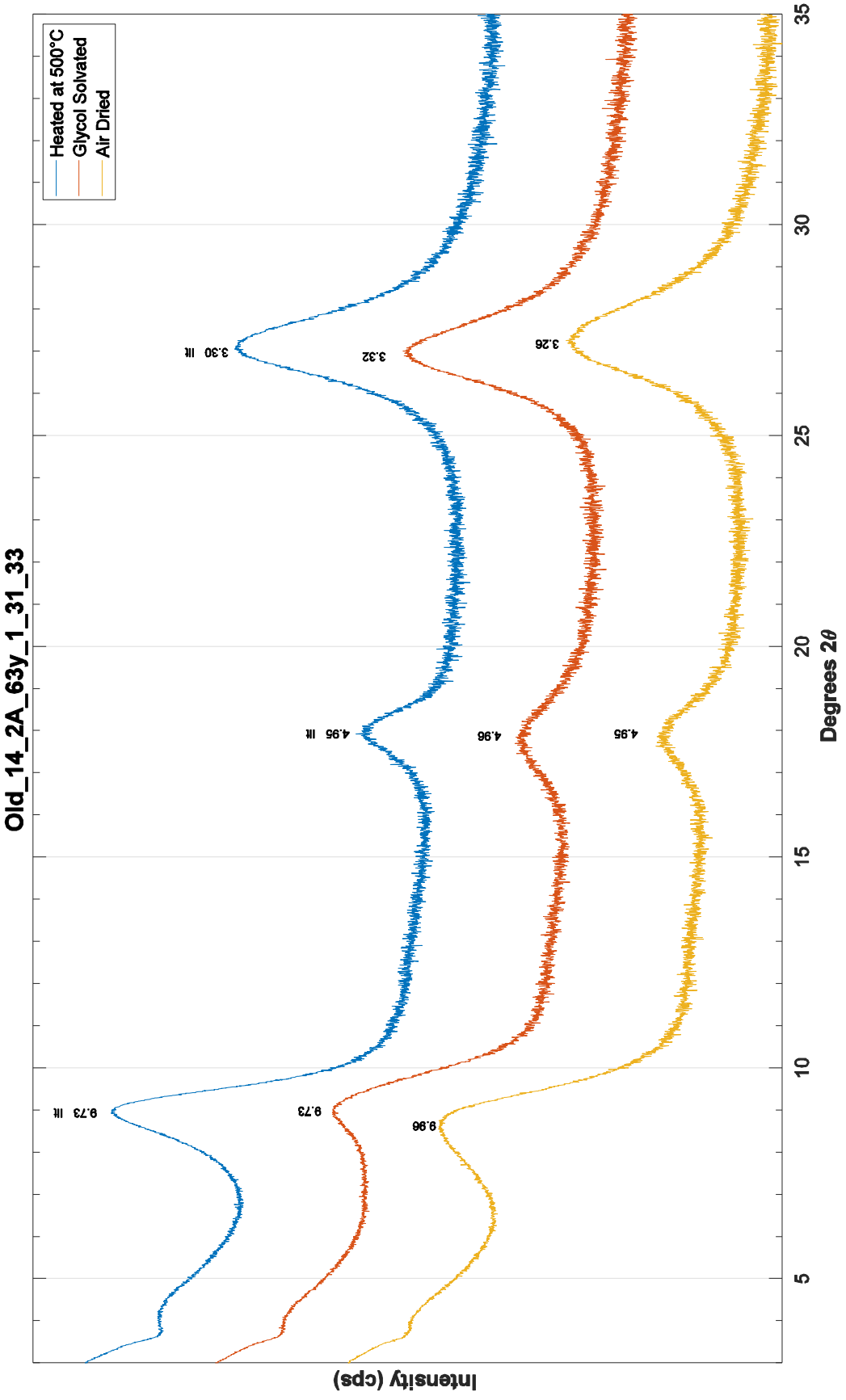
Old_14_2A_63y_1_31_33
Heated at 500°C
Glycol Solvated
Air Dried
Intensity (cps)
Degrees 2θ
5
10
15
20
25
30
35
9.73 IR
9.73
9.96
4.95 IR
4.96
4.95
3.30 IR
3.32
3.26

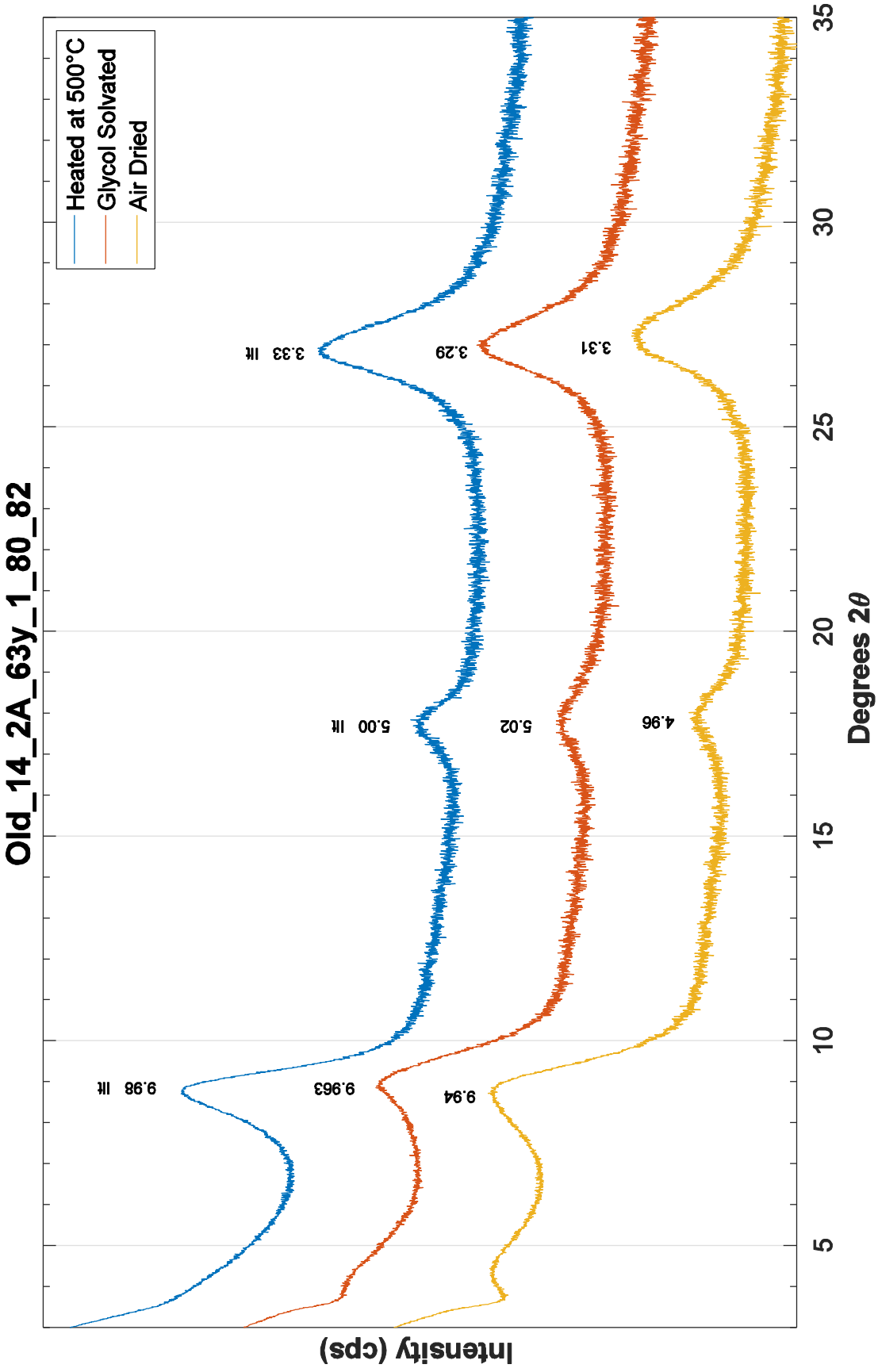
Old_14_2A_63y_1_80_82
Heated at 500°C
Glycol Solvated
Air Dried
Intensity (cps)
Degrees 2θ
5
10
15
20
25
30
35
9.98 Ilt
9.963
9.94
5.00 Ilt
5.02
4.96
3.33 Ilt
3.29
3.31

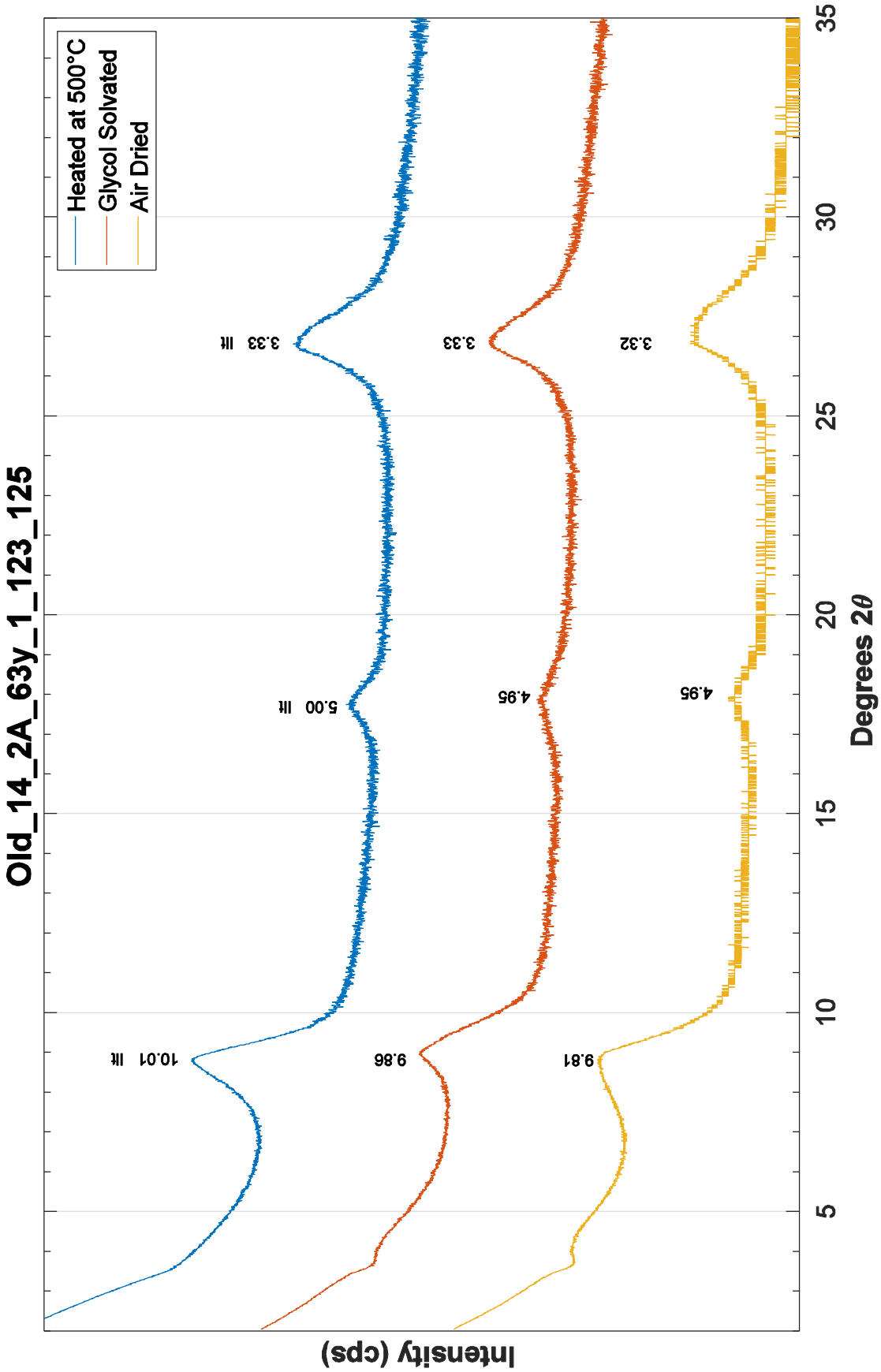
Old_14_2A_63y_1_123_125
Heated at 500°C
Glycol Solvated
Air Dried
10.01 Ilt
9.86
9.81
5.00 Ilt
4.95
4.95
3.33 Ilt
3.33
3.32
Intensity (cps)
Degrees 2θ
5
10
15
20
25
30
35

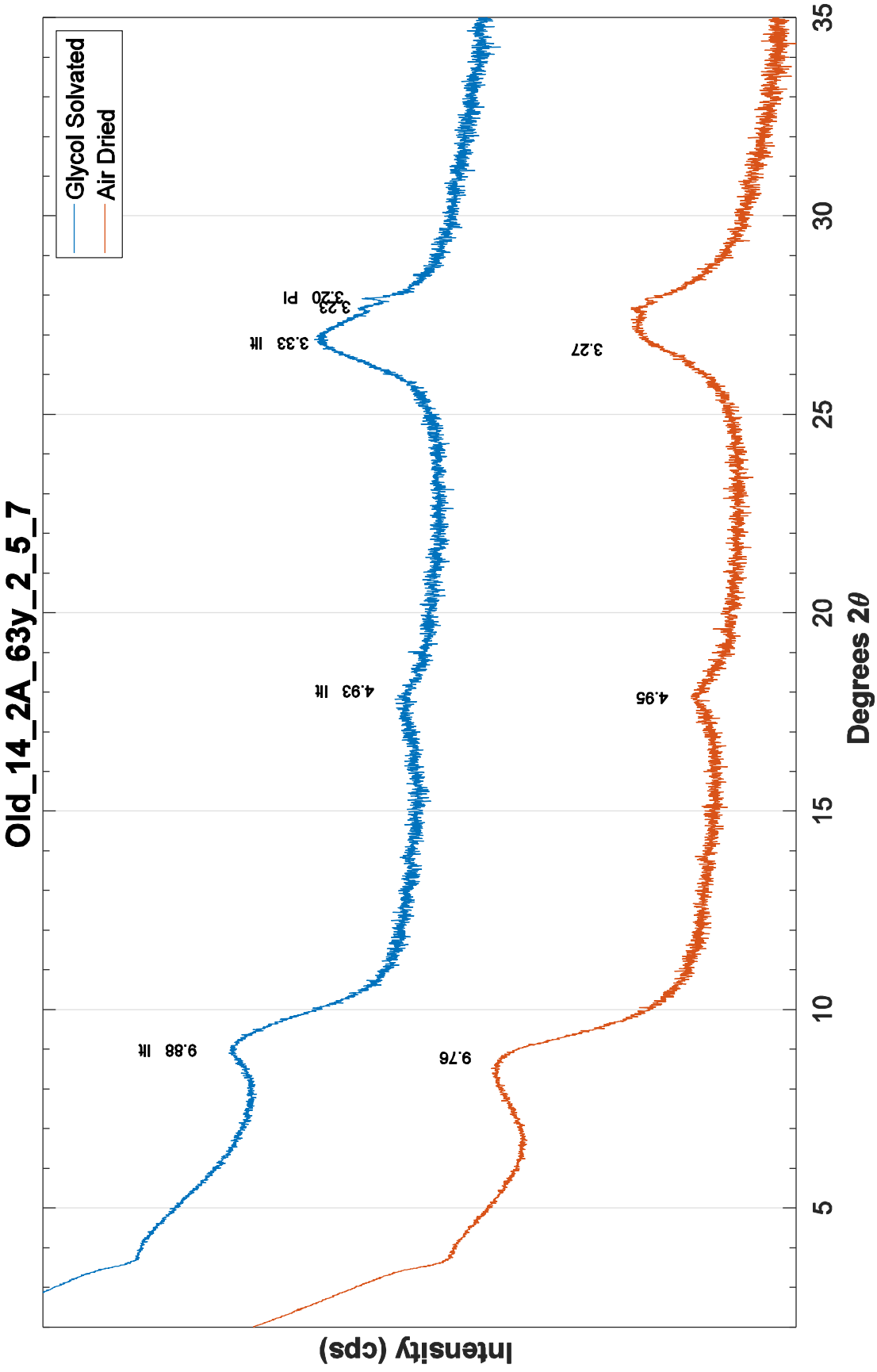
Old_14_2A_63y_2_5_7
Glycol Solvated
Air Dried
Intensity (cps)
Degrees 2θ
5
10
15
20
25
30
35
9.88 lit
4.93 lit
3.33 lit
3.23
3.20 Pl
9.76
4.95
3.27

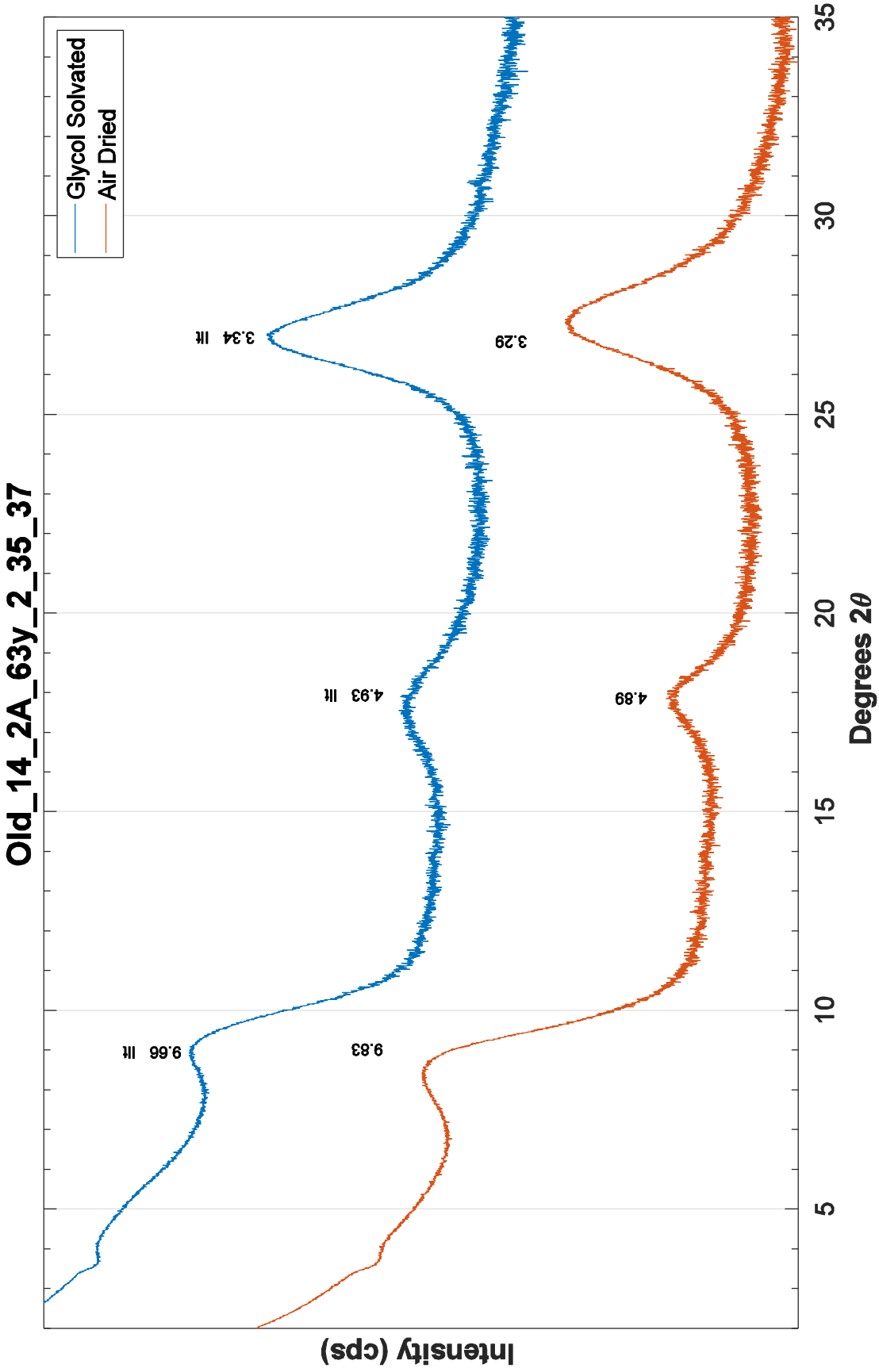
Old_14_2A_63y_2_35_37
Glycol Solvated
Air Dried
Intensity (cps)
Degrees 2θ
5
10
15
20
25
30
35
9.66 Ilt
9.83
4.93 Ilt
4.89
3.34 Ilt
3.29

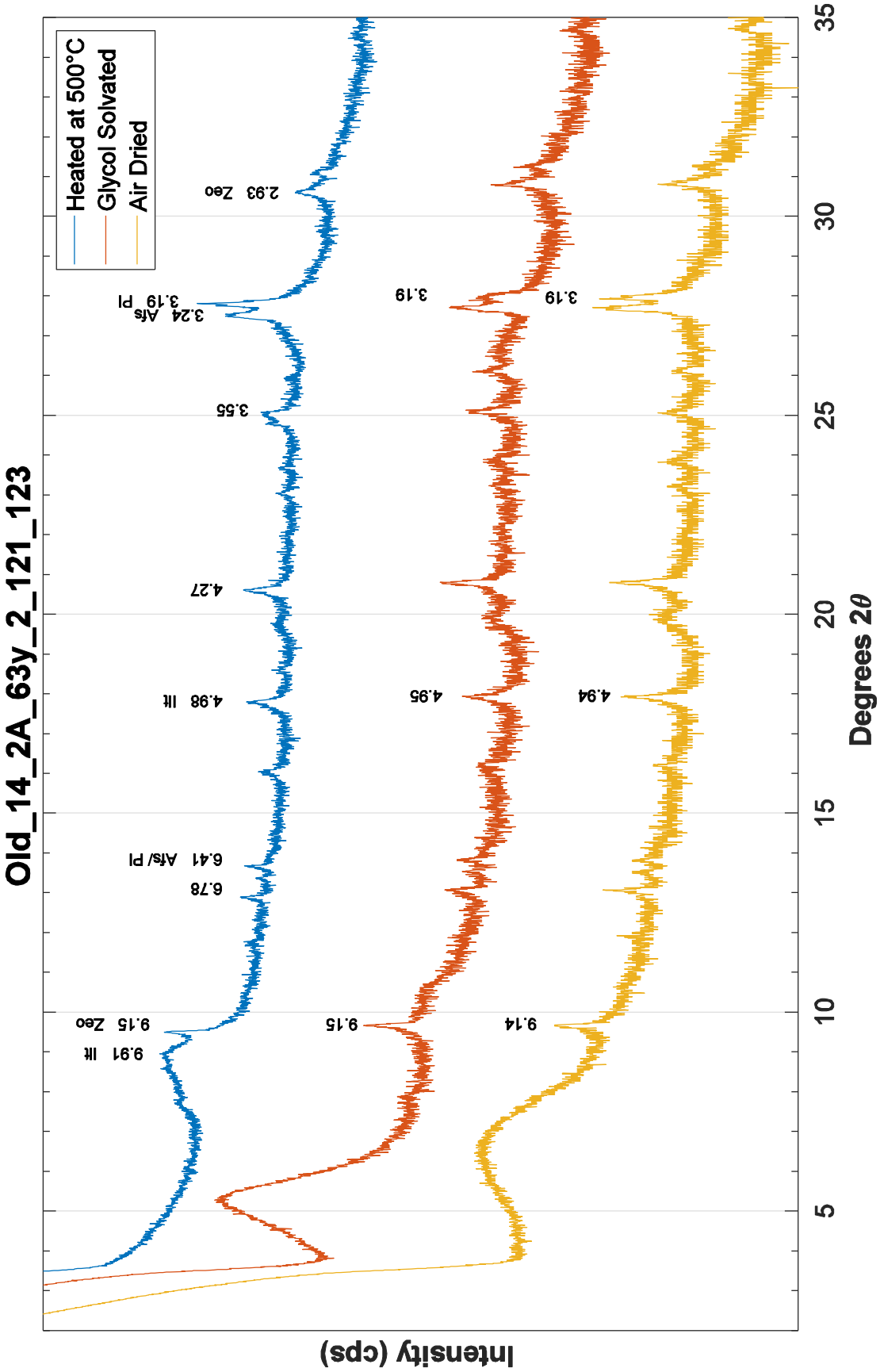
Old_14_2A_63y_2_121_123
Heated at 500°C
Glycol Solvated
Air Dried
Intensity (cps)
Degrees 2θ
5
10
15
20
25
30
35
9.91 Ilt
9.15 Zeo
6.78
6.41 Afs/Pl
4.98 Ilt
4.27
3.55
3.24 Afs
3.19 Pl
2.93 Zeo
9.15
3.19
4.95
9.14
3.19
4.94

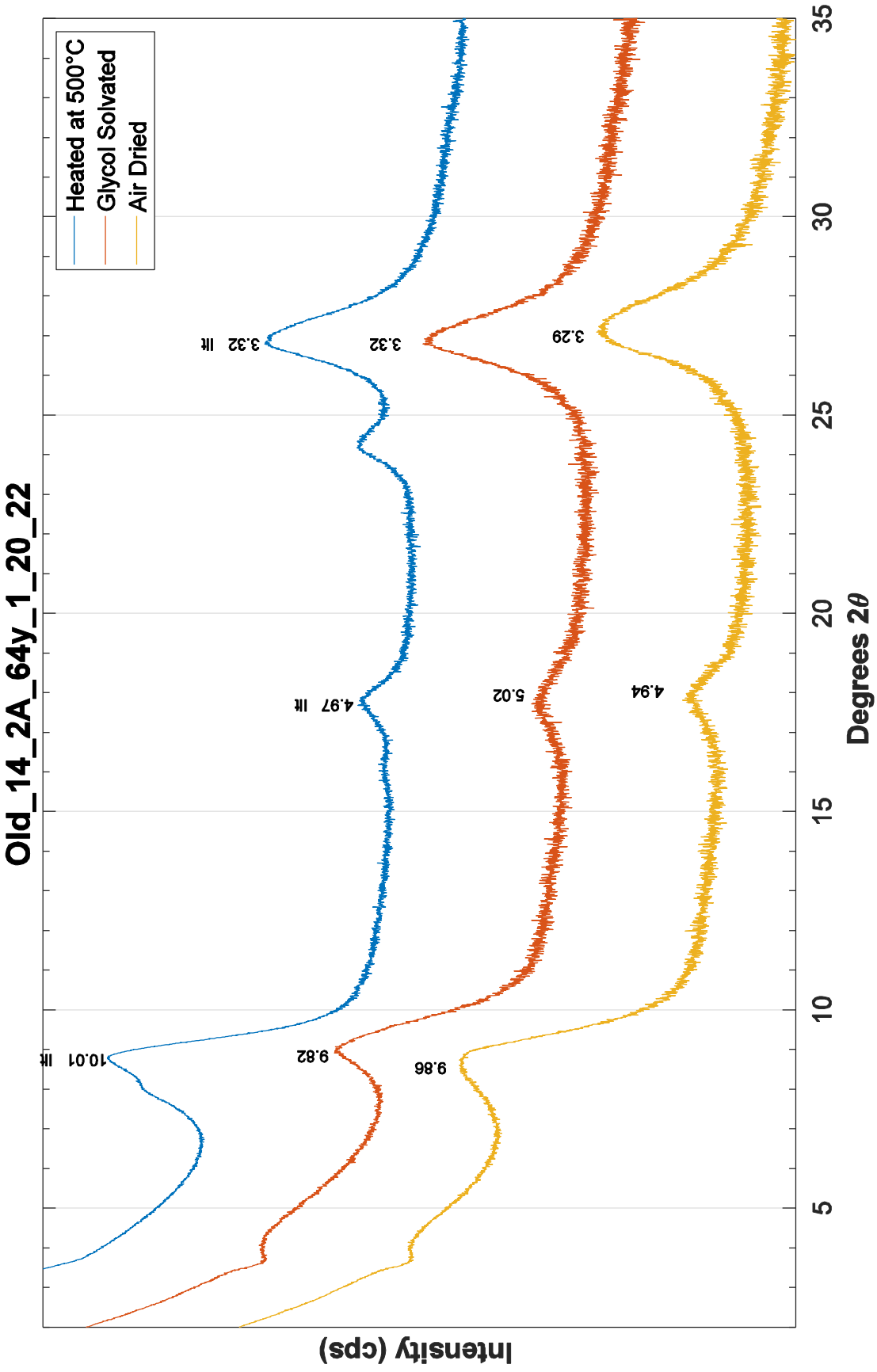
Old_14_2A_64y_1_20_22
Heated at 500°C
Glycol Solvated
Air Dried
10.01 lit
9.82
9.86
4.97 lit
5.02
4.94
3.32 lit
3.32
3.29
Intensity (cps)
Degrees 2θ
5
10
15
20
25
30
35

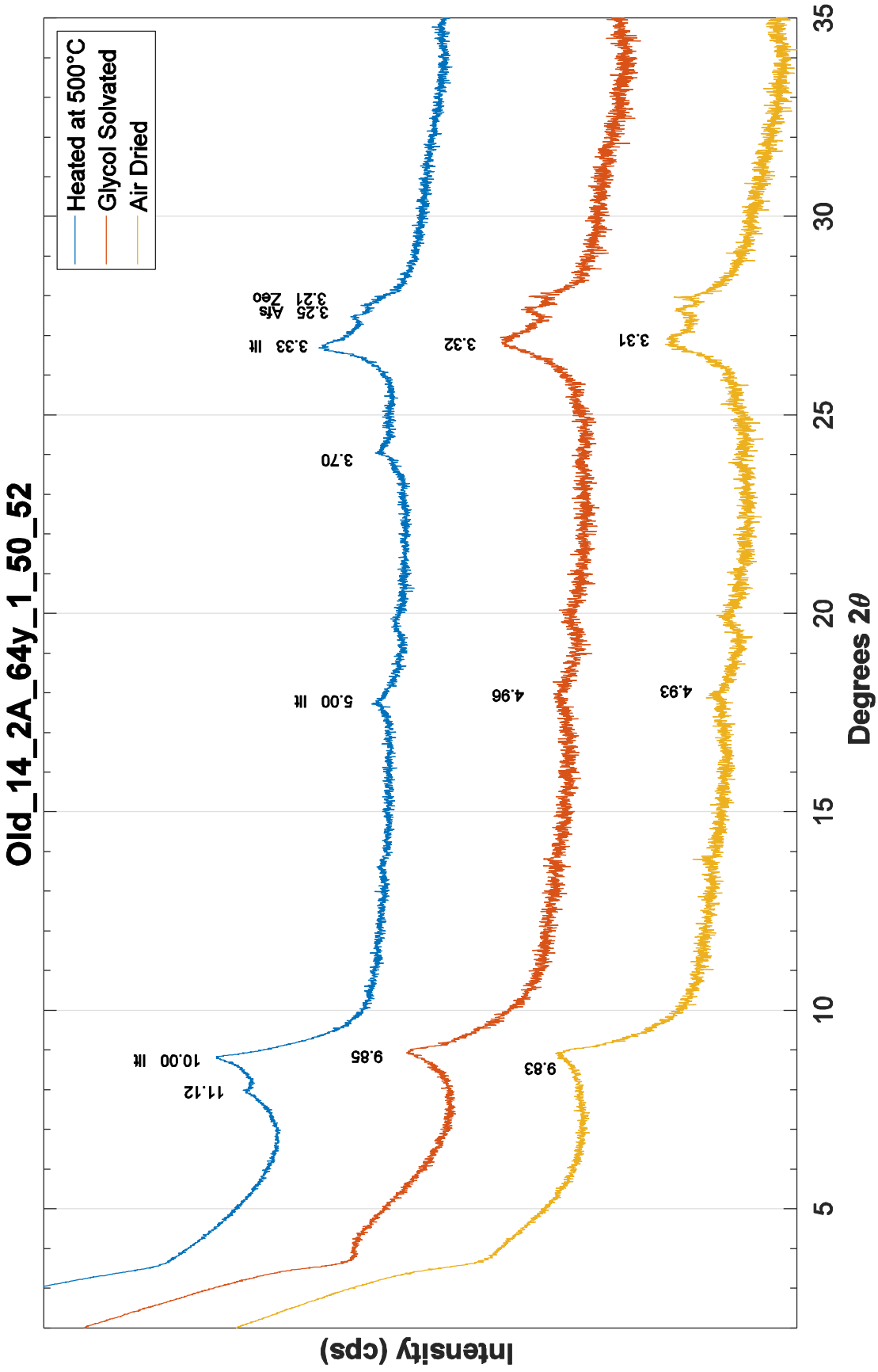
Old_14_2A_64y_1_50_52
Heated at 500°C
Glycol Solvated
Air Dried
Intensity (cps)
Degrees 2θ
5
10
15
20
25
30
35
11.12
10.00 IIt
9.85
9.83
5.00 IIt
4.96
4.93
3.70
3.33 IIt
3.25 Ats
3.21 Zeo
3.32
3.31

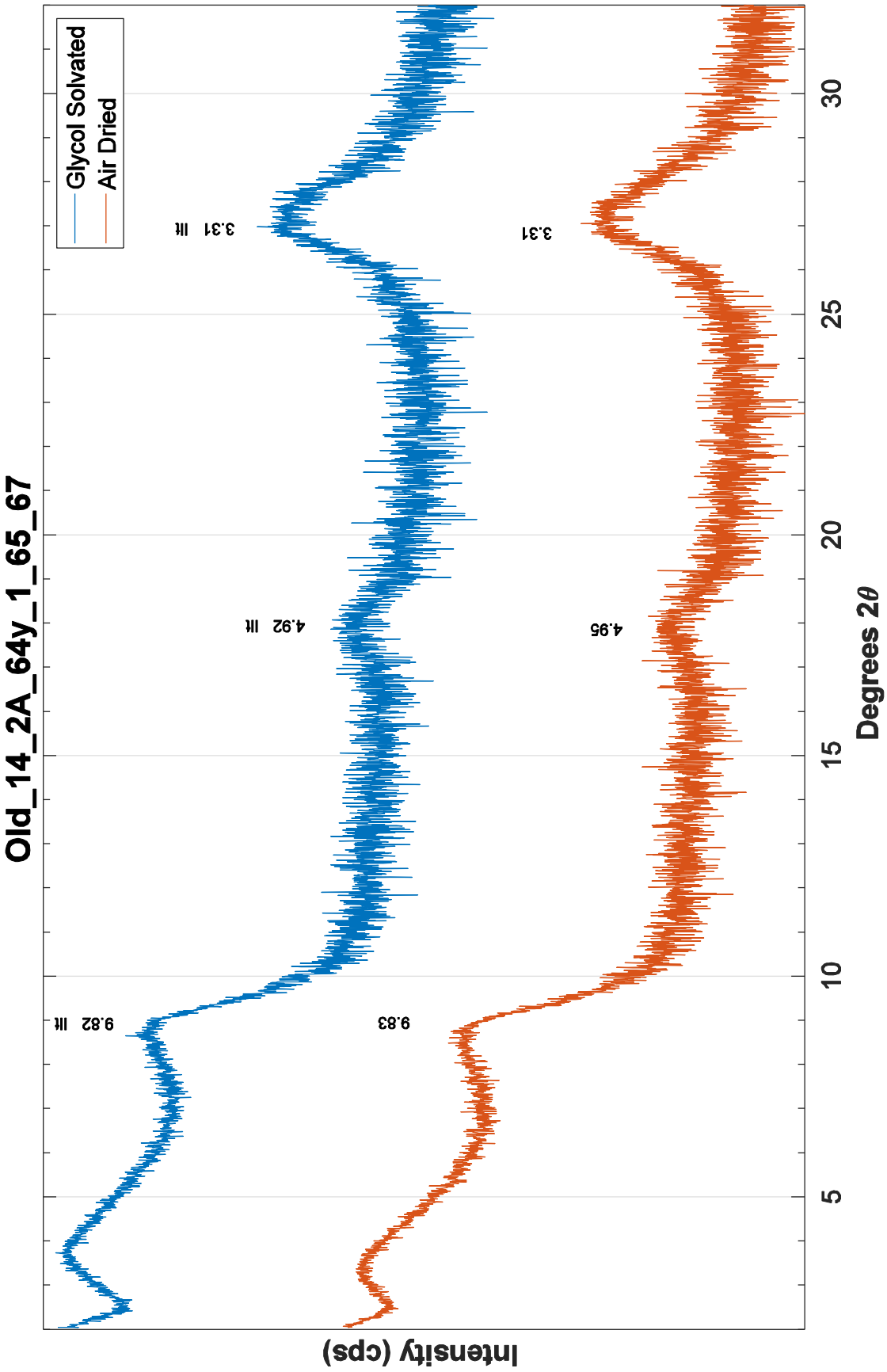
Old_14_2A_64y_1_65_67
Glycol Solvated
Air Dried
9.82 Å
4.92 Å
3.31 Å
9.83
4.95
3.31
Intensity (cps)
Degrees 2θ
5
10
15
20
25
30

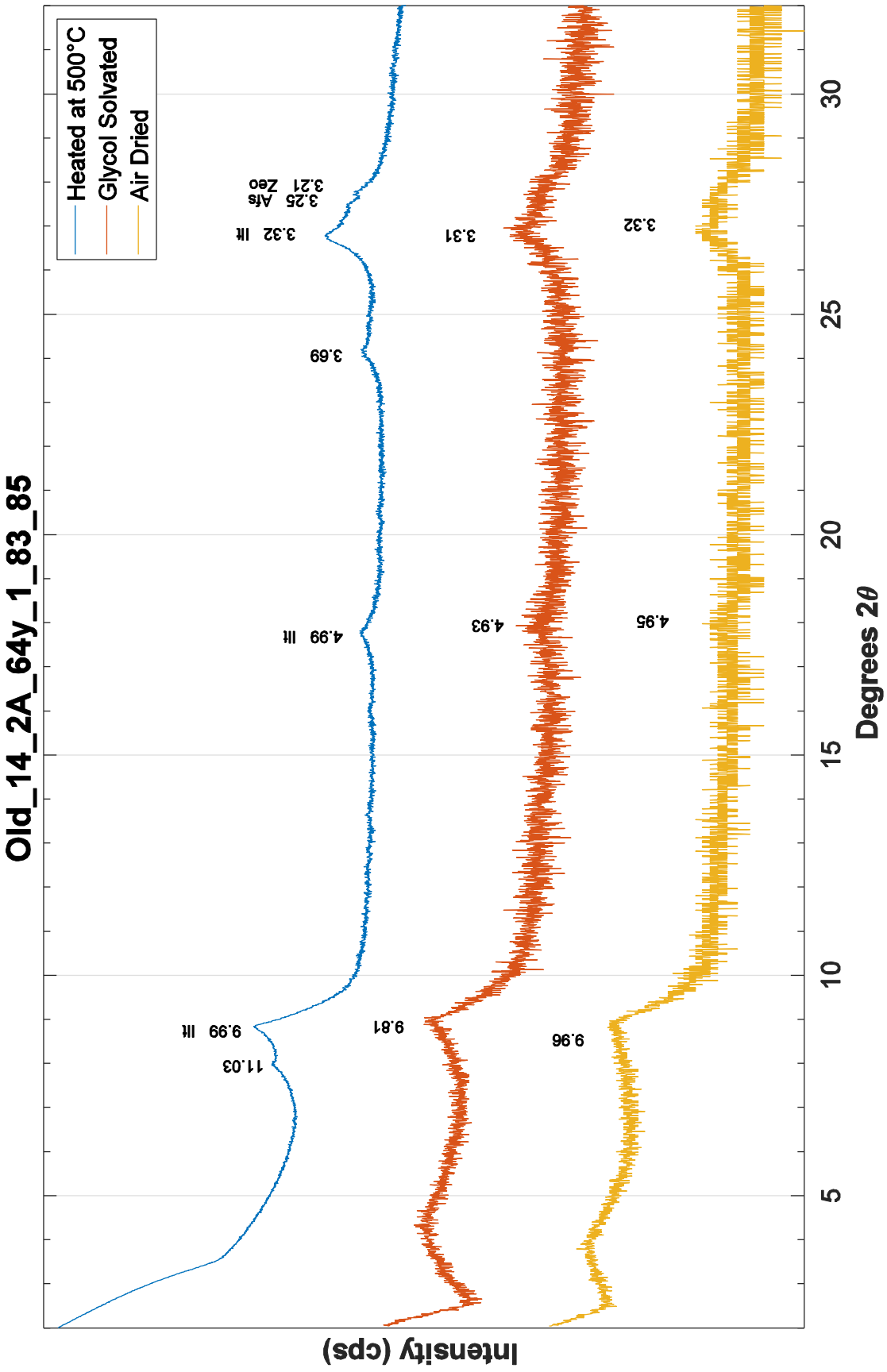
Old_14_2A_64y_1_83_85
Heated at 500°C
Glycol Solvated
Air Dried
Intensity (cps)
Degrees 2θ
5
10
15
20
25
30
11.03
9.99 Ilt
4.99 Ilt
3.69
3.32 Ilt
3.25 Als
3.21 Zeo
9.81
4.93
3.31
9.96
4.95
3.32

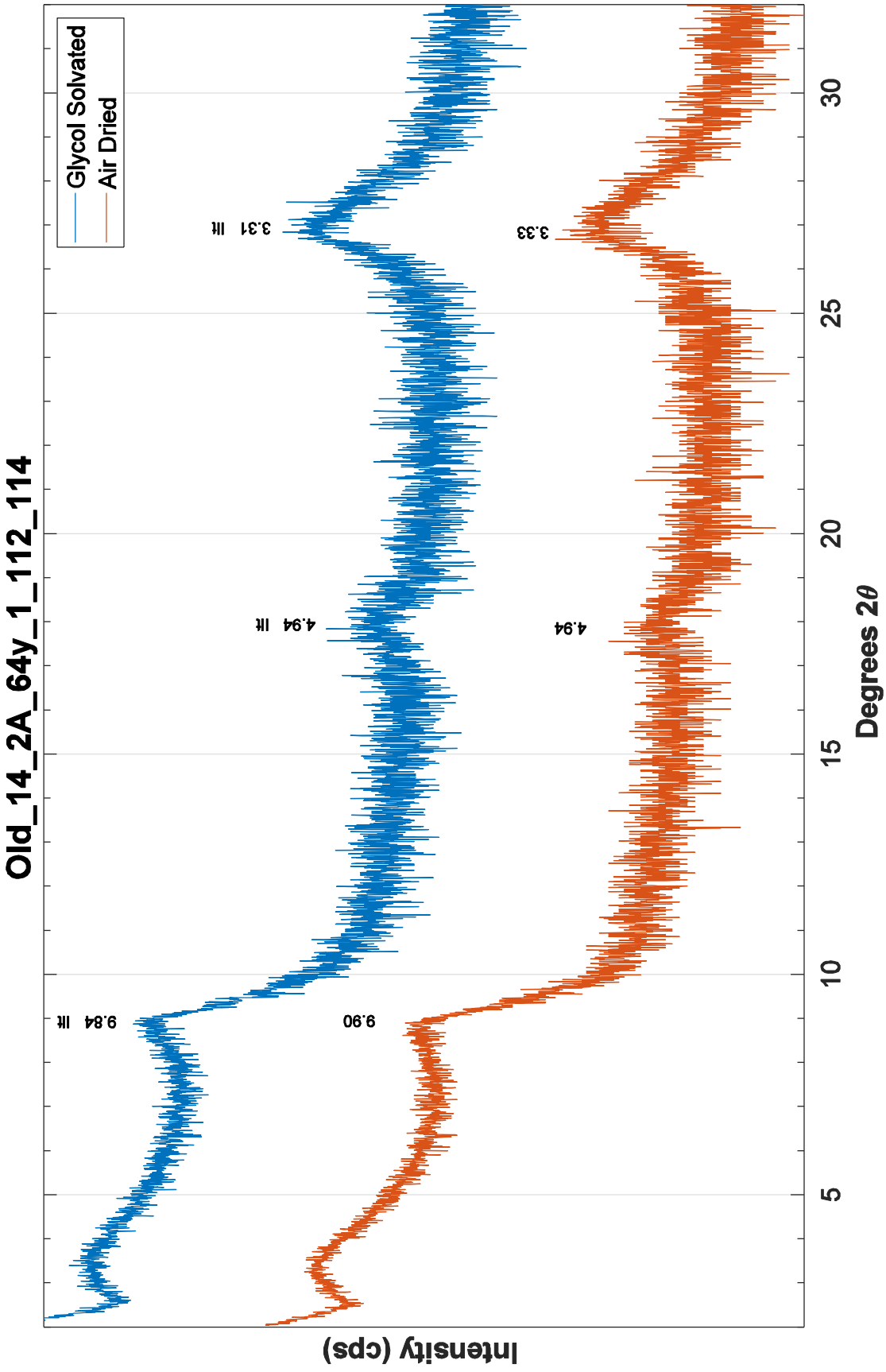
Old_14_2A_64y_1_112_114
Glycol Solvated
Air Dried
9.84 Ilt
4.94 Ilt
3.31 Ilt
9.90
4.94
3.33
Intensity (cps)
Degrees 2θ
5
10
15
20
25
30

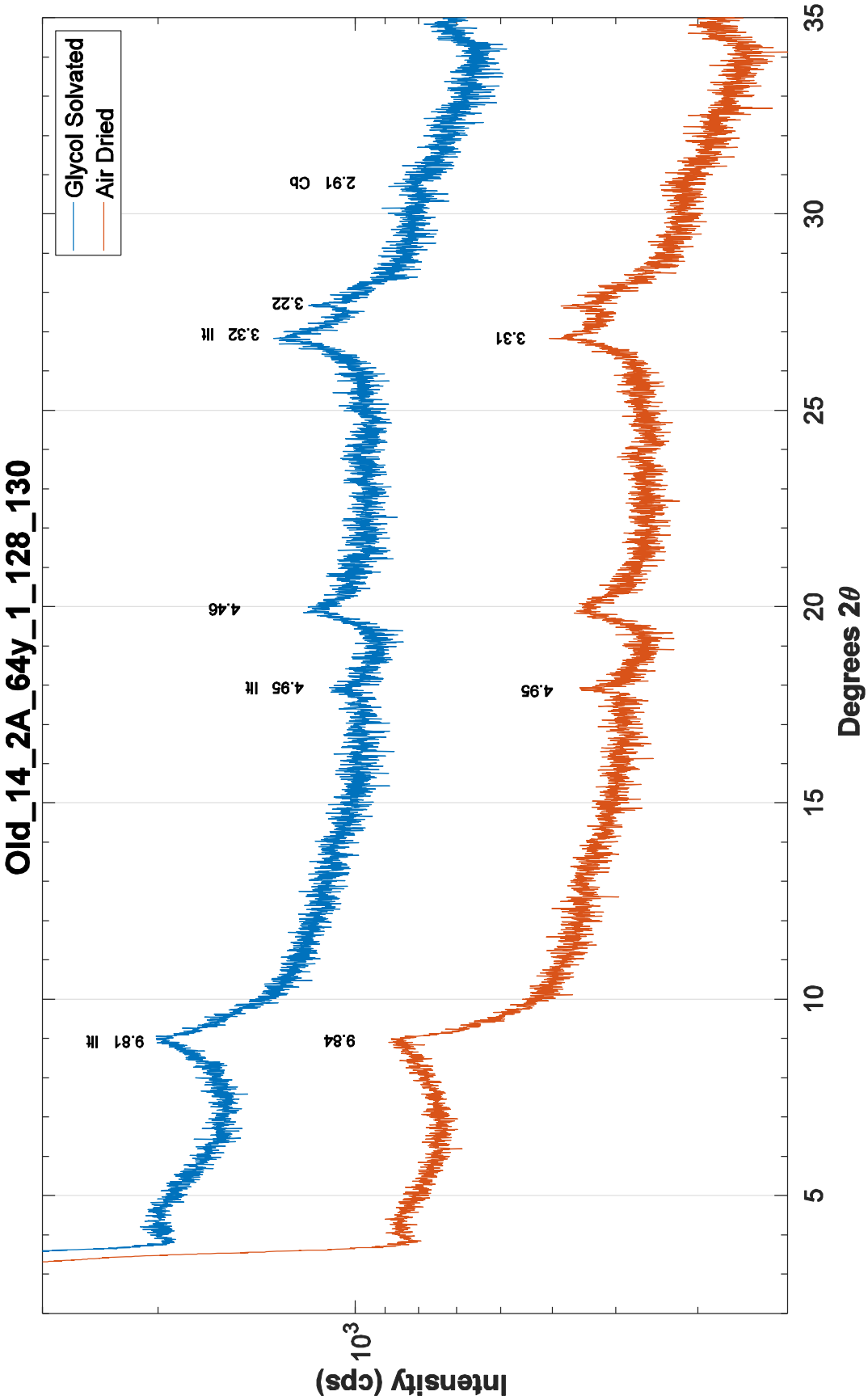
Old_14_2A_64y_1_128_130
Glycol Solvated
Air Dried
9.81 lit
9.84
4.95 lit
4.46
3.32 lit
3.22
2.91 Cb
4.95
3.31
Intensity (cps)
10^3
Degrees 2θ
5
10
15
20
25
30
35

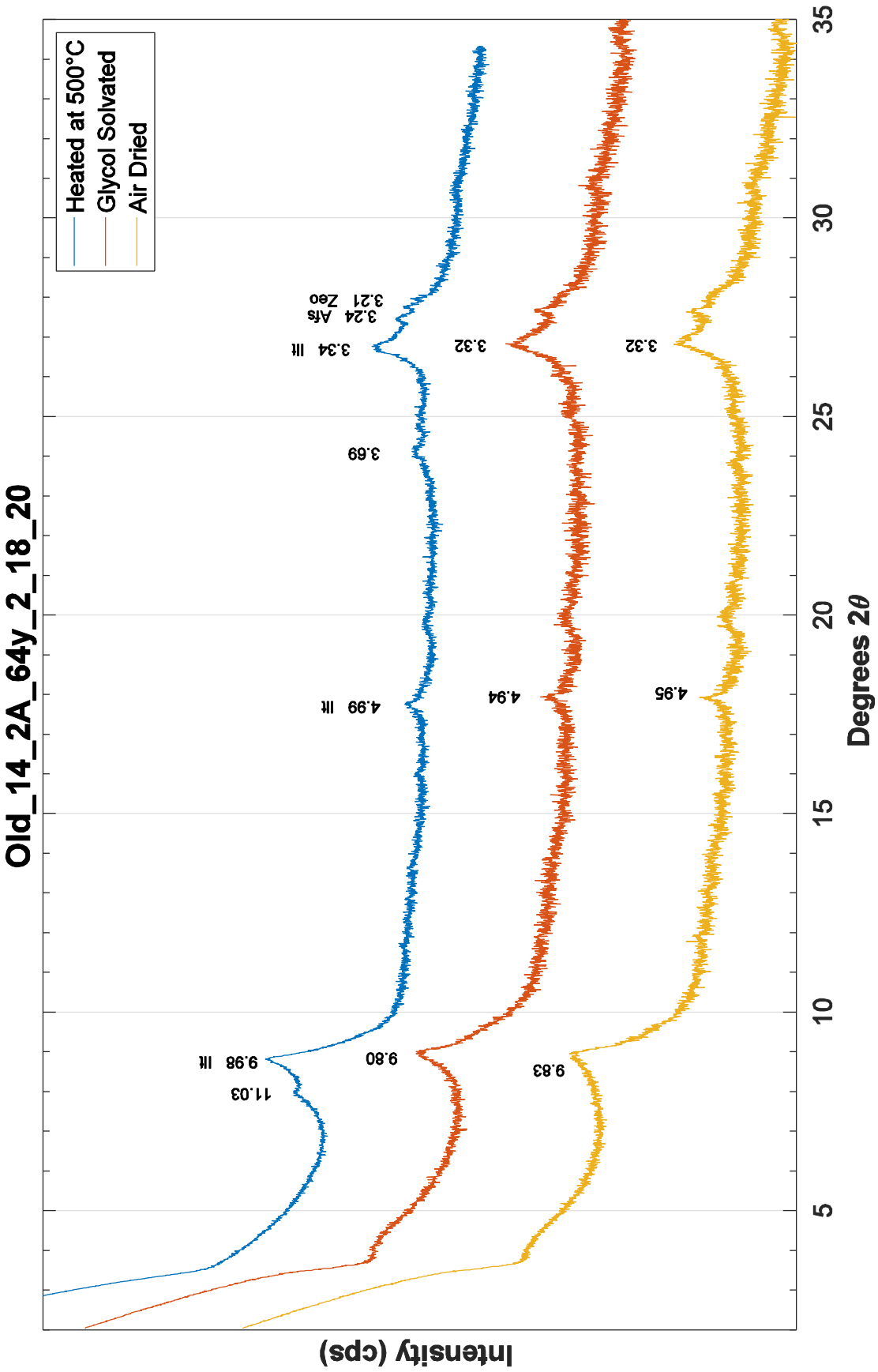
Old_14_2A_64y_2_18_20
Heated at 500°C
Glycol Solvated
Air Dried
Intensity (cps)
Degrees 2θ
5
10
15
20
25
30
35
11.03
9.98 Ilt
9.80
9.83
4.99 Ilt
4.94
4.95
3.69
3.34 Ilt
3.24 Afs
3.21 Zeo
3.32
3.32

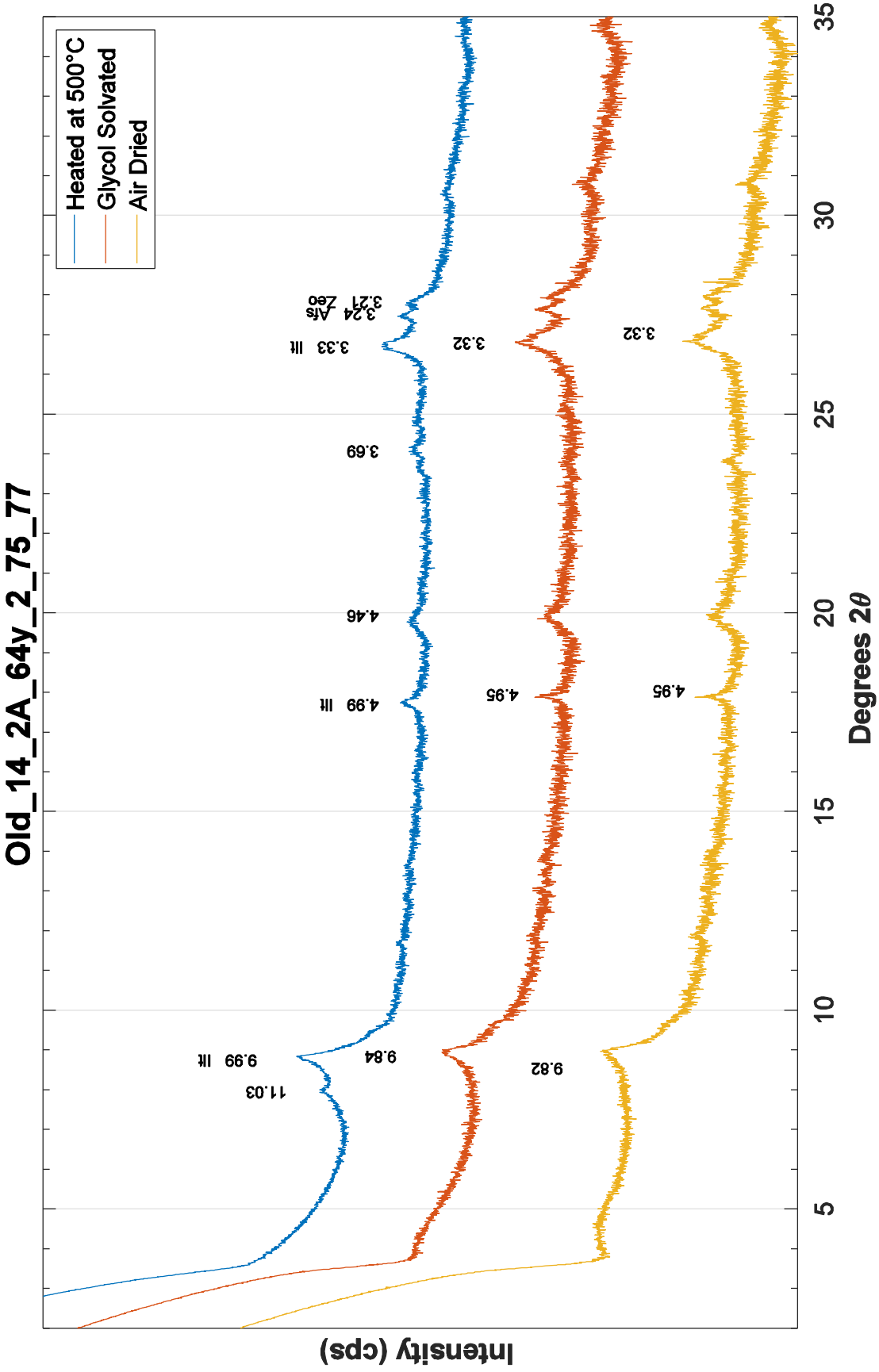
Old_14_2A_64y_2_75_77
Heated at 500°C
Glycol Solvated
Air Dried
Intensity (cps)
Degrees 2θ
5
10
15
20
25
30
35
11.03
9.99 Ilt
9.84
4.99 Ilt
4.46
3.69
3.33 Ilt
3.24 Ats
3.21 Zeo
9.82
4.95
3.32
3.32
4.95
3.32

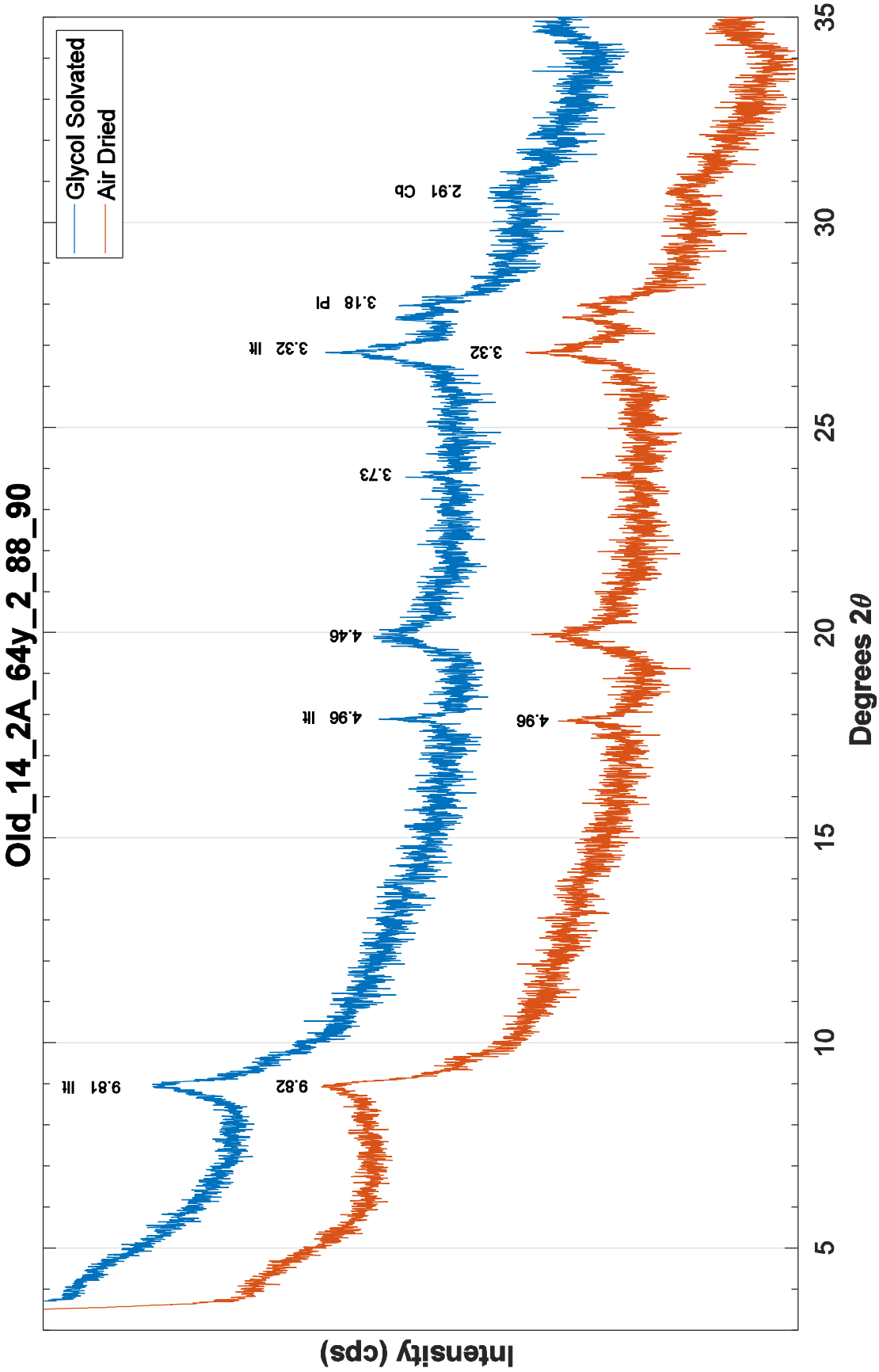
Old_14_2A_64y_2_88_90
Glycol Solvated
Air Dried
9.81 Ilt
9.82
4.96 Ilt
4.96
4.46
3.73
3.32 Ilt
3.32
3.18 Pl
2.91 Cb
Intensity (cps)
Degrees 2θ
5
10
15
20
25
30
35

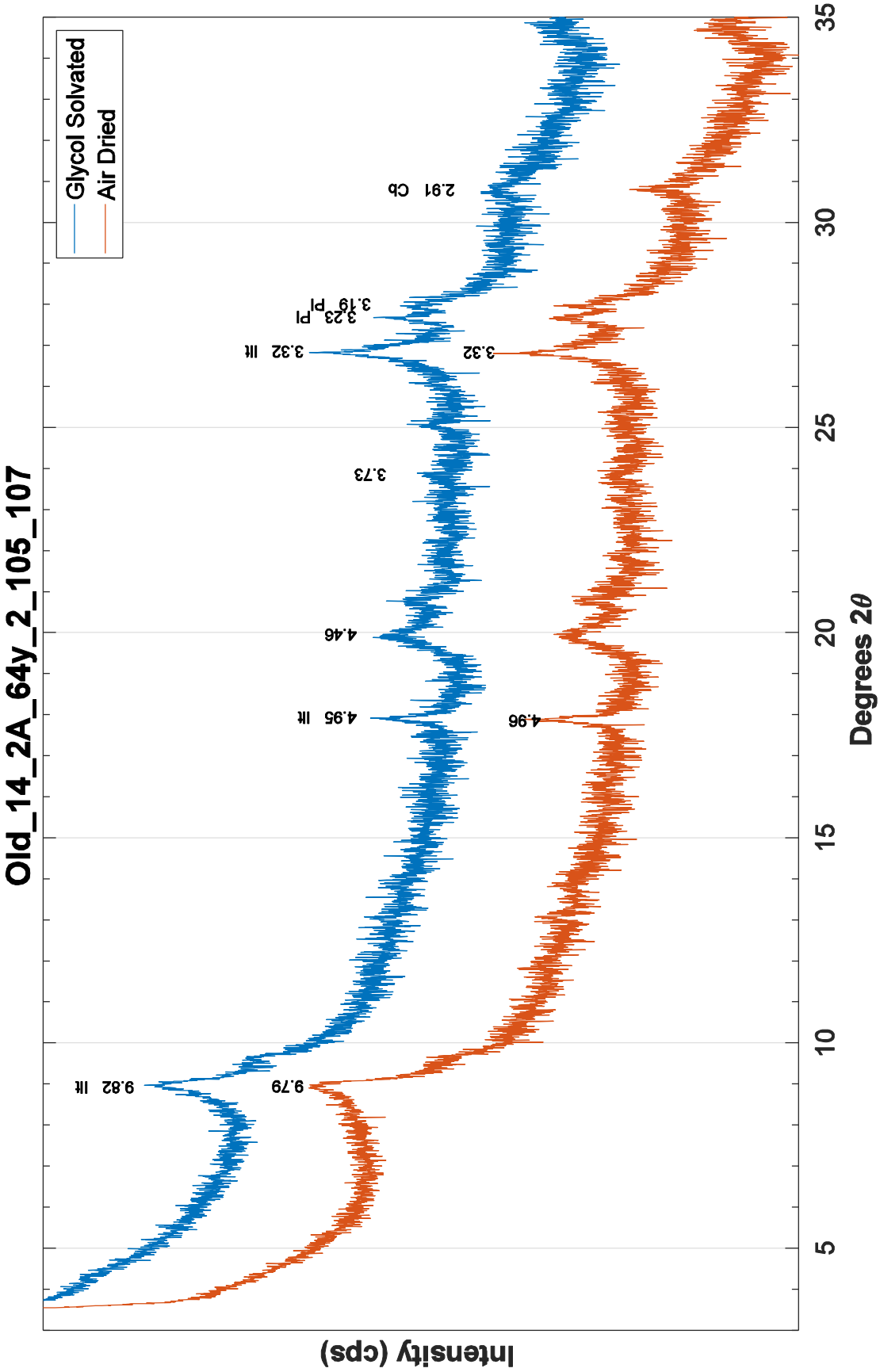
Old_14_2A_64y_2_105_107
Glycol Solvated
Air Dried
Intensity (cps)
Degrees 2θ
5
10
15
20
25
30
35
9.82 Ilt
9.79
4.95 Ilt
4.96
4.46
3.73
3.32 Ilt
3.32
3.23 Pl
3.19 Pl
2.91 Cb

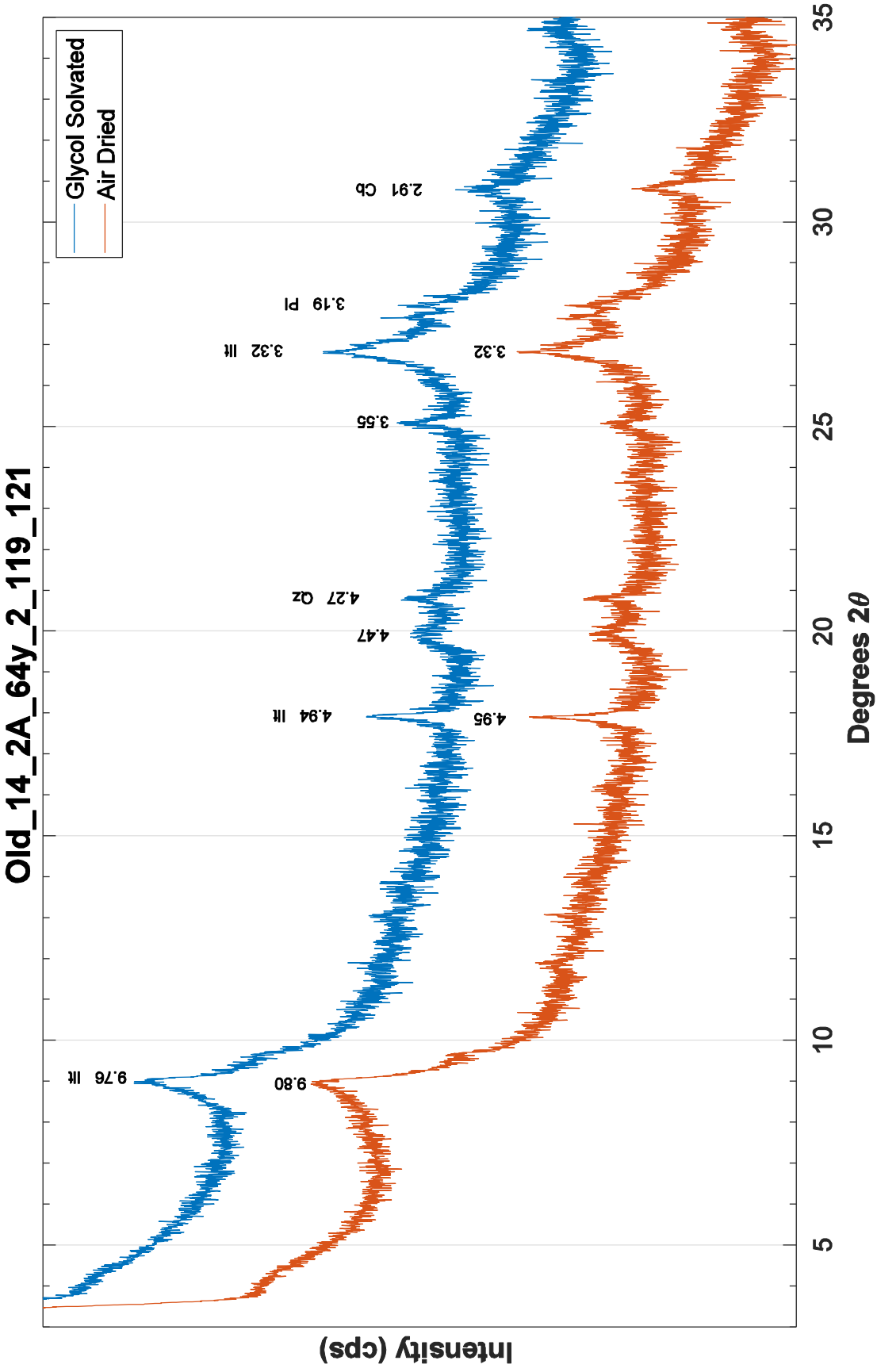
Old_14_2A_64y_2_119_121
Glycol Solvated
Air Dried
9.76 Ilt
9.80
4.94 Ilt
4.95
4.47
4.27 Qz
3.55
3.32 Ilt
3.32
3.19 Pl
2.91 Cb
Intensity (cps)
Degrees 2θ
5
10
15
20
25
30
35

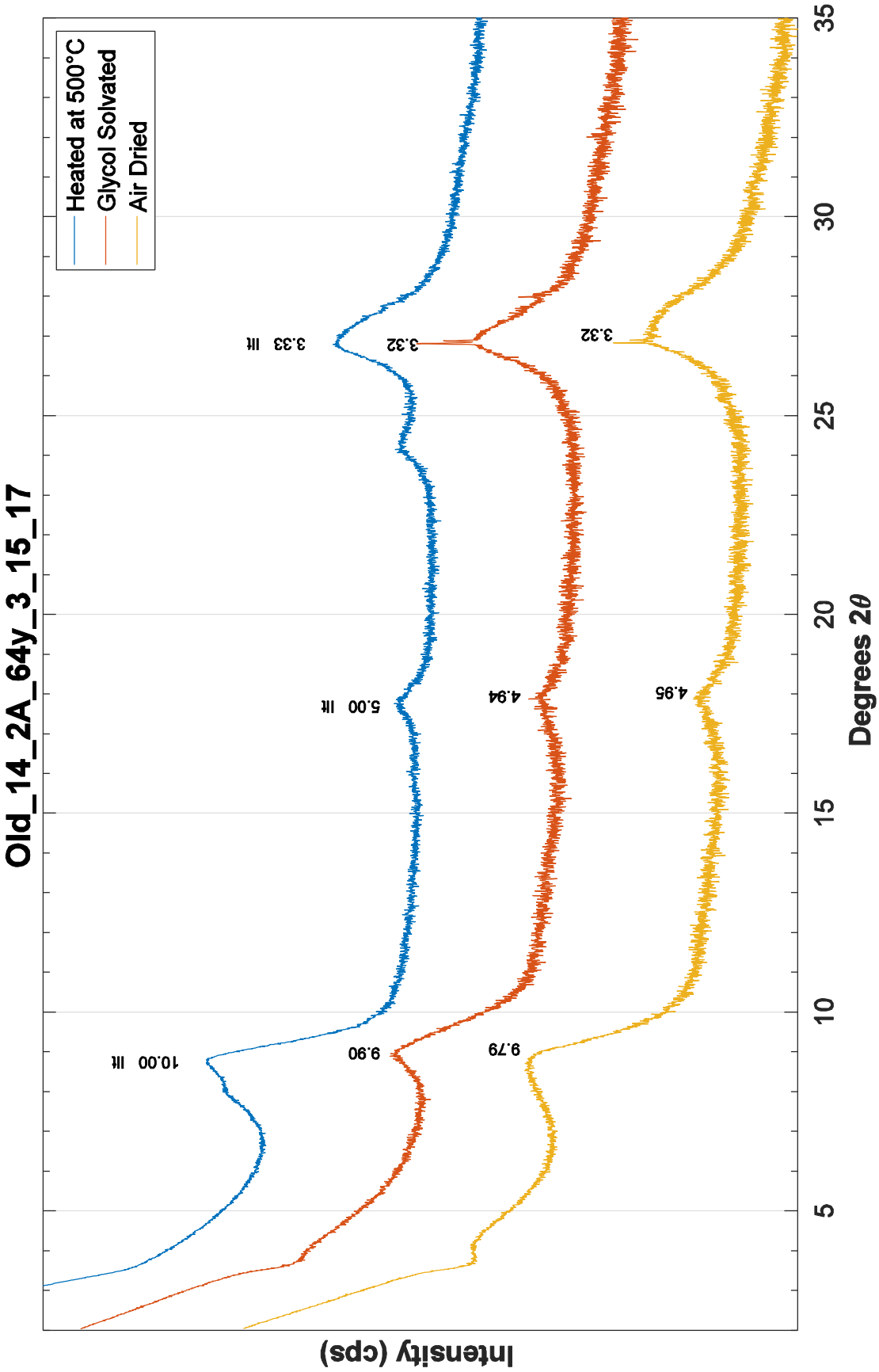
Old_14_2A_64y_3_15_17
Heated at 500°C
Glycol Solvated
Air Dried
10.00 Å
9.90
9.79
5.00 Å
4.94
4.95
3.33 Å
3.32
3.32
Intensity (cps)
Degrees 2θ
5
10
15
20
25
30
35

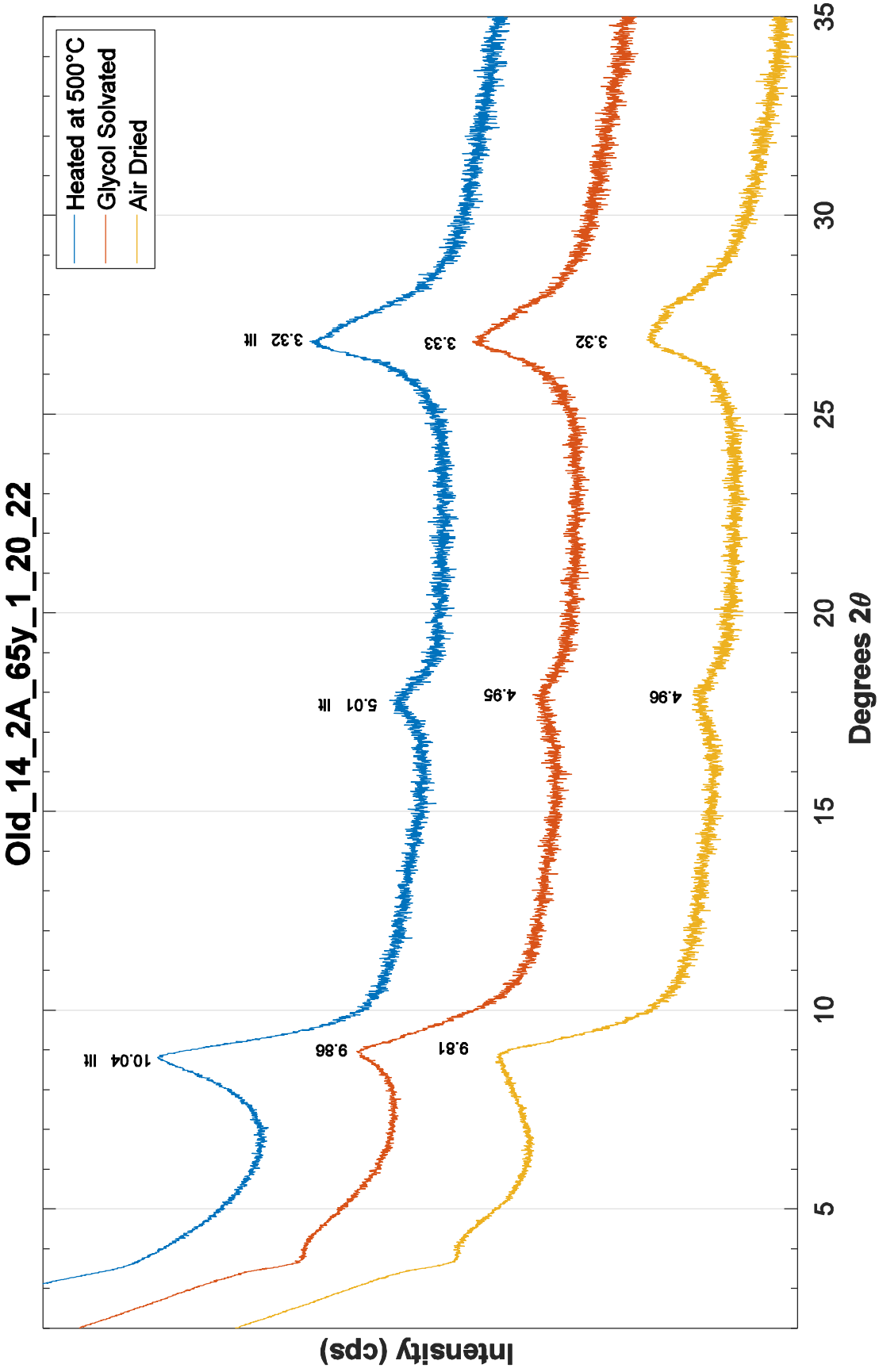
Old_14_2A_65y_1_20_22
Heated at 500°C
Glycol Solvated
Air Dried
10.04 Å
9.86
9.81
5.01 Å
4.95
4.96
3.32 Å
3.33
3.32
Intensity (cps)
Degrees 2θ
5
10
15
20
25
30
35

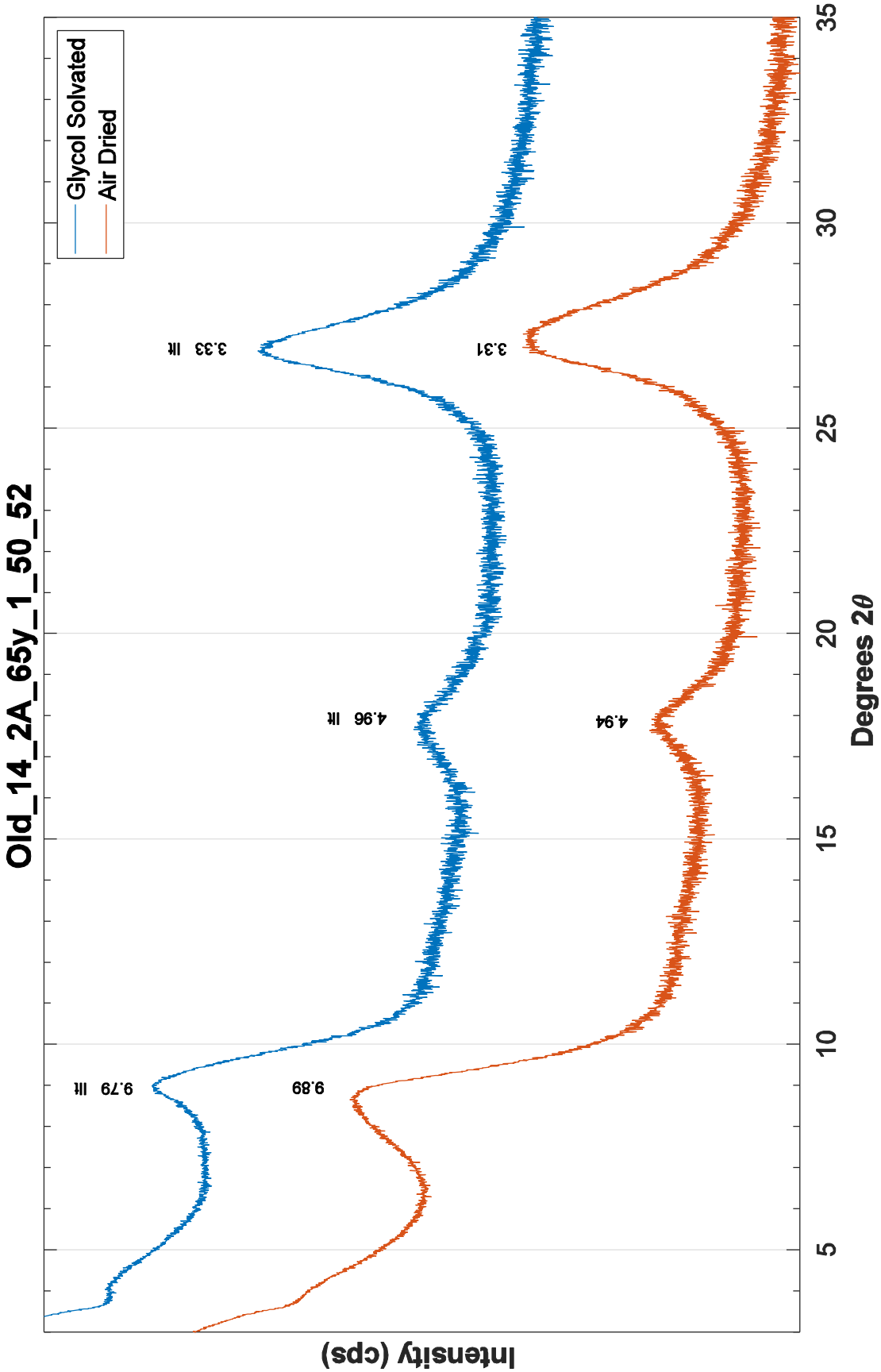
Old_14_2A_65y_1_50_52
Glycol Solvated
Air Dried
9.79 Ilt
9.89
4.96 Ilt
4.94
3.33 Ilt
3.31
Intensity (cps)
Degrees 2θ
5
10
15
20
25
30
35

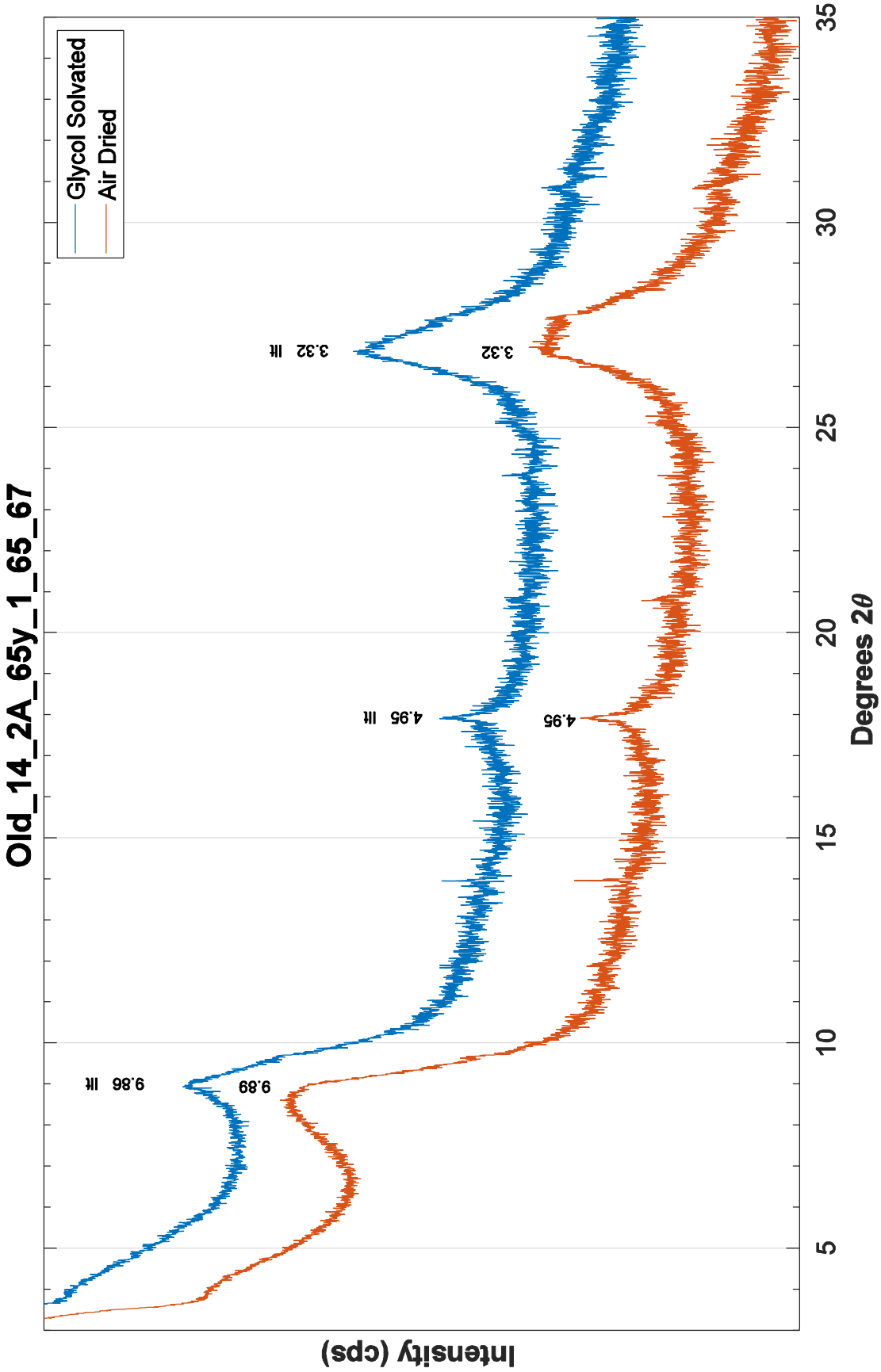
Old_14_2A_65y_1_65_67
Glycol Solvated
Air Dried
9.86 Å
9.89
4.95 Å
4.95
3.32 Å
3.32
Intensity (cps)
Degrees 2θ
5
10
15
20
25
30
35

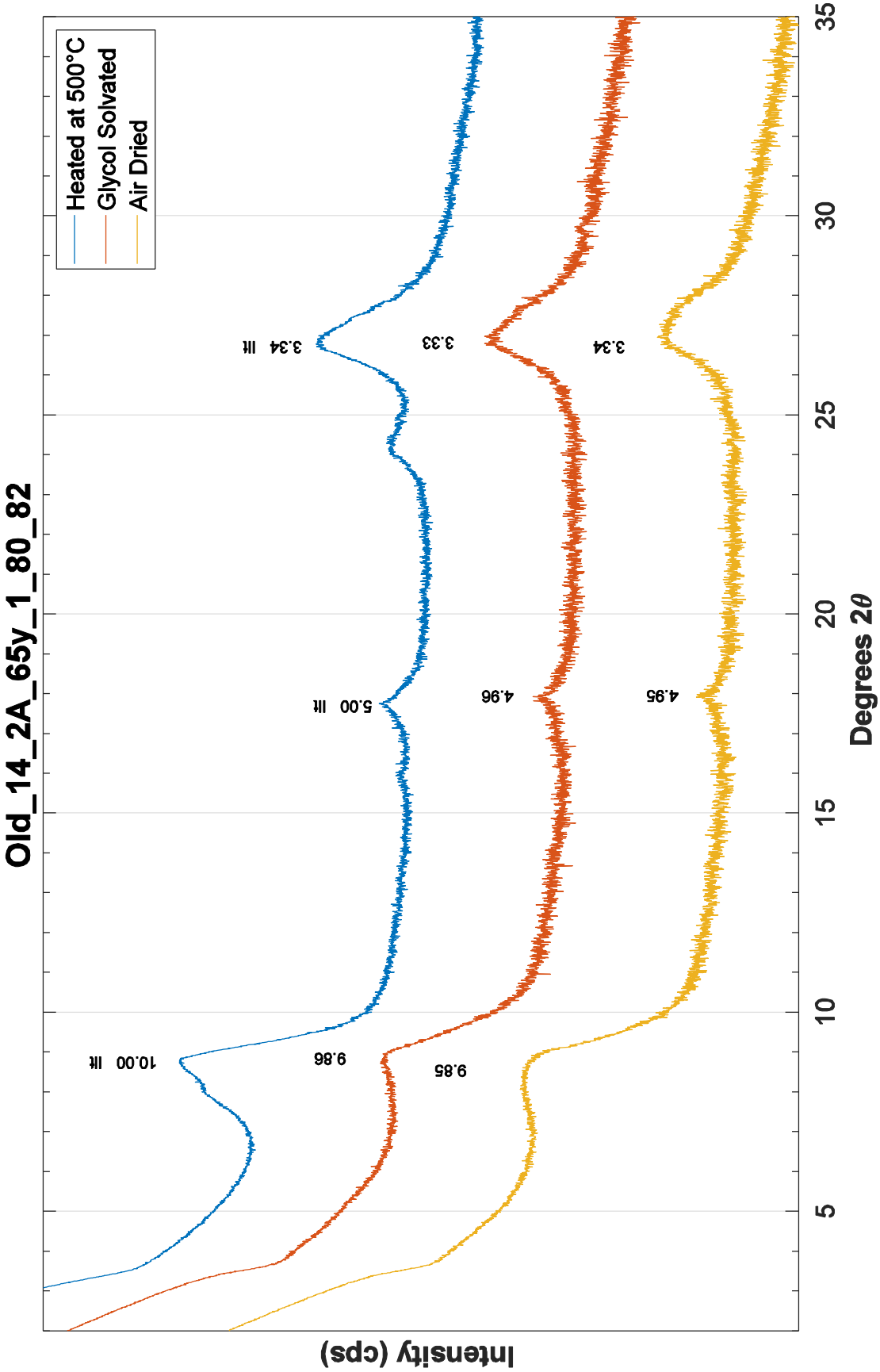
Old_14_2A_65y_1_80_82
Heated at 500°C
Glycol Solvated
Air Dried
10.00 Ilt
9.86
5.00 Ilt
3.34 Ilt
9.85
4.96
3.33
4.95
3.34
Intensity (cps)
Degrees 2θ
5
10
15
20
25
30
35

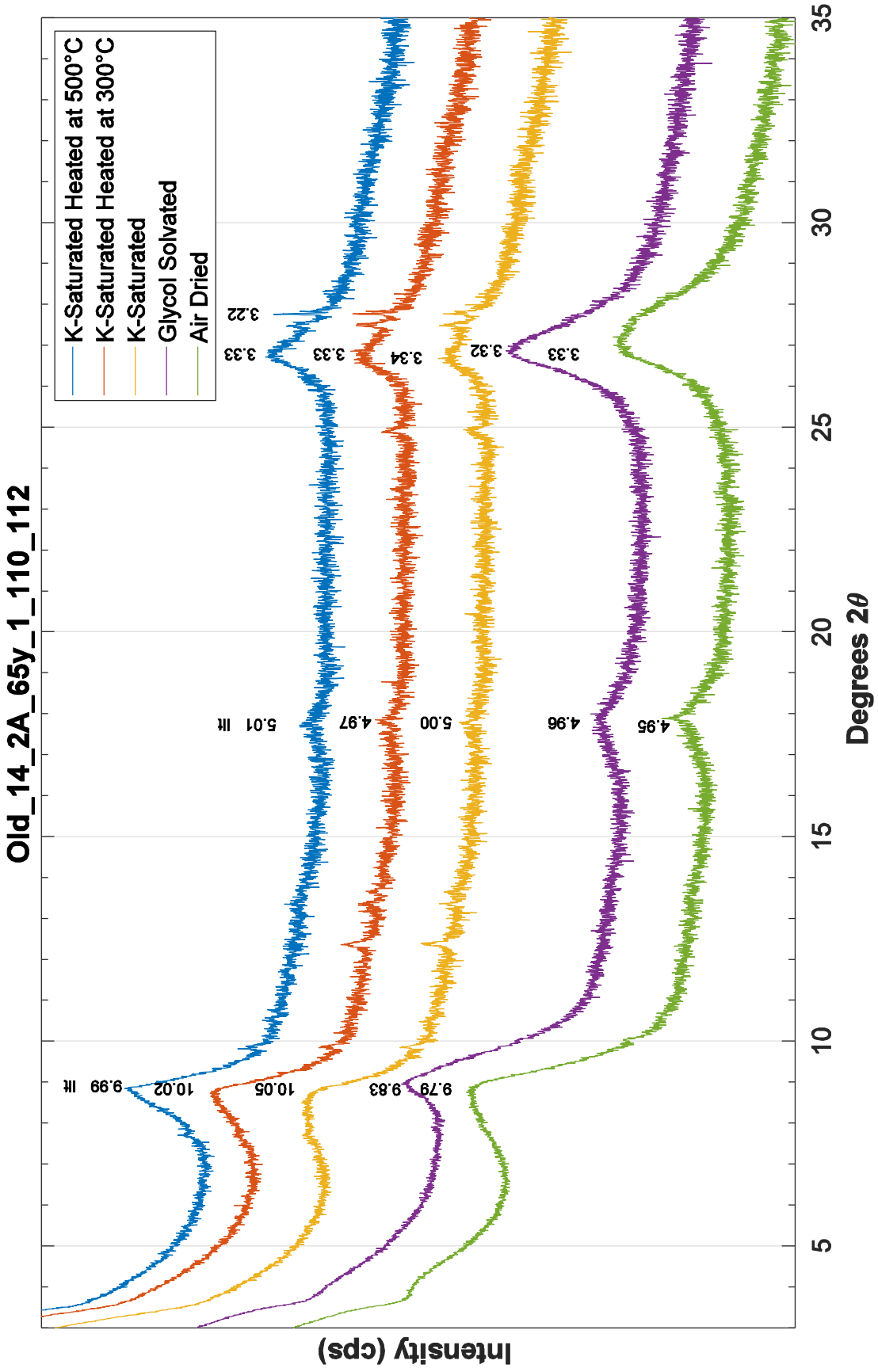
Old_14_2A_65y_1_110_112
K-Saturated Heated at 500°C
K-Saturated Heated at 300°C
K-Saturated
Glycol Solvated
Air Dried
Intensity (cps)
Degrees 2θ
5
10
15
20
25
30
35
9.99
10.02
10.05
9.83
9.79
5.01
4.97
5.00
4.96
4.95
3.33
3.34
3.33
3.32
3.33
3.22

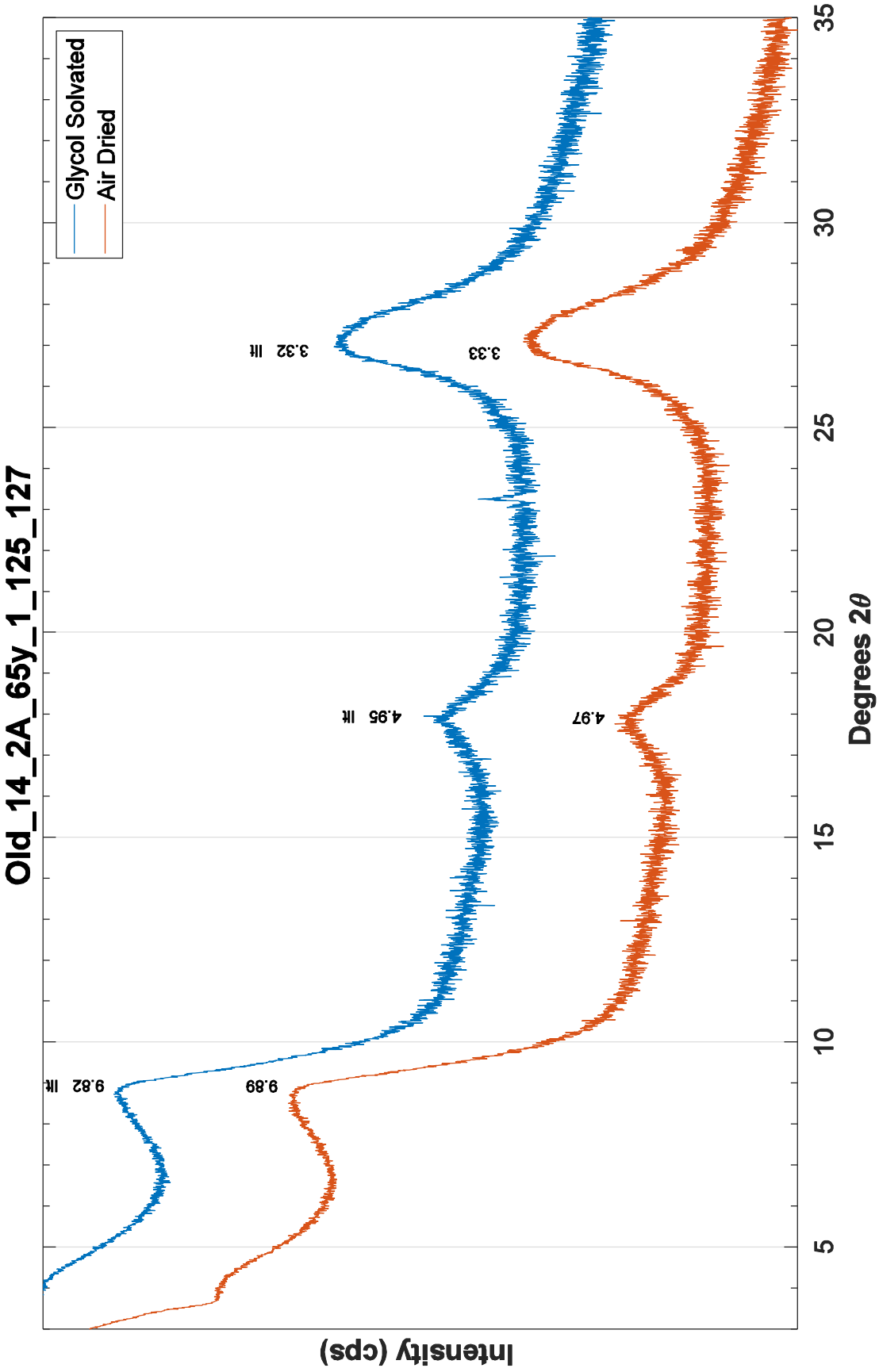
Old_14_2A_65y_1_125_127
Glycol Solvated
Air Dried
9.82 lit
9.89
4.95 lit
4.97
3.32 lit
3.33
Intensity (cps)
Degrees 2θ
5
10
15
20
25
30
35

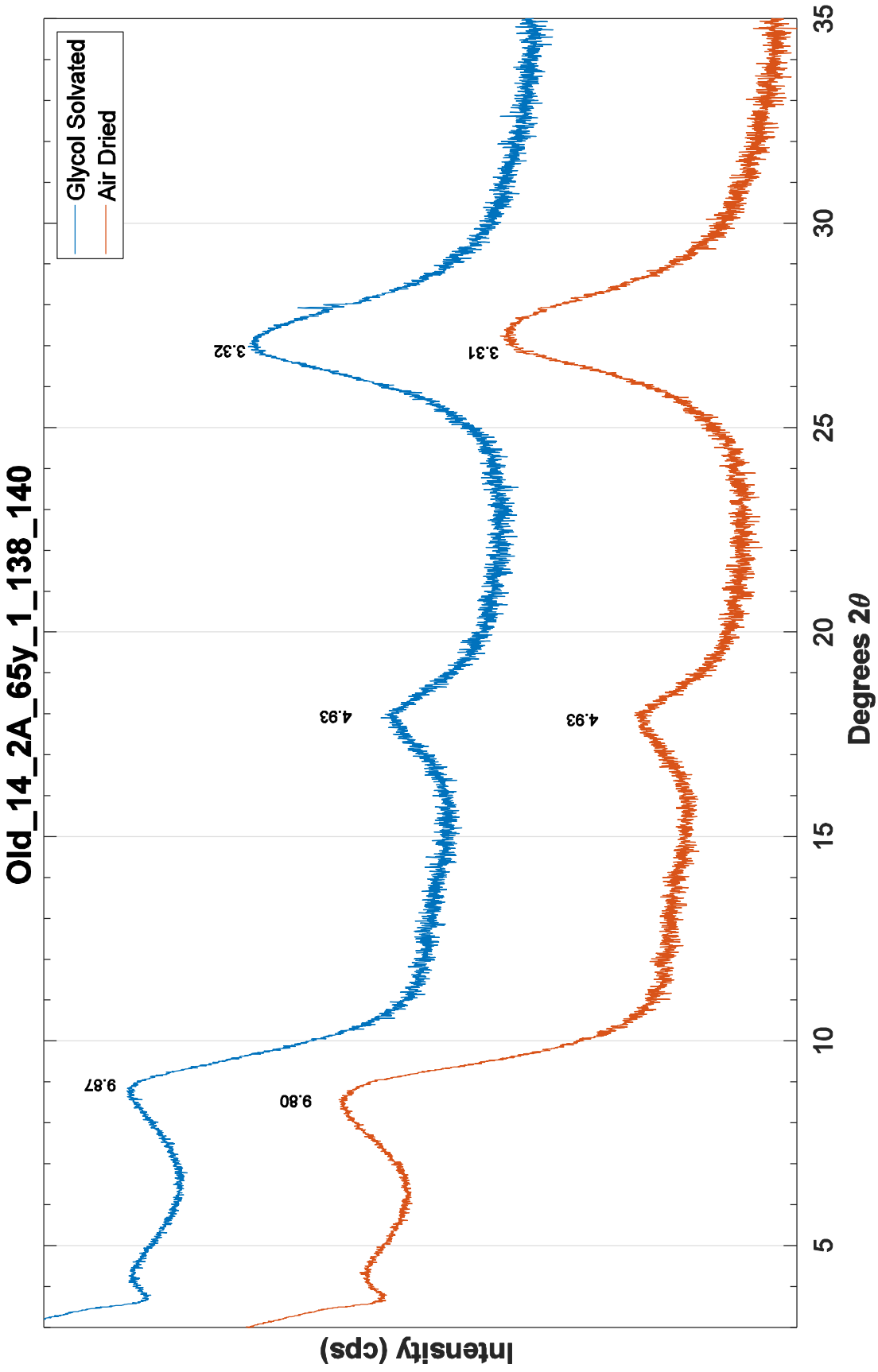
Old_14_2A_65y_1_138_140
Glycol Solvated
Air Dried
9.87
9.80
4.93
4.93
3.32
3.31
Intensity (cps)
5
10
15
20
25
30
35
Degrees 2θ

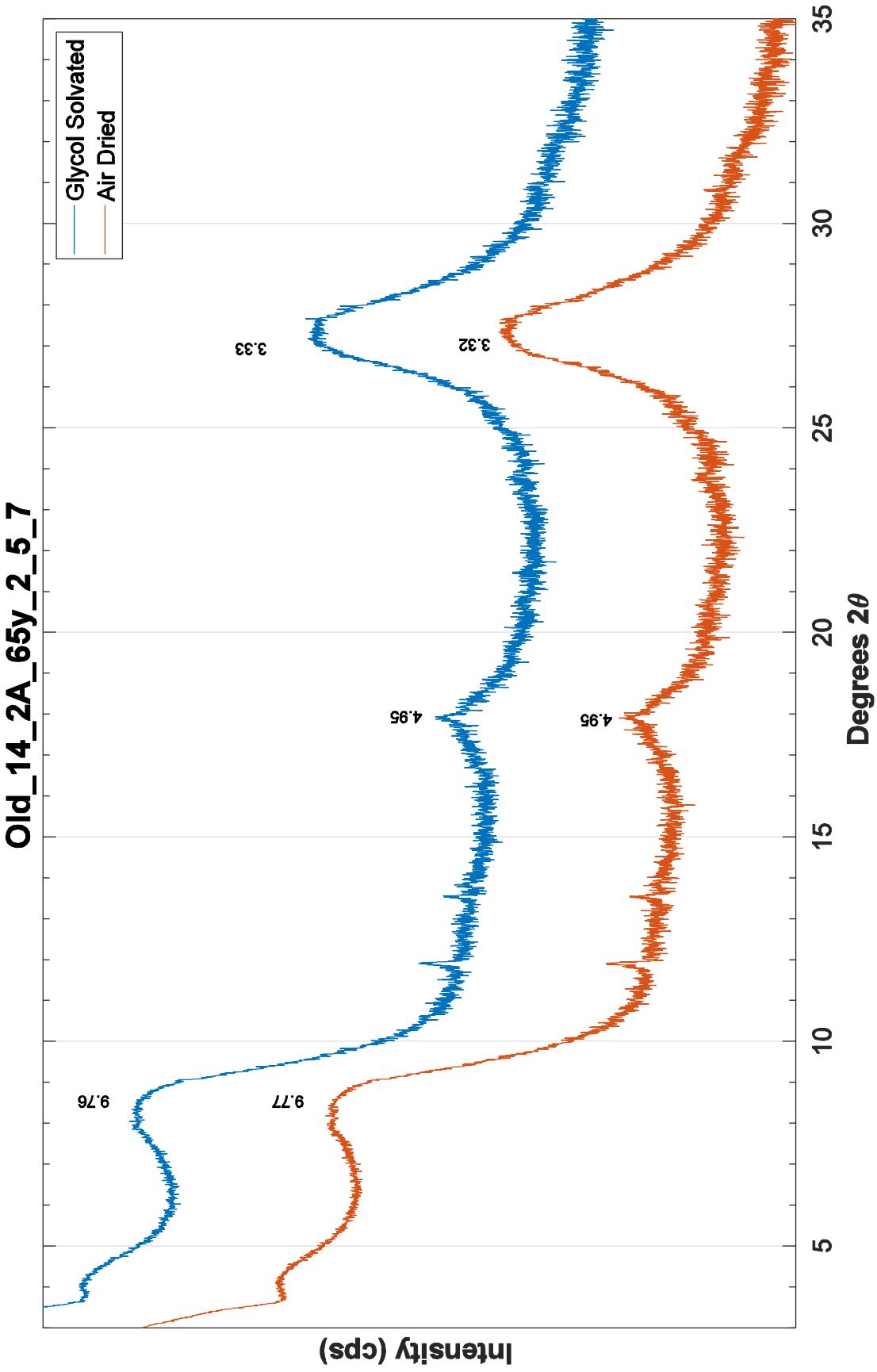
Old_14_2A_65y_2_5_7
Glycol Solvated
Air Dried
9.76
9.77
4.95
4.95
3.33
3.32
Intensity (cps)
Degrees 2θ
5
10
15
20
25
30
35

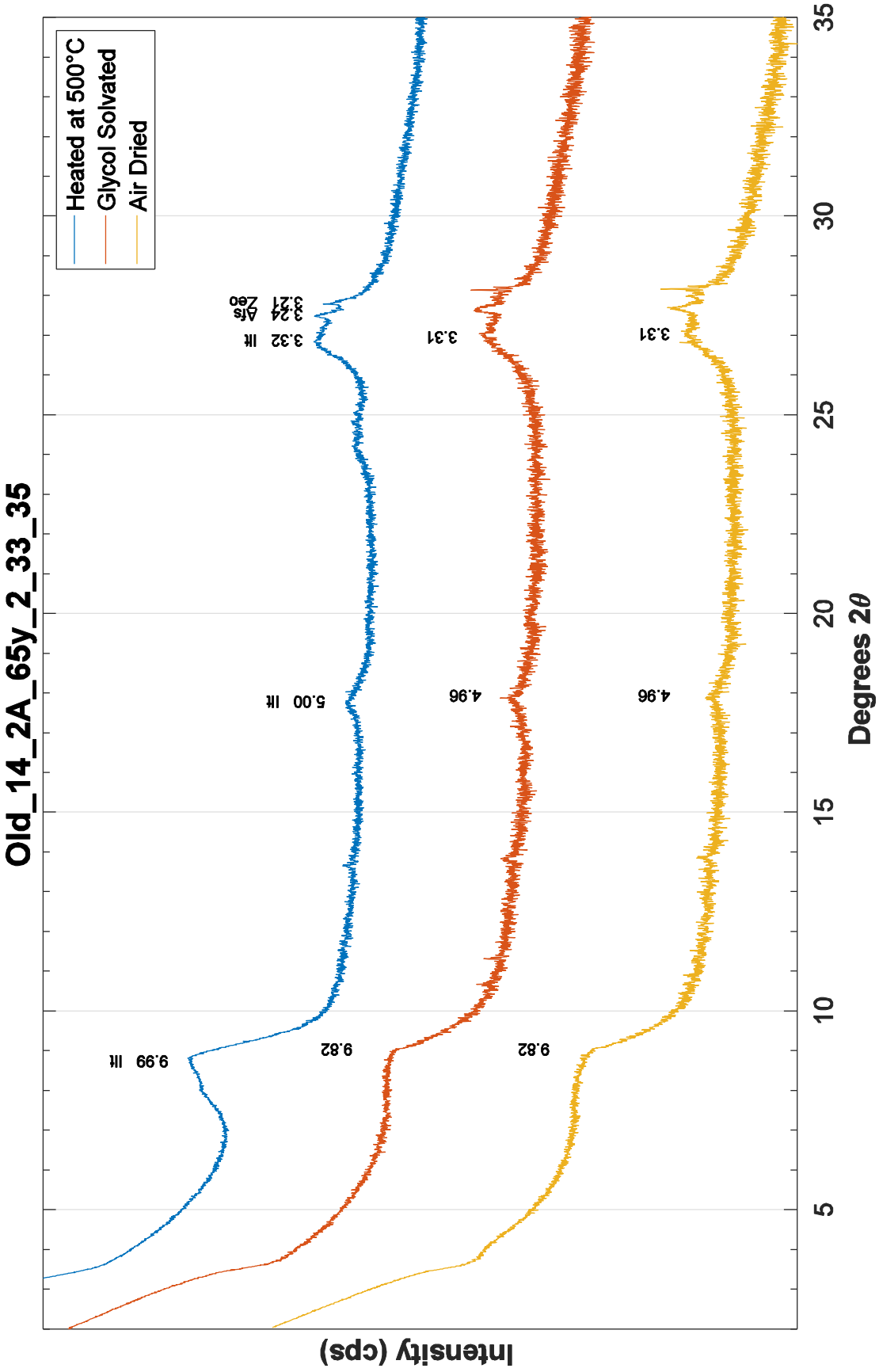
Old_14_2A_65y_2_33_35
Heated at 500°C
Glycol Solvated
Air Dried
9.99 Ilt
9.82
5.00 Ilt
4.96
3.32 Ilt
3.24 Afs
3.21 Zeo
3.31
9.82
4.96
3.31
Intensity (cps)
Degrees 2θ
5
10
15
20
25
30
35

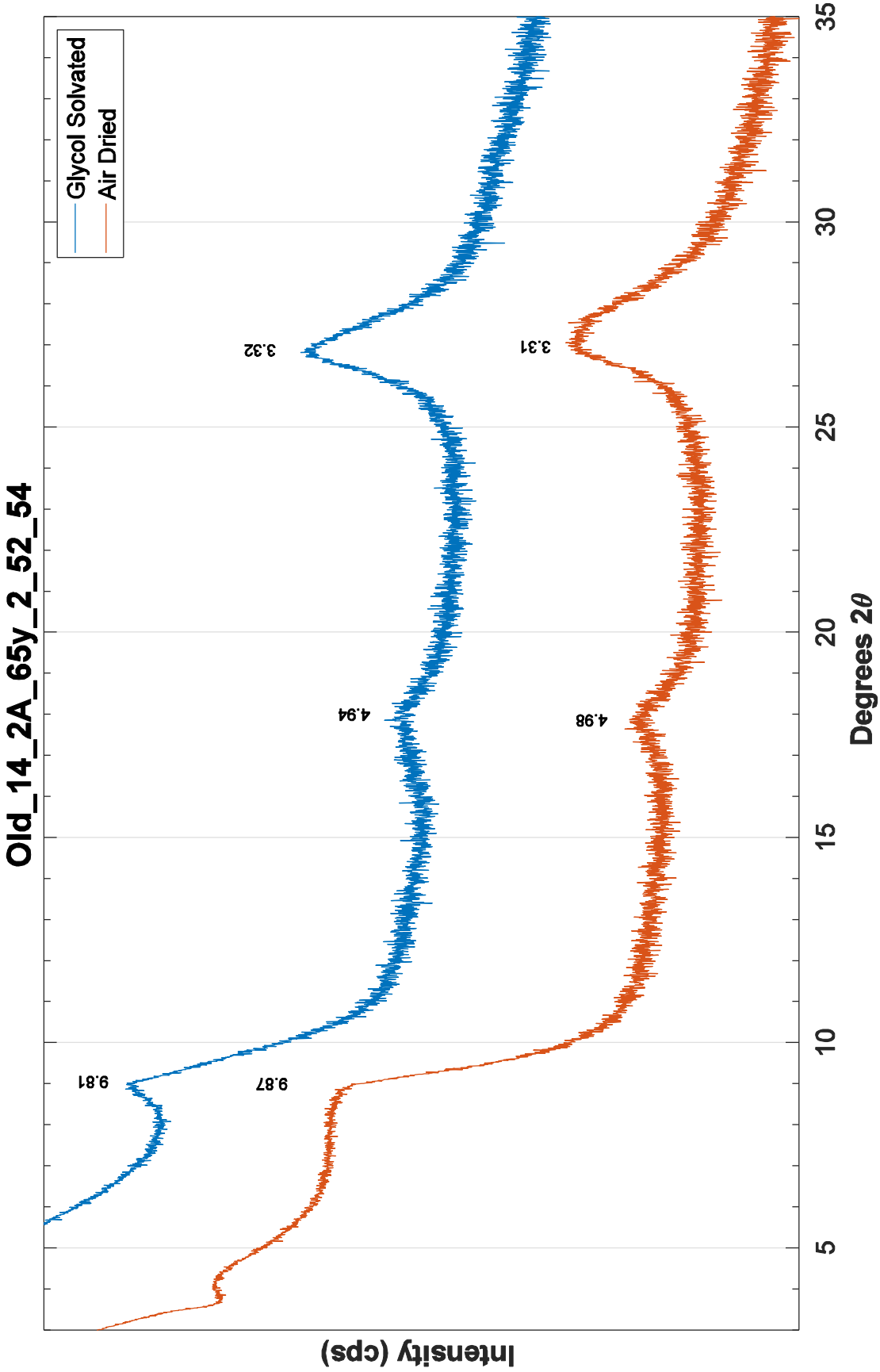
Old_14_2A_65y_2_52_54
Glycol Solvated
Air Dried
9.81
9.87
4.94
4.98
3.32
3.31
Intensity (cps)
Degrees 2θ
5
10
15
20
25
30
35

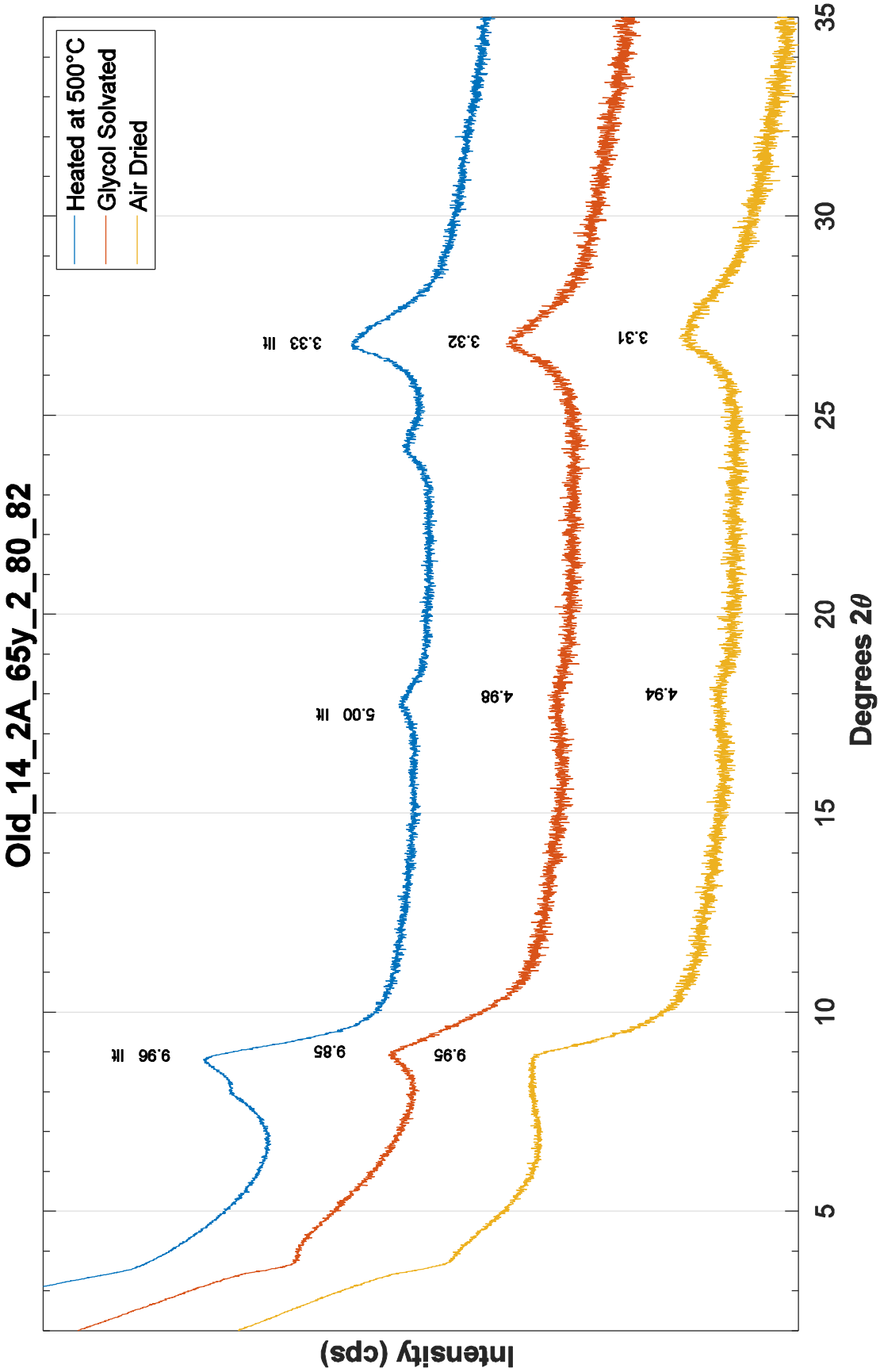
Old_14_2A_65y_2_80_82
Heated at 500°C
Glycol Solvated
Air Dried
9.96 Ilt
9.85
5.00 Ilt
3.33 Ilt
9.95
4.98
3.32
4.94
3.31
Intensity (cps)
Degrees 2θ
5
10
15
20
25
30
35

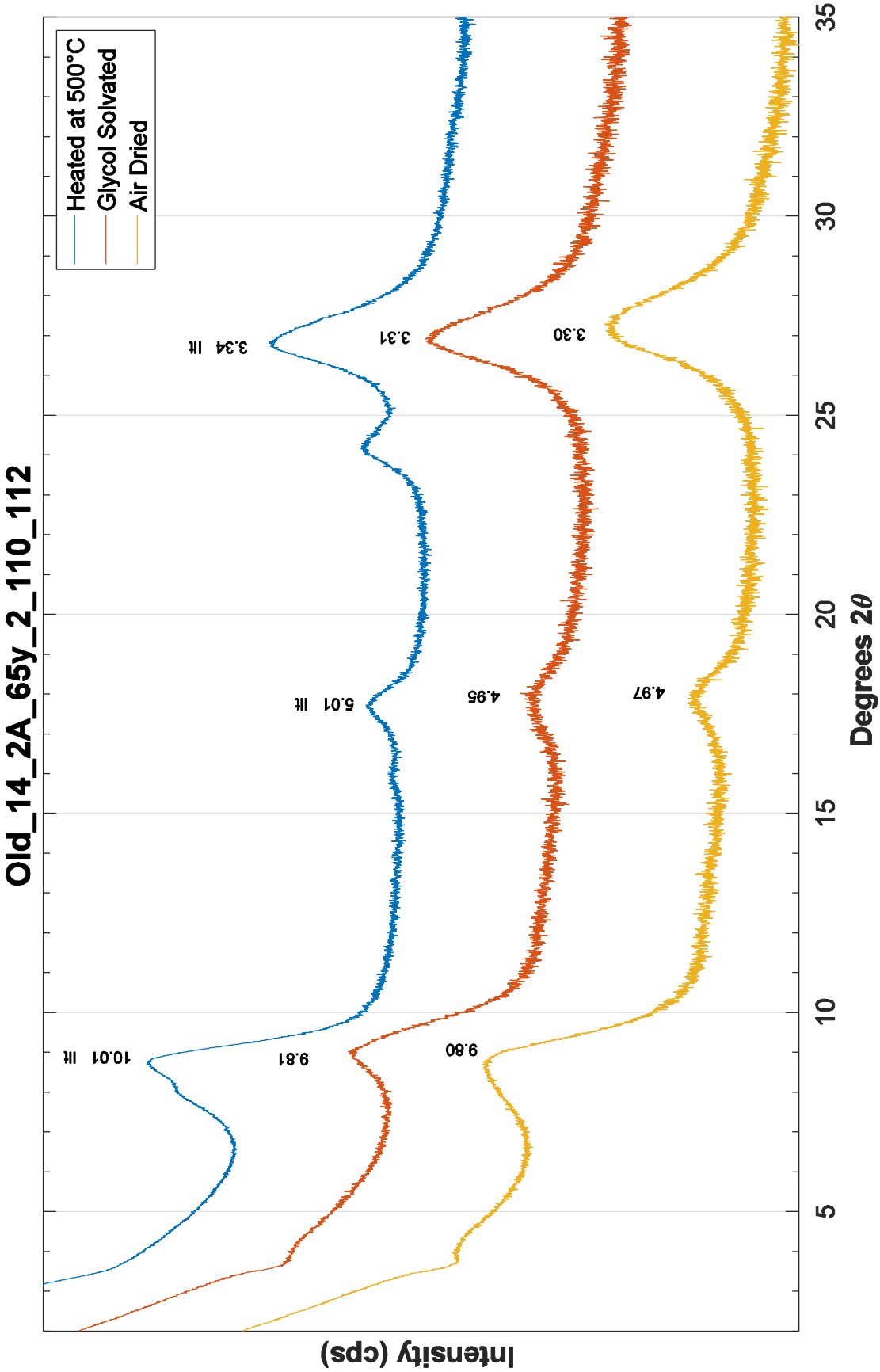
Old_14_2A_65y_2_110_112
Heated at 500°C
Glycol Solvated
Air Dried
10.01 Å
9.81
9.80
5.01 Å
4.95
4.97
3.34 Å
3.31
3.30
Intensity (cps)
Degrees 2θ
5
10
15
20
25
30
35

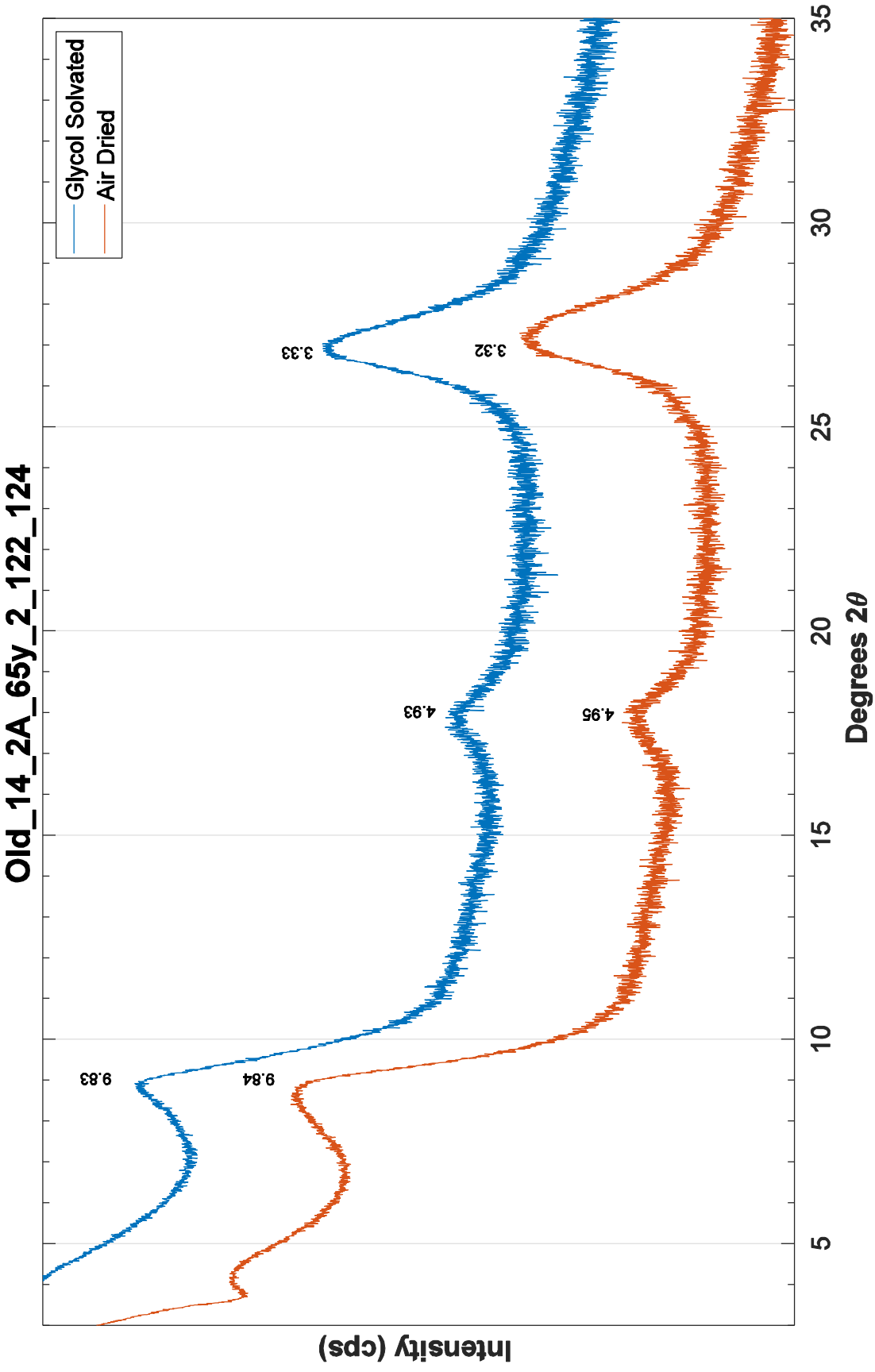
Old_14_2A_65y_2_122_124
Glycol Solvated
Air Dried
9.83
9.84
4.93
4.95
3.33
3.32
Intensity (cps)
Degrees 2θ
5
10
15
20
25
30
35

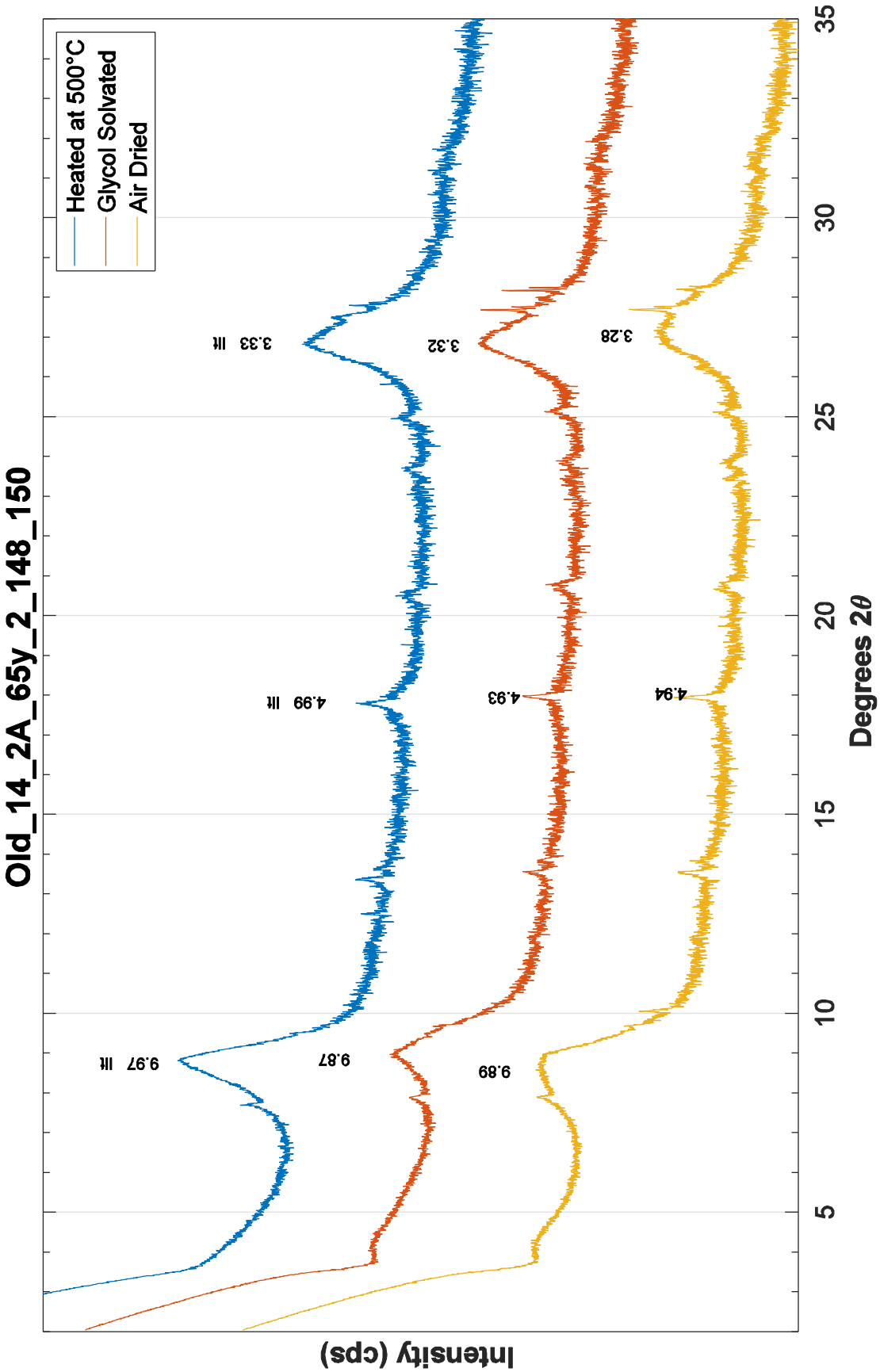
Old_14_2A_65y_2_148_150
Heated at 500°C
Glycol Solvated
Air Dried
9.97 Ilt
9.87
9.89
4.99 Ilt
4.93
4.94
3.33 Ilt
3.32
3.28
Intensity (cps)
Degrees 2θ
5
10
15
20
25
30
35

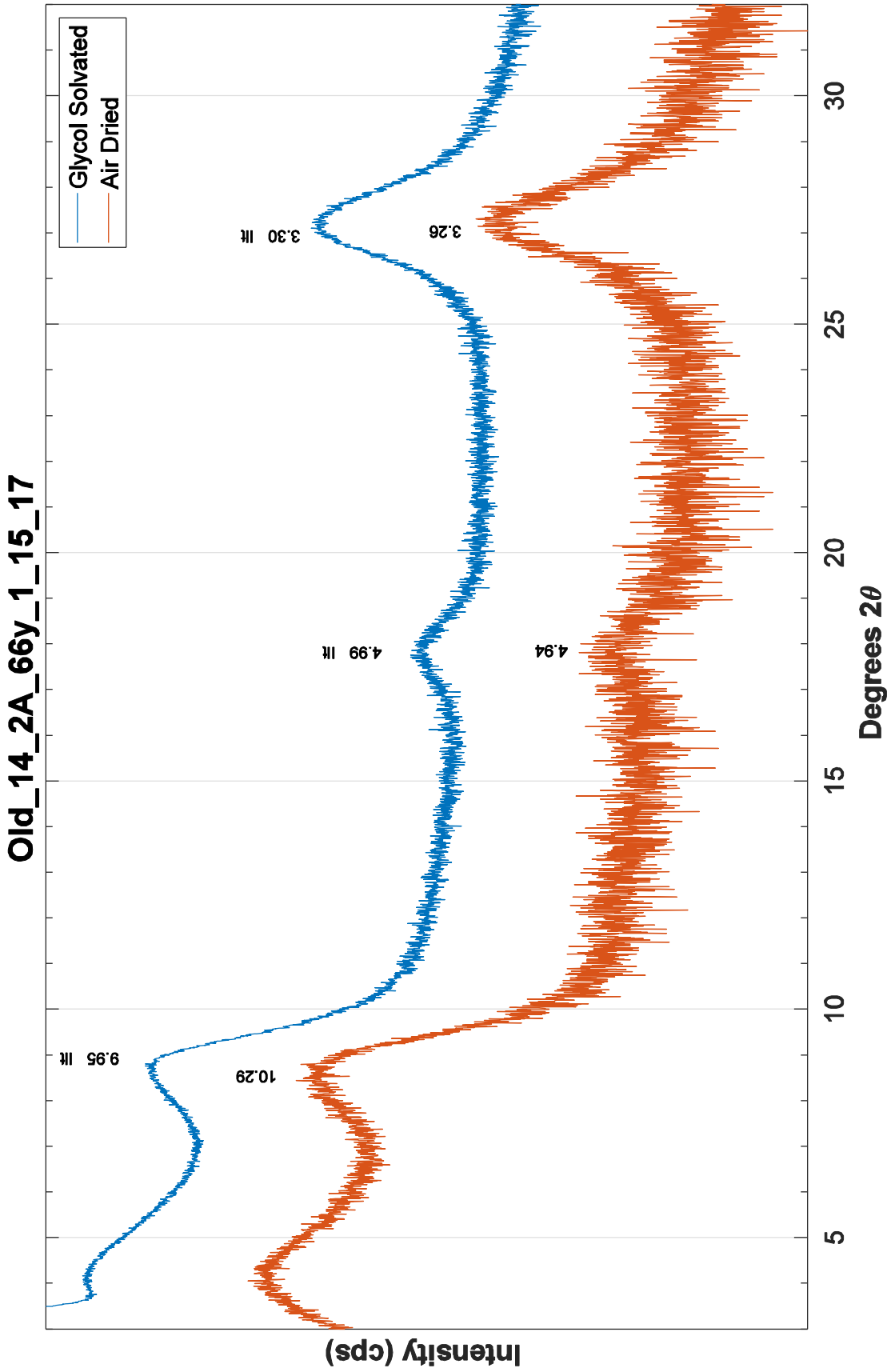
Old_14_2A_66y_1_15_17
Glycol Solvated
Air Dried
9.95 Å
10.29
4.99 Å
4.94
3.30 Å
3.26
Intensity (cps)
Degrees 2θ
5
10
15
20
25
30

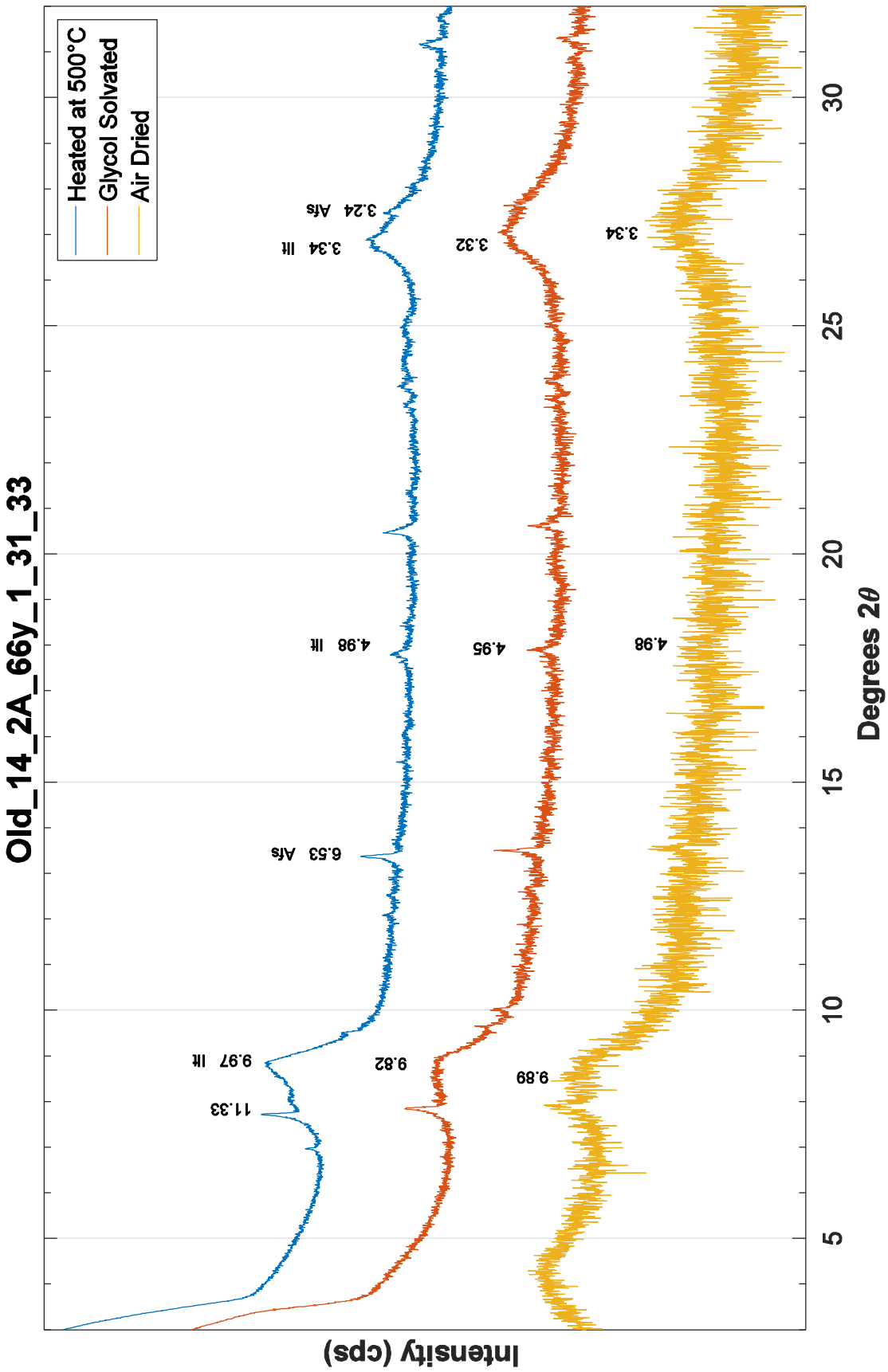
Old_14_2A_66y_1_31_33
Heated at 500°C
Glycol Solvated
Air Dried
Intensity (cps)
Degrees 2θ
5
10
15
20
25
30
11.33
9.97 Ilt
6.53 Afs
4.98 Ilt
3.34 Ilt
3.24 Afs
9.89
9.82
4.95
3.32
4.98
3.34

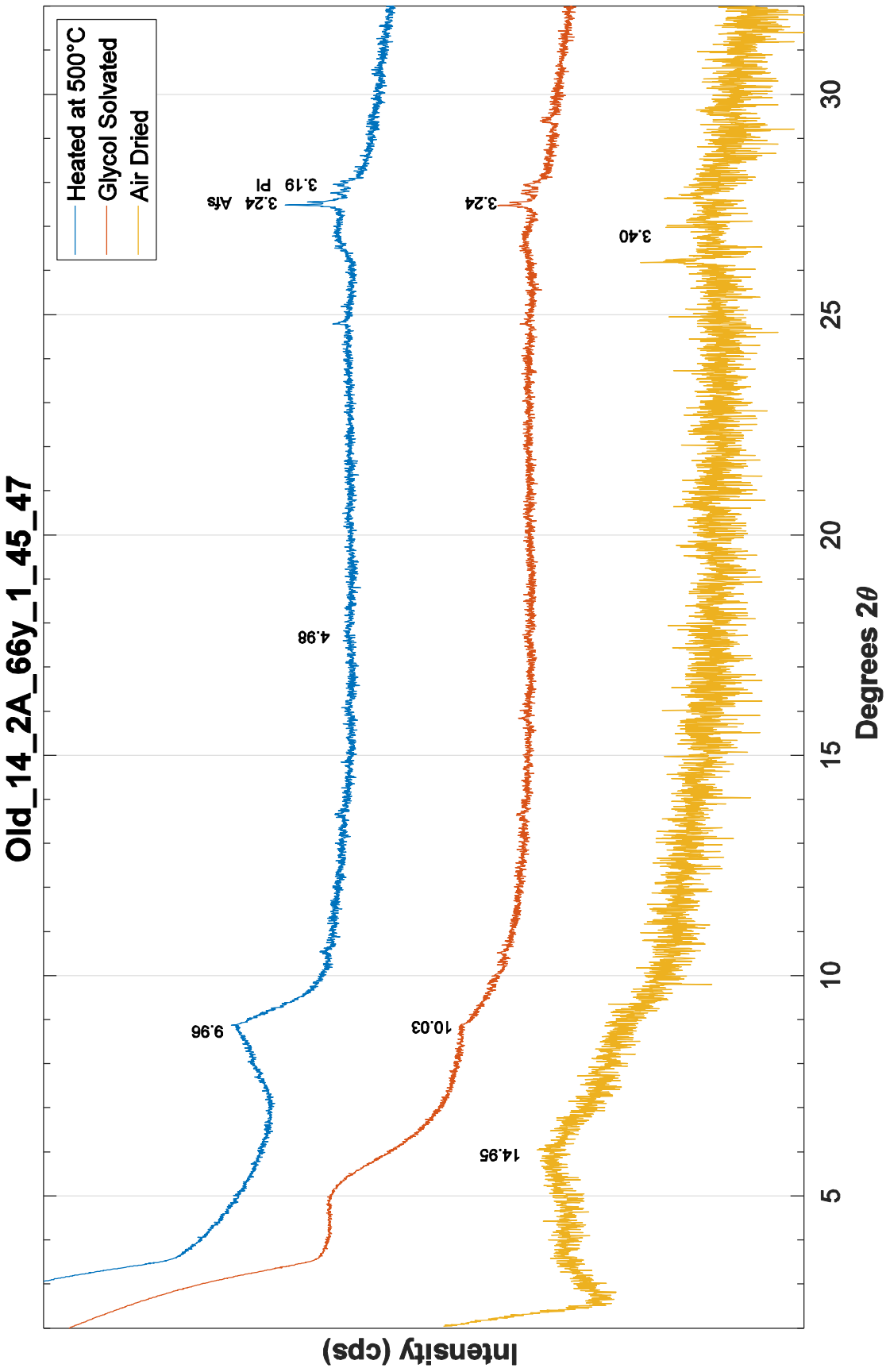
Old_14_2A_66y_1_45_47
Heated at 500°C
Glycol Solvated
Air Dried
3.24 Ats
3.19 Pl
4.98
9.96
3.24
10.03
3.40
14.95
Intensity (cps)
Degrees 2θ
5
10
15
20
25
30

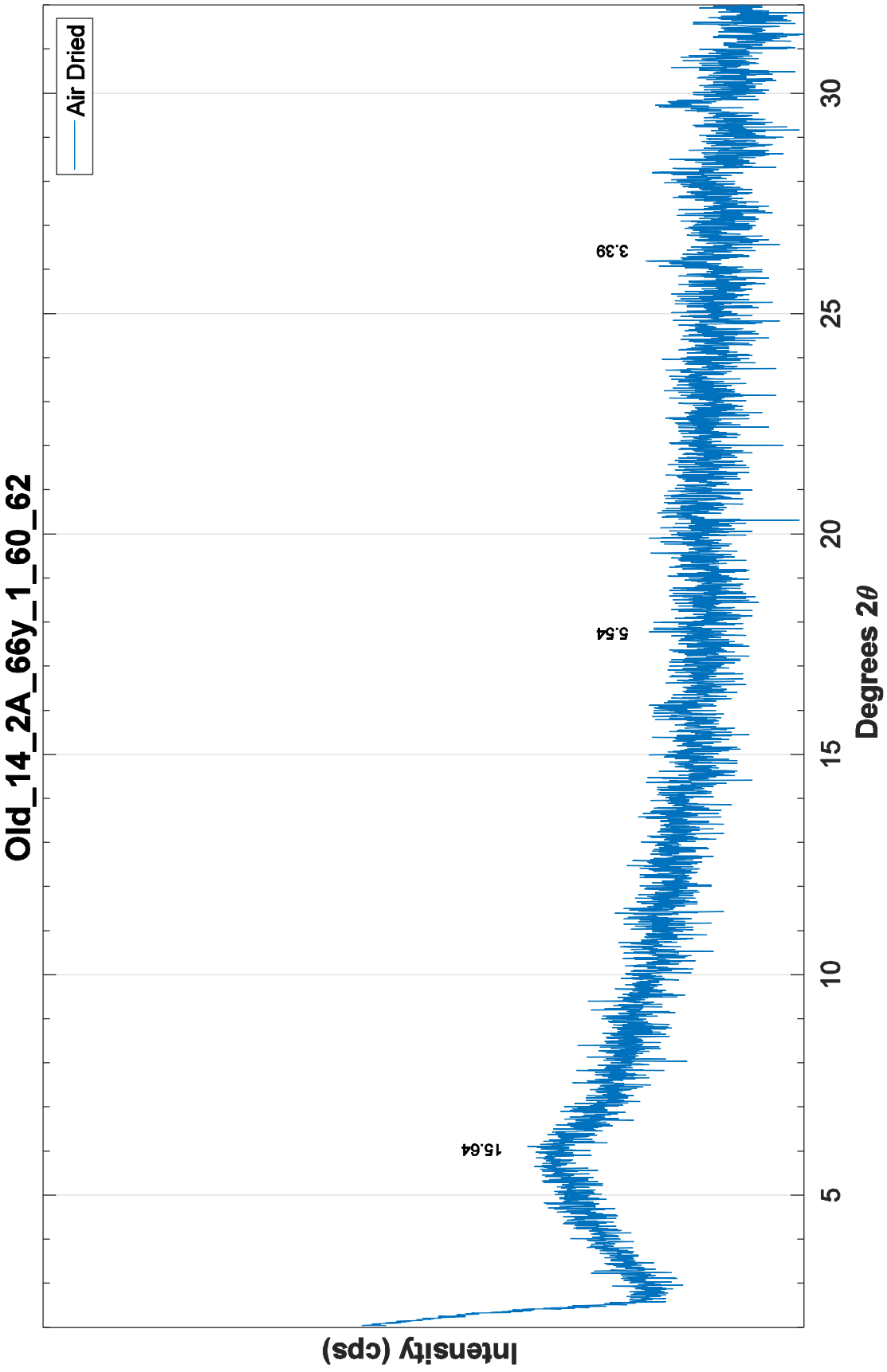
Old_14_2A_66y_1_60_62
Air Dried
15.64
5.54
3.39
Intensity (cps)
Degrees 2θ
5
10
15
20
25
30

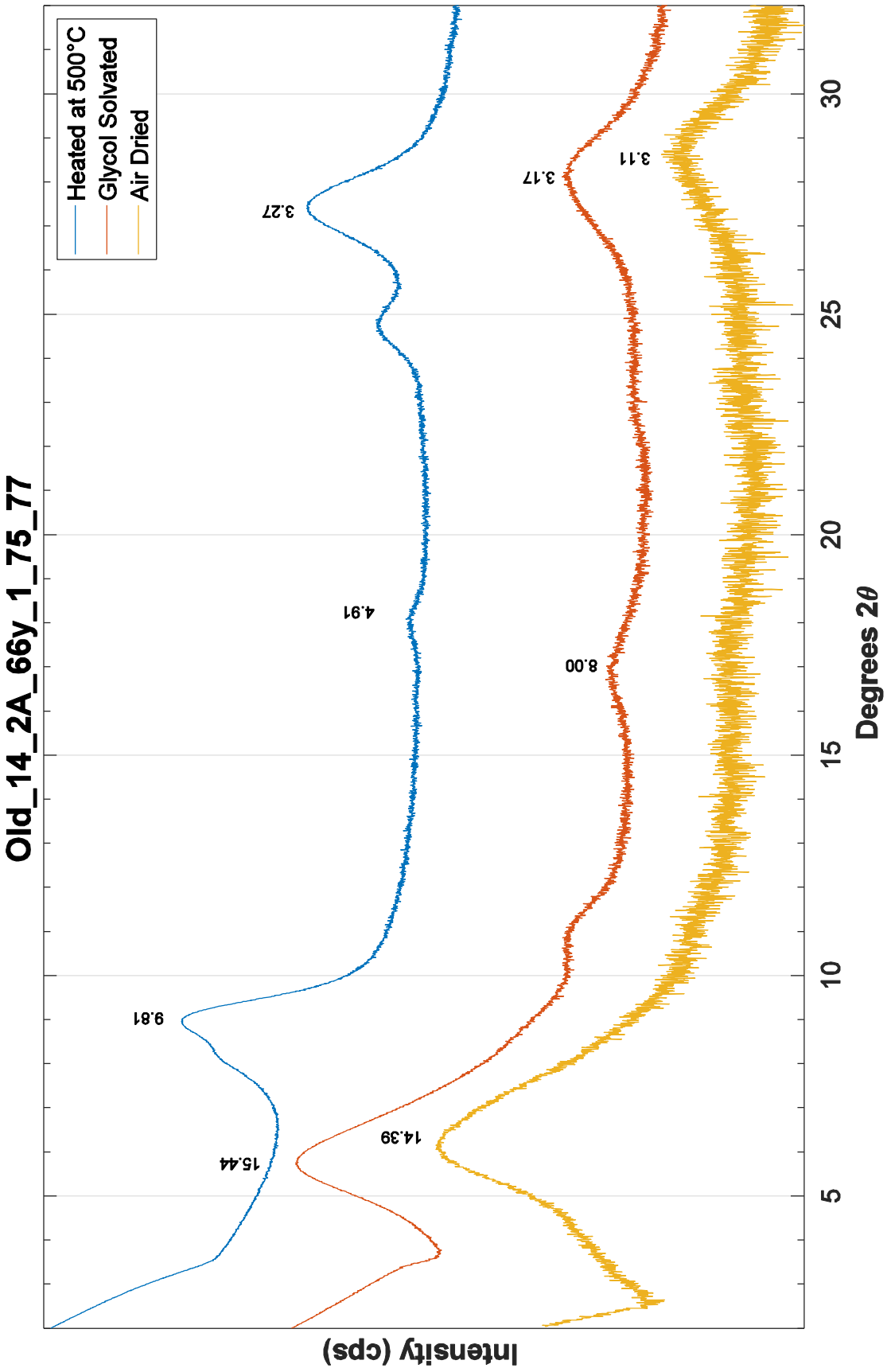
Old_14_2A_66y_1_75_77
Heated at 500°C
Glycol Solvated
Air Dried
Intensity (cps)
Degrees 2θ
5
10
15
20
25
30
15.44
9.81
4.91
3.27
14.39
8.00
3.17
3.11

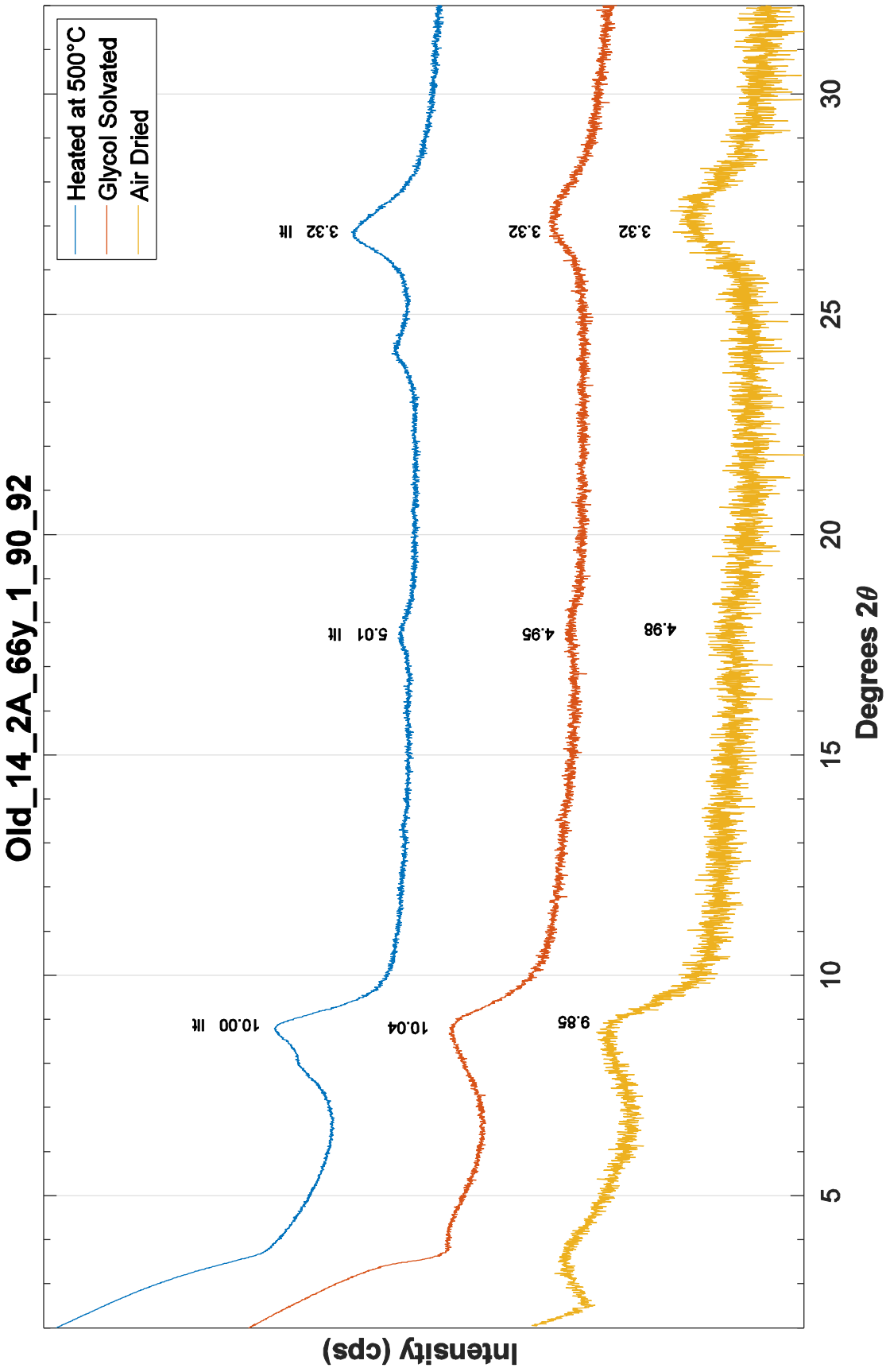
Old_14_2A_66y_1_90_92
Heated at 500°C
Glycol Solvated
Air Dried
10.00 Å
5.01 Å
3.32 Å
10.04
4.95
3.32
9.85
4.98
3.32
Intensity (cps)
Degrees 2θ
5
10
15
20
25
30

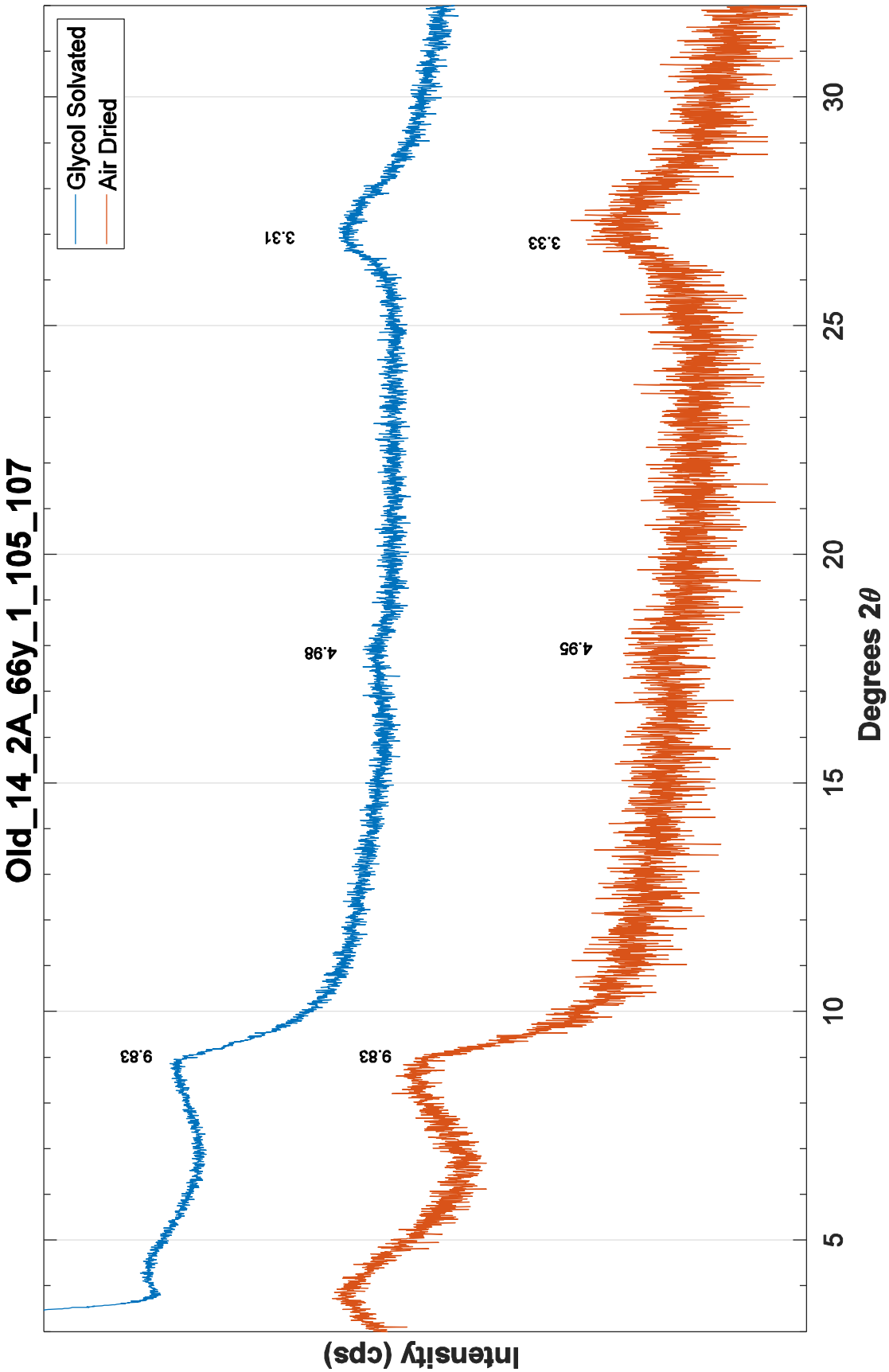
Old_14_2A_66y_1_105_107
Glycol Solvated
Air Dried
9.83
4.98
3.31
9.83
4.95
3.33
Intensity (cps)
Degrees 2θ
5
10
15
20
25
30

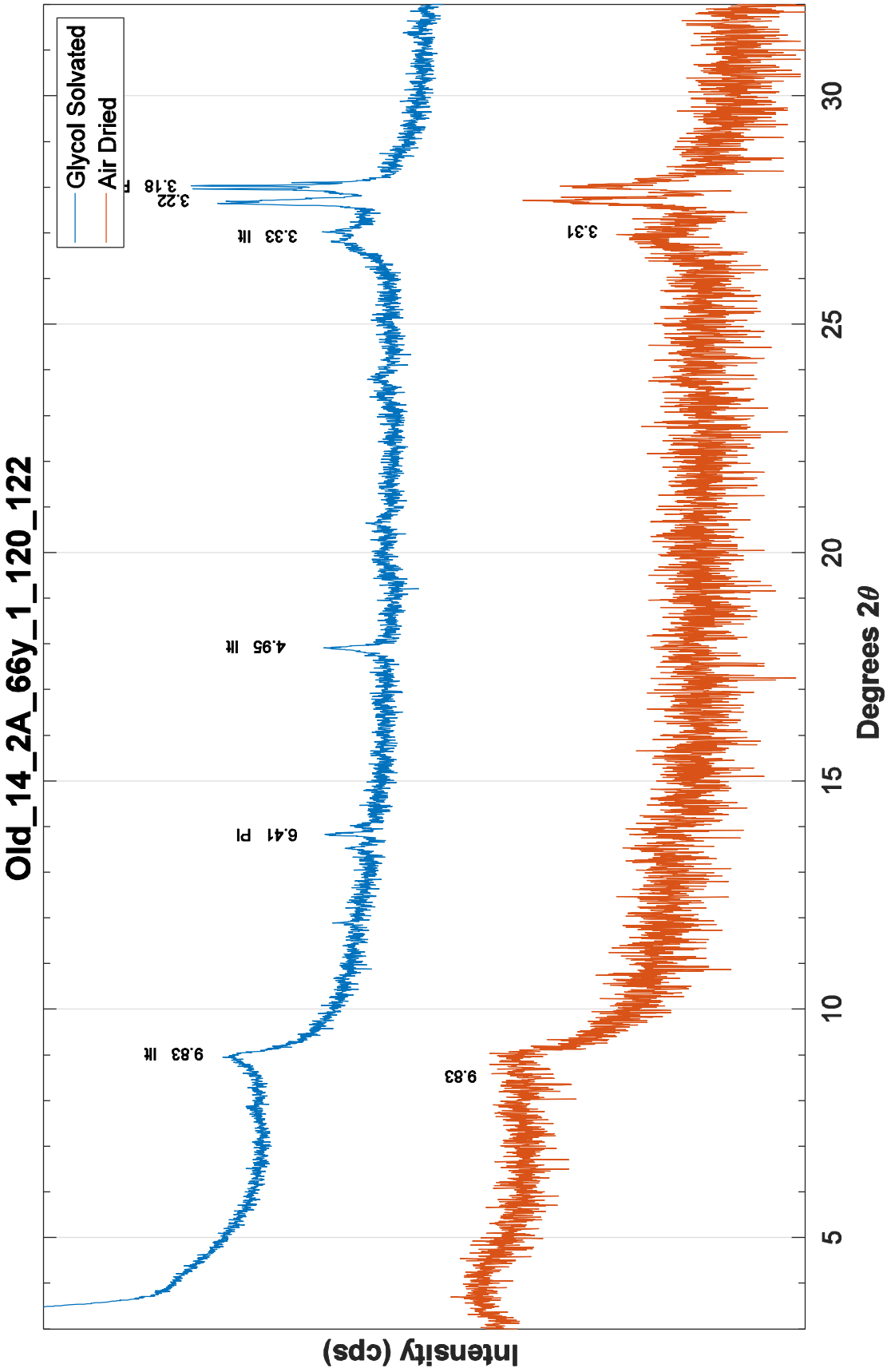
Old_14_2A_66y_1_120_122
Glycol Solvated
Air Dried
3.18 F
3.22
3.33 Ilt
4.95 Ilt
6.41 Pl
9.83 Ilt
3.31
9.83
Intensity (cps)
Degrees 2θ
5
10
15
20
25
30

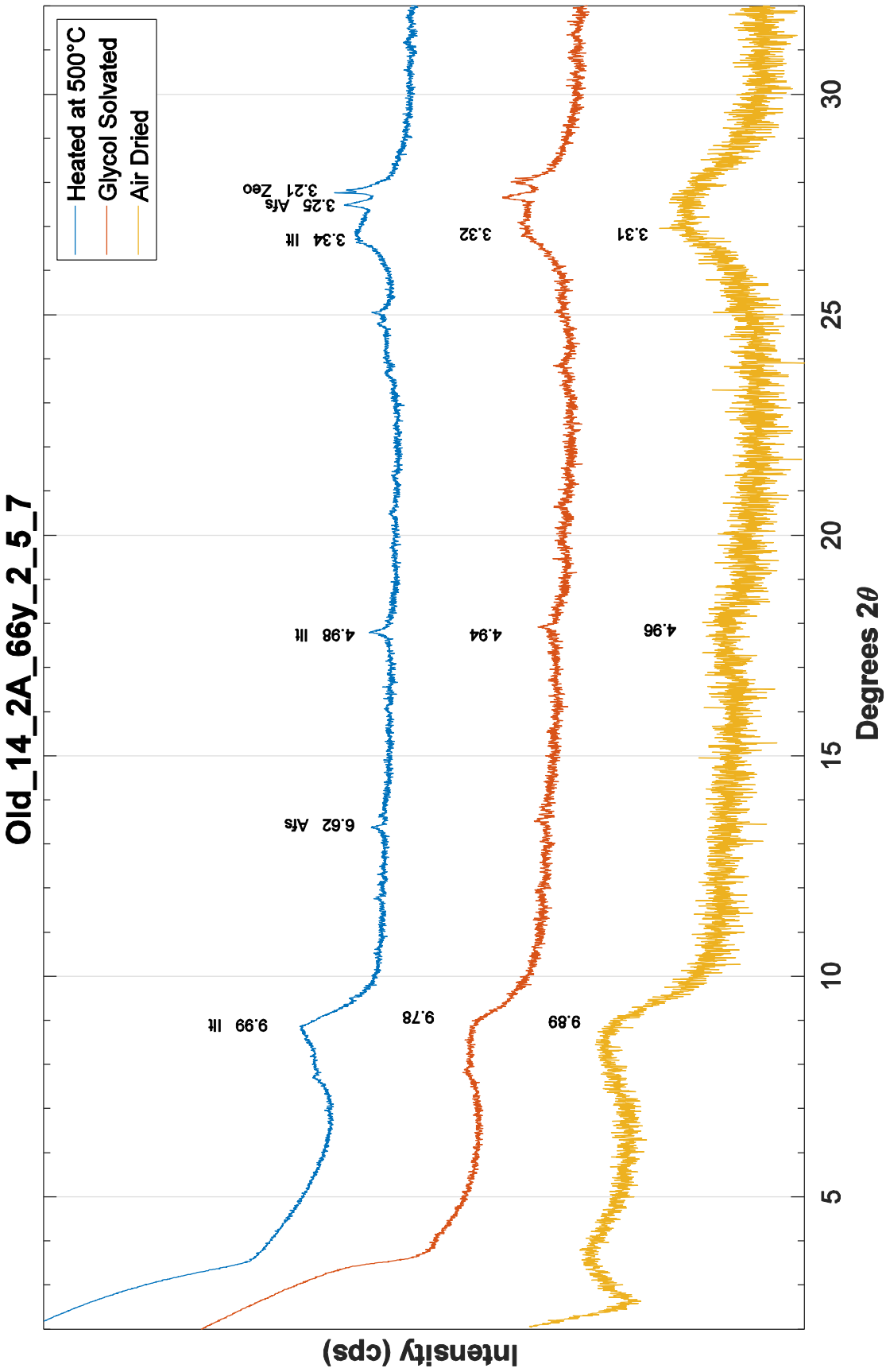
Old_14_2A_66y_2_5_7
Heated at 500°C
Glycol Solvated
Air Dried
Intensity (cps)
Degrees 2θ
5
10
15
20
25
30
9.99 Ilt
9.78
9.89
6.62 Afs
4.98 Ilt
4.94
4.96
3.34 Ilt
3.32
3.31
3.25 Afs
3.21 Zeo

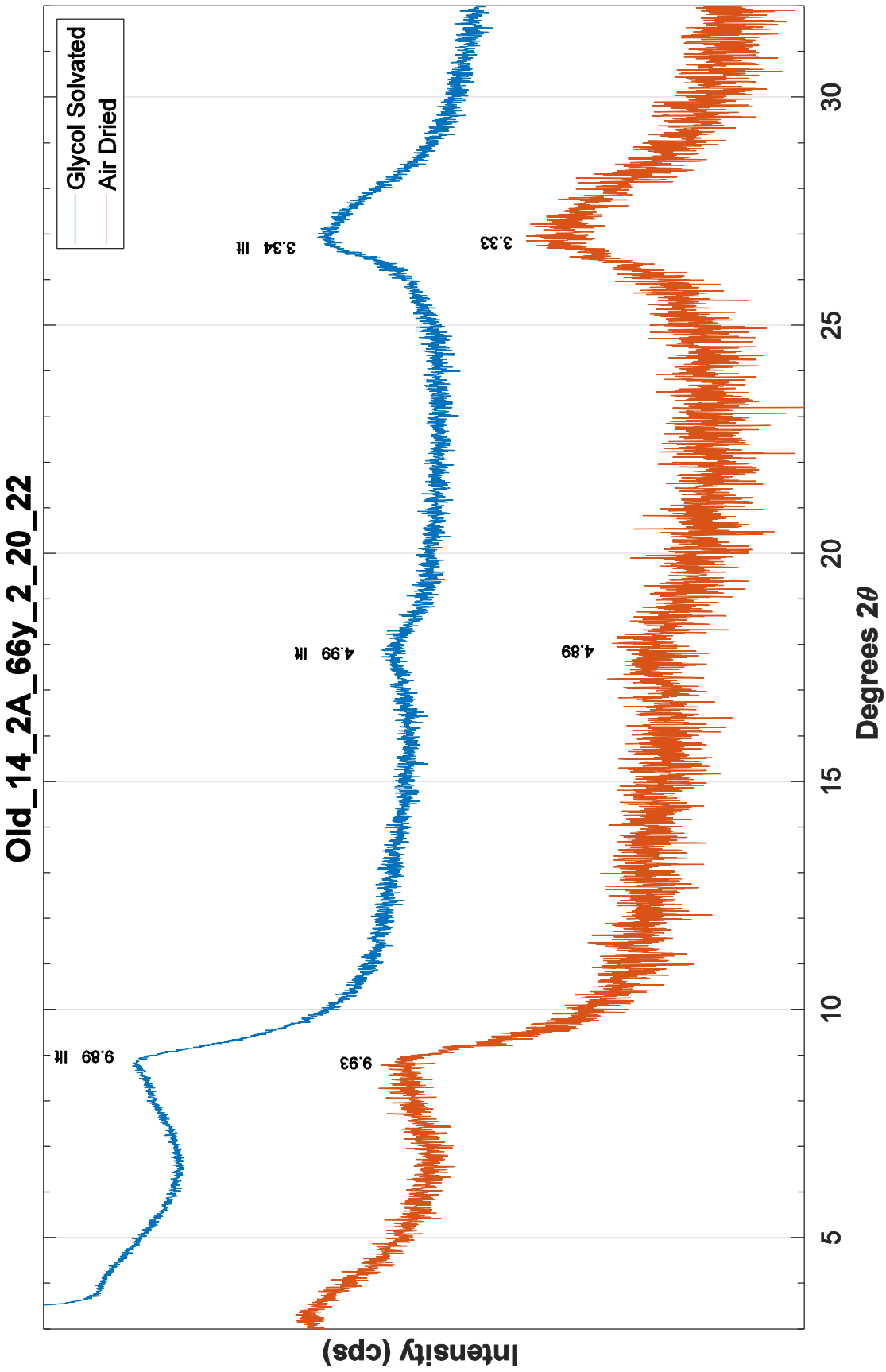
Old_14_2A_66y_2_20_22
Glycol Solvated
Air Dried
9.89 Å
4.99 Å
3.34 Å
9.93
4.89
3.33
Intensity (cps)
Degrees 2θ
5
10
15
20
25
30

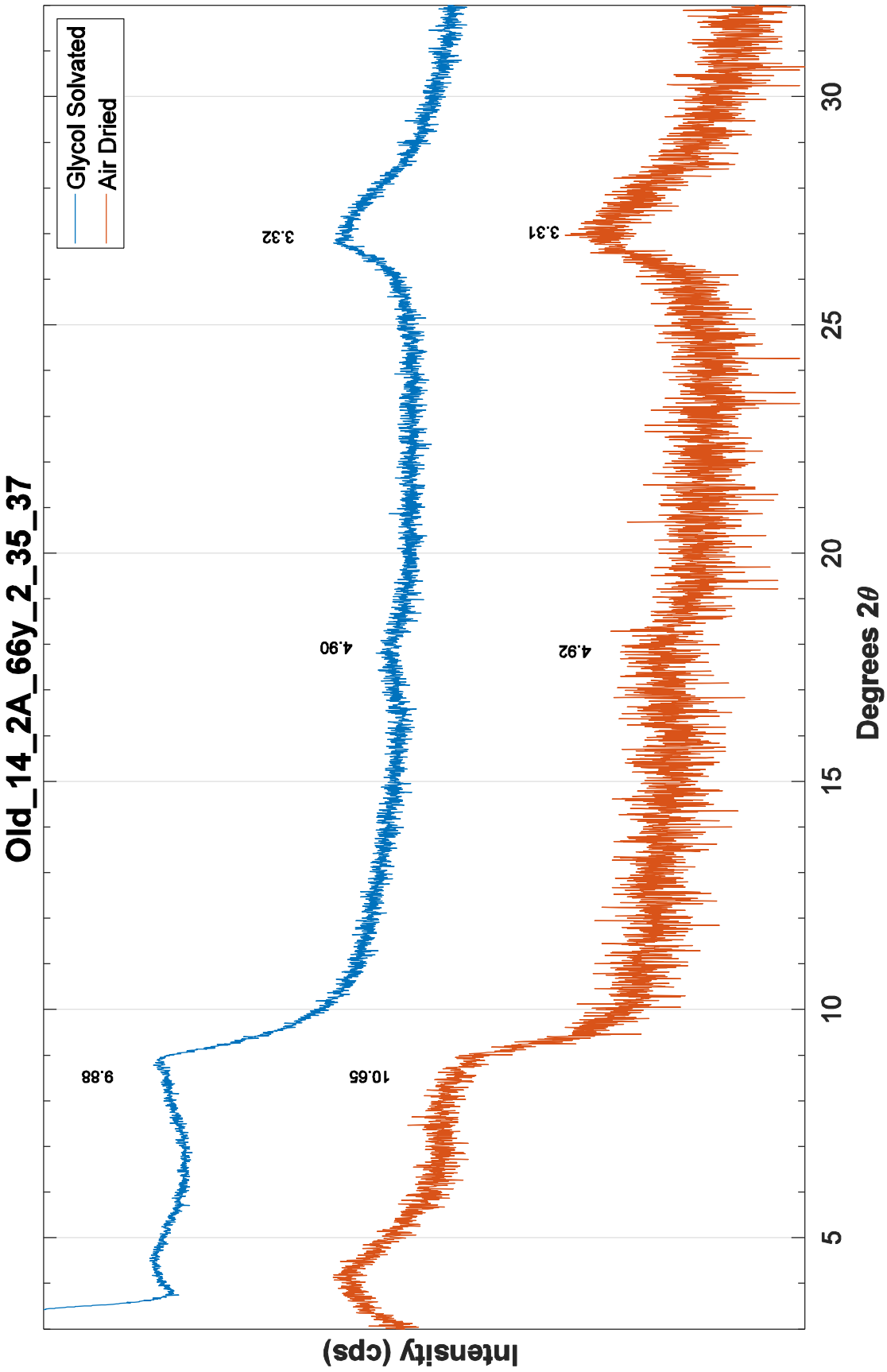
Old_14_2A_66y_2_35_37
Glycol Solvated
Air Dried
9.88
10.65
4.90
4.92
3.32
3.31
Intensity (cps)
Degrees 2θ
5
10
15
20
25
30

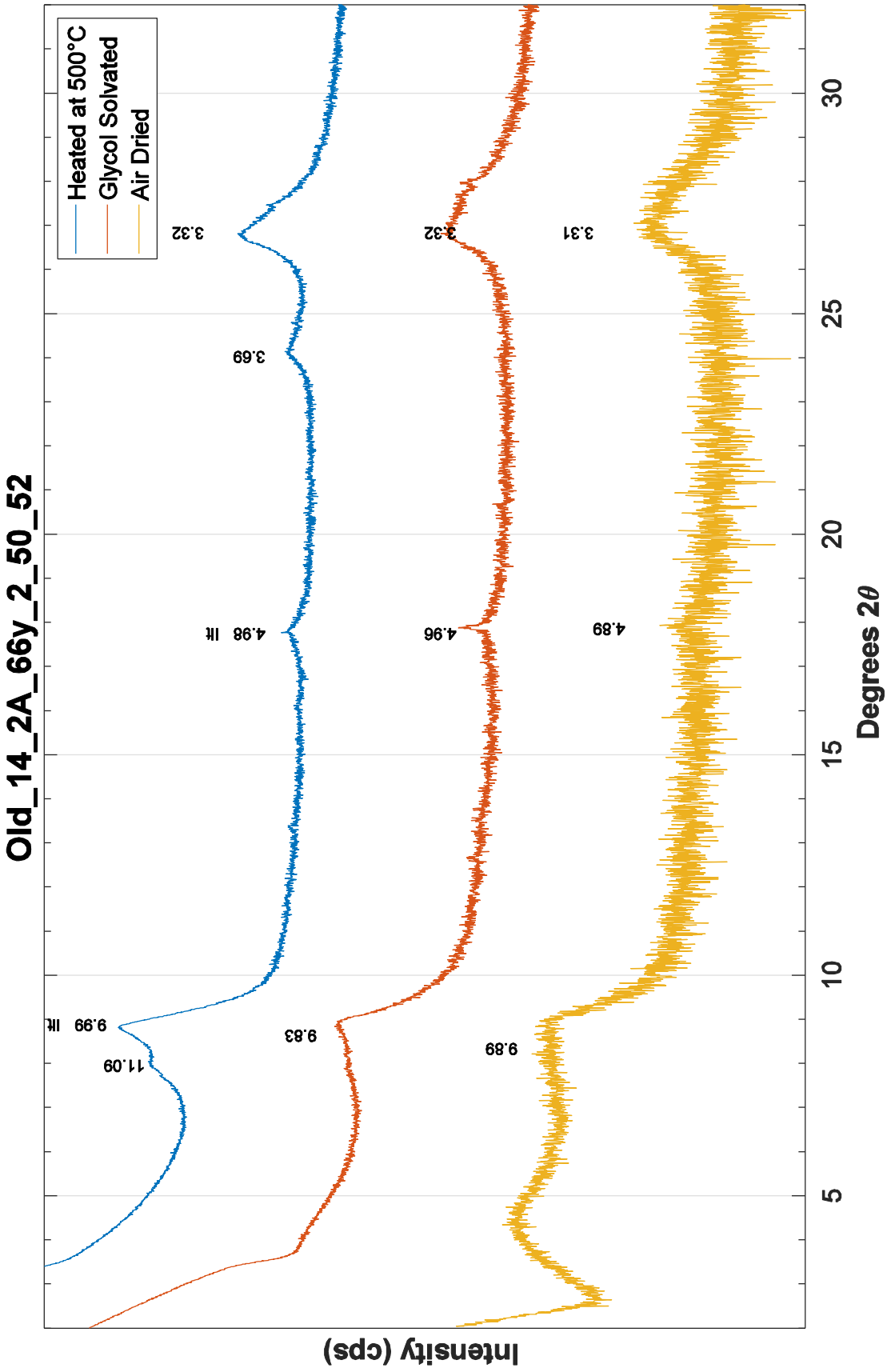
Old_14_2A_66y_2_50_52
Heated at 500°C
Glycol Solvated
Air Dried
Intensity (cps)
Degrees 2θ
5
10
15
20
25
30
11.09
9.99
9.83
9.89
4.98
4.96
4.89
3.69
3.32
3.32
3.31

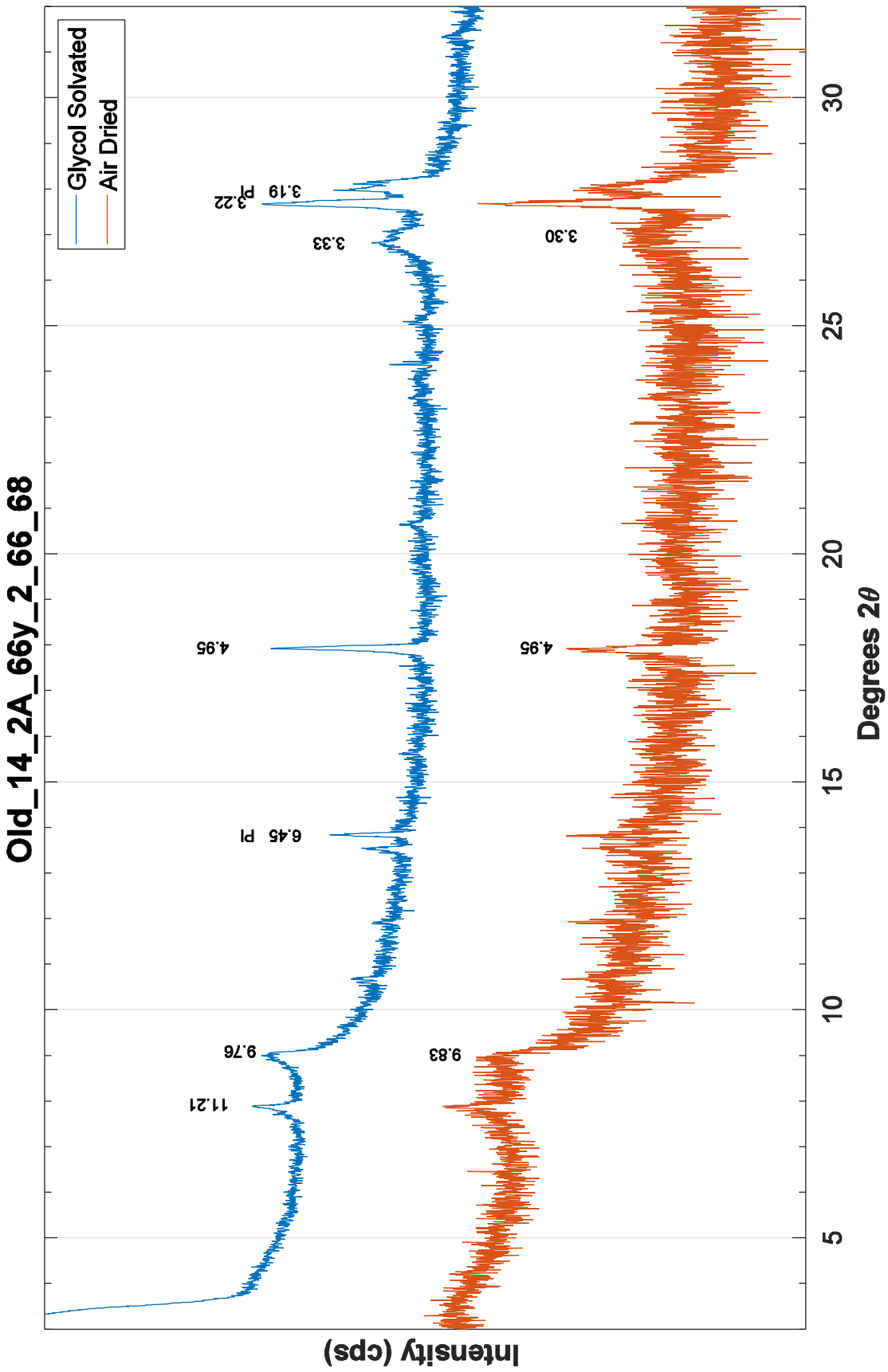
Old_14_2A_66y_2_66_68
Glycol Solvated
Air Dried
Intensity (cps)
Degrees 2θ
5
10
15
20
25
30
11.21
9.76
6.45 Pl
4.95
3.33
3.19 Pl 3.22
9.83
4.95
3.30

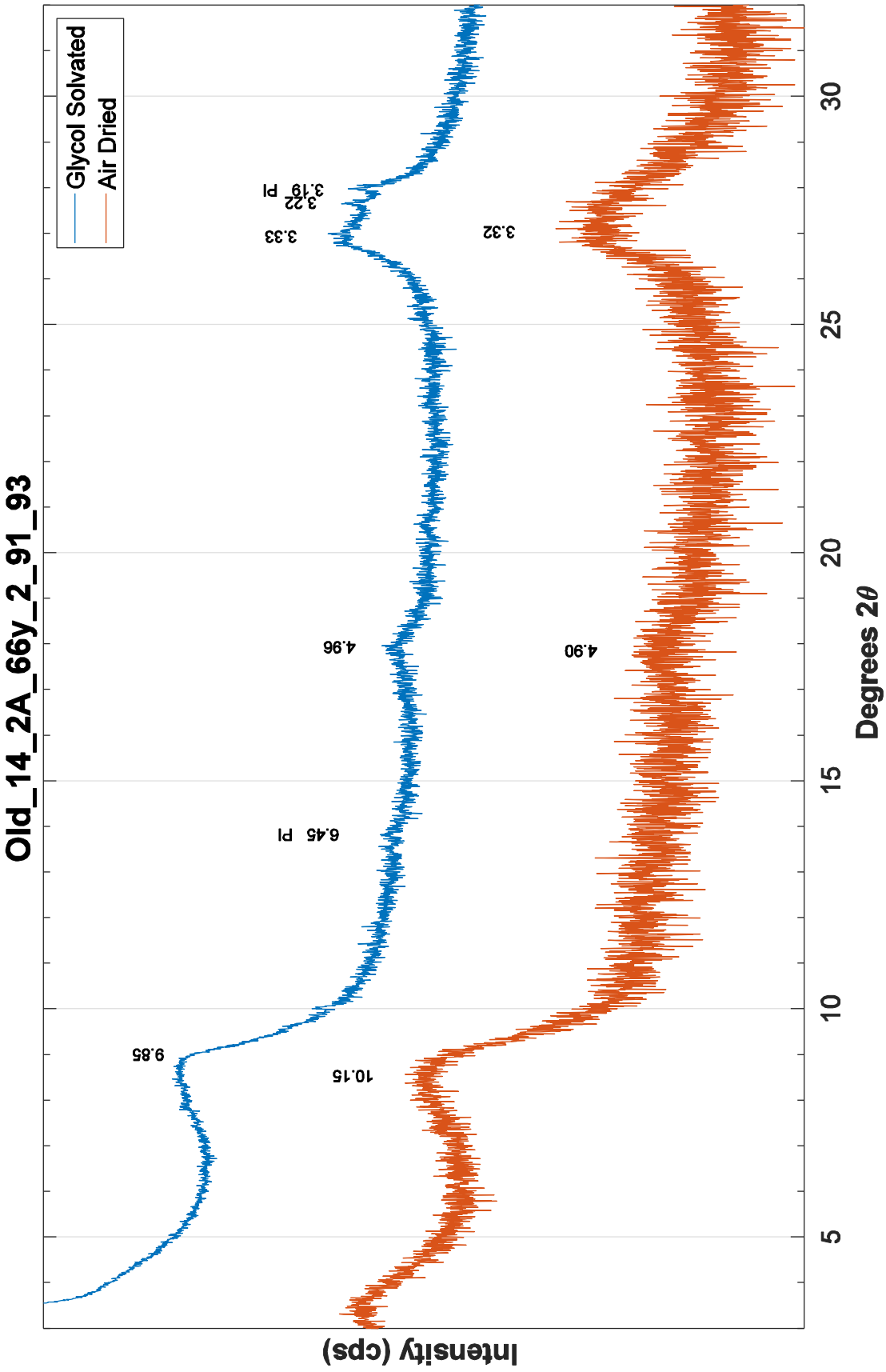
Old_14_2A_66y_2_91_93
Glycol Solvated
Air Dried
Intensity (cps)
Degrees 2θ
5
10
15
20
25
30
9.85
10.15
6.45 Pl
4.96
4.90
3.33
3.32
3.22
3.19 Pl

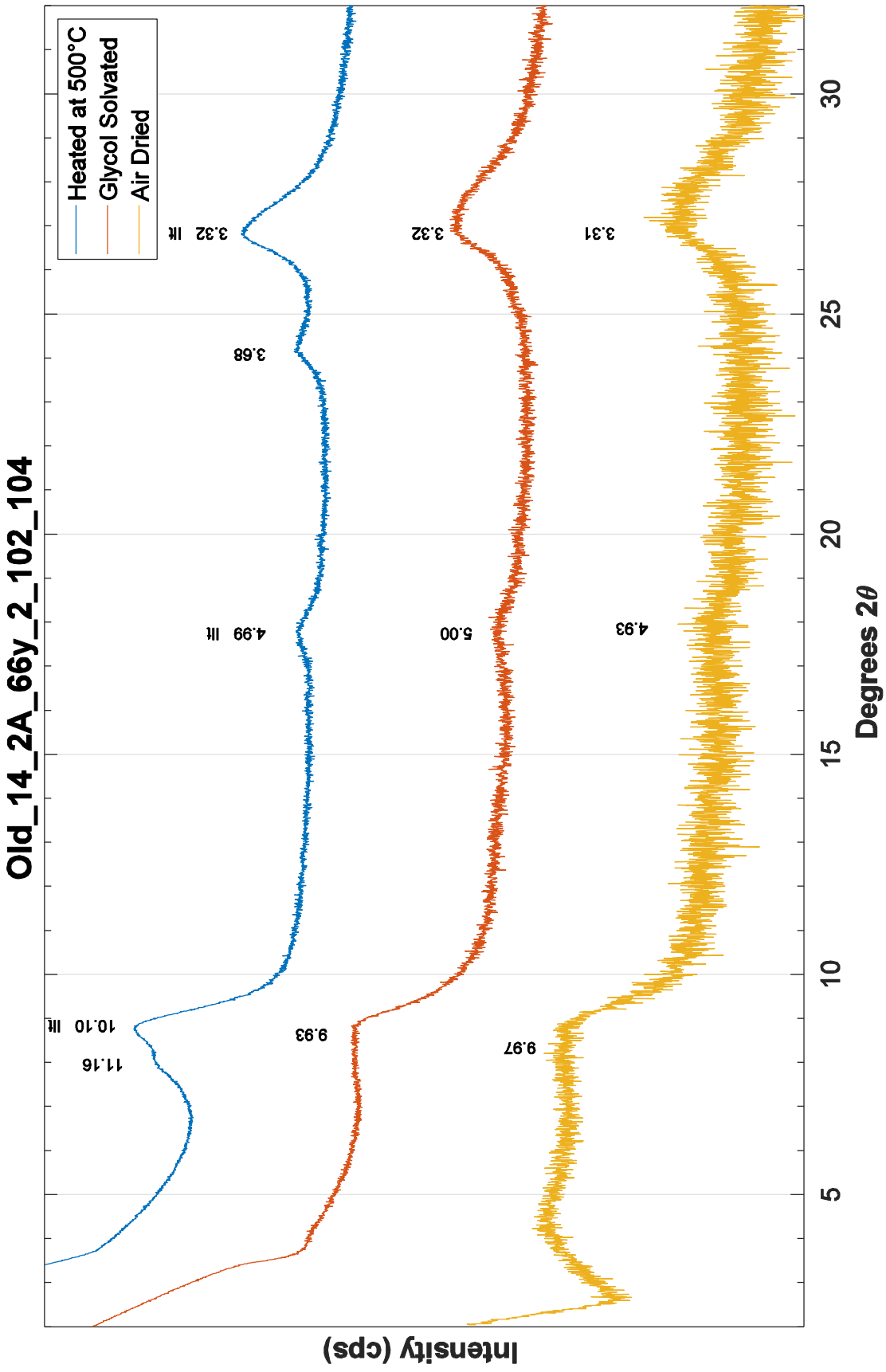
Old_14_2A_66y_2_102_104
Heated at 500°C
Glycol Solvated
Air Dried
Intensity (cps)
Degrees 2θ
5
10
15
20
25
30
11.16
10.10 IR
9.93
9.97
3.68
4.99 IR
5.00
4.93
3.32 IR
3.32
3.31

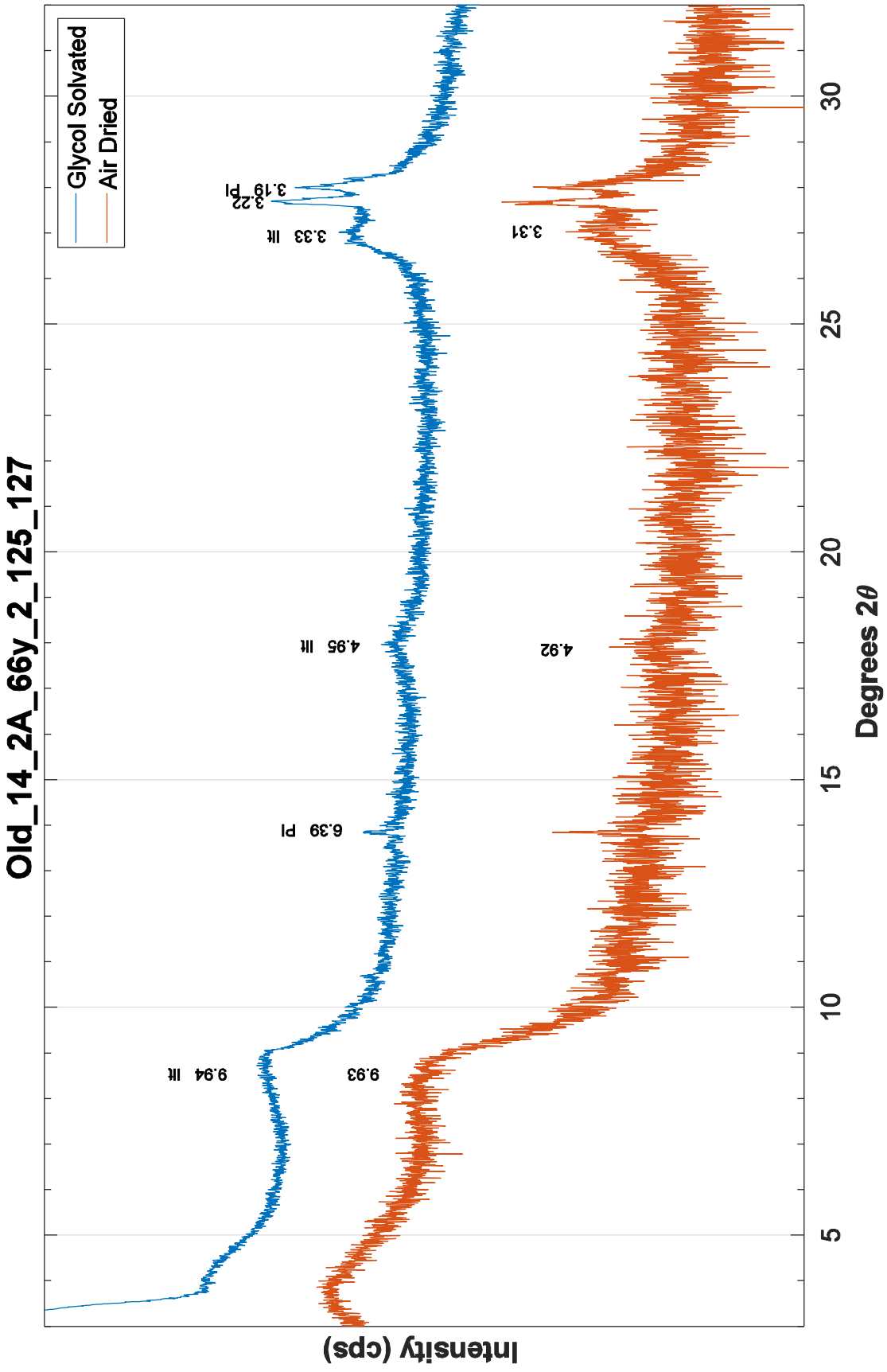
Old_14_2A_66y_2_125_127
Glycol Solvated
Air Dried
9.94 Ilt
9.93
6.39 Pl
4.95 Ilt
4.92
3.33 Ilt
3.31
3.22
3.19 Pl
Intensity (cps)
Degrees 2θ
5
10
15
20
25
30

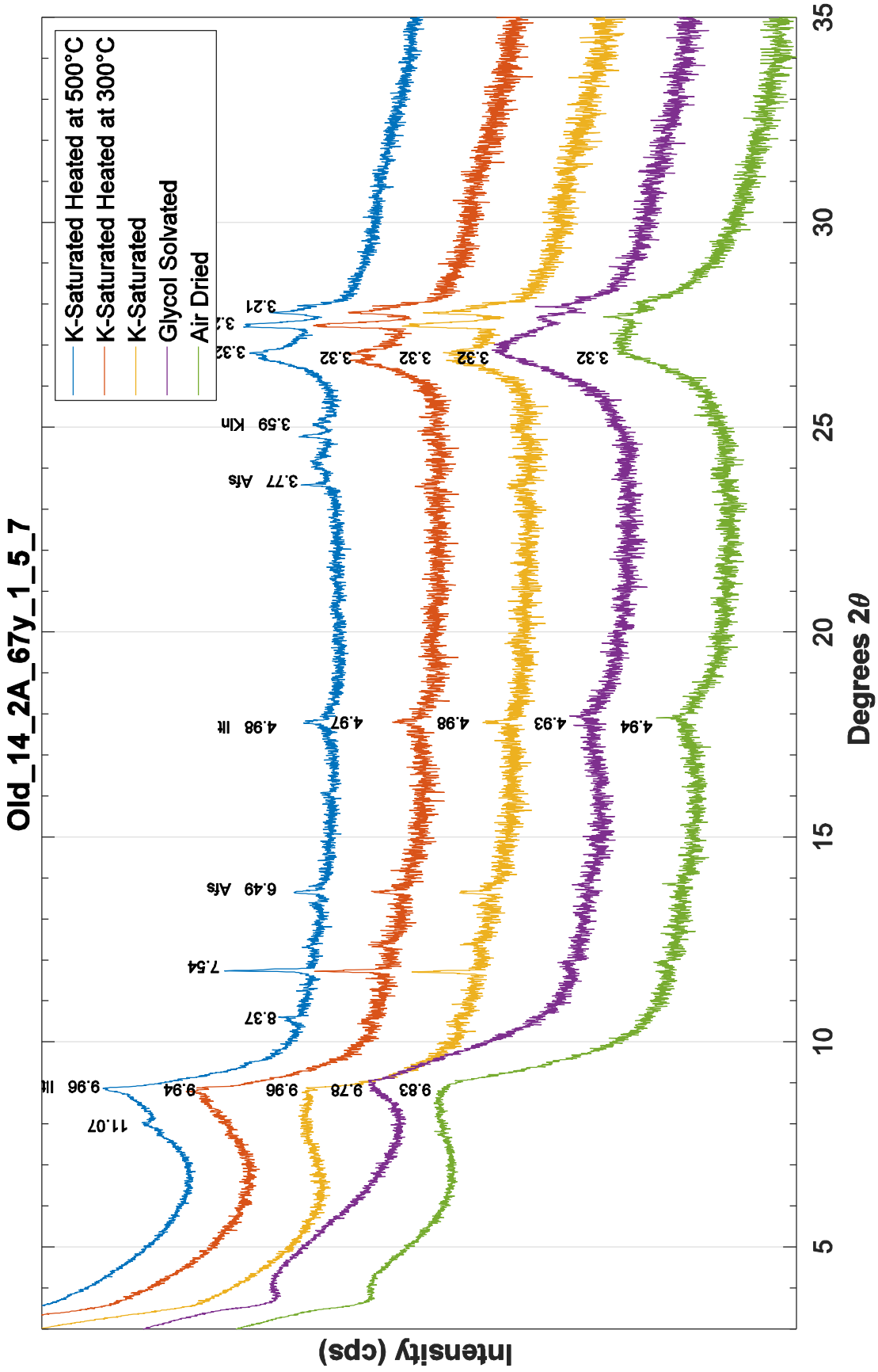
Old_14_2A_67y_1_5_7
K-Saturated Heated at 500°C
K-Saturated Heated at 300°C
K-Saturated
Glycol Solvated
Air Dried
Intensity (cps)
Degrees 2θ
5
10
15
20
25
30
35
11.07
9.96
9.94
9.83
9.78
9.96
8.37
7.54
6.49 Afs
4.98 Ilt
4.97
4.98
4.93
4.94
3.77 Afs
3.59 Kln
3.32
3.32
3.32
3.32
3.32
3.21

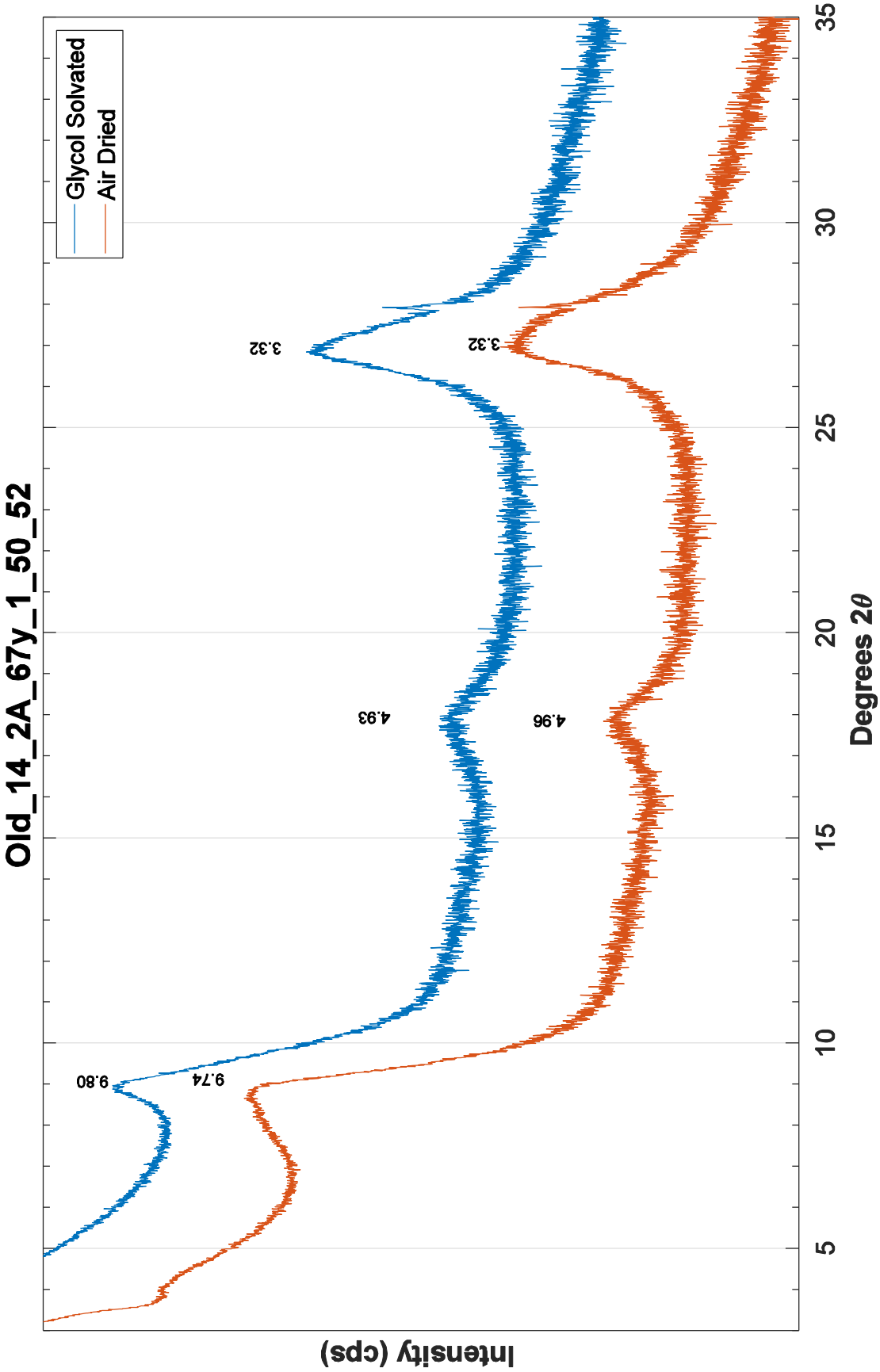
Old_14_2A_67y_1_50_52
Glycol Solvated
Air Dried
9.80
9.74
4.93
4.96
3.32
3.32
Intensity (cps)
Degrees 2θ
5
10
15
20
25
30
35

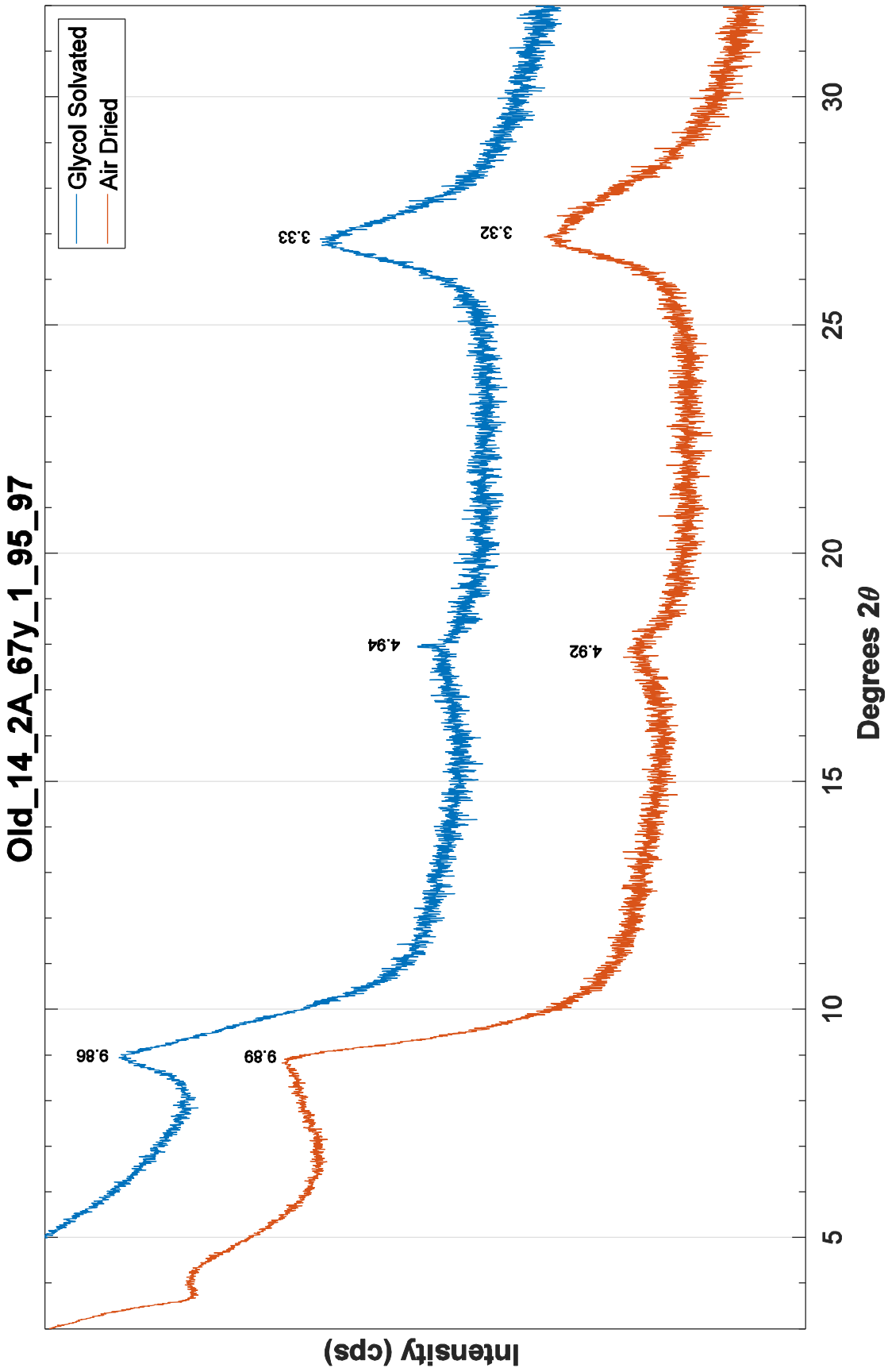
Old_14_2A_67y_1_95_97
Glycol Solvated
Air Dried
9.86
9.89
4.94
4.92
3.33
3.32
Intensity (cps)
Degrees 2θ
5
10
15
20
25
30

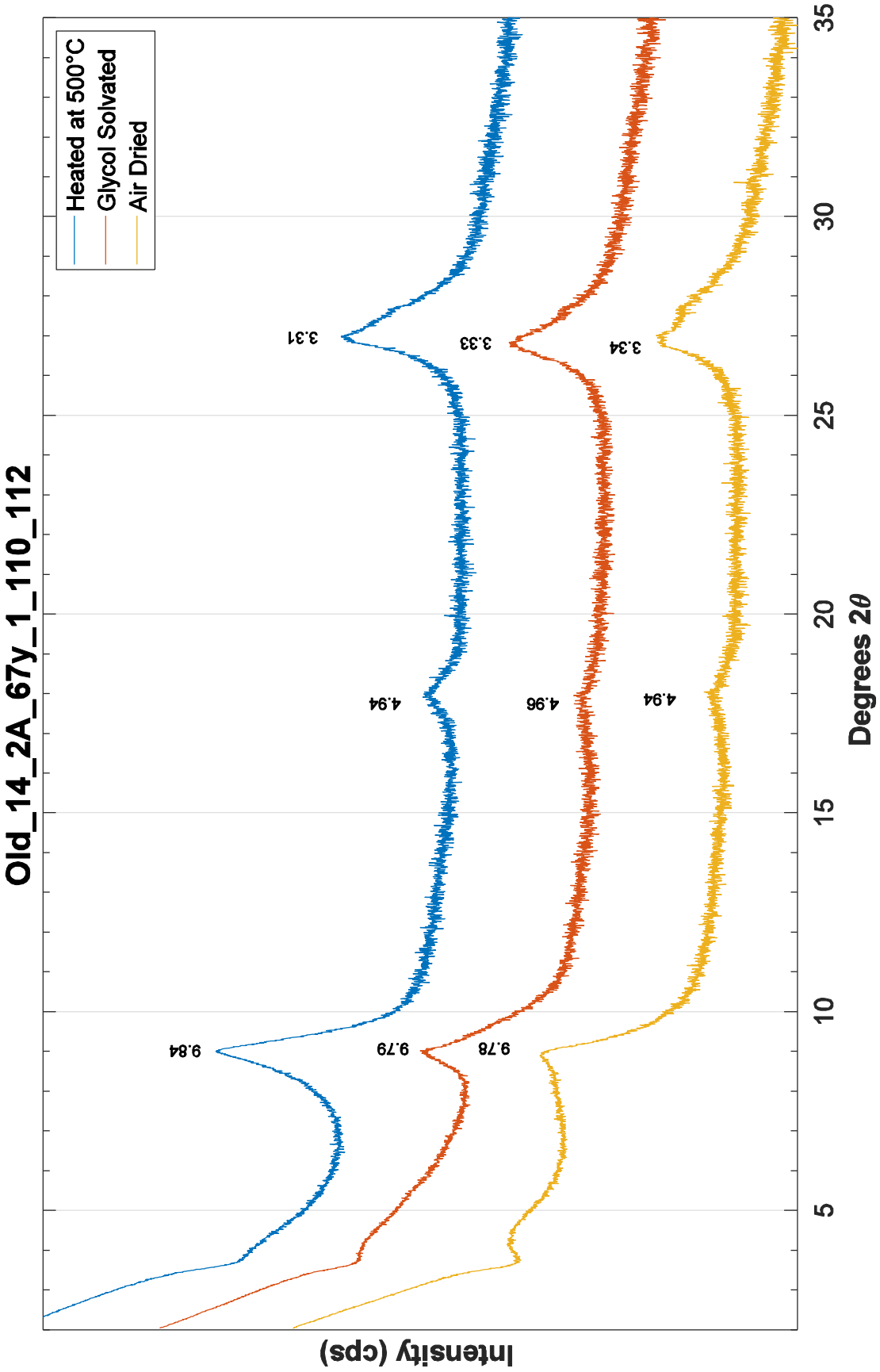
Old_14_2A_67y_1_110_112
Heated at 500°C
Glycol Solvated
Air Dried
Intensity (cps)
Degrees 2θ
5
10
15
20
25
30
35
9.84
9.79
9.78
4.94
4.96
4.94
3.31
3.33
3.34

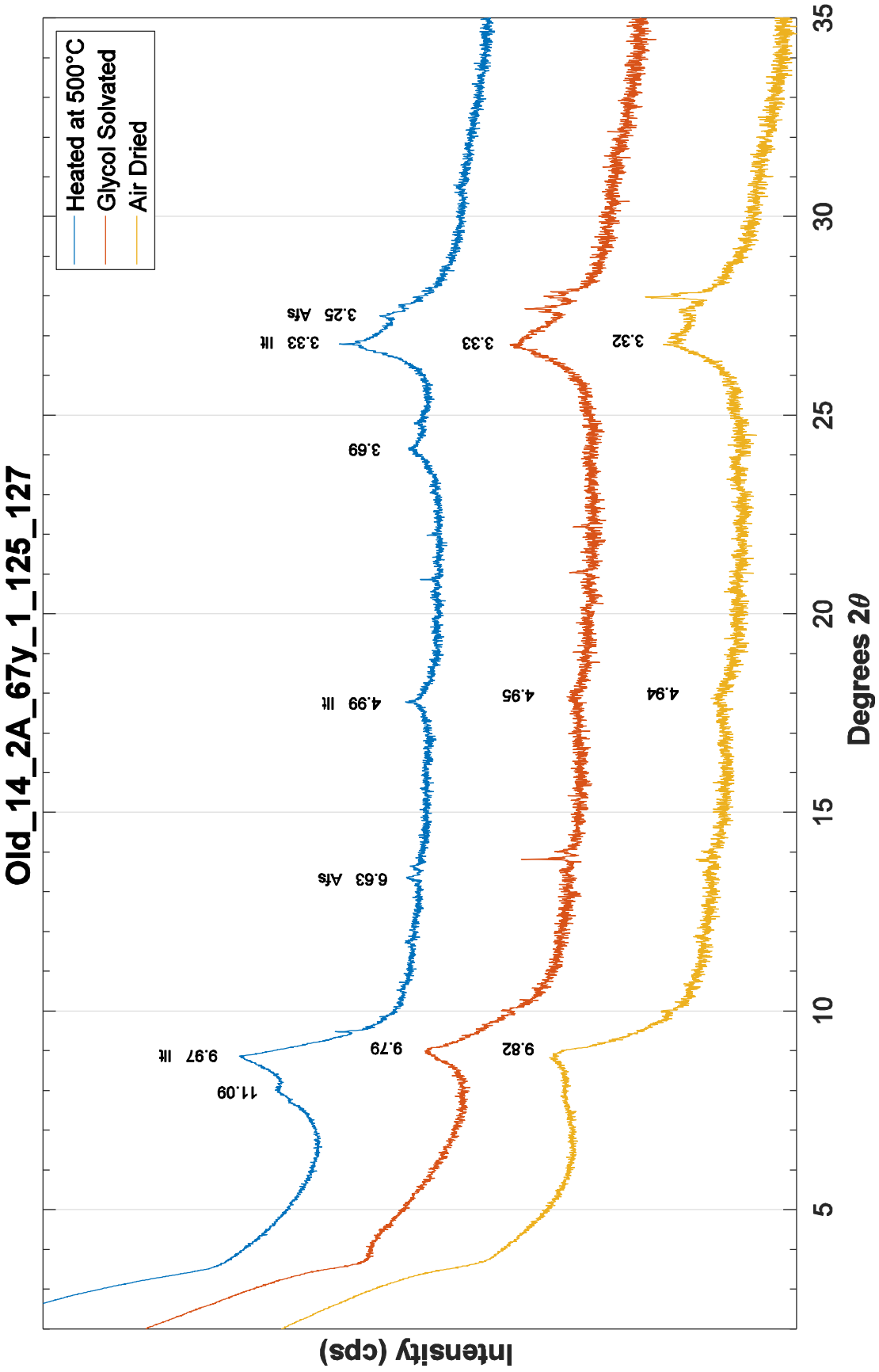
Old_14_2A_67y_1_125_127
Heated at 500°C
Glycol Solvated
Air Dried
Intensity (cps)
Degrees 2θ
5
10
15
20
25
30
35
11.09
9.97 Ilt
9.79
6.63 Als
3.69
4.99 Ilt
3.33 Ilt
3.25 Als
9.82
4.95
3.33
4.94
3.32

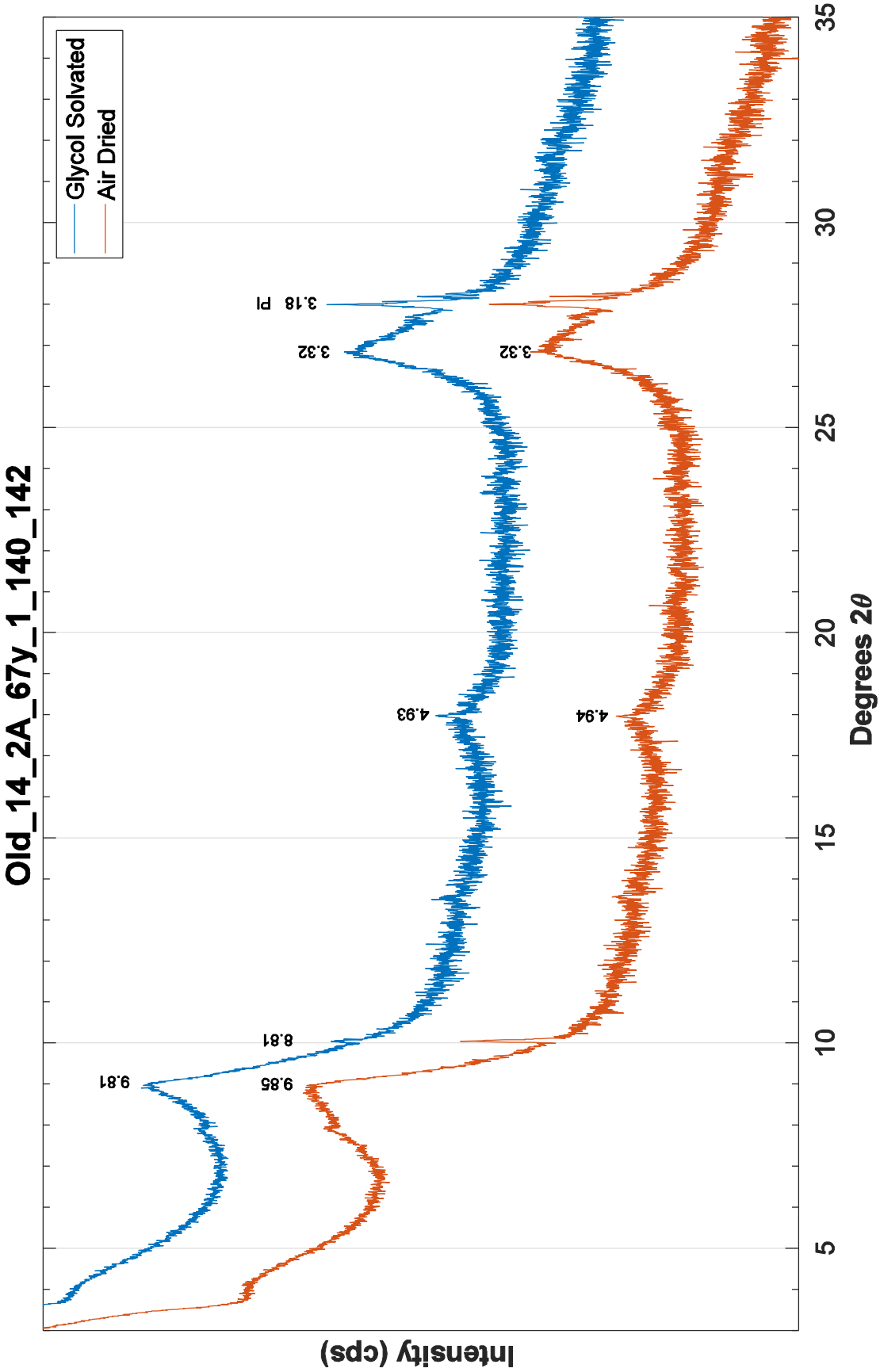
Old_14_2A_67y_1_140_142
Glycol Solvated
Air Dried
3.18 PI
3.32
3.32
4.93
4.94
8.81
9.85
9.81
Intensity (cps)
Degrees 2θ
5
10
15
20
25
30
35

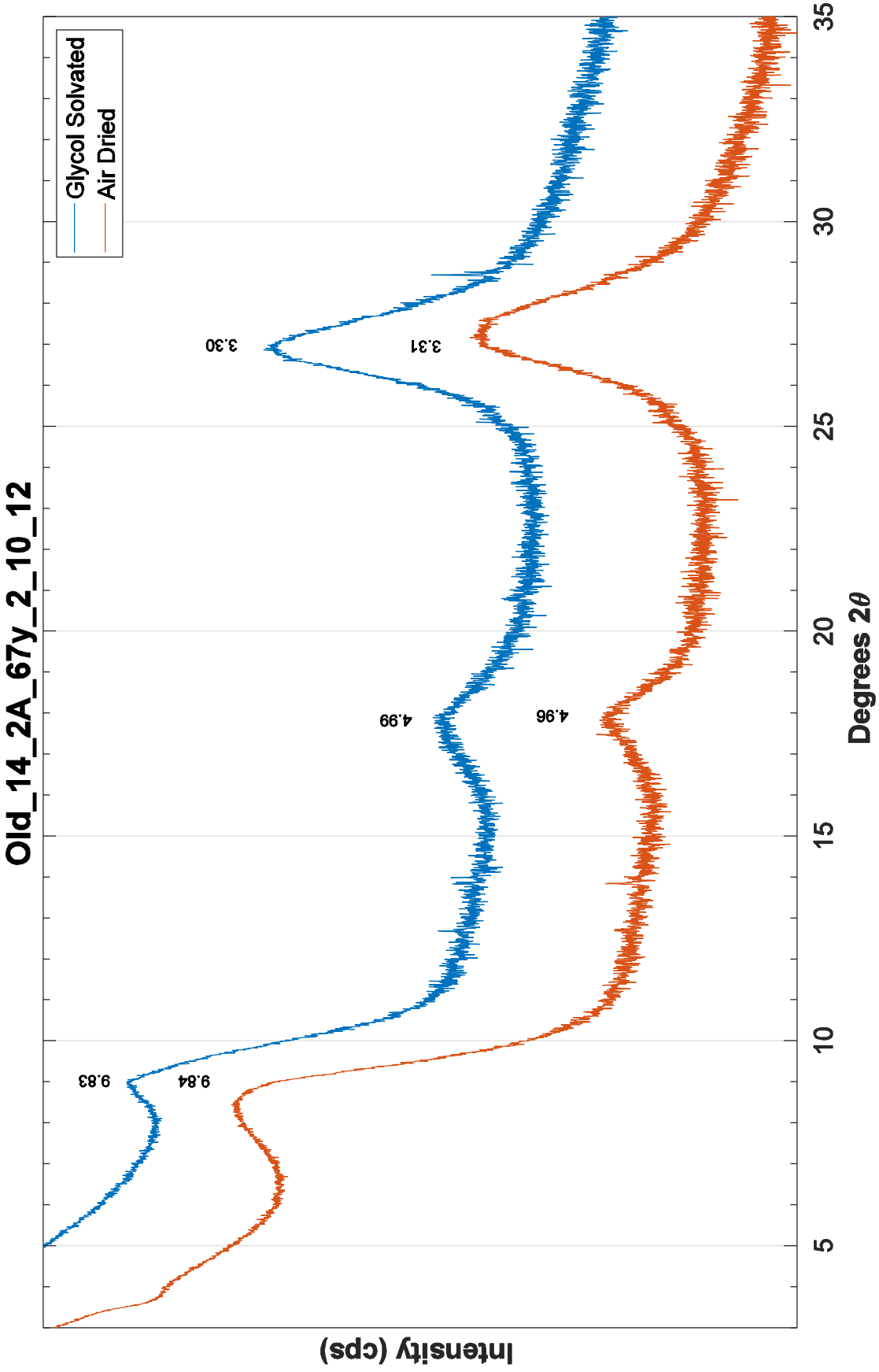
Old_14_2A_67y_2_10_12
Glycol Solvated
Air Dried
9.83
9.84
4.99
4.96
3.30
3.31
Intensity (cps)
Degrees 2θ
5
10
15
20
25
30
35

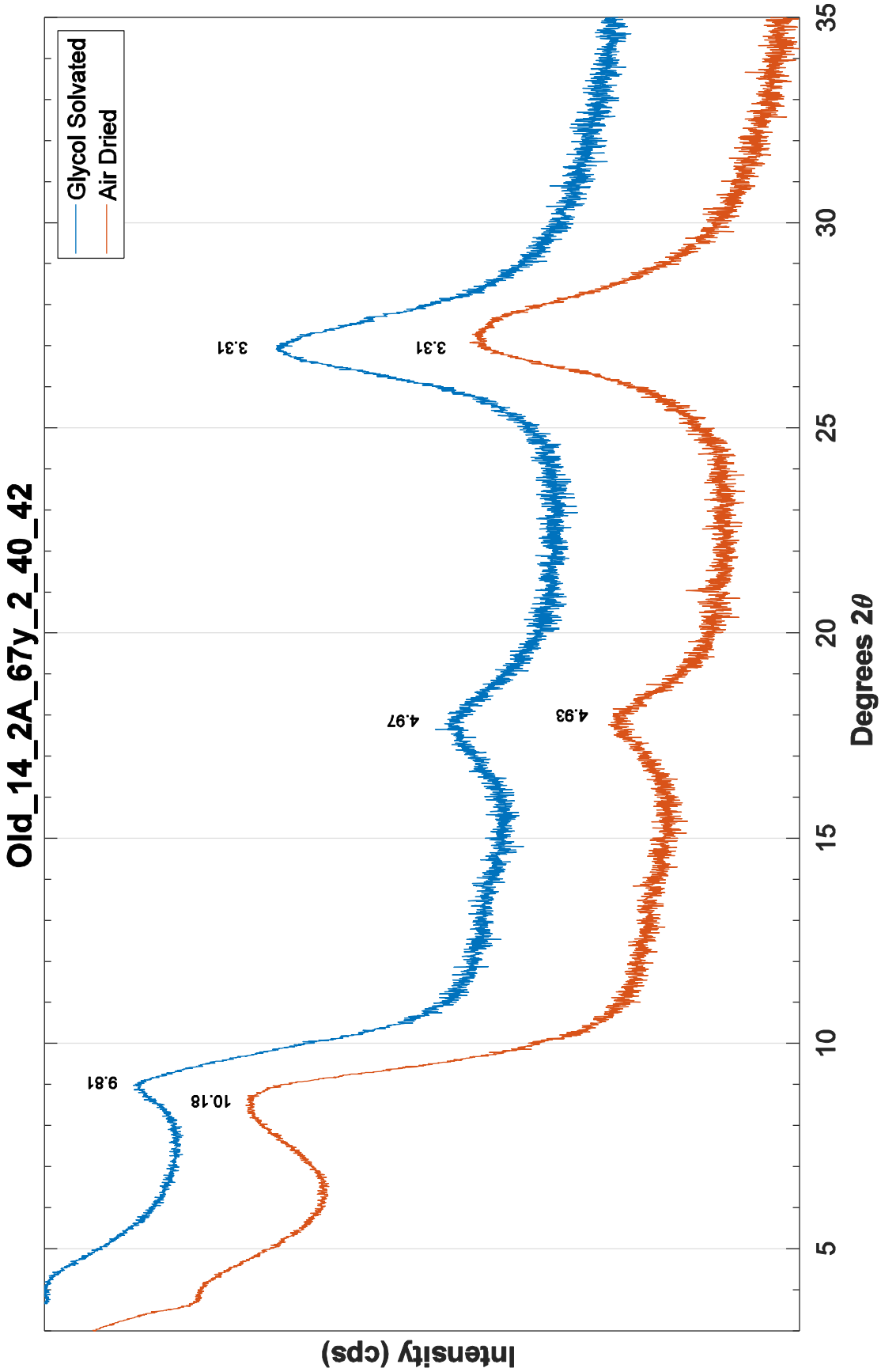
Old_14_2A_67y_2_40_42
Glycol Solvated
Air Dried
9.81
10.18
4.97
4.93
3.31
3.31
Intensity (cps)
Degrees 2θ
5
10
15
20
25
30
35

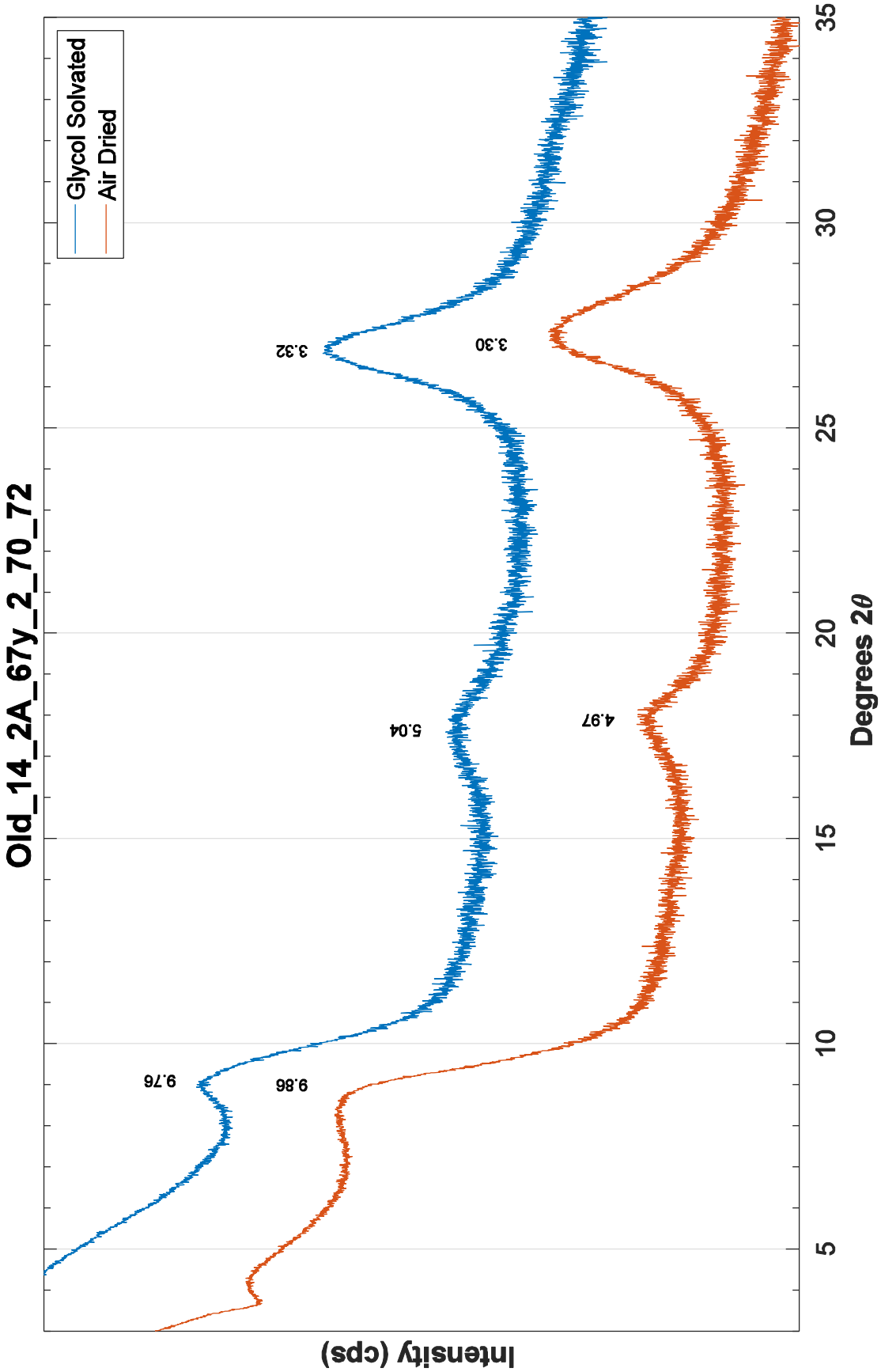
Old_14_2A_67y_2_70_72
Glycol Solvated
Air Dried
9.76
9.86
5.04
4.97
3.32
3.30
Intensity (cps)
Degrees 2θ
5
10
15
20
25
30
35

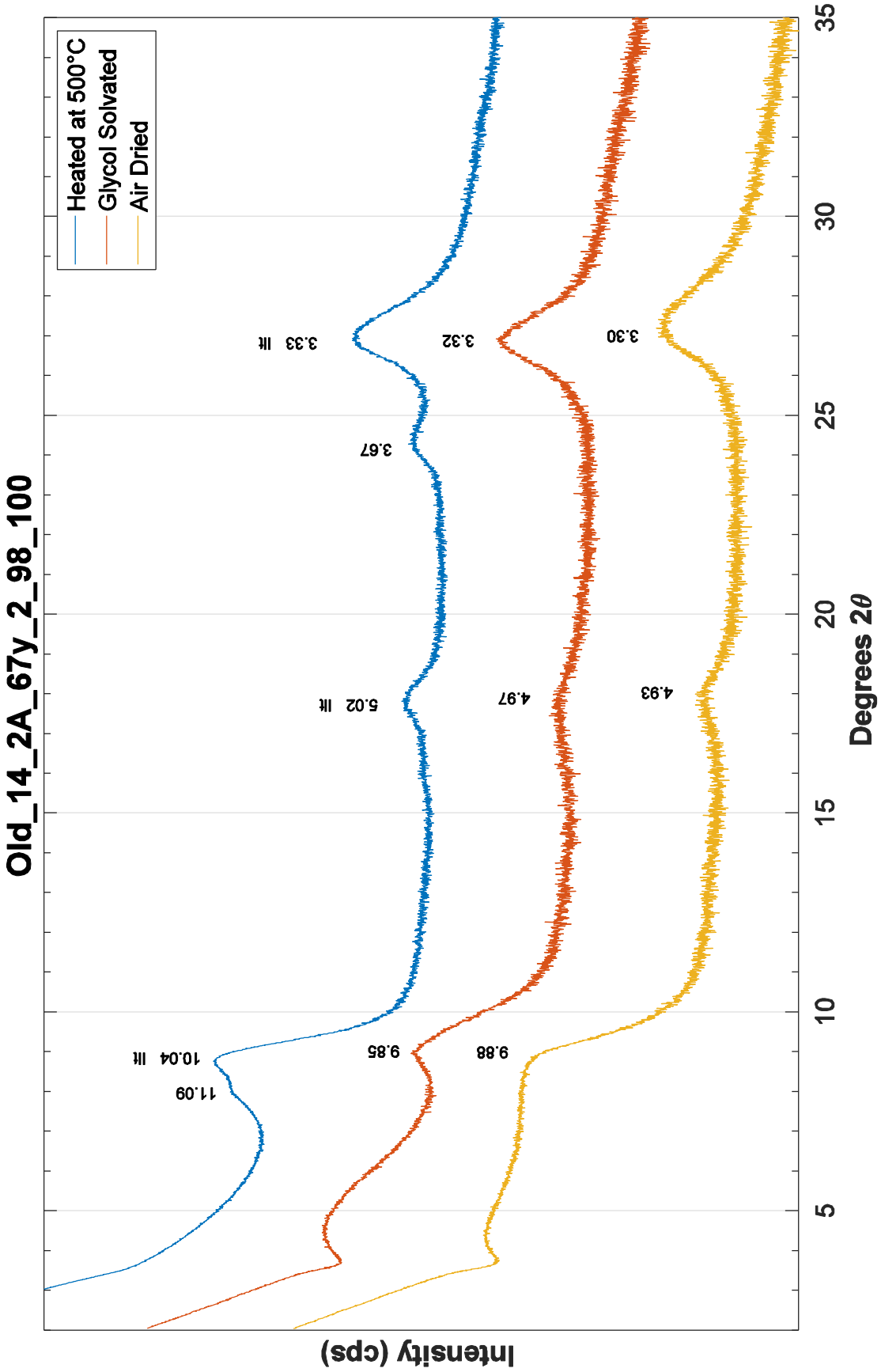
Old_14_2A_67y_2_98_100
Heated at 500°C
Glycol Solvated
Air Dried
Intensity (cps)
Degrees 2θ
5
10
15
20
25
30
35
11.09
10.04 Ilt
9.85
9.88
5.02 Ilt
4.97
4.93
3.67
3.33 Ilt
3.32
3.30

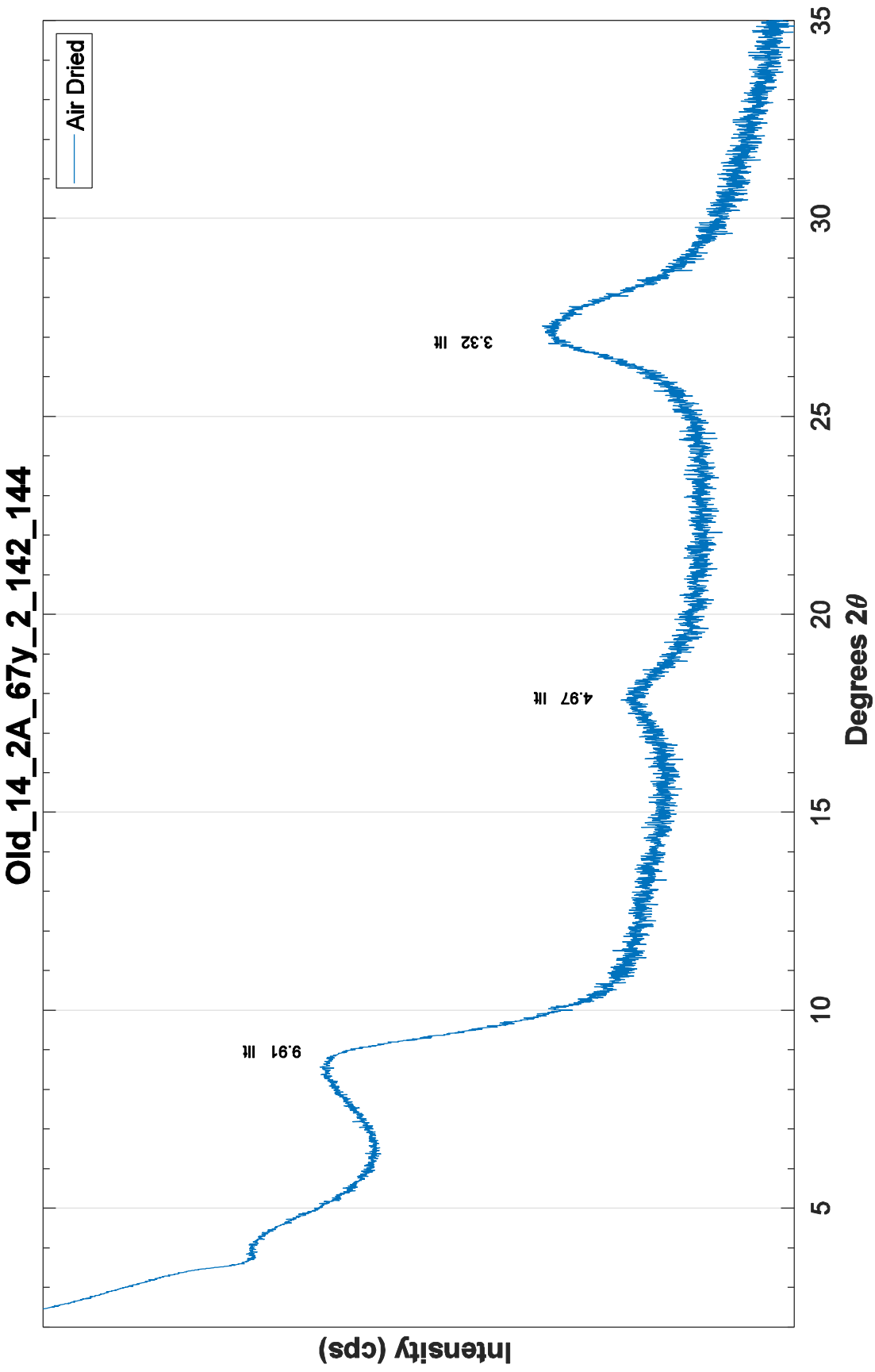
Old_14_2A_67y_2_142_144
Air Dried
9.91 Å
4.97 Å
3.32 Å
Intensity (cps)
Degrees 2θ
5
10
15
20
25
30
35

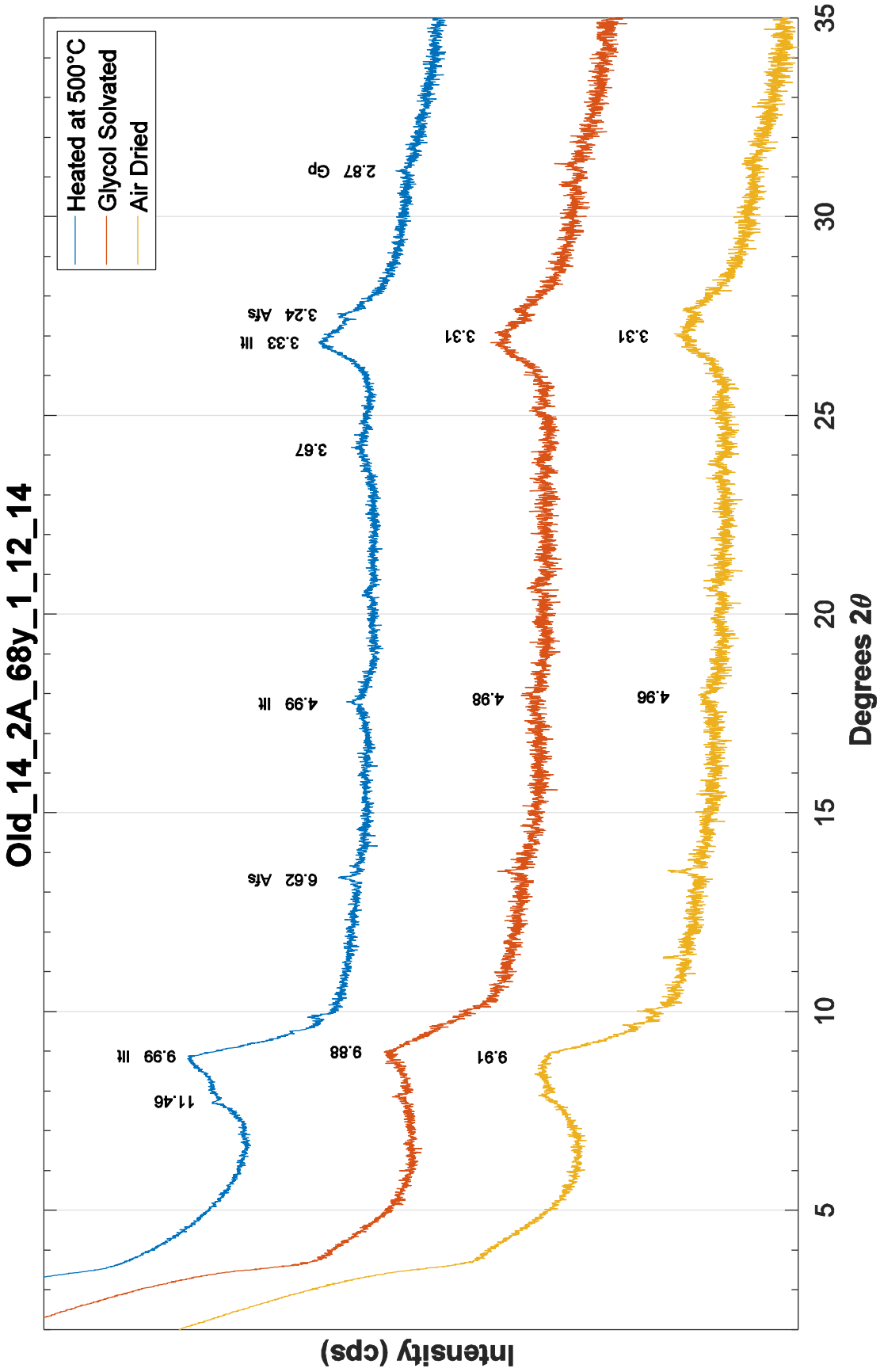
Old_14_2A_68y_1_12_14
Heated at 500°C
Glycol Solvated
Air Dried
Intensity (cps)
Degrees 2θ
5
10
15
20
25
30
35
11.46
9.99 Ilt
9.88
9.91
6.62 Afs
3.67
4.99 Ilt
4.98
4.96
3.33 Ilt
3.24 Afs
3.31
3.31
2.87 Gp

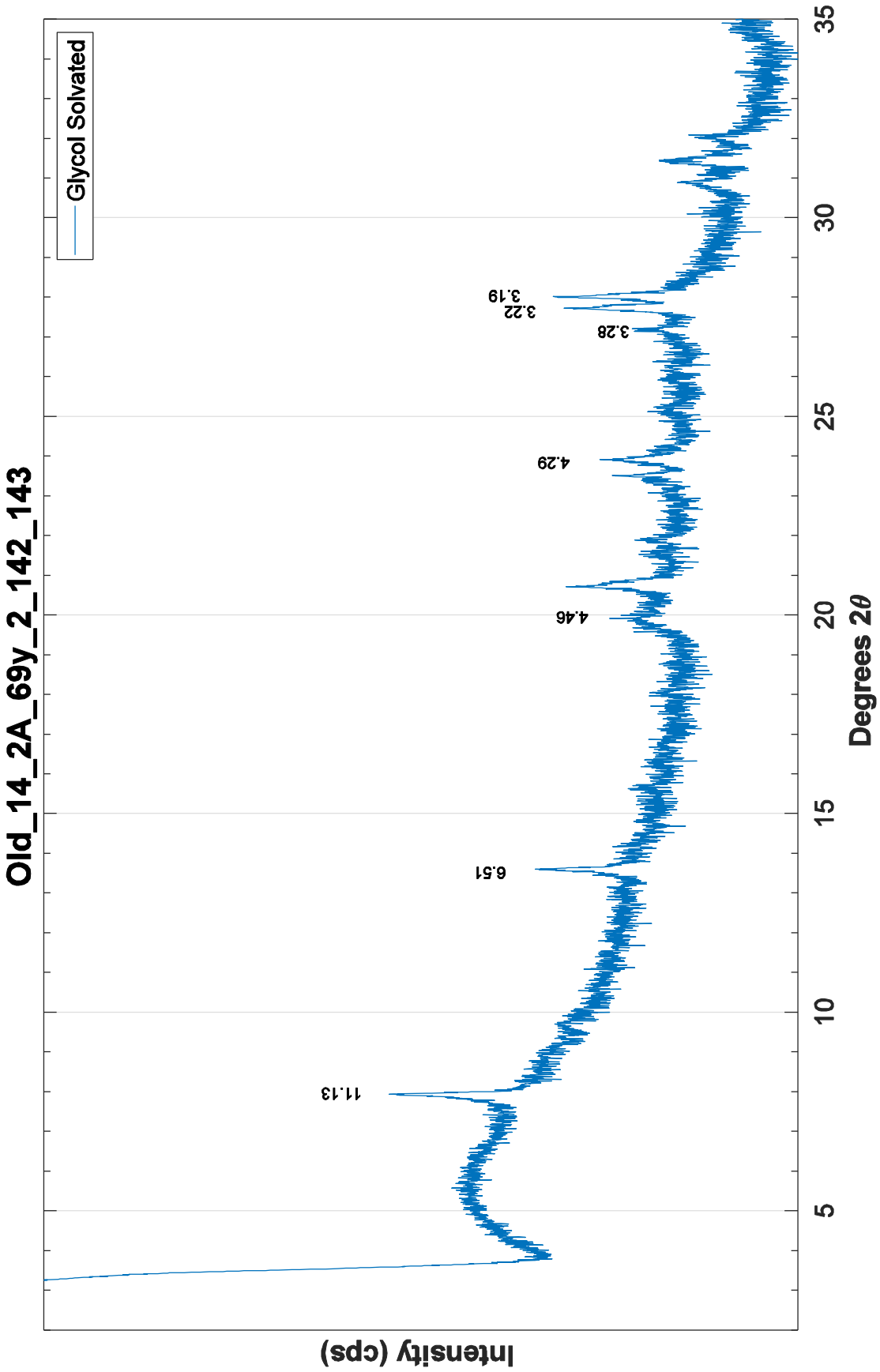
Old_14_2A_69y_2_142_143
Glycol Solvated
Intensity (cps)
Degrees 2θ
5
10
15
20
25
30
35
11.13
6.51
4.46
4.29
3.28
3.22
3.19

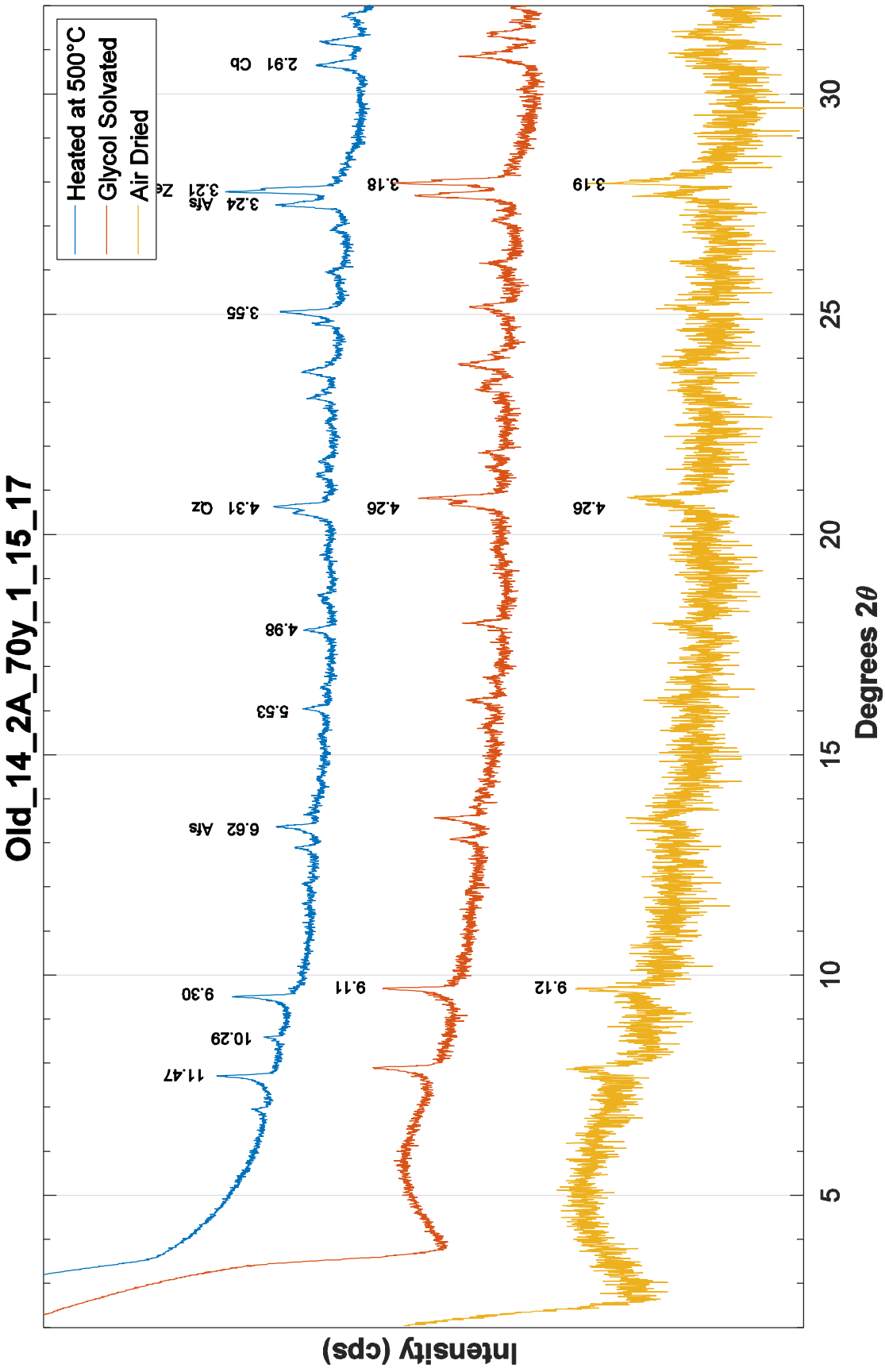
Old_14_2A_70y_1_15_17
Heated at 500°C
Glycol Solvated
Air Dried
Intensity (cps)
Degrees 2θ
5
10
15
20
25
30
11.47
10.29
9.30
9.11
9.12
6.62 Afs
5.53
4.98
4.31 Qz
4.26
4.26
3.55
3.24 Afs
3.21
3.18
3.19
2.91 Cb

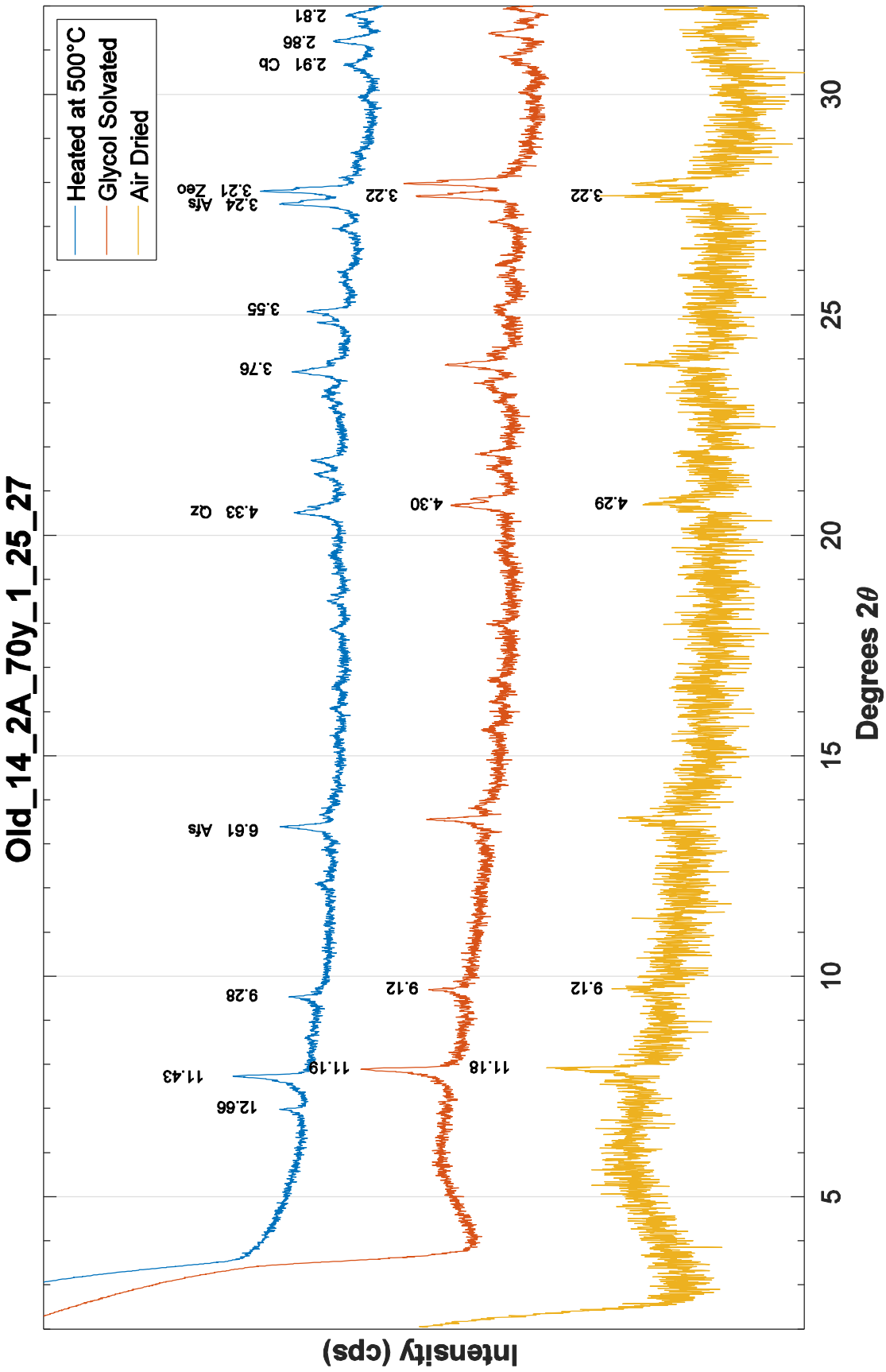
Old_14_2A_70y_1_25_27
Heated at 500°C
Glycol Solvated
Air Dried
Intensity (cps)
Degrees 2θ
5
10
15
20
25
30
12.66
11.43
11.19
9.28
6.61 Afs
4.33 Qz
3.76
3.55
3.24 Afs
3.21 Zeo
2.91 Cb
2.86
2.81
11.18
9.12
4.30
3.22
9.12
4.29
3.22

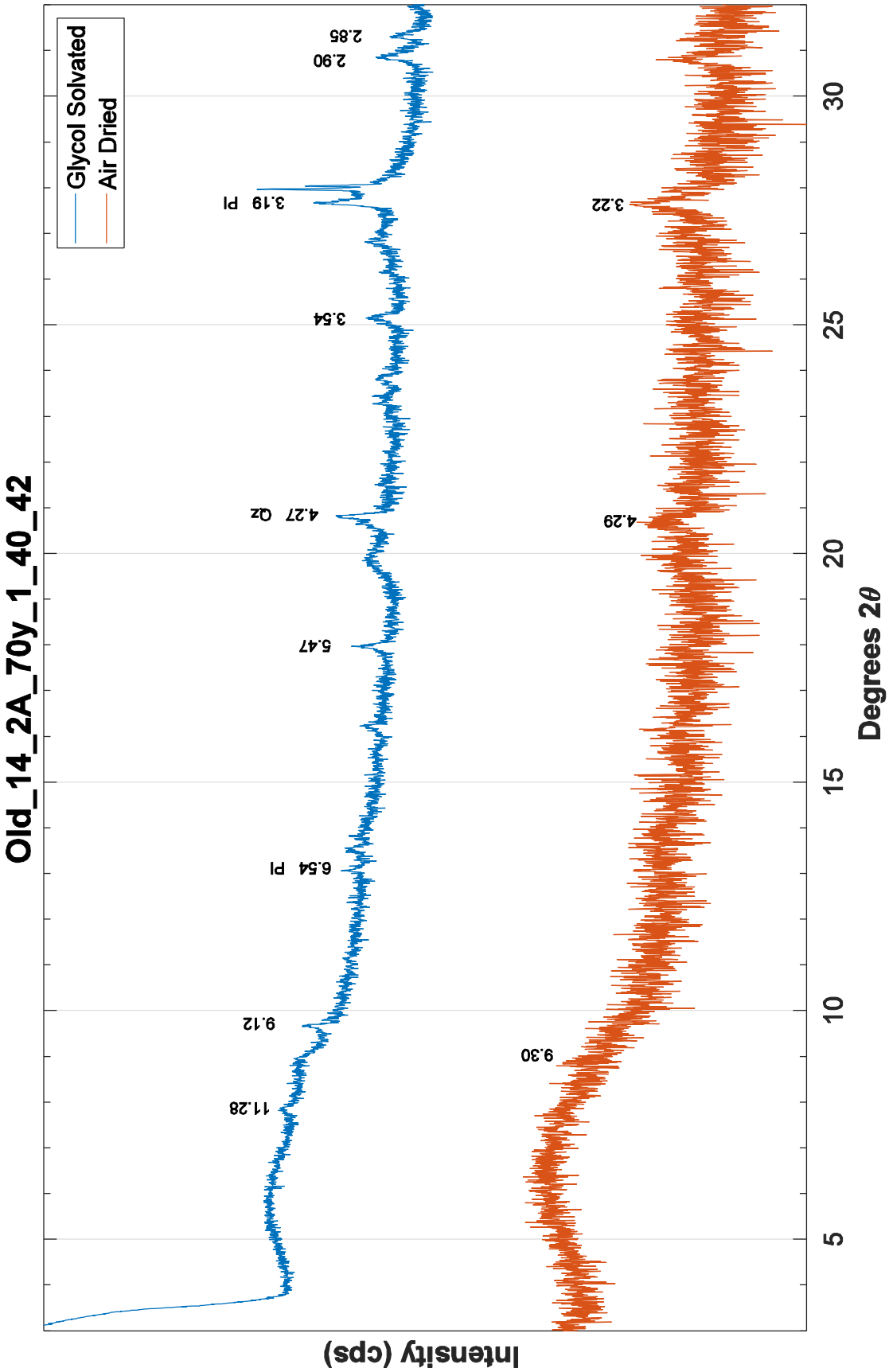
Old_14_2A_70y_1_40_42
Glycol Solvated
Air Dried
Intensity (cps)
Degrees 2θ
5
10
15
20
25
30
2.85
2.90
3.19 Pl
3.54
4.27 Qz
5.47
6.54 Pl
9.12
11.28
3.22
4.29
9.30

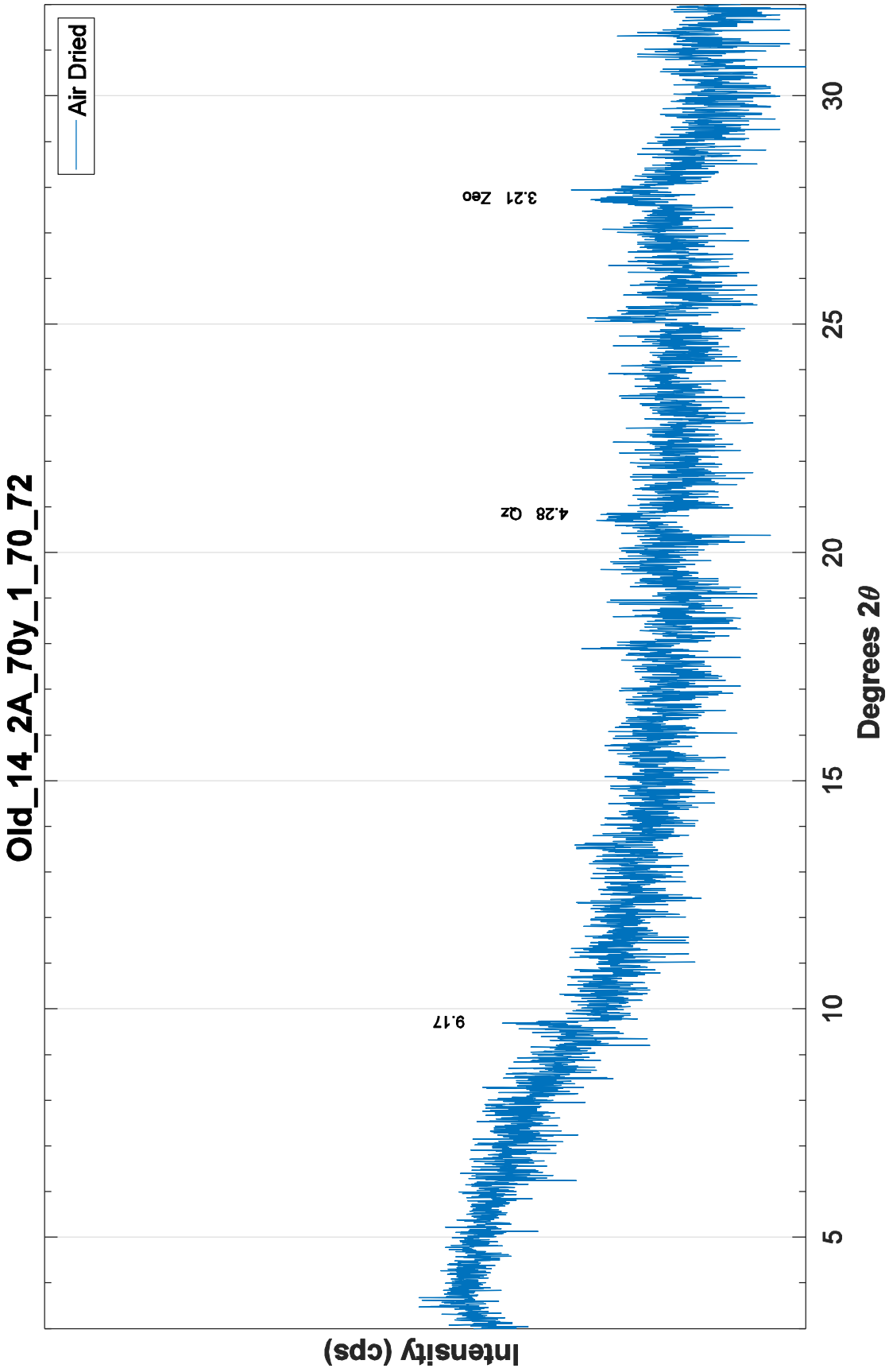
Old_14_2A_70y_1_70_72
Air Dried
Intensity (cps)
Degrees 2θ
5
10
15
20
25
30
9.17
4.28 Qz
3.21 Zeo

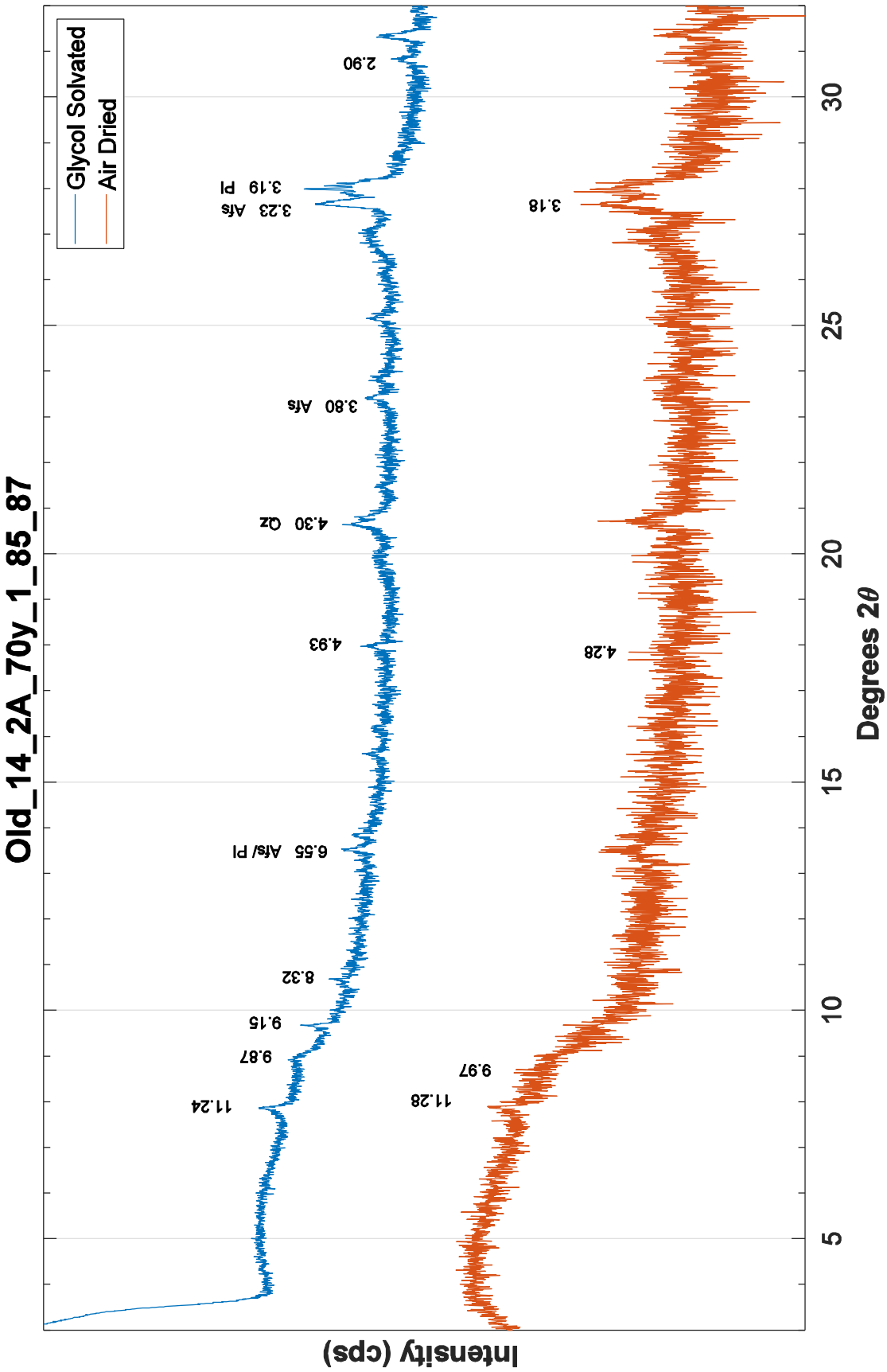
Old_14_2A_70y_1_85_87
Glycol Solvated
Air Dried
Intensity (cps)
Degrees 2θ
5
10
15
20
25
30
11.24
9.87
9.15
8.32
6.55 Afs/ Pl
4.93
4.30 Qz
3.80 Afs
3.23 Afs
3.19 Pl
2.90
11.28
9.97
4.28
3.18

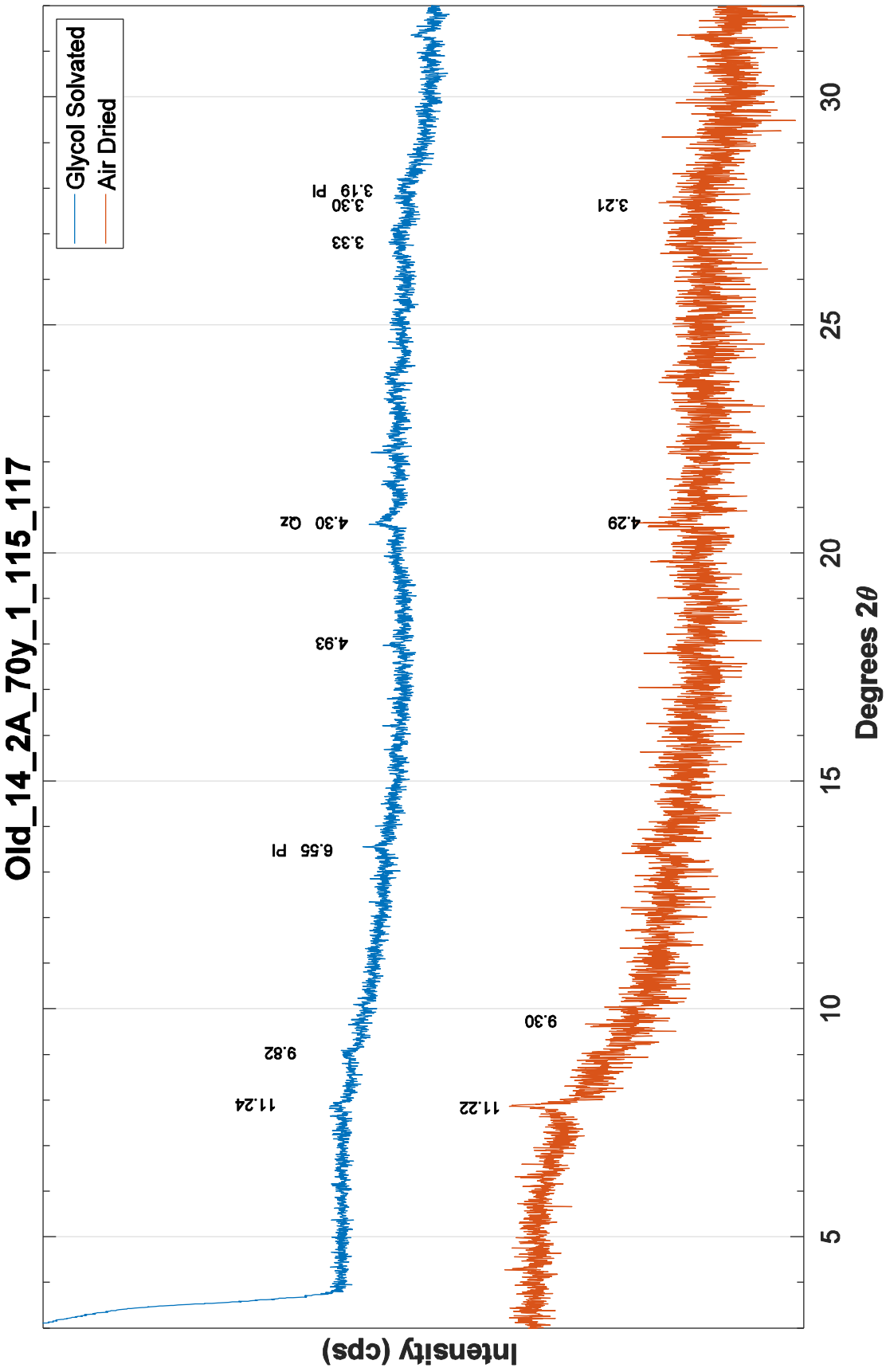
Old_14_2A_70y_1_115_117
Glycol Solvated
Air Dried
Intensity (cps)
Degrees 2θ
5
10
15
20
25
30
11.24
9.82
6.55 Pl
4.93
4.30 Qz
3.33
3.30
3.19 Pl
11.22
9.30
4.29
3.21

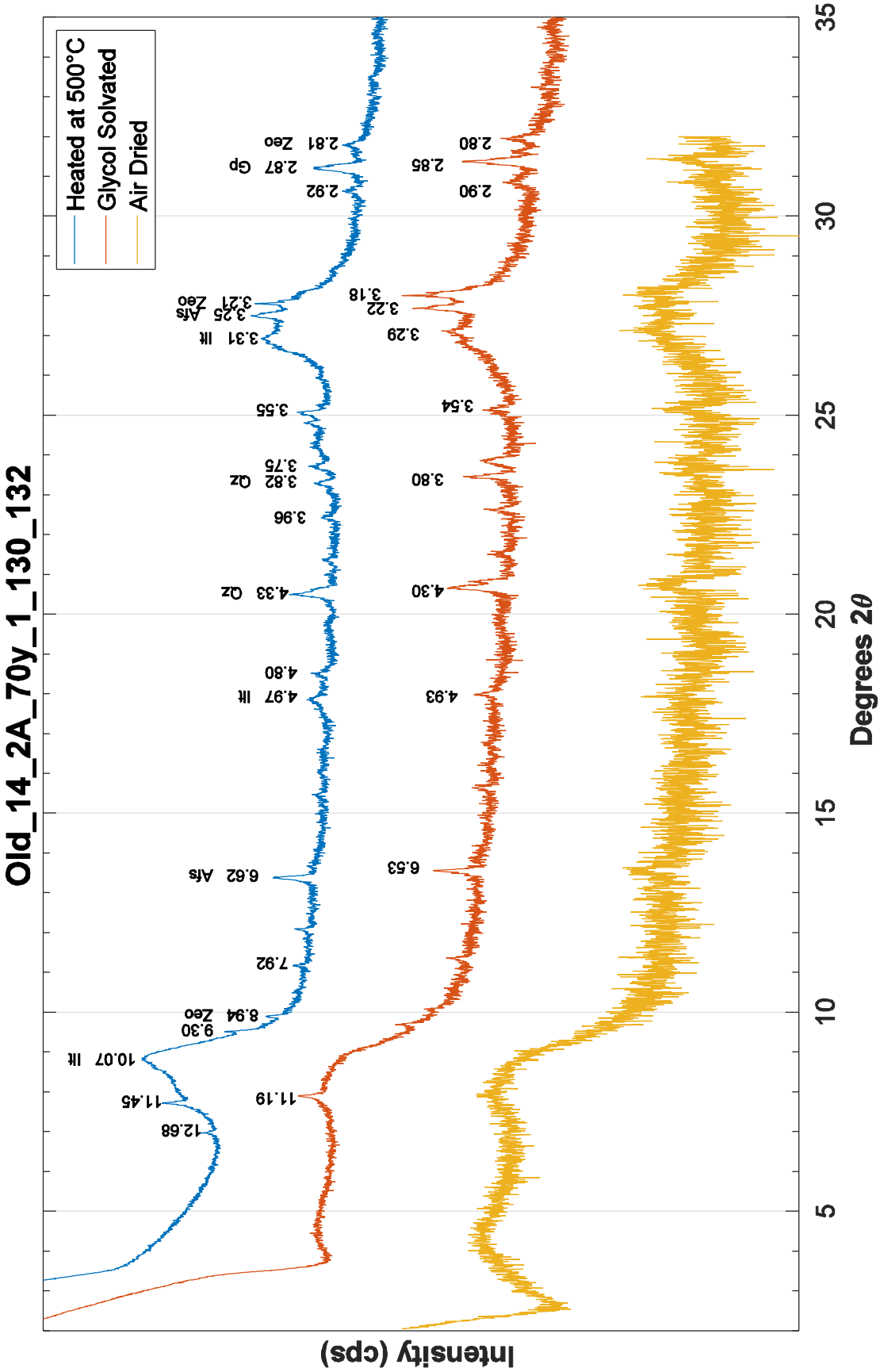
Old_14_2A_70y_1_130_132
Heated at 500°C
Glycol Solvated
Air Dried
Intensity (cps)
Degrees 2θ
5
10
15
20
25
30
35
12.68
11.45
10.07 Ilt
9.30
8.94 Zeo
7.92
6.62 Afs
4.97 Ilt
4.80
4.33 Qz
3.96
3.82
3.75 Qz
3.55
3.31 Ilt
3.25 Afs
3.21 Zeo
2.92
2.87 Gp
2.81 Zeo
11.19
6.53
4.93
4.30
3.80
3.54
3.29
3.22
3.18
2.90
2.85
2.80

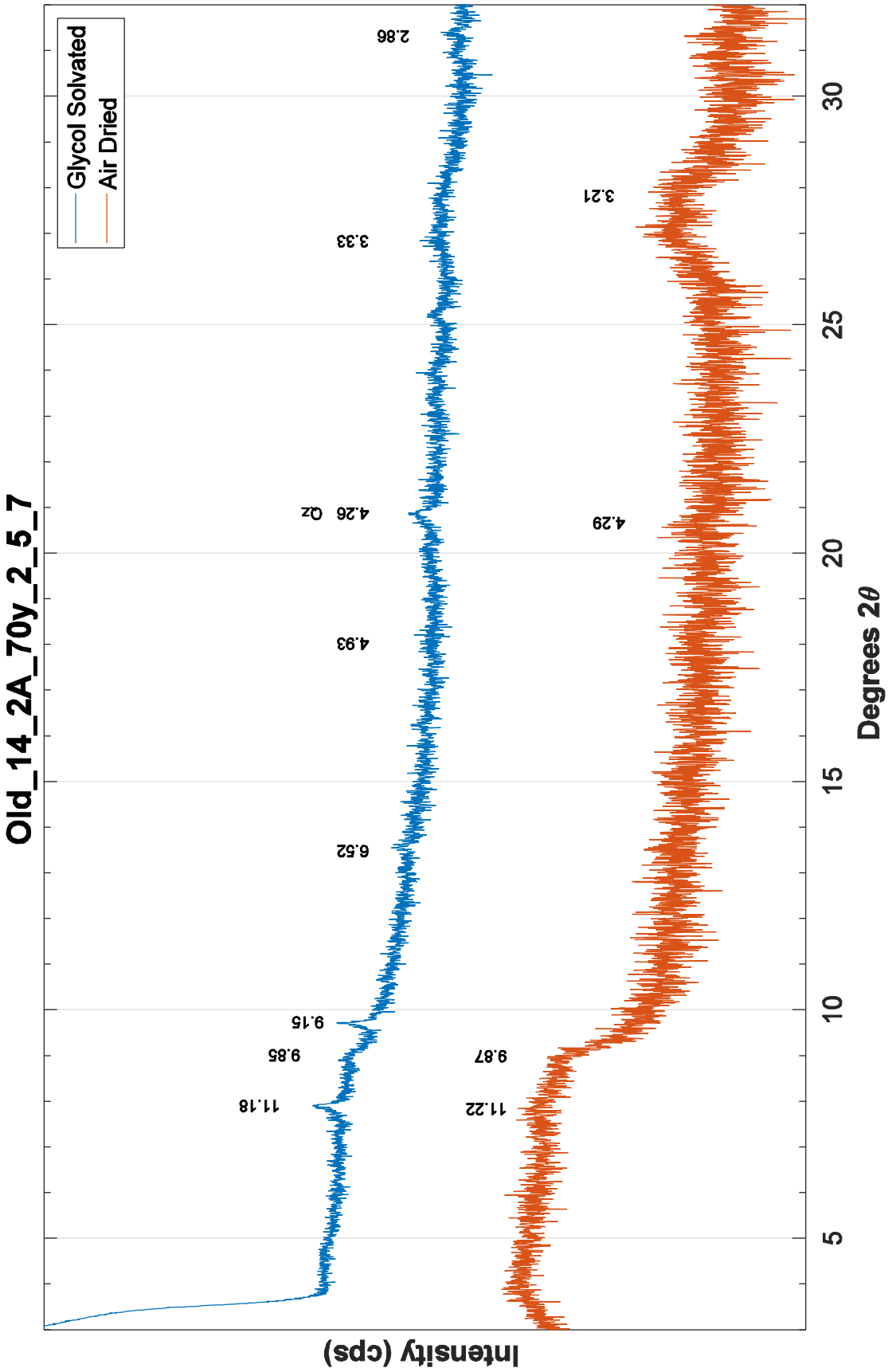
Old_14_2A_70y_2_5_7
Glycol Solvated
Air Dried
Intensity (cps)
Degrees 2θ
5
10
15
20
25
30
11.18
9.85
9.15
6.52
4.93
4.26 Qz
3.33
2.86
11.22
9.87
4.29
3.21

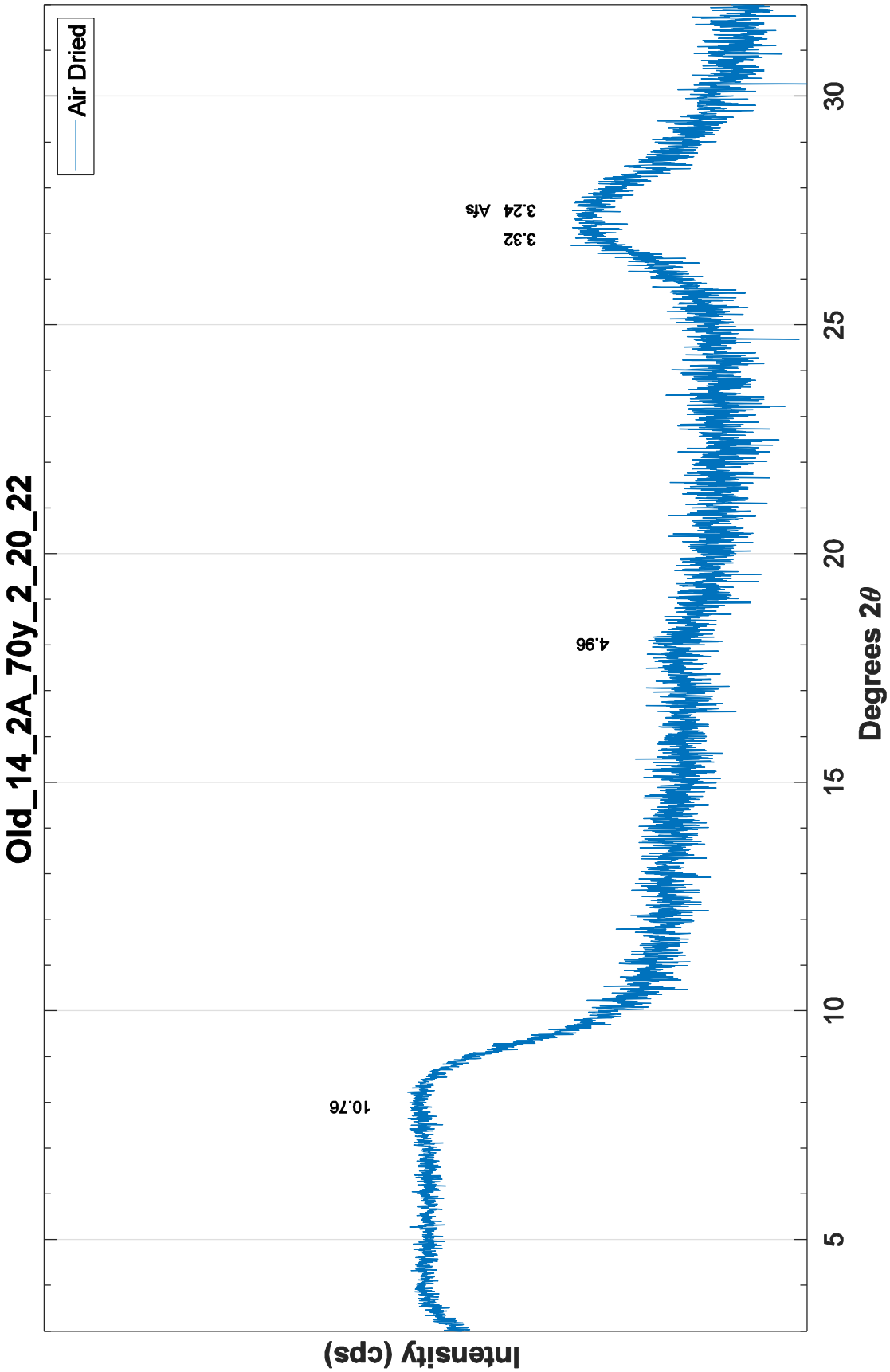
Old_14_2A_70y_2_20_22
Air Dried
Intensity (cps)
Degrees 2θ
5
10
15
20
25
30
10.76
4.96
3.32
3.24 Å

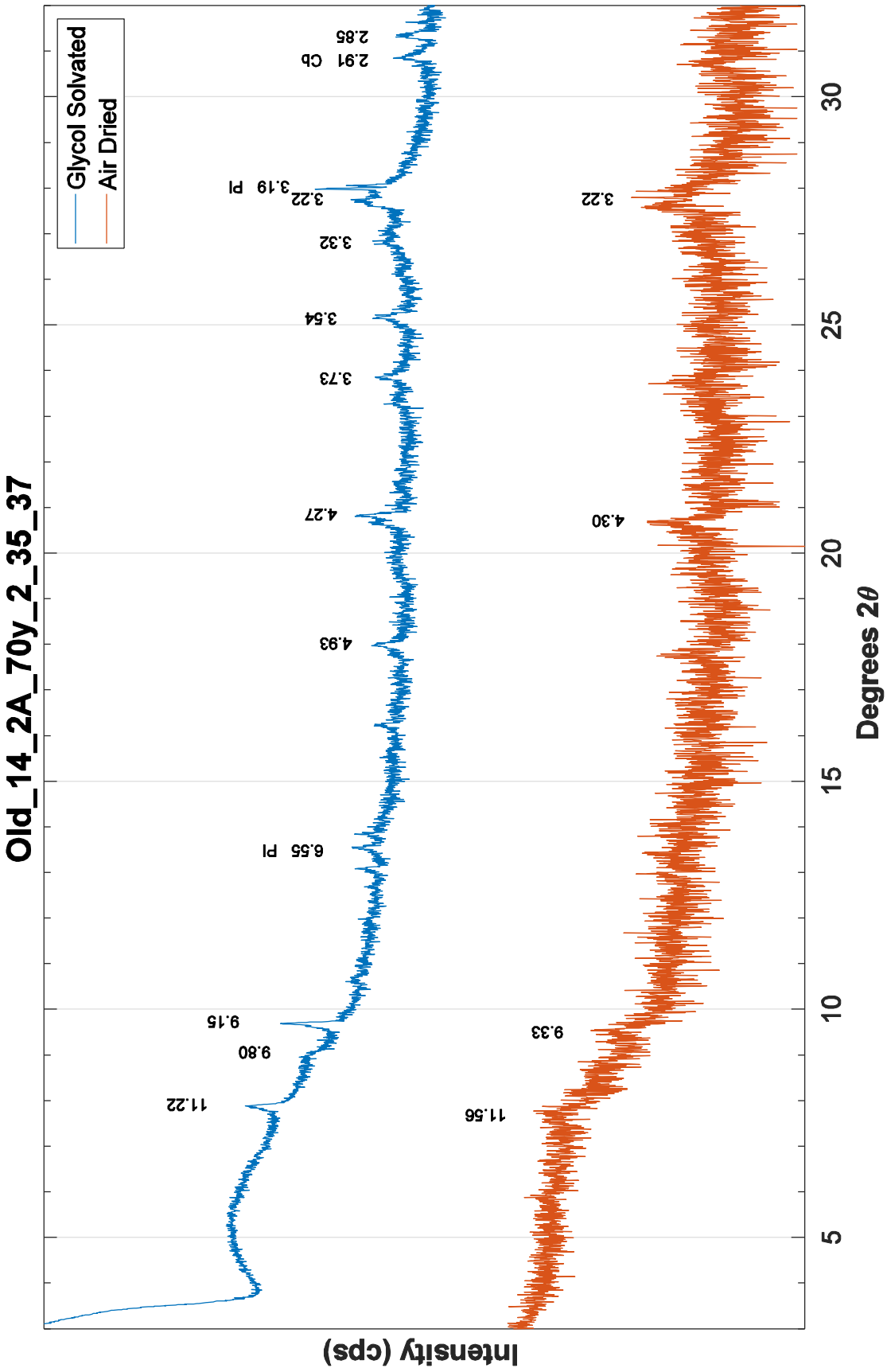
Old_14_2A_70y_2_35_37
Glycol Solvated
Air Dried
Intensity (cps)
Degrees 2θ
5
10
15
20
25
30
11.22
9.80
9.15
6.55 Pl
4.93
4.27
3.73
3.54
3.32
3.22
3.19 Pl
2.91 Cb
2.85
11.56
9.33
4.30
3.22

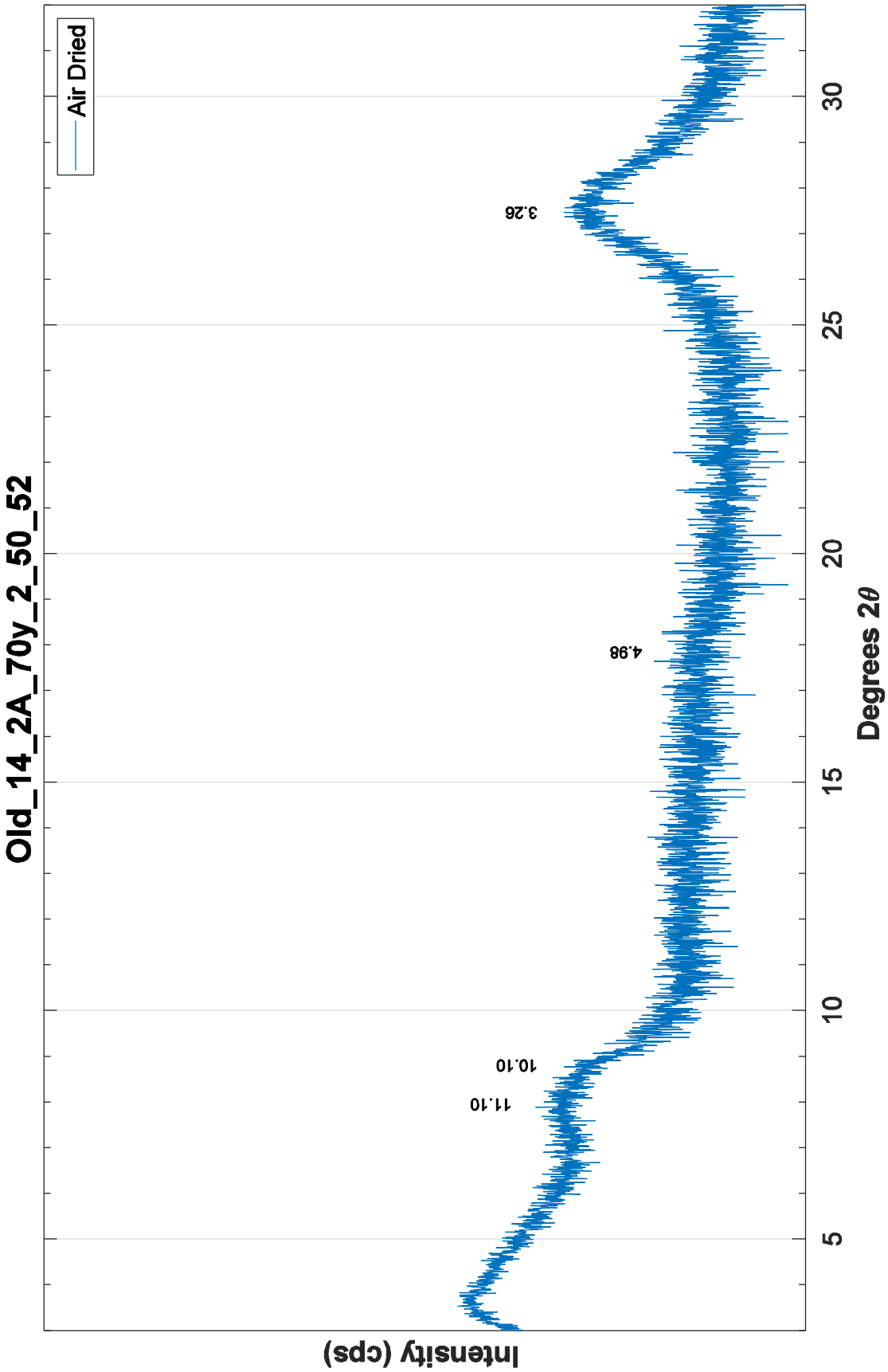
Old_14_2A_70y_2_50_52
Air Dried
Intensity (cps)
Degrees 2θ
5
10
15
20
25
30
11.10
10.10
4.98
3.26

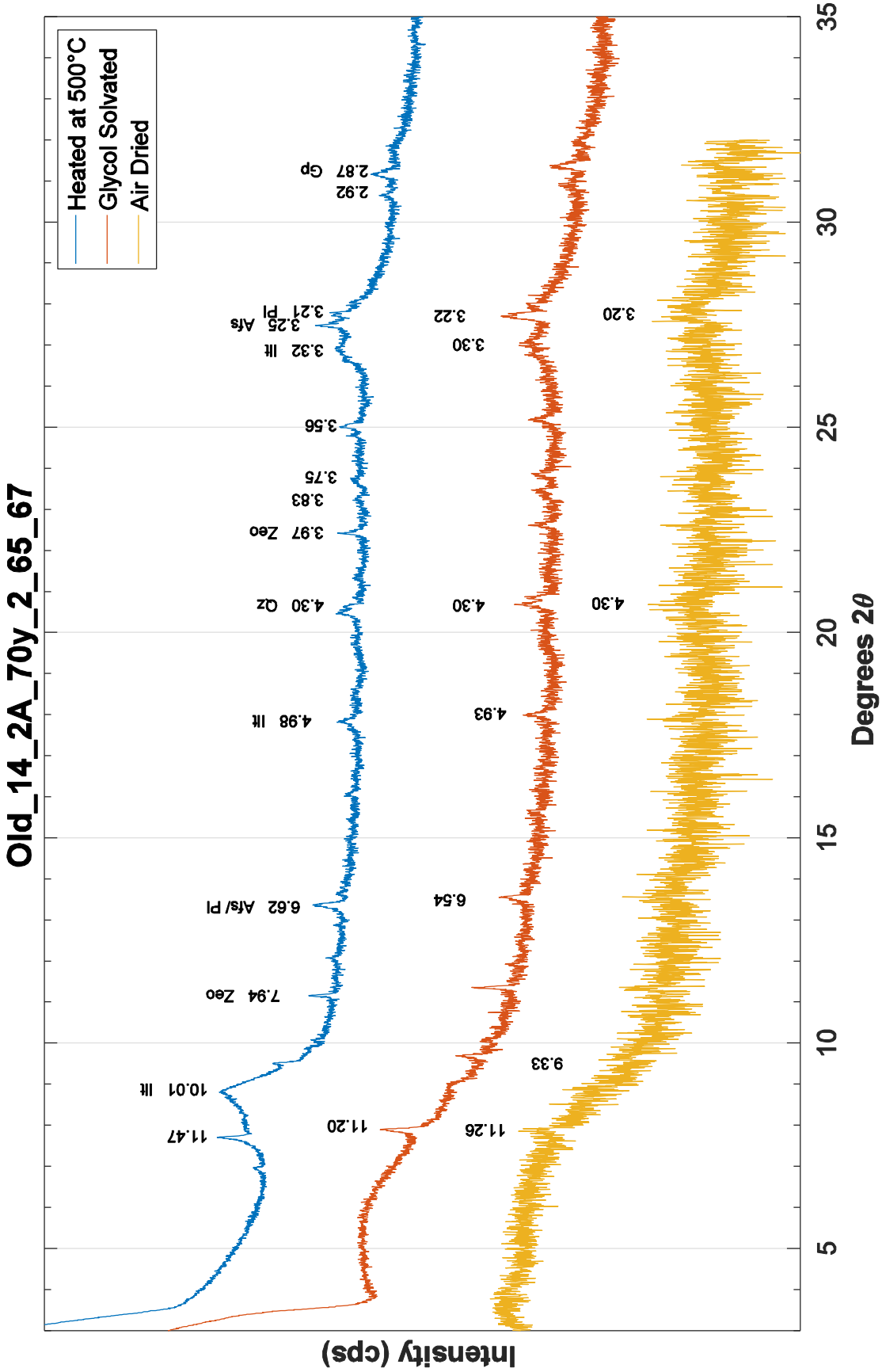
Old_14_2A_70y_2_65_67
Heated at 500°C
Glycol Solvated
Air Dried
Intensity (cps)
Degrees 2θ
5
10
15
20
25
30
35
11.47
10.01 Ilt
7.94 Zeo
6.62 Afs/ Pl
4.98 Ilt
4.30 Qz
3.97 Zeo
3.83
3.75
3.56
3.32 Ilt
3.25 Afs
3.21 Pl
2.92
2.87 Gp
11.20
9.33
6.54
4.93
4.30
3.30
3.22
11.26
4.30
3.20

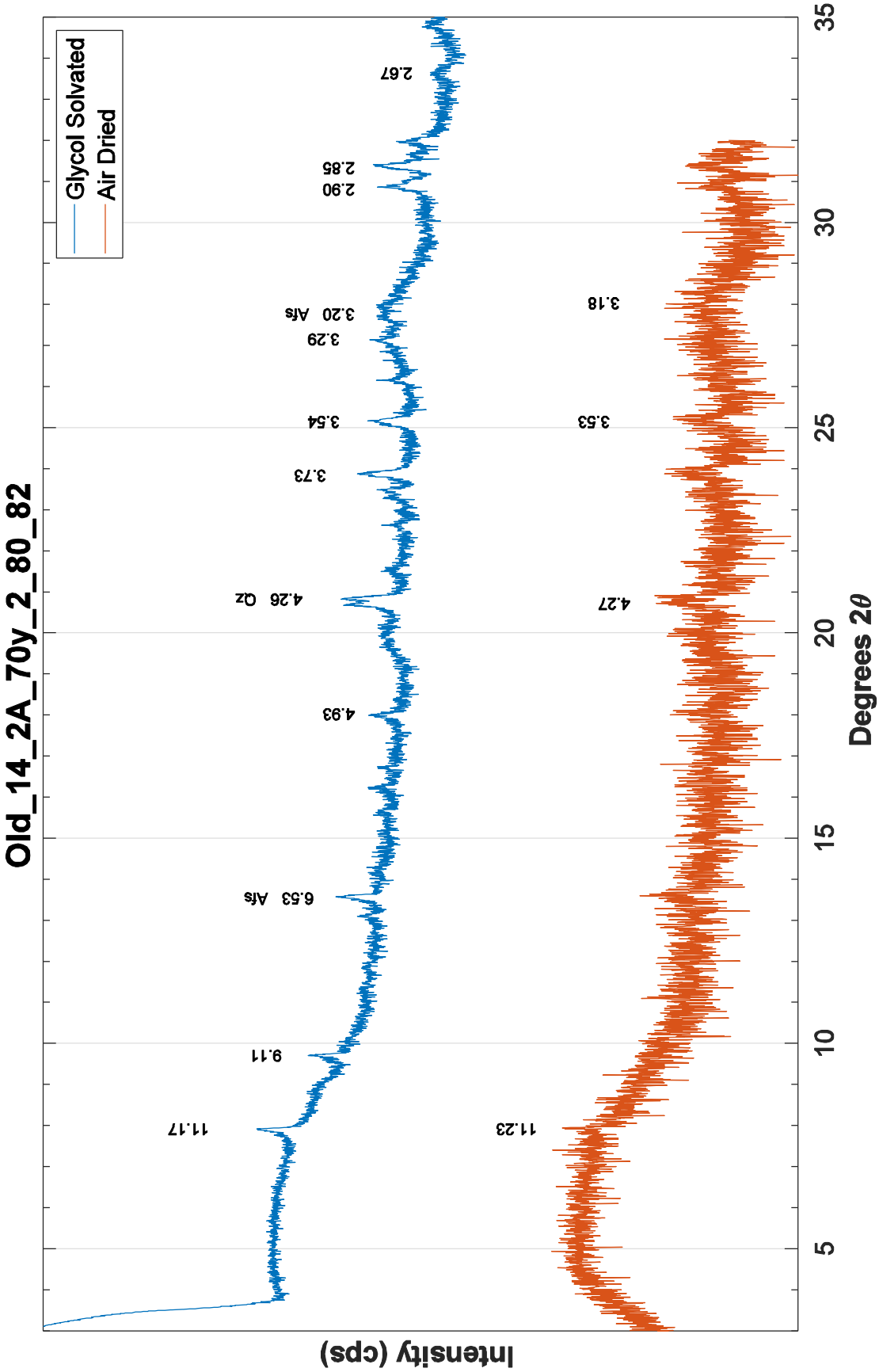
Old_14_2A_70y_2_80_82
Glycol Solvated
Air Dried
Intensity (cps)
Degrees 2θ
5
10
15
20
25
30
35
11.17
9.11
6.53 Afs
4.93
4.26 Qz
3.73
3.54
3.29
3.20 Afs
2.90
2.85
2.67
11.23
4.27
3.53
3.18

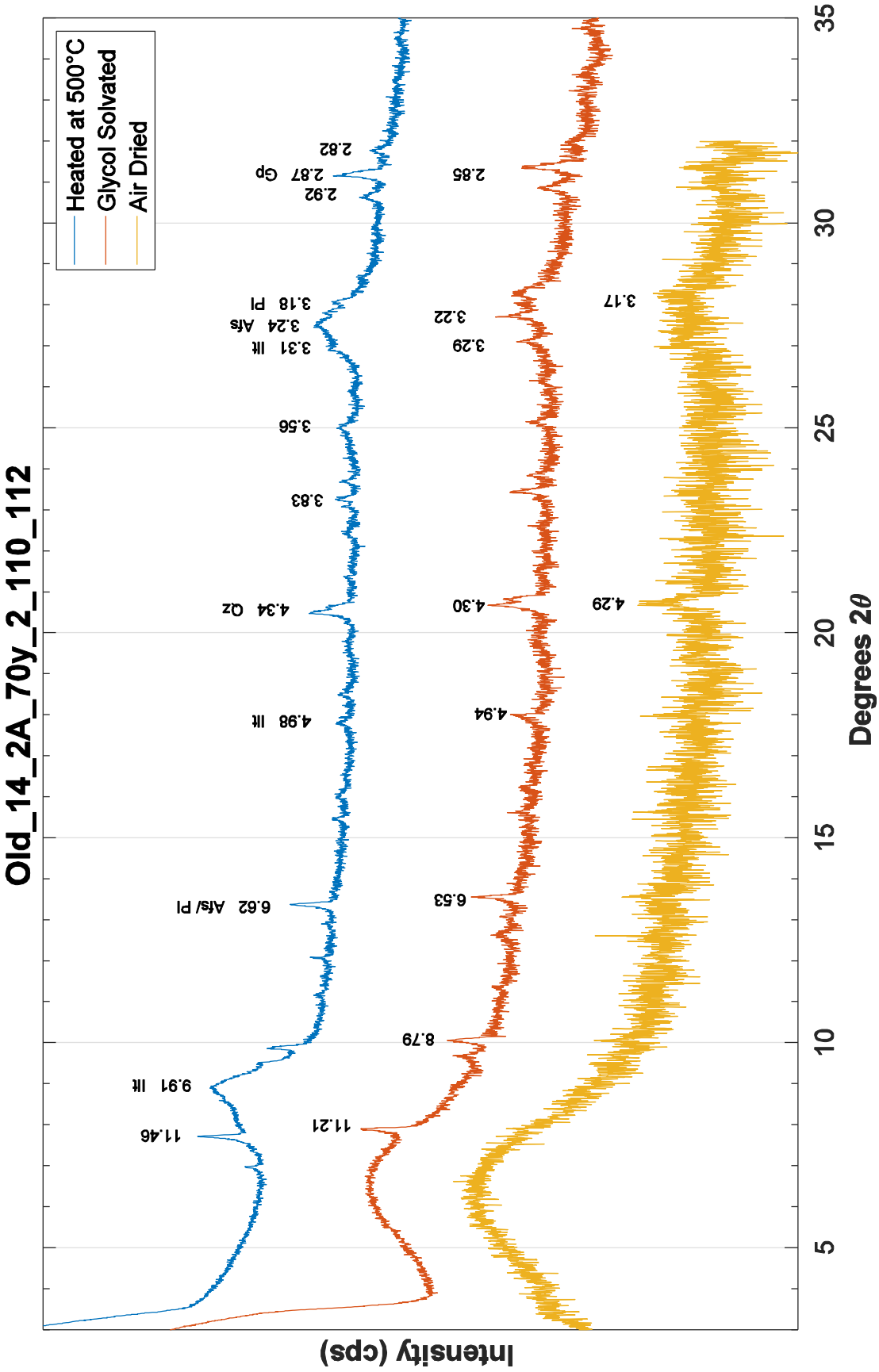
Old_14_2A_70y_2_110_112
Heated at 500°C
Glycol Solvated
Air Dried
Intensity (cps)
Degrees 2θ
5
10
15
20
25
30
35
11.46
9.91 Ilt
11.21
8.79
6.62 Afs/ Pl
6.53
4.98 Ilt
4.94
4.34 Qz
4.30
4.29
3.83
3.56
3.31 Ilt
3.24 Afs
3.18 Pl
3.29
3.22
3.17
2.92
2.87 Gp
2.82
2.85

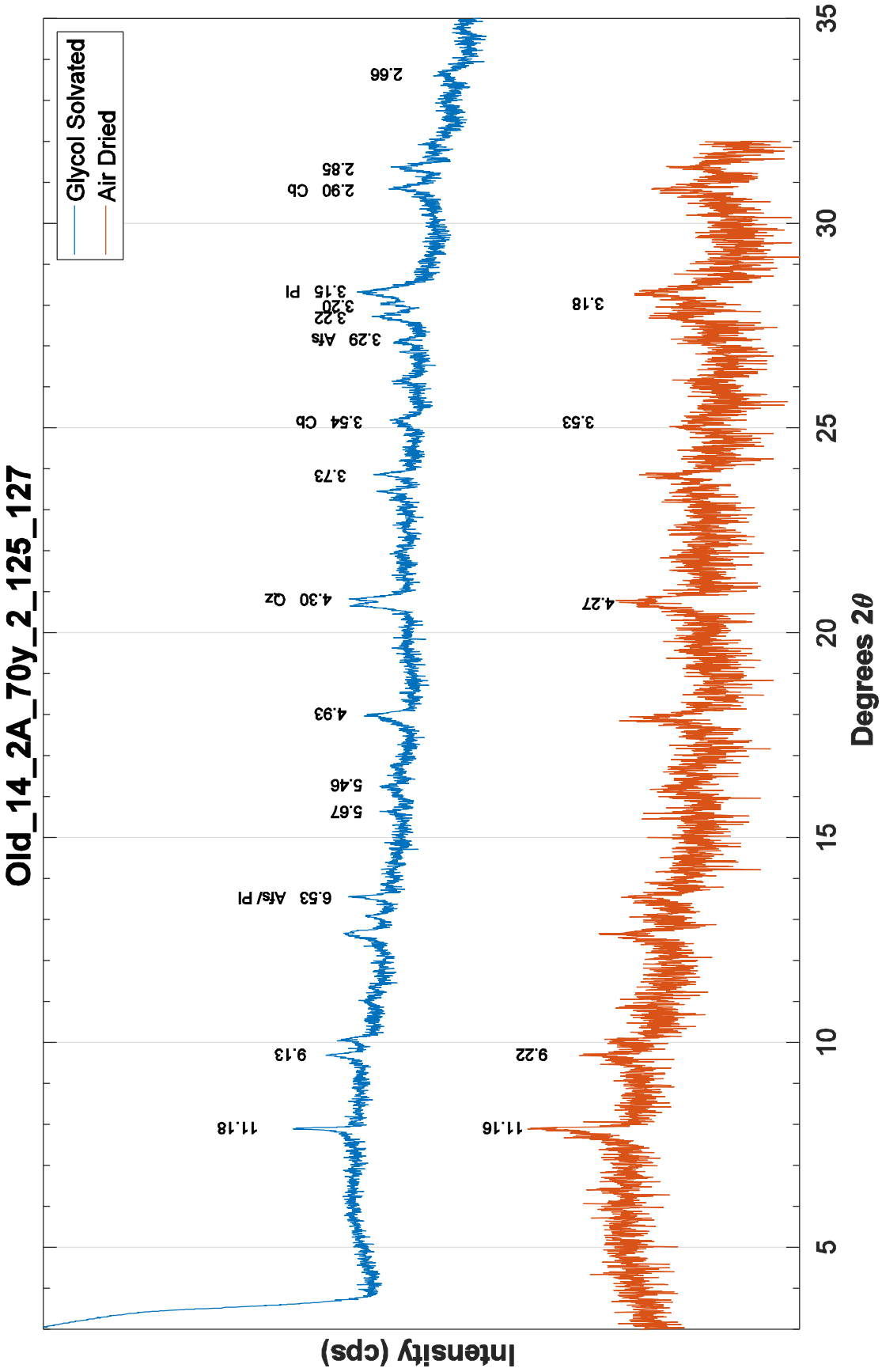
Old_14_2A_70y_2_125_127
Glycol Solvated
Air Dried
Intensity (cps)
Degrees 2θ
5
10
15
20
25
30
35
11.18
9.13
6.53 Afs/ Pl
5.67
5.46
4.93
4.30 Qz
3.73
3.54 Cb
3.29 Afs
3.22
3.20
3.15 Pl
2.90 Cb
2.85
2.66
11.16
9.22
4.27
3.53
3.18

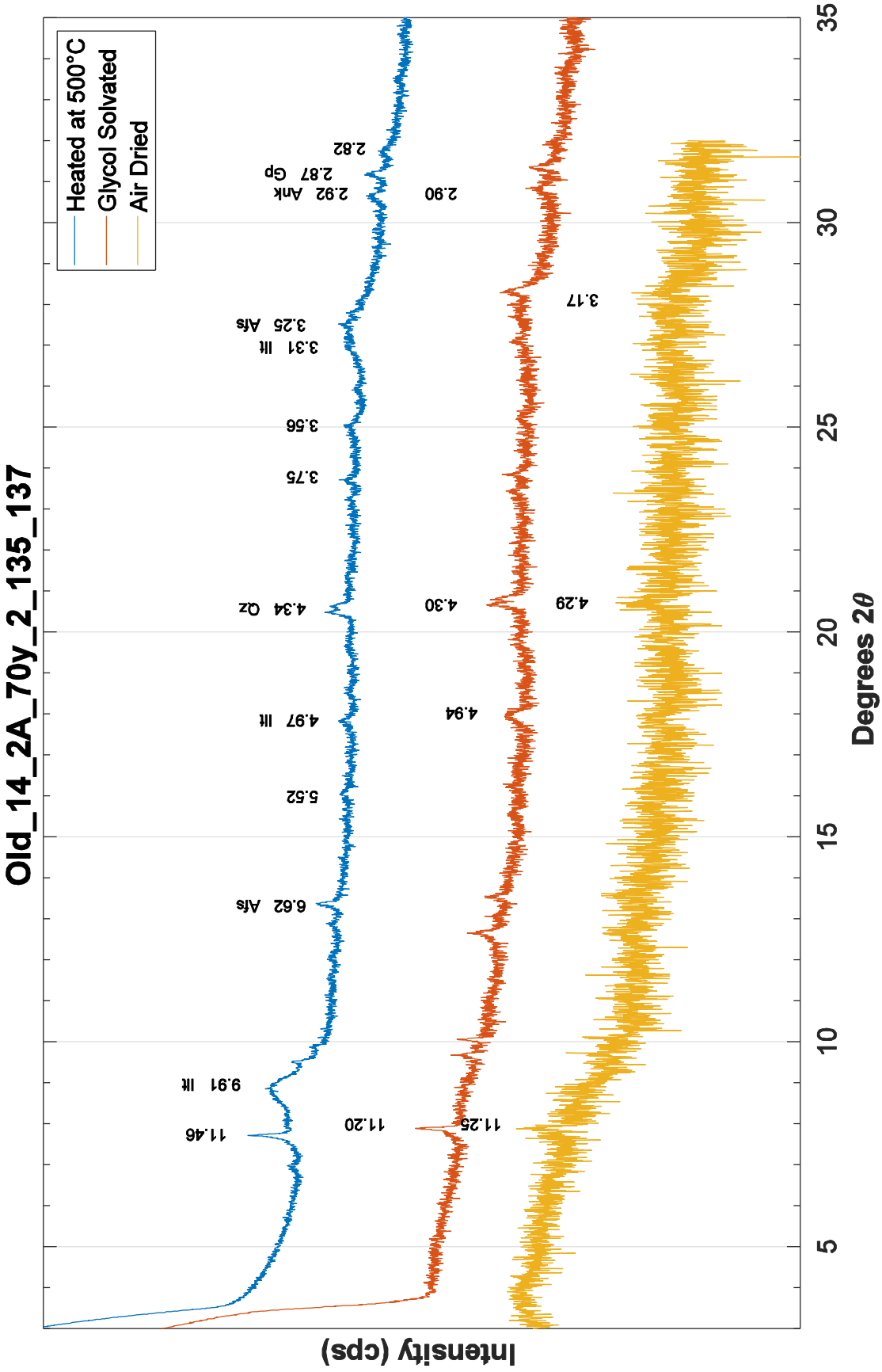
Old_14_2A_70y_2_135_137
Heated at 500°C
Glycol Solvated
Air Dried
Intensity (cps)
Degrees 2θ
5
10
15
20
25
30
35
11.46
9.91 Ilt
11.20
11.25
6.62 Afs
5.52
4.97 Ilt
4.94
4.34 Qz
4.30
4.29
3.75
3.56
3.31 Ilt
3.25 Afs
3.17
2.92 Ank
2.87 Gp
2.90
2.82

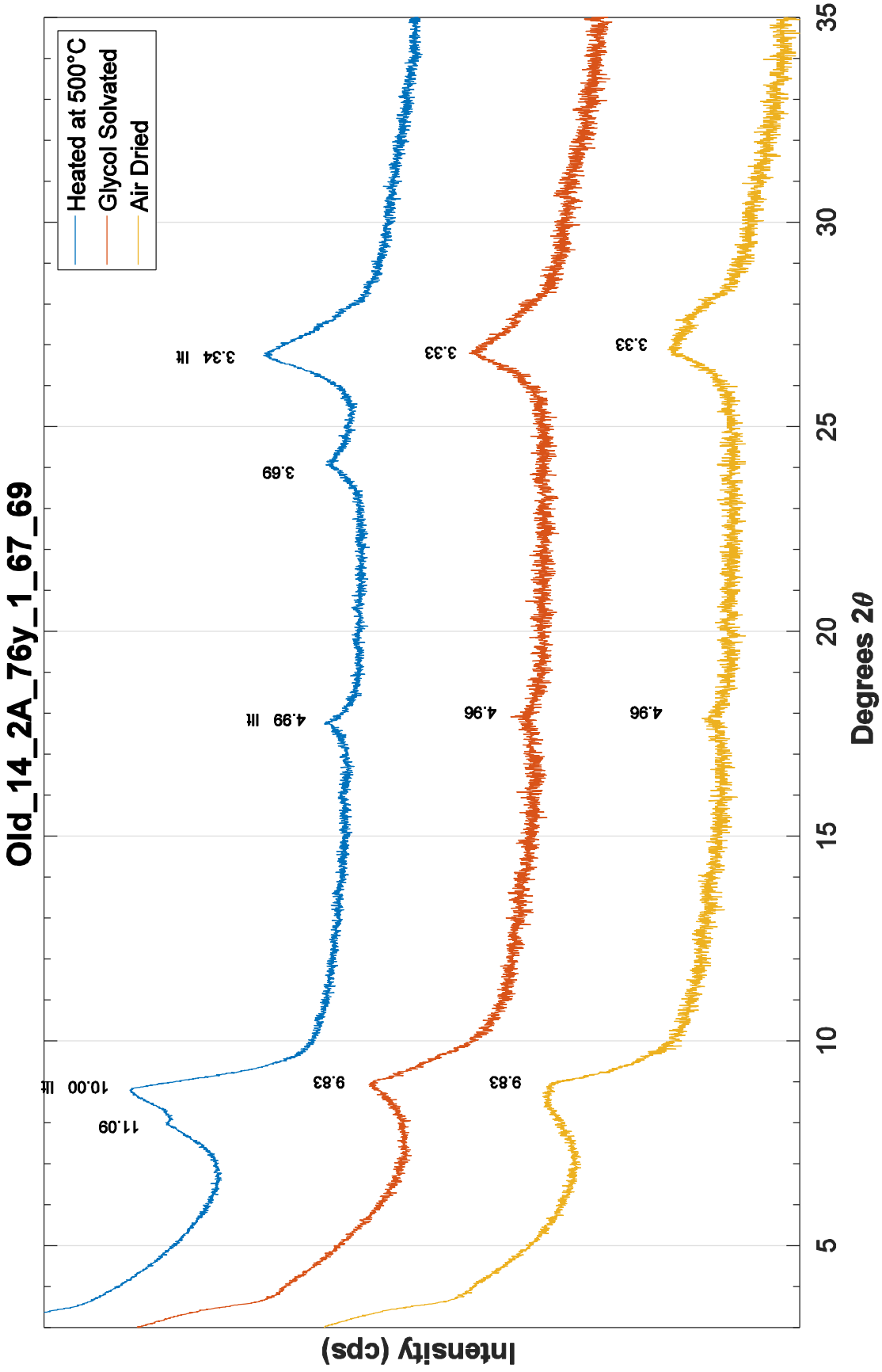
Old_14_2A_76y_1_67_69
Heated at 500°C
Glycol Solvated
Air Dried
Intensity (cps)
Degrees 2θ
5
10
15
20
25
30
35
10.00 IR
11.09
9.83
4.99 IR
3.69
3.34 IR
9.83
4.96
3.33
9.83
4.96
3.33

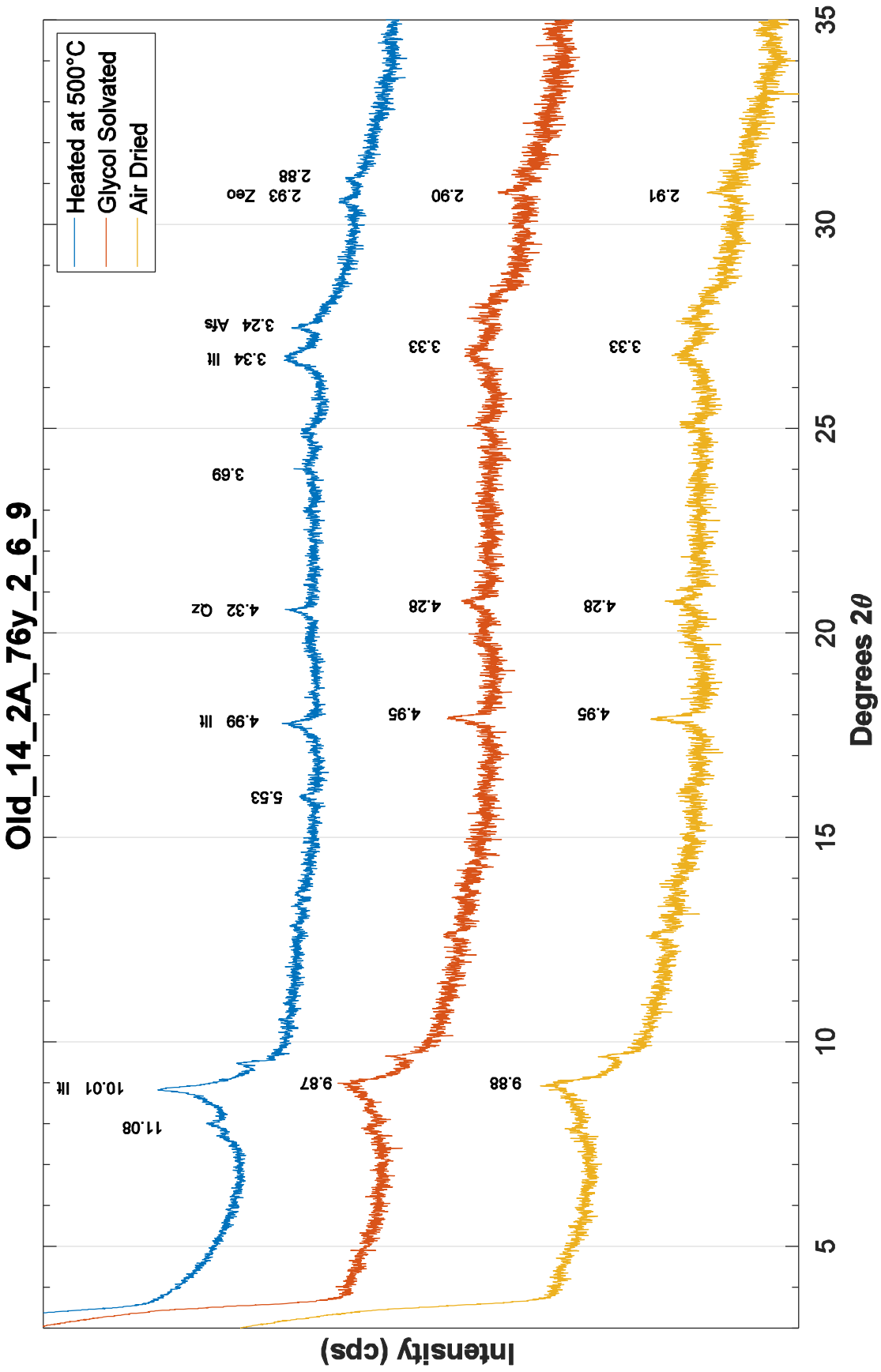
Old_14_2A_76y_2_6_9
Heated at 500°C
Glycol Solvated
Air Dried
Intensity (cps)
Degrees 2θ
5
10
15
20
25
30
35
11.08
10.01 Ilt
9.87
9.88
5.53
4.99 Ilt
4.95
4.95
4.32 Qz
4.28
4.28
3.69
3.34 Ilt
3.33
3.33
3.24 Afs
2.93 Zeo
2.88
2.90
2.91

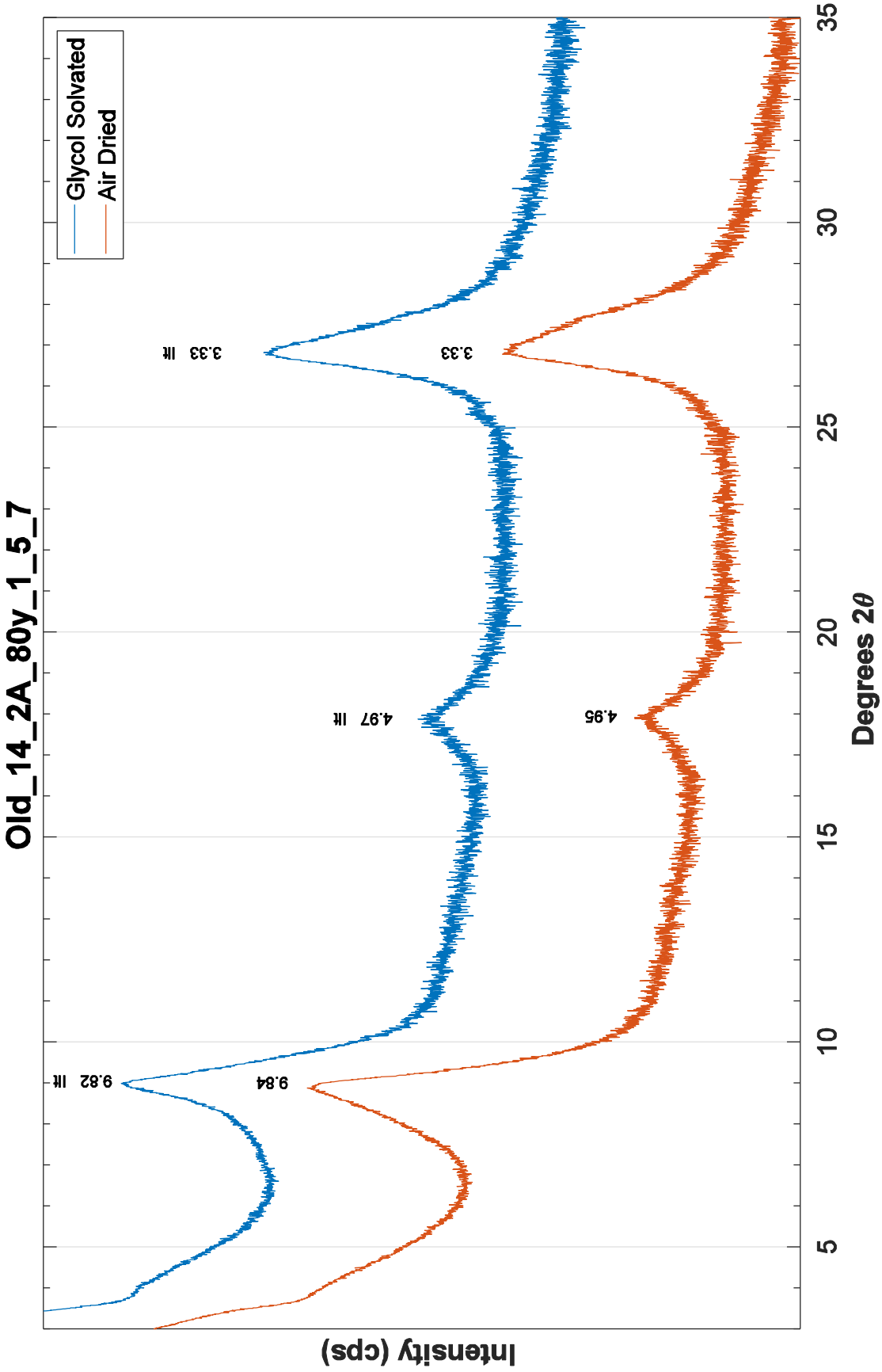
Old_14_2A_80y_1_5_7
Glycol Solvated
Air Dried
9.82 lit
9.84
4.97 lit
4.95
3.33 lit
3.33
Intensity (cps)
Degrees 2θ
5
10
15
20
25
30
35

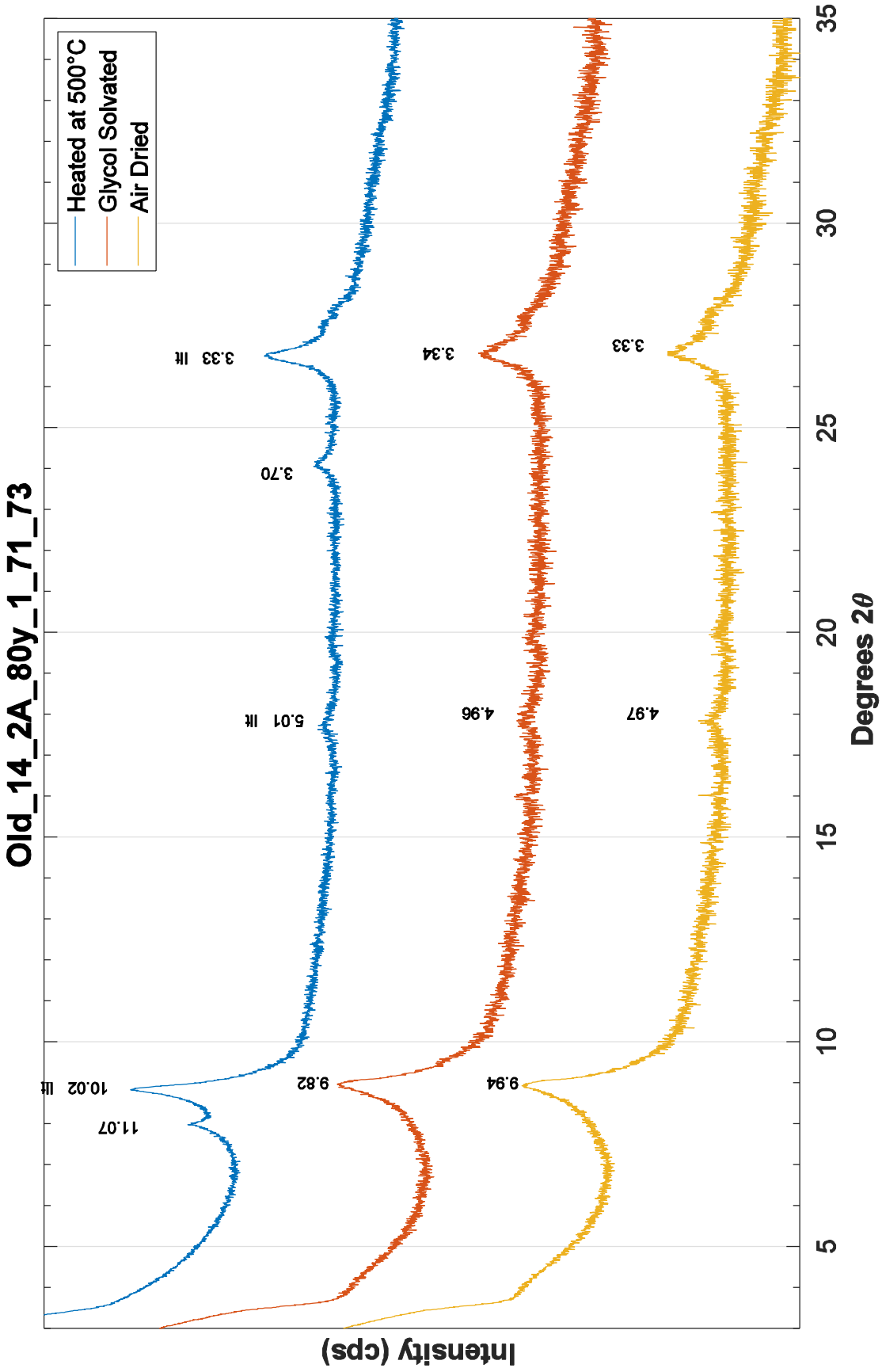
Old_14_2A_80y_1_71_73
Heated at 500°C
Glycol Solvated
Air Dried
Intensity (cps)
Degrees 2θ
5
10
15
20
25
30
35
10.02 Ilt
11.07
9.82
9.94
5.01 Ilt
3.70
4.96
4.97
3.33 Ilt
3.34
3.33

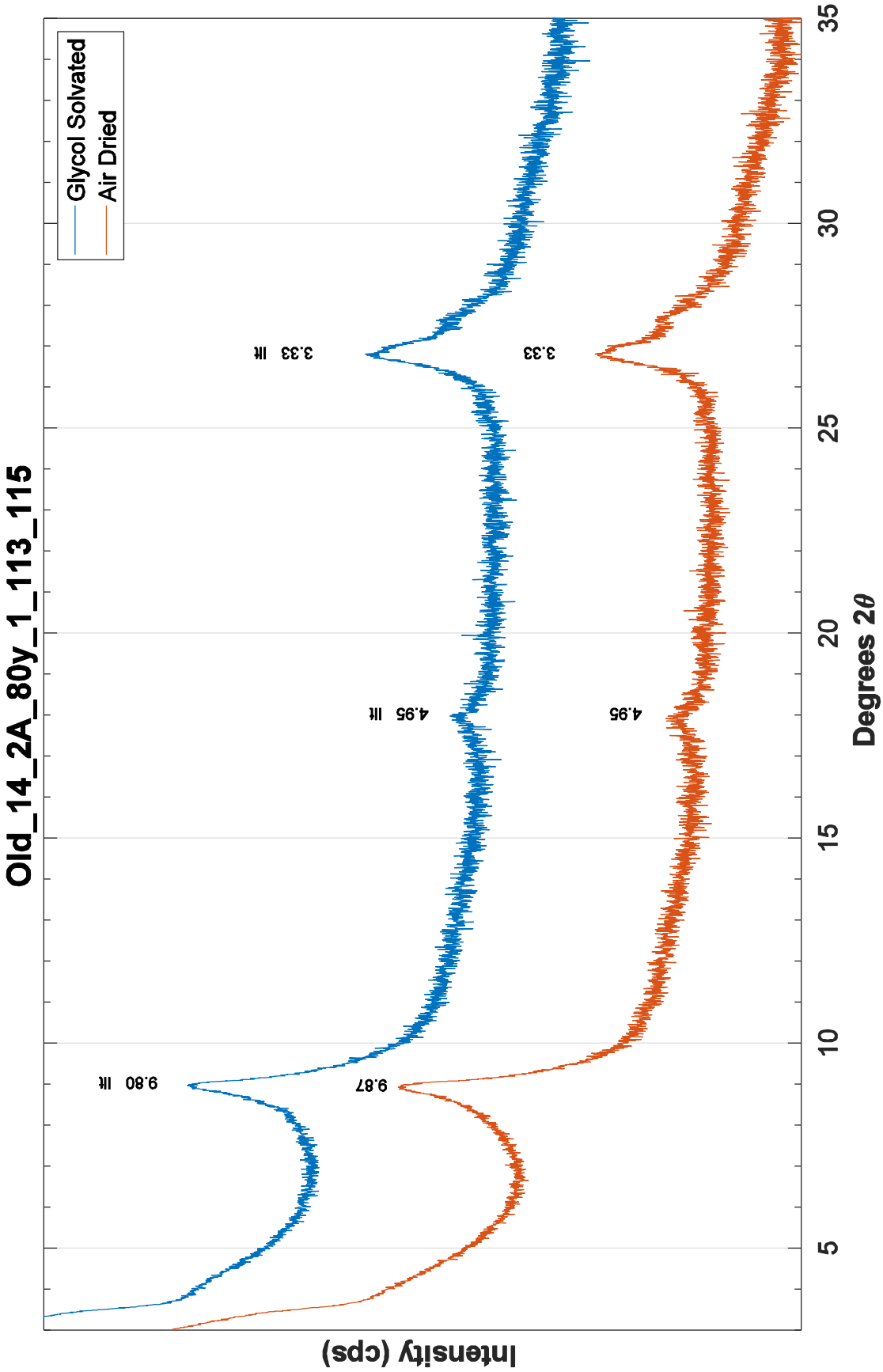
Old_14_2A_80y_1_113_115
Glycol Solvated
Air Dried
9.80 lit
9.87
4.95 lit
4.95
3.33 lit
3.33
Intensity (cps)
Degrees 2θ
5
10
15
20
25
30
35

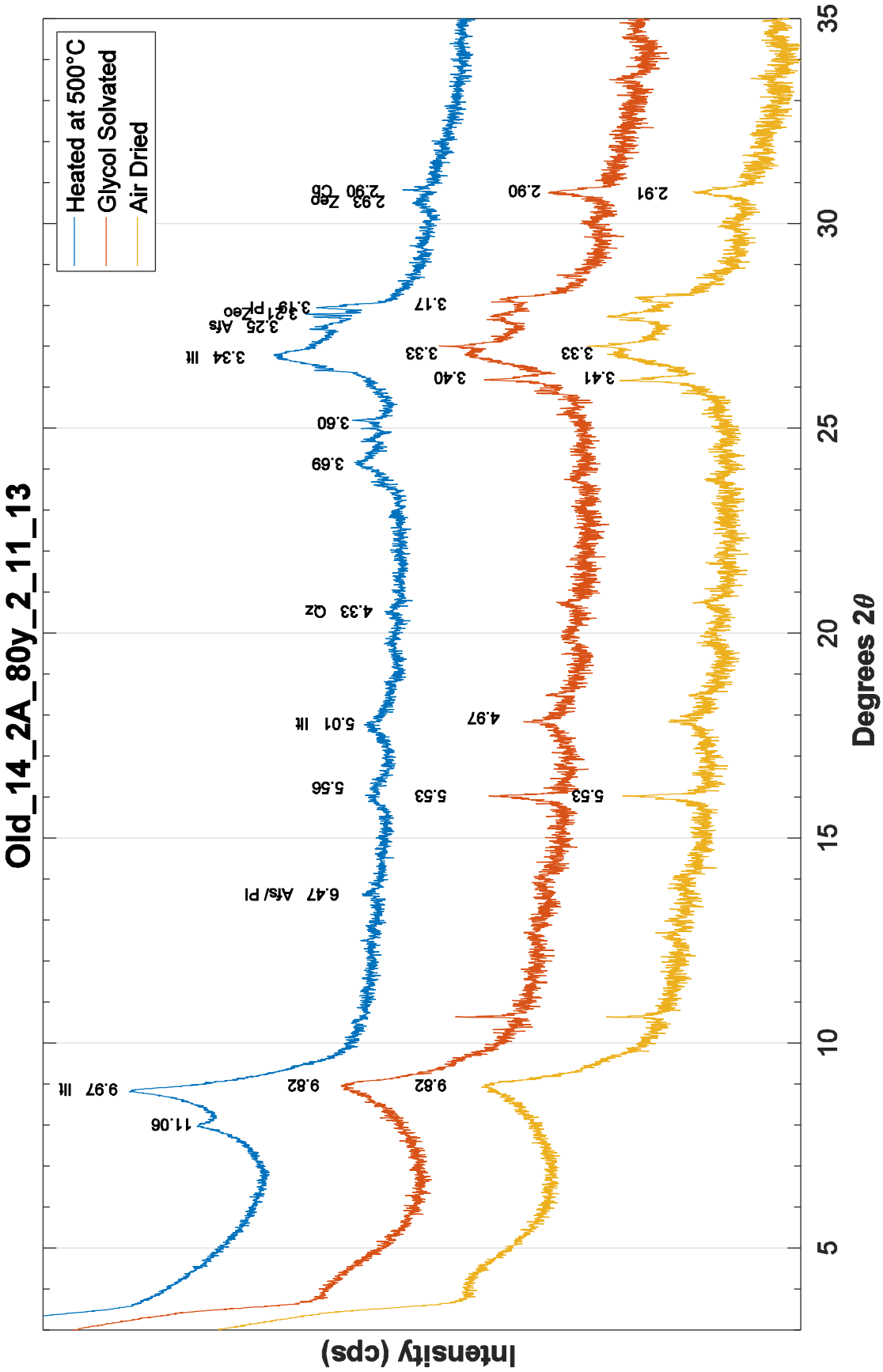
Old_14_2A_80y_2_11_13
Heated at 500°C
Glycol Solvated
Air Dried
Intensity (cps)
Degrees 2θ
5
10
15
20
25
30
35
9.97 Ilt
11.06
9.82
9.82
6.47 Afs/ Pl
5.56
5.53
5.01 Ilt
5.53
4.97
4.33 Qz
3.69
3.60
3.34 Ilt
3.25 Afs
3.21 Plag
3.17
2.93 Zep
2.90 Cb
3.41
3.33
3.40
3.33
2.91
2.90

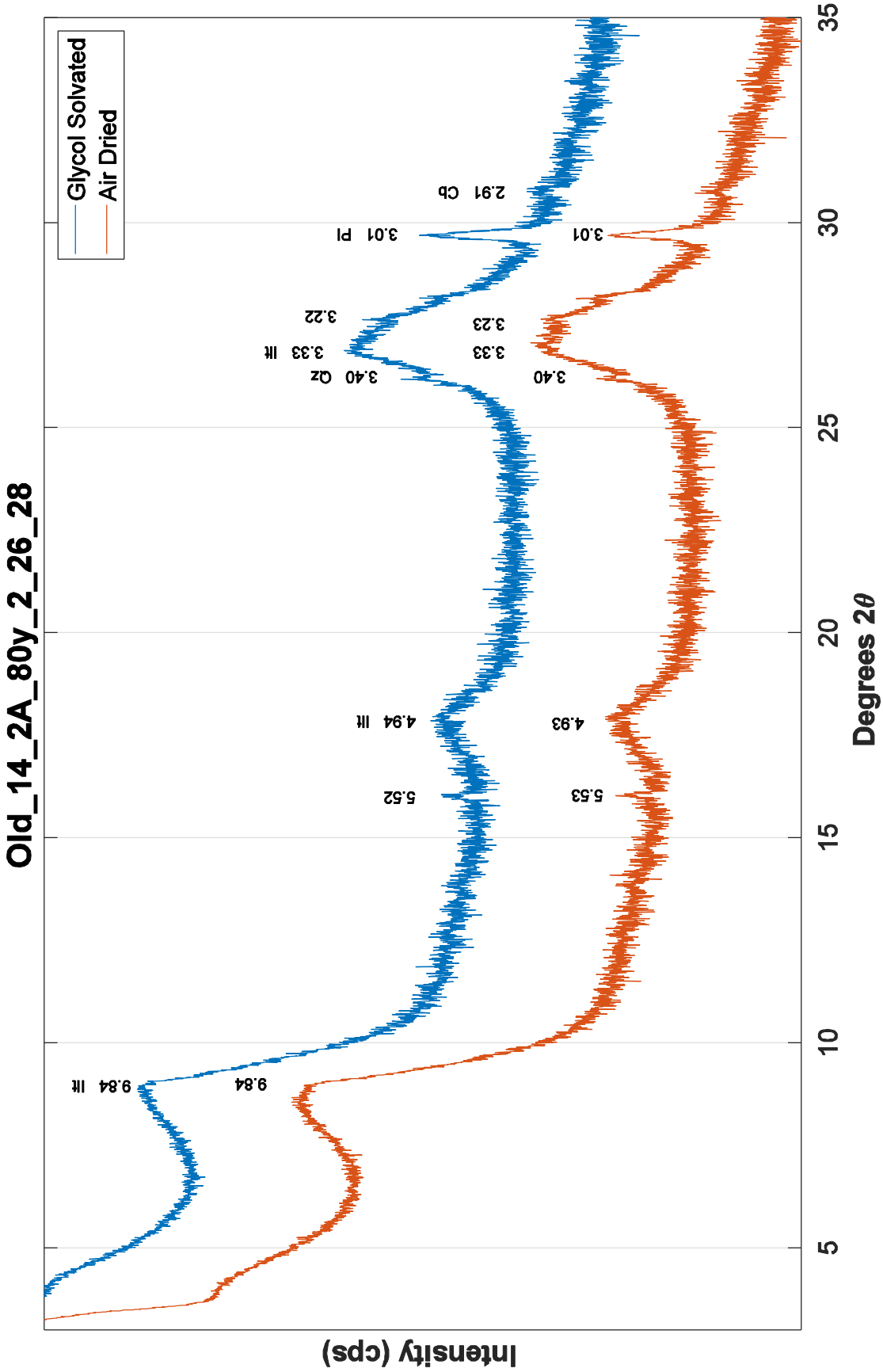
Old_14_2A_80y_2_26_28
Glycol Solvated
Air Dried
Intensity (cps)
Degrees 2θ
5
10
15
20
25
30
35
9.84 Ilt
9.84
4.94 Ilt
5.52
5.53
4.93
3.40 Qz
3.33 Ilt
3.22
3.01 Pl
2.91 Cb
3.40
3.33
3.23
3.01

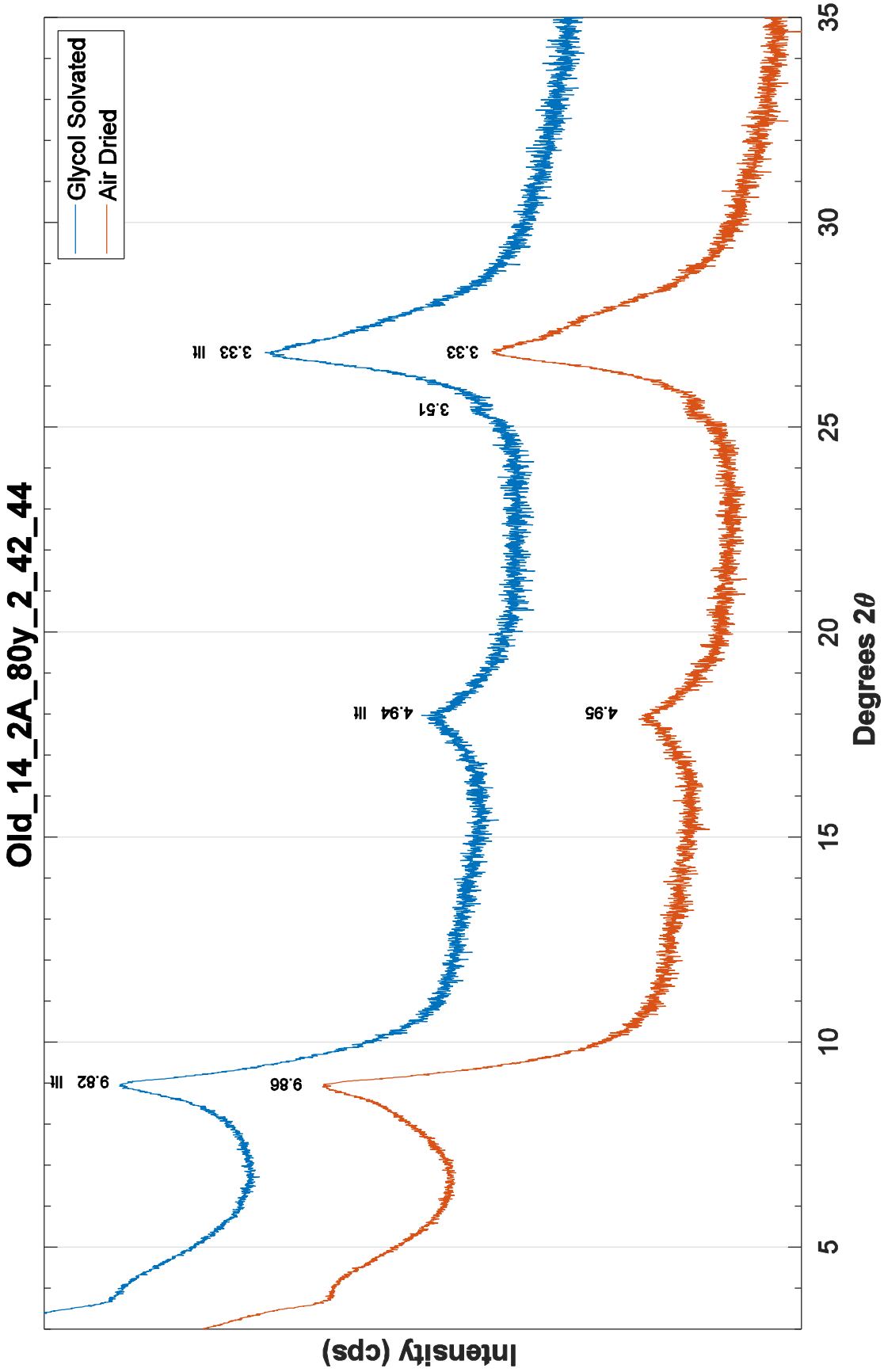
Old_14_2A_80y_2_42_44
Glycol Solvated
Air Dried
9.82 III
9.86
4.94 III
4.95
3.51
3.33 III
3.33
Intensity (cps)
Degrees 2θ
5
10
15
20
25
30
35

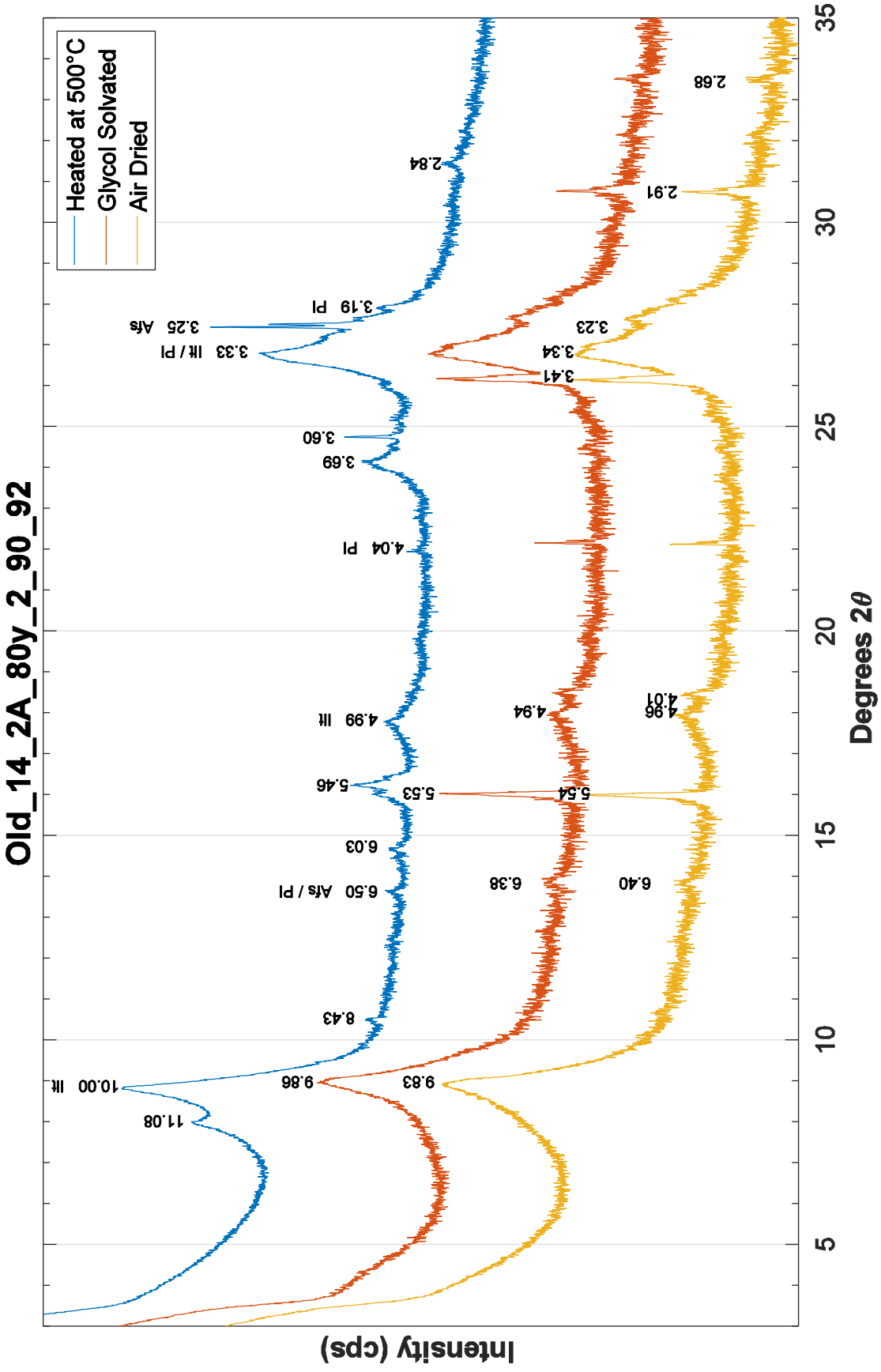
Old_14_2A_80y_2_90_92
Heated at 500°C
Glycol Solvated
Air Dried
Intensity (cps)
Degrees 2θ
5
10
15
20
25
30
35
10.00 Ilt
11.08
9.86
9.83
8.43
6.50 Afs / Pl
6.38
6.40
6.03
5.53
5.54
5.46
4.99 Ilt
4.94
4.96
4.01
4.04 Pl
3.69
3.60
3.33 Ilt / Pl
3.25 Afs
3.19 Pl
3.41
3.34
3.23
2.91
2.84
2.68

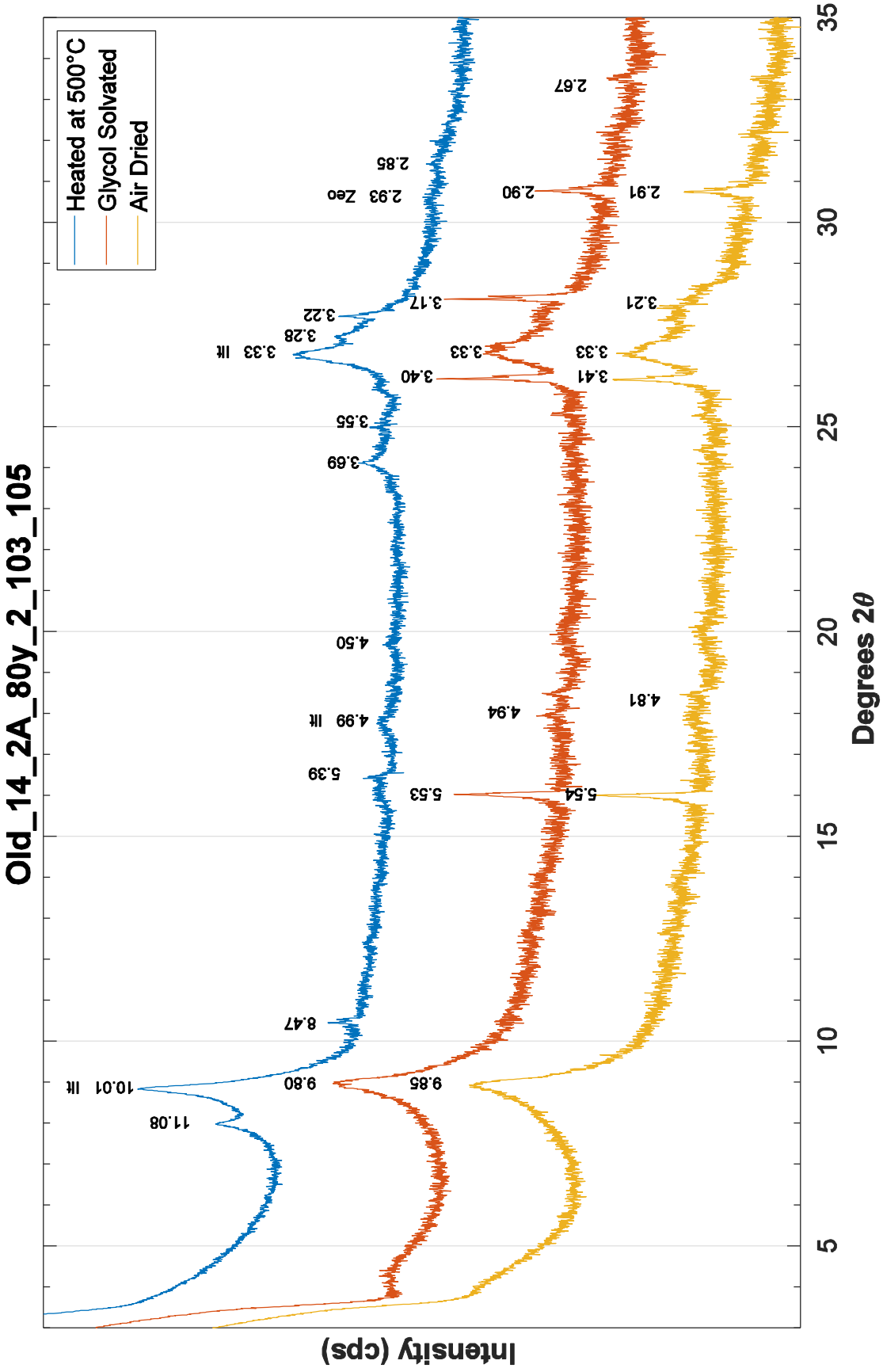
Old_14_2A_80y_2_103_105
Heated at 500°C
Glycol Solvated
Air Dried
Intensity (cps)
Degrees 2θ
5
10
15
20
25
30
35
10.01 llt
11.08
9.80
9.85
8.47
5.39
5.53
5.54
4.99 llt
4.94
4.81
4.50
3.69
3.55
3.40
3.41
3.33 llt
3.28
3.33
3.22
3.17
3.21
2.93 Zeo
2.90
2.91
2.85
2.67

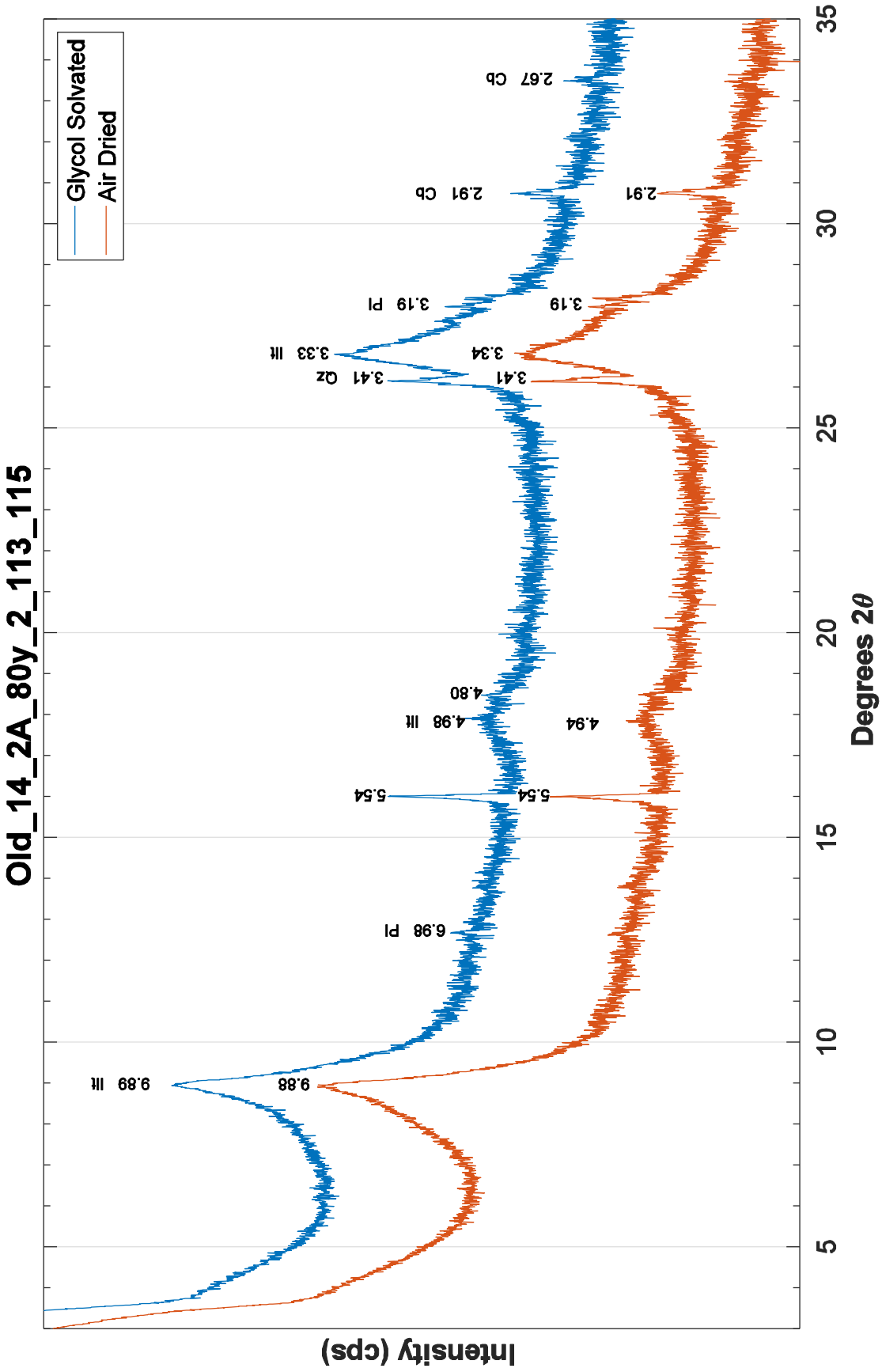
Old_14_2A_80y_2_113_115
Glycol Solvated
Air Dried
Intensity (cps)
Degrees 2θ
5
10
15
20
25
30
35
9.89 Ilt
9.88
6.98 Pl
5.54
5.54
4.98 Ilt
4.80
4.94
3.41 Qz
3.41
3.33 Ilt
3.34
3.19 Pl
3.19
2.91 Cb
2.91
2.67 Cb

Appendix E.2

The patterns for 060 reflections for selected samples

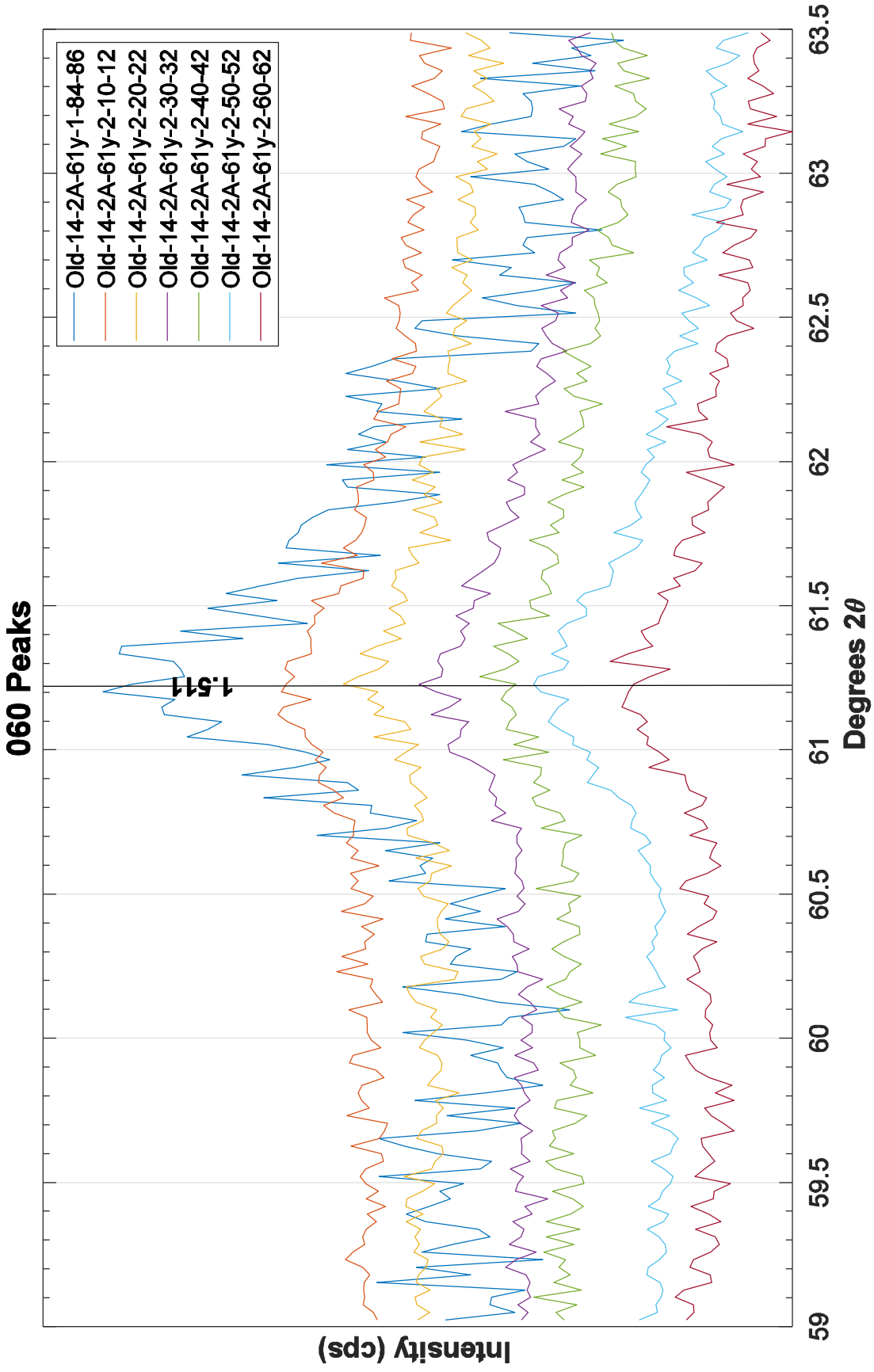
060 Peaks
1.511
Old-14-2A-61y-1-84-86
Old-14-2A-61y-2-10-12
Old-14-2A-61y-2-20-22
Old-14-2A-61y-2-30-32
Old-14-2A-61y-2-40-42
Old-14-2A-61y-2-50-52
Old-14-2A-61y-2-60-62
Intensity (cps)
59
59.5
60
60.5
61
61.5
62
62.5
63
63.5
Degrees 2θ

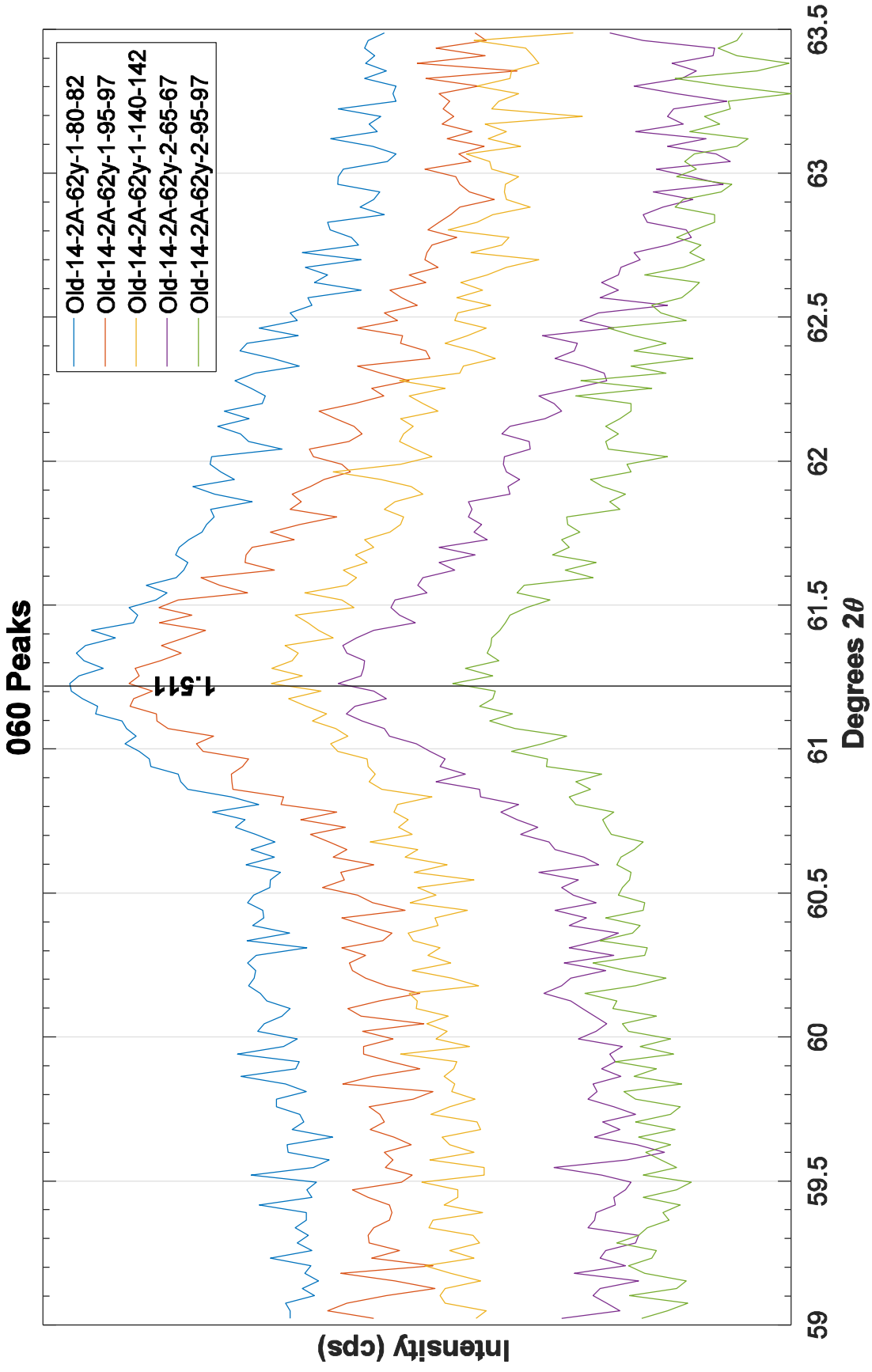
060 Peaks
1.511
Old-14-2A-62y-1-80-82
Old-14-2A-62y-1-95-97
Old-14-2A-62y-1-140-142
Old-14-2A-62y-2-65-67
Old-14-2A-62y-2-95-97
Intensity (cps)
Degrees 2θ
59
59.5
60
60.5
61
61.5
62
62.5
63
63.5

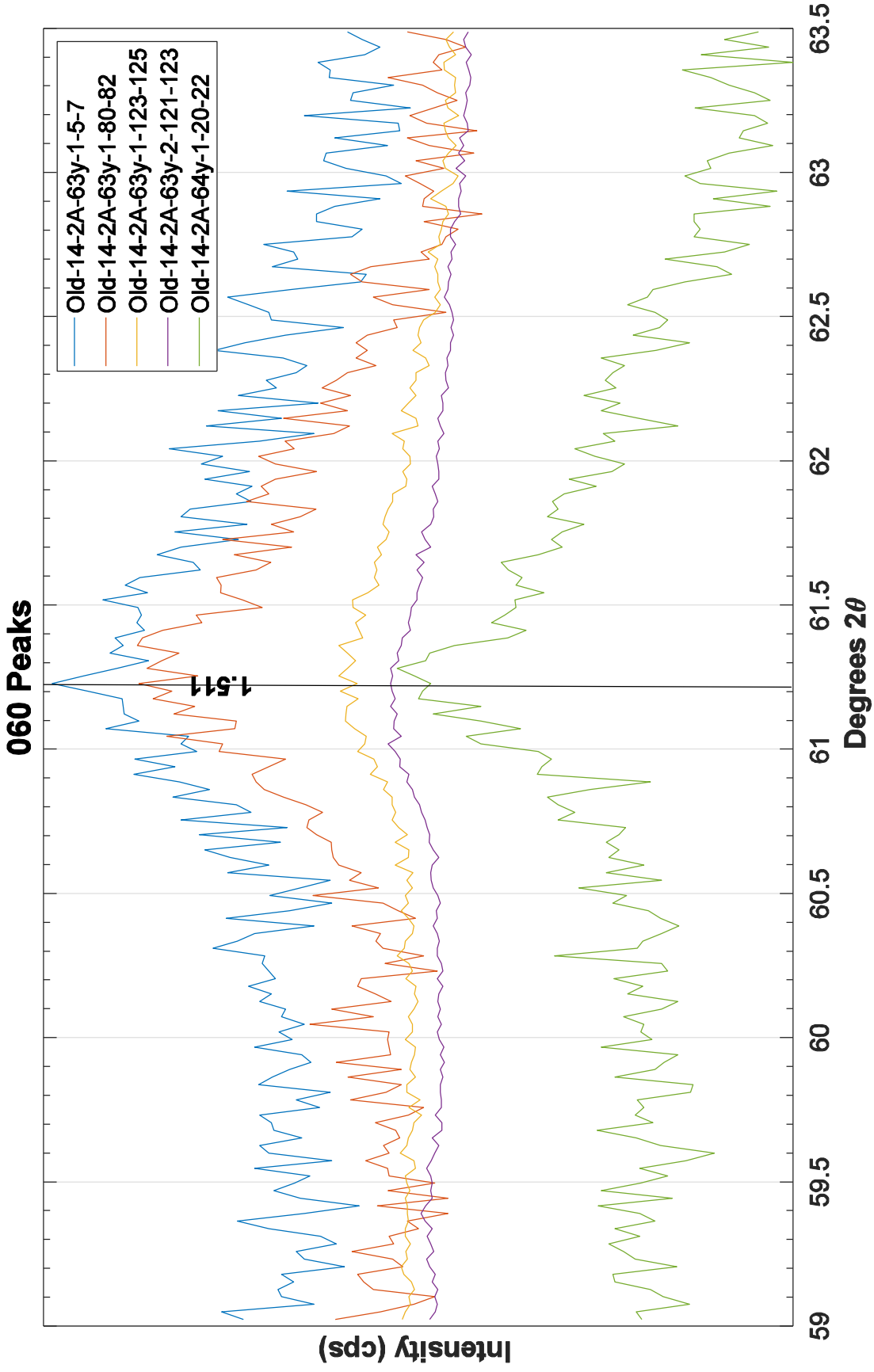
060 Peaks
1.511
Old-14-2A-63y-1-5-7
Old-14-2A-63y-1-80-82
Old-14-2A-63y-1-123-125
Old-14-2A-63y-2-121-123
Old-14-2A-64y-1-20-22
Intensity (cps)
Degrees 2θ
59
59.5
60
60.5
61
61.5
62
62.5
63
63.5

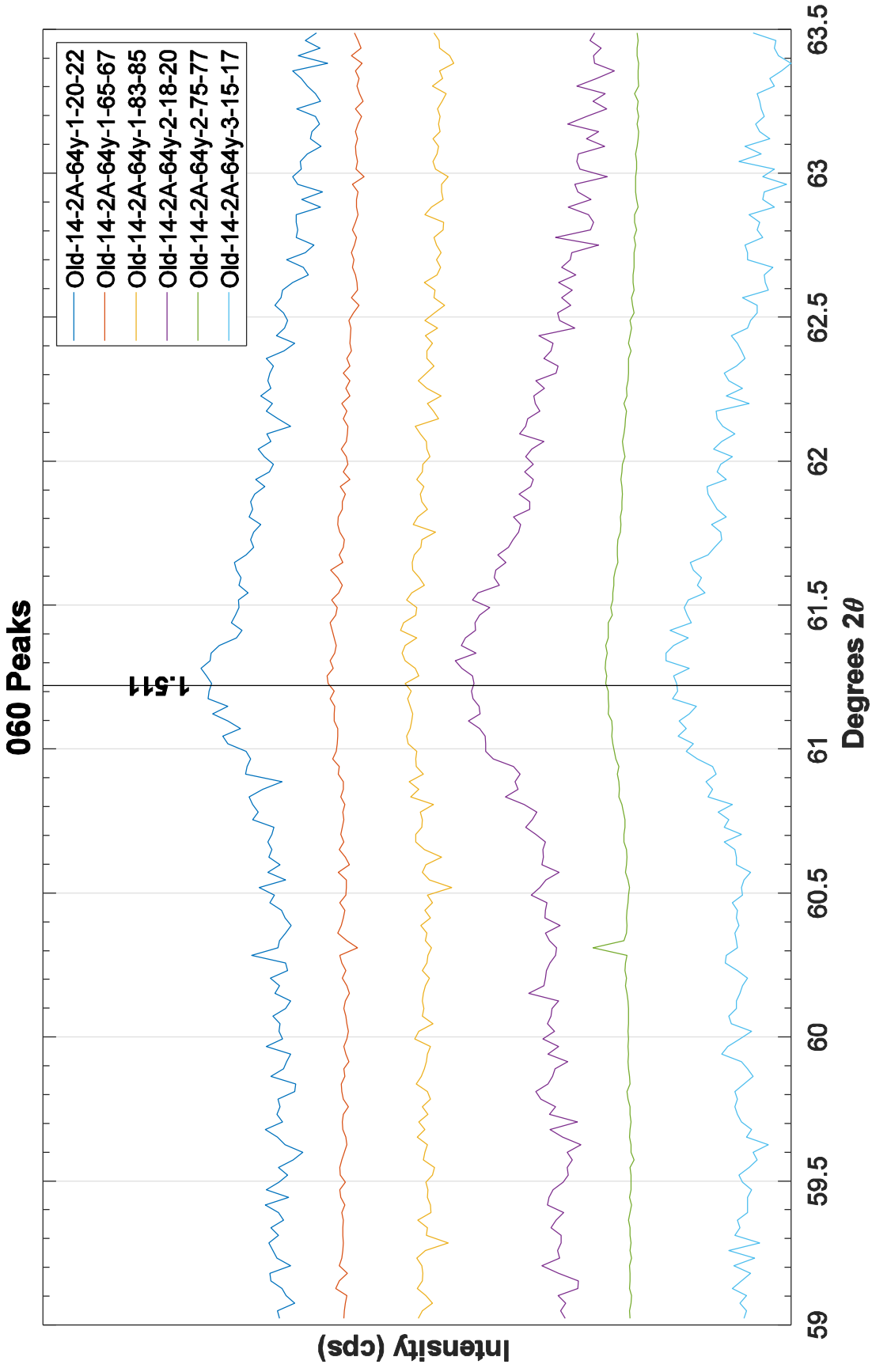
060 Peaks
1.511
Old-14-2A-64y-1-20-22
Old-14-2A-64y-1-65-67
Old-14-2A-64y-1-83-85
Old-14-2A-64y-2-18-20
Old-14-2A-64y-2-75-77
Old-14-2A-64y-3-15-17
Intensity (cps)
Degrees 2θ
59
59.5
60
60.5
61
61.5
62
62.5
63
63.5

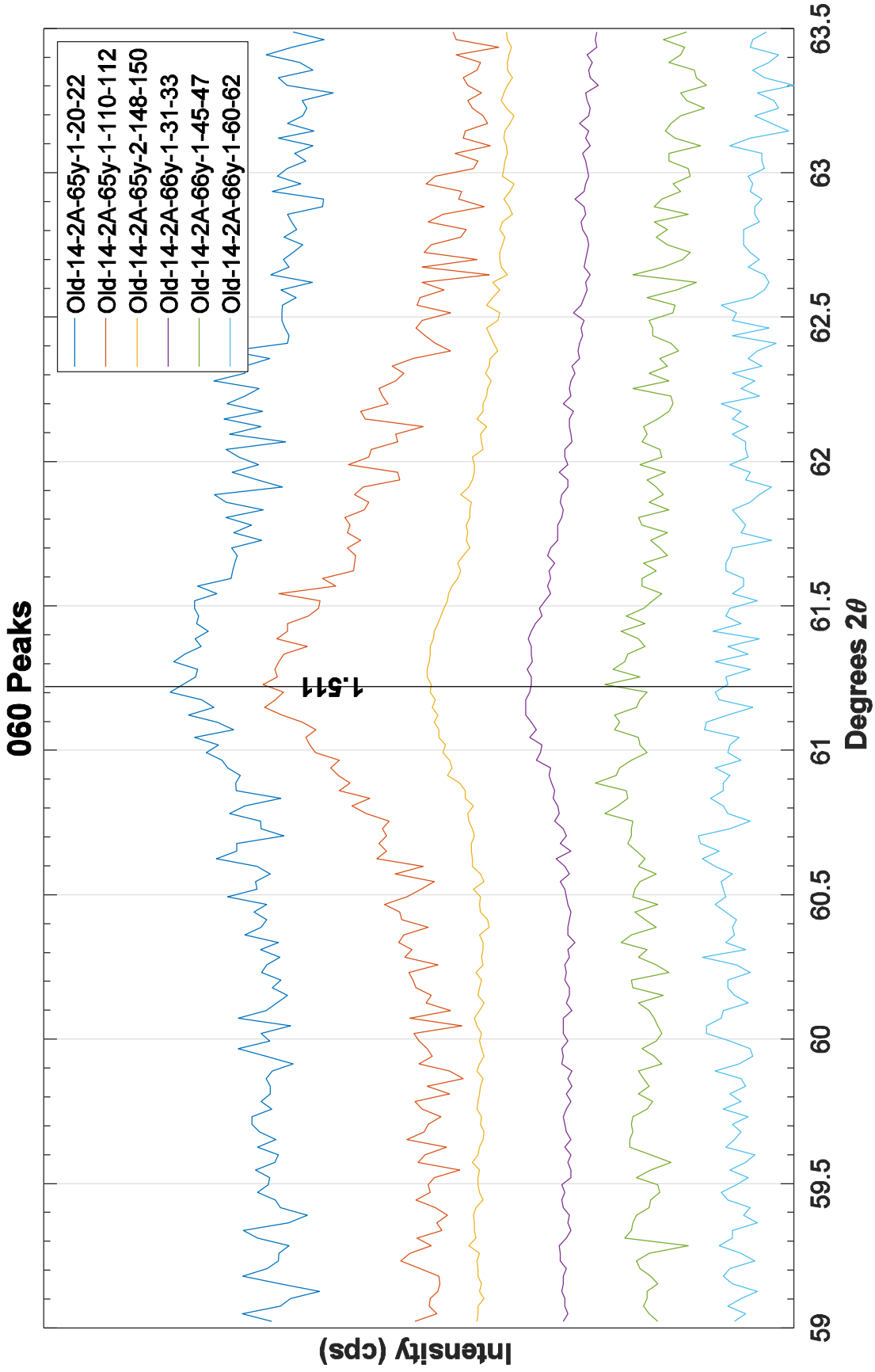
060 Peaks
Old-14-2A-65y-1-20-22
Old-14-2A-65y-1-110-112
Old-14-2A-65y-2-148-150
Old-14-2A-66y-1-31-33
Old-14-2A-66y-1-45-47
Old-14-2A-66y-1-60-62
1.511
Intensity (cps)
Degrees 2θ
59
59.5
60
60.5
61
61.5
62
62.5
63
63.5

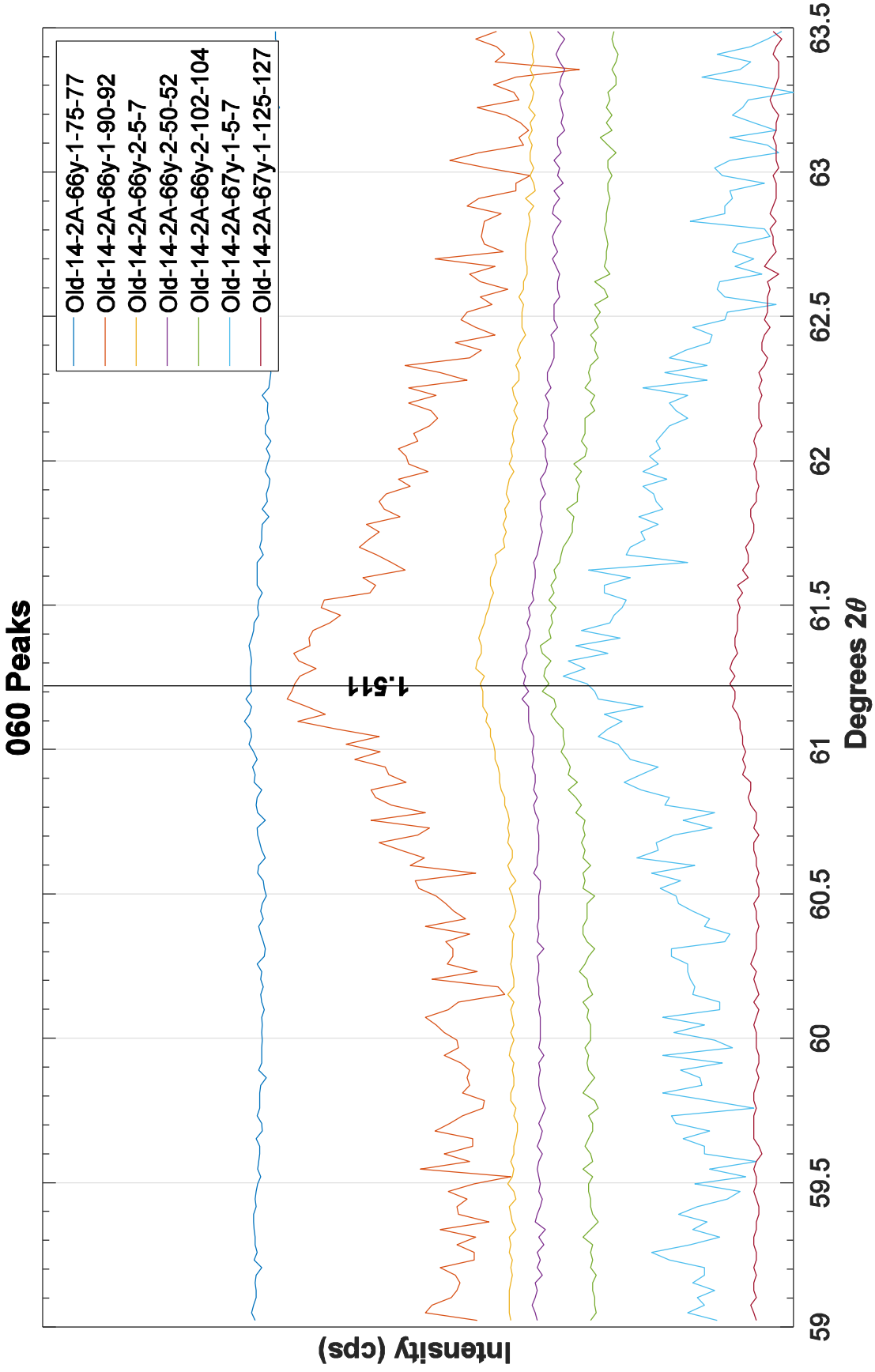
060 Peaks
Old-14-2A-66y-1-75-77
Old-14-2A-66y-1-90-92
Old-14-2A-66y-2-5-7
Old-14-2A-66y-2-50-52
Old-14-2A-66y-2-102-104
Old-14-2A-67y-1-5-7
Old-14-2A-67y-1-125-127
1.511
Intensity (cps)
Degrees 2θ
59
59.5
60
60.5
61
61.5
62
62.5
63
63.5

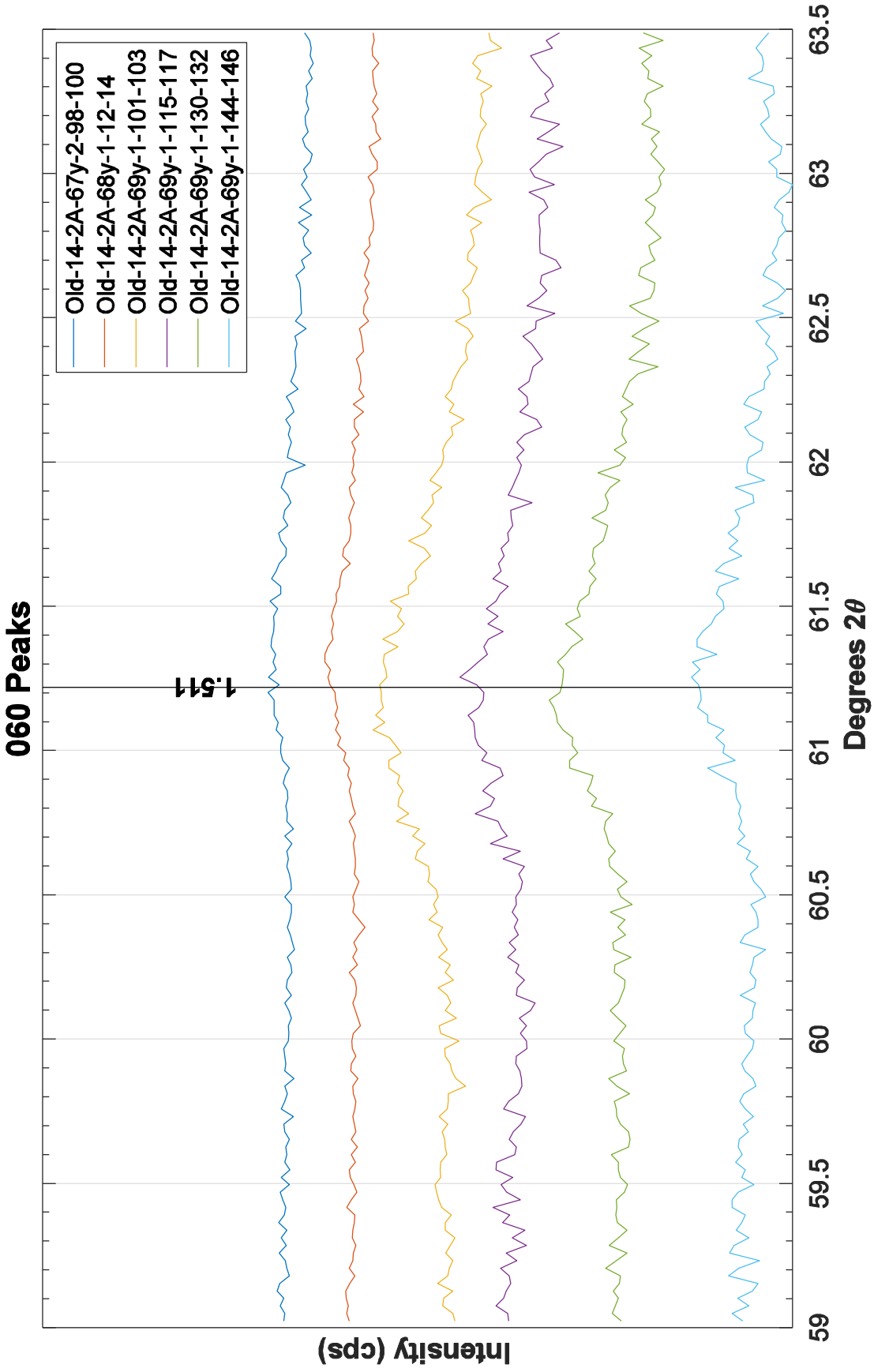
060 Peaks
1.511
Old-14-2A-67y-2-98-100
Old-14-2A-68y-1-12-14
Old-14-2A-69y-1-101-103
Old-14-2A-69y-1-115-117
Old-14-2A-69y-1-130-132
Old-14-2A-69y-1-144-146
Intensity (cps)
Degrees 2θ
59
59.5
60
60.5
61
61.5
62
62.5
63
63.5

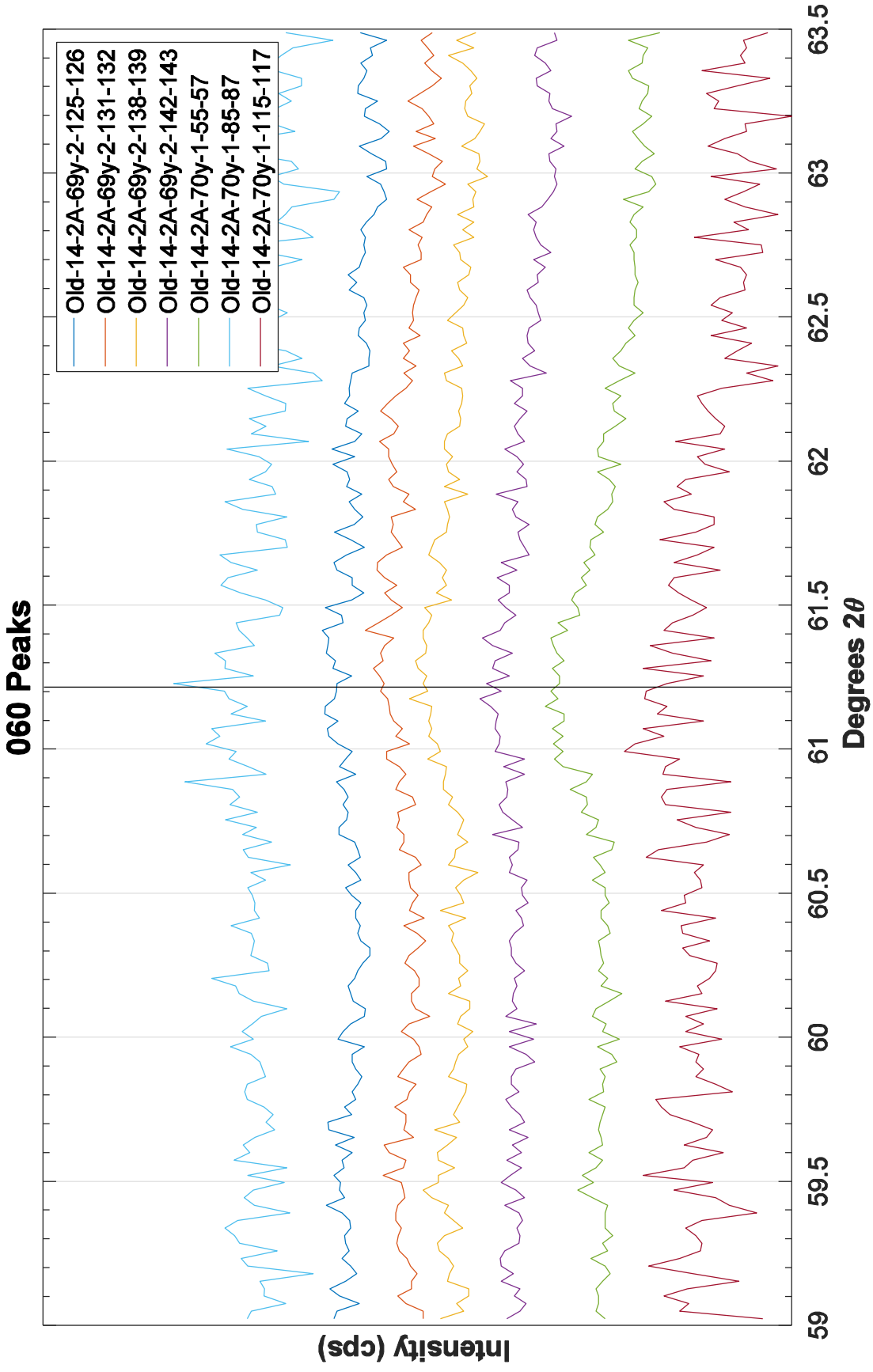
060 Peaks
Intensity (cps)
Degrees 2θ
59
59.5
60
60.5
61
61.5
62
62.5
63
63.5
Old-14-2A-69y-2-125-126
Old-14-2A-69y-2-131-132
Old-14-2A-69y-2-138-139
Old-14-2A-69y-2-142-143
Old-14-2A-70y-1-55-57
Old-14-2A-70y-1-85-87
Old-14-2A-70y-1-115-117

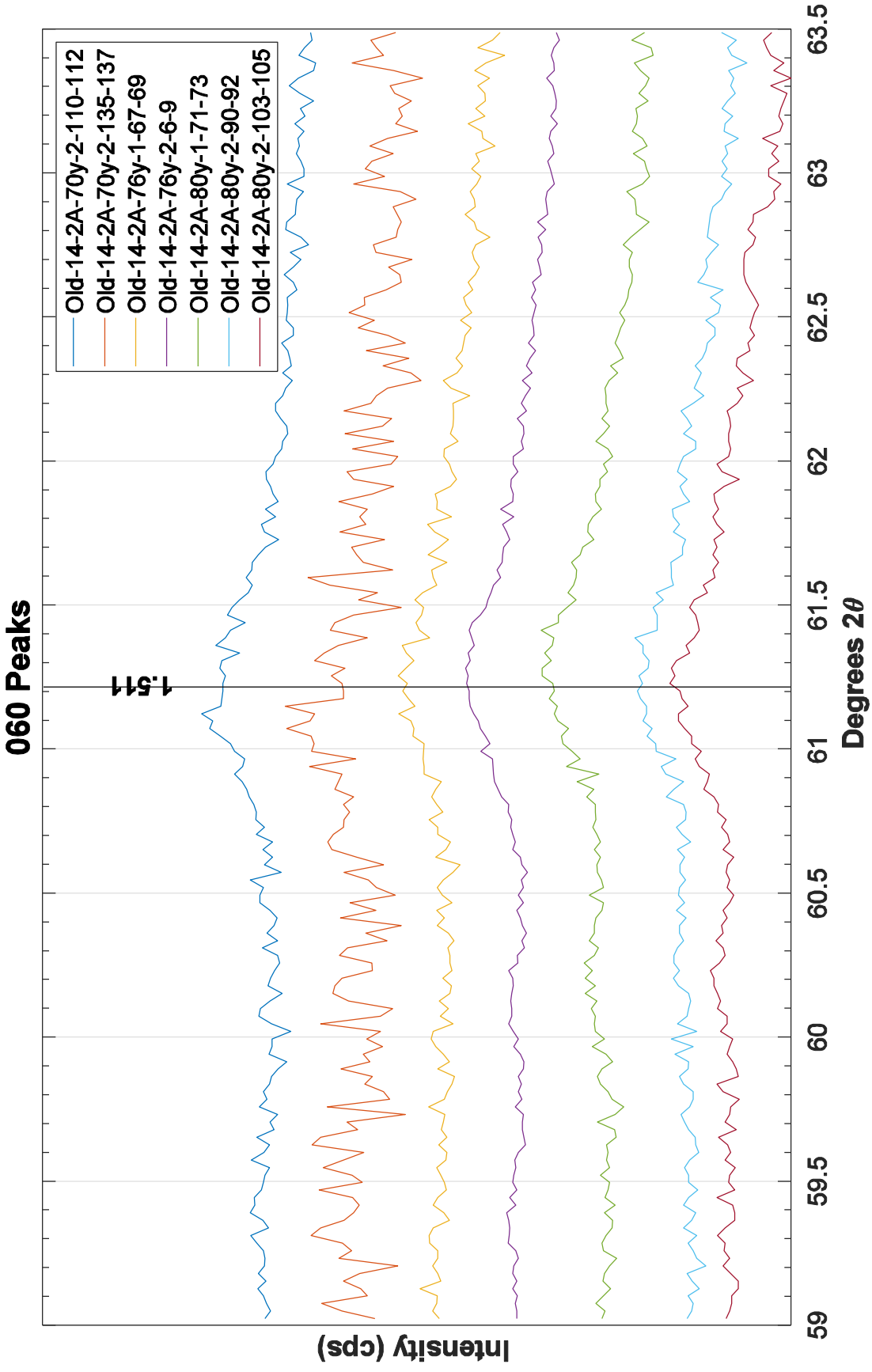
060 Peaks
1.511
Old-14-2A-70y-2-110-112
Old-14-2A-70y-2-135-137
Old-14-2A-76y-1-67-69
Old-14-2A-76y-2-6-9
Old-14-2A-80y-1-71-73
Old-14-2A-80y-2-90-92
Old-14-2A-80y-2-103-105
Intensity (cps)
Degrees 2θ
59
59.5
60
60.5
61
61.5
62
62.5
63
63.5